Università degli Studi della Tuscia di Viterbo

Dipartimento di Scienze Ecologiche e Biologiche (DEB)

Corso di Dottorato di Ricerca in

Ecology and Sustainable management of environmental resources - **XXXVI cycle**

TITOLO TESI DI DOTTORATO DI RICERCA

Innovative nano-biotechnology applications in pharmaceutical, cosmeceutical and advanced biomaterial sciences.

Settore scientifico-disciplinare
(**s.s.d. CHIM/06**)

Tesi di dottorato di:
Dott.ssa Elisabetta Tomaino

Tomaino Elisabetta

Coordinatore del corso
Prof. Claudio Carere

Firma

Tutor
Prof. Raffaele Saladino

Raffaele Saladino

Co-tutor
Dott.ssa Eliana Capecchi

Eliana Capecchi

(A.Y. 2022/23)

Thesis advisor

Prof. Raffaele Saladino

Author

Elisabetta Tomaino

Innovative nano-biotechnology applications in pharmaceutical, cosmeceutical and advanced biomaterial sciences

Abstract

This study focused on novel nano-biotechnology applications in the context of green chemistry and circular economy, with a primary attention to valorisation of natural polyphenols, such as lignin as sustainable nanomaterials and carriers for the immobilization of enzymes in biocatalysis. Three main topics have been discussed, each addressing different aspects of lignin nanoparticles utilization: I) nanofillers for biodegradable and home-compostable plastic blends; II) protective nanocarriers in cosmetic formulations; and III) nano-biocatalysts for green organic synthesis.

In the first section of the thesis, innovative lignin nanoparticles enriched with saccharides from fishery wastes, such as chitosan and chito-oligosaccharides, are developed as versatile bio-filler for advanced bioplastic formulation. These nanoparticles showed remarkable physical, chemical, and biological properties. In particular, they demonstrate UV-shielding, antioxidant, and antimicrobial activities, with the added benefits of a synergistic antioxidant effect between lignin and chito-oligosaccharides.

Next, the study explores the application of lignin nanoparticles in cosmetic and cosmeceutical formulations, with a particular focus on sunscreen products. In this latter case, lignin nanoparticles have been applied as carriers for commercially available UV chemical filters, such as avobenzone and octyl methoxycinnamate, enhancing their stability and photoprotective properties. Furthermore, lignin nanoparticles were used as capsules for the protection of ascorbic acid esters from degradation, contributing to the development of sustainable and effective cosmetic formulations.

Finally, sustainable bio-catalysts have been developed for biotechnology applications by functionalization of lignin nanoparticles with enzymatic cascades. They comprised the co-immobilization of lipase M and tyrosinase on lignin-chitosan nanoparticles by layer-by-layer (LbL) deposition technique. The enzymatic cascade retained high catalytic activity over numerous cycles in the one-pot synthesis of a large panel of bioactive lipophilic esters of natural hydroxytyrosol, starting from tyrosol and long chain carboxylic acids, under environmentally friendly experimental conditions. Detailed description of the activity parameters and kinetic properties of these novel catalysts are described in detail. Notably, the co-immobilization of the enzymes was facilitated by the use of natural concanavalin A as molecular spacer, ensuring the correct orientation and appropriate spatial distance between the two enzymes. In a subsequent investigation, the integration of multicomponent chemistry with previously described multienzymes cascade was reported in order to synthesized bioactive 1,4-benzoxazines under favourable heterogeneous conditions. Benzoxazines represent an important privileged scaffolds in medicinal chemistry due to their pharmacological properties. The synthetic approach

involved the selective oxidative functionalization of tyrosol esters via nucleophilic 1,6-Michael addiction of selected α–amino acid methyl esters, followed by consecutive intramolecular lactonization and aromatization processes.
In summary, this study significantly contributed to green chemistry and circular economy applications by showcasing the versatility of lignin nanoparticles. They were used as a versatile nanoplatform for the design of sustainable materials and biocatalysts, offering promising entries for environmentally friendly industrial processes. This work underscores the potential of lignin nanoparticles to play a pivotal role in advancing sustainable and eco-conscious technologies.

Table of Contents

Title page……...1
Abstract…….....2
Table of contents……....4
List of figures and tables……6
Acknowledgments……10
List of papers……11
Conclusions …….....141

1. INTRODUCTION……14
1.1 Green chemistry and Circular economy……15
1.2 Chemistry of renewable biopolymers…….....16
1.2.1 Lignin properties and applications……...…17
References……21

2. BIONANOTECHNOLOGY APPLICATIONS OF LIGNIN……23
2.1.Innovative bio-nanotechnology……...24
2.2.Lignin nanoparticles……24
2.2.1 Lignin nanoparticles valorisation and applications……..26
2.2.2 Lignin nanoparticles functionalisation ……27
2.2.3 Lignin nanoparticles as functional supports for enzyme immobilization…….29
2.2.4 Multienzymes cascade immobilization……30
References……..32

3. ADVANCED MATERIAL APPLICATIONS OF LIGNIN NANOPARTICLES: THE BIOPLASTIC CASE……..36
3.1.Nanoparticles of Lignins and Saccharides from Fishery Wastes as Sustainable UV-Shielding, Antioxidant, and Antimicrobial Bio-fillers
3.1.1 Aim of work……37
3.1.2 Experimental part……38
3.1.3 Results and discussions……...41
References……50

4. COSMECEUTICAL APPLICATIONS OF LIGNIN NANOPARTICLES…… 53
4.1.Nano-Structured Lignin as Green Antioxidant and UV Shielding Ingredient for Sunscreen Applications (Review)……..54
4.1.1 Aim of work……...54
4.1.2 Results and discussions……..56

4.2. Lignin Nanoparticles as Sustainable Photoprotective Carriers for Sunscreen Filters……66
4.2.1 Aim of work……66
4.2.2 Experimental part……68
4.2.3 Results and discussions……....70

4.3. Biosynthesis of Novel Ascorbic Acid Esters and Their Encapsulation in Lignin Nanoparticles as Carriers and Stabilizing Systems……...76
4.3.1 Aim of work……..76
4.3.2 Experimental part……..77
4.3.3 Results and discussions……81
References……...88

5. MULTIENZYME CASCADE APPLICATION OF LIGNIN NANOPARTICLES……97
5.1. Lignin Nanoparticles Support Lipase-Tyrosinase Enzymatic Cascade in the Synthesis of Lipophilic Hydroxytyrosol Ester Derivatives……98
5.1.1 Aim of work……..98
5.1.2 Experimental part……..99
5.1.3 Results and discussions……103

5.2. Synthesis of Bioactive Hydroxytyrosol Esters via Multienzyme Cascade on Electroactive Melanin Lignin Nanoparticles: A One-Pot Approach without Extra Reducing Agents……...113
5.2.1 Aim of work……113
5.2.2 Experimental part……114
5.2.3 Results and discussions……117

5.3. Synthesis of benzoxazines by heterogeneous multicomponent bio-chemo multienzymes cascade reaction……125
5.3.1 Aim of work……125
5.3.2 Experimental part……126
5.3.3 Results and discussions……131
References……..135

6. CONCLUSIONS……141

List of figures and tables

Figure 1.1. Convergence of Circular economy and Green chemistry

Table 1 Summary of chemical structures and advantages of various biopolymers

Figure 1.2 (A). Cross-section of a wood trunk. (**B).** A multi-layer structure wraps around the plant cell cytoplasm (the lumen), starting with the plasma membrane, developing with three layers (S1-S2-S3) of lignin-rich secondary cell walls and ending with the more external primary walls that are surrounded by the pectin-rich middle lamella, which also provides connection to adjacent cells. (**C**) cellulose microfibrils (MF, gray rods) embedded in a matrix of hemicelluloses (in orange), pectin (in green, only present in the primary walls) and lignin microparticles (lignin–carbohydrate complexes, LCC).

Figure 1.3 In the upper part, the lignin biosynthetic pathway. In the bottom part, the major structural unit in the polymer and the structure of lignin.

Figure 1.4 Main properties of common technical lignin.

Figure 2.1 a) The layers of nanoparticles**. b)** Types of nanoparticles.

Figure 2.2. Representation of the different shapes of LNPs.

Figure 2.3. LNPs preparation methods.

Figure 2.4 Different applications of LNPs.

Figure 2.5 a) Main chemical interactions between lignin nanoparticles and proteins; **b)** General methods for loading and releasing active substances from various lignin-based particulate and capsule carriers.

Figure 2.6. Five chemical approaches to construct multienzymatic complex.

Figure 3.1 Schematic representation of the nanoprecipitation for the preparation of mixed lignin nanoparticles bearing chitosan (CH/LNPs) and chito-oligosaccharides (COS/OLNPs). Panel A: dissolution of Kraft lignin in THF (the upper part) and Organosolv lignin (bottom part). Panel B: dissolution of CH and COS in acetic acid (upper part) and in deionized water (bottom part), respectively. Panel C: nanoprecipitation procedure at two different times (few seconds). Panel D: CH/KLNPs and CH/OLNPs obtained after freeze-dry.

Figure 3.2. Pictures of CH/KLNPs (Panel A) and CH/OLNPs (Panel B) obtained from the nanoprecipitation process and classified depending on the CH type. Samples 1 and 8: commercial medium molecular weight CH. Samples 2 and 9: commercial low molecular weight CH. Samples 2 and 9: commercial low molecular weight CH. Samples 3 and 10: commercial shrimp CH. Samples 4 and 11: CH from fishery waste with 57-80% de-acetylation degree. Samples 5 and 12: CH from fishery waste with 57%-70% de-acetylation degree. Samples 6 and 13: CH from fishery waste with 64% de-acetylation degree. Samples 7 and 14: CH from fishery waste with 30% de-acetylation degree.

Table 2 Yield, ratio of components, melting point and DPPH scavenging activity (IC_{50}, µg/mL) of CH/KLNPs, CH/OLNPs and COS/OLNPs.

Figure 3.3. FT-IR spectra of CH/OLNPs. Panel A: CH/OLNPs bearing CH with high DD value. Panel B: CH/OLNPs bearing CH with low DD value.

Figure 3.4. SEM images of CH/OLNPs and COS/OLNPs. Panel A: CH/OLNPs bearing CH with high DD (CH5/OLNPs and CH1/OLNPs) and low DD (CH4/OLNPs), respectively. Panel B: COS/OLNPs bearing COS with high DD (COS3/OLNPs and COS5/OLNPs) and low DD (COS9/OLNPs and COS10/OLNPs), respectively.

Table 3 DLS and z-potential of CH/OLNPs and COS/OLNPs.

Table 4 Determination of synergistic or additive antioxidant effect of lignin and saccharide for COS/OLNPs.

Figure 3.5. UV-absorbing capacity of CH/OLNPs and COS/OLNPs. Panel A: CH/OLNPs. Panel B: COS/OLNPs characterized by high MW saccharides. Panel C: COS/OLNPs characterized by low MW saccharides.

Figure 3.6. Antibacterial activity of COS1-10/OLNPs. Panel A: doubling time for the referred Gram-negative and Gram-positive bacteria. Panel B: minimum inhibitory concentration (MIC50) of COS1/OLNPs, COS2/OLNPs, COS4/OLNPs, COS5/OLNPs and COS7/OLNPs evaluated against E. coli and S. aureus. All the data included the standard error of the mean of three independent assays.

Figure 4.1. Schematic representation of photodegradation processes operative in the case of avobenzone (AVOB) (**A**) and octyl methoxycinnamate (OCM) (**B**).

Table 5. Toxic effects of some of the most representative OCFs applied in sunscreen formulations.

Table 6. Cosmetic and cosmeceutical application of lignin**.**

Figure 4.2. Chemical structure of the main components in lignin. (A) Monolignols; (B) representation of the main type of inter-units in lignin.

Table 7. Classification of different types of lignin depending on the amount of para-hydroxyphenyl (H), guaiacyl (G), and syringyl (S) sub-units.

Table 8. Major technologies available for the production of LNPs.

Figure 4.3. Classification and structural representation of lignin sub-units with antioxidant activity and chromophoric groups.

Table 9. Antioxidant activity comparison of main lignin subunit.

Figure 4.4. UV-VIS assay to evidence of bathochromic effect of organosolv lignin nanoparticles (OLNPs; green line) after the nanostructuration of starting technical organosolv lignin (OL; red line).

Figure 4.5. Photodegradation pathway of 1 (panel A) and 5 (panel B) after UV irradiation. (i) Z/E isomerization process; (ii) side chain cleavage; and (iii) [2 + 2]π cycloaddition.

Scheme 4.1. General Procedure for the Preparation and Characterization of Loaded LNPs.

Table 10. Encapsulation Parameters, Hydrodynamic Diameter, ζ-Potential, and Polydispersive Index of LNPs-1, LNPs-5, LNPs-1/5, LNPs-1/10, and LNPs-5/10.

Figure 4.6. Results of (top) FESEM analysis of LNPs-1 (panel A), LNPs-5 (panel B), and LNPs-1/5 (panel C) and (bottom) DLS analysis.

Figure 4.7. SAXS profiles of LNP samples. (A) The intensity vs q data in a double logarithmic scale are shown as colored dots and lines (LNPs, red; LNPs-1, green; LNPs-5, blue; and LNPs-1/5, purple), while the model function of the Porod law decay (c/q4, with $c = 3.2 \times 10^{-4}$ cm^{-1} nm^{-4}, reference slope indicated as dotted gray line) and the Guinier contribution (I(0)exp(−Rg2q2/3) with $I(0) = 8 \times 10^{-3}$ cm^{-1} and Rg = 1.33 nm) with a flat background (3×10^{-3} cm^{-1}) are shown as a solid black line. The latter contribution is also reported as a dashed black line. The most evident diffraction peak position is indicated. (B) The wider-angle scattering region presenting the diffraction peaks for samples LNPs-1 and LNPs-1/5 ($q > nm^{-1}$) is highlighted by plotting data as a function of 2θ rather than q. The data are vertically shifted on the intensity scale for better visualization and the peak positions are indicated by dotted gray lines.

Figure 4.8. In vitro UV–vis absorbance of aqueous suspensions of LNPs-1 (panel A), LNPs-5 (panel B), and LNPs-5/10 (panel C).

Figure 4.9. DPPH scavenging activity of loaded lignin nanoparticles presented as % of DPPH radical inhibitions and IC50 values (μg/mL).

Figure 4.10. Photostability evaluation of loaded LNPs compared to the corresponding dissolved SSF.

Scheme 4.2. Degradation pathway of AA. AA: ascorbic acid; L-XY: L-xylosone, 2-AF: 2-furanoic acid; DHA: dehydroascorbic acid; DKG: di-ketogulonic acid; FU: furfural. The numbering of the carbon atoms of ascorbic acid is highlighted by the red numbers.

Figure 4.11. Schematic representation of preparation steps of **biocatalyst I**.

Table 11. Kinetic parameters of **biocatalyst I**.

Scheme 4.3. Synthesis of 3-O-ethyl ascorbic acid esters 4 and 5 by using biocatalyst I in 2-MeTHF.

Figure 4.12. Schematic representation of the encapsulation protocol of esters 4 and 5. DMI: dimethyl isosorbide; AA: ascorbic acid; DLS: dynamic light scattering; SEM: scanning electron microscopy.

Table 12. Efficiency of loading of ascorbic acid esters and other AA derivatives into LNPs.

Table 13. Morphology and size characterization of loaded LNPs.

Figure 4.13 Panel (A) Release profile of esters 4 and 5 at selected pH values (pH 3.0 and pH 5.4). Panel (B) Zero-order, first-order, Higuchi and Korsmeyerñ–Peppas kinetic models for the release of esters 4 and 5 at pH 3.0.

Table 14. The antioxidant activity was expressed in IC_{50} values (μg/mL).

Figure 4.14. Evaluation of stability of AA derivatives under selected pH and temperature conditions.

Scheme 5.1. Schematic representation of Catalyst I and Catalyst II. Random immobilization (pathway A); Oriented co-immobilization (pathway B).

Figure 5.1. Field emission scanning electron microscopy (FE-SEM) images of **Catalyst I** (panel A) and **Catalyst II** (panel B). Panel C−D: magnification (x800k) of **Catalyst I** and Catalyst II, respectively.

Table 15. DLS and ζ-potential of OLNPs/CH and OLNPs/CH/Con A intermediates and **Catalyst I–II**.

Figure 5.2. FT-IR spectra of **Catalyst I** (red line) and **Catalyst II** (blue line). The FT-IR spectra of free MJL (green line) and Ty (purple line) are reported as reference.

Table 16. Immobilization and activity parameters of **Catalyst I** and **Catalyst II**.[a]

Table 17. Kinetic parameters of **Catalyst I** and **Catalyst II**.[a]

Figure 5.3. Laser confocal scanning microscopy of **Catalyst I–II**. Panel a: MJL labelled with FITC in the donor channel at 490 nm (green pixels) of **Catalyst I**. Panel b: Ty labelled with Rho B in the acceptor channel at 560 nm (red pixels) of **Catalyst I**. Panel c: FRET channel of merged fluorescence effect of **Catalyst I**. Panel d: original FRET signal of **Catalyst I**. PANEL e-h: donor, acceptor, FRET and original FRET channels respectively of **Catalyst II**.

Scheme 5.2. Synthesis of tyrosol oleate **5** by reaction of tyrosol **1** and oleic acid **2** in the presence of Catalyst I and **Catalyst II**. The tyrosinase activity of **Catalyst I** and **Catalyst II** was inhibited by performing the reaction under argon atmosphere.

Table 18. Synthesis of tyrosol oleate **5** from tyrosol **1** and oleic acid **2** in the presence of **Catalyst I** and **Catalyst II**.[a]

Scheme 5.3. Synthesis of hydroxytyrosol esters **8–10** from tyrosol 1 and carboxylic acids **2–4** in the presence of **Catalyst I** and **Catalyst II**. The reaction was performed under dioxygen atmosphere to activate also tyrosinase.

Table 19. Synthesis of lipophilic hydroxytyrosol esters **8–10** from 1 by **Catalyst I** and **Catalyst II**[a]

Scheme 5.4. Synthesis of hybrid melanin-lignin nanoparticles. Pathway A: preparation of EHLNPs/EM. Pathway B: preparation of EHLNPs/PM.

Table 20. Yields, HOMO-LUMO energy gap values and electrochemical parameters of EHLNPs/EM and EHLNPs/PM by using EHLNPs as reference.

Figure 5.4. FTIR spectra of hybrid melanin lignin nanoparticles. Panel (A): EHLNPs/EM, green line. Panel (B) EHLNPs/PM, green line. EHLNPs orange line.

Figure 5.5. FE-SEM images of hybrid melanin lignin nanoparticles. Panel (A): EHLNPs/EM. Panel (B) EHLNPs/PM.

Figure 5.6. CVs of EHLNPs/EM (red line), EHLNPs/PM (blue line) and EHLNPs (green line). Redox probe: 5 mM $[Fe(CN)_6]3^-/4^-$ containing 0.1 M KCl. Scan rate: 25 mV/s.

Table 21. Immobilization and activity parameters of EHLNPs/EM/Con A/Ty, EHLNPs/PM/Con A/Ty and EHLNPs/Con A/Ty.

Scheme 5.5. Preparation of **Catalyst I–III**.

Table 22. Activity parameters of **Catalyst I–III**.

Table 23. Synthesis of lipophilic hydroxytyrosol esters.

Scheme 5.6. Heterogeneous multi-component bio-chemo multienzymes cascade synthesis of 2(H)-benzo-1,4-oxazin-2-one 1,4-benzoxazine **6a** and catechol **5a**.

Scheme 5.7. Proposed reaction pathway for the synthesis of 2(H)-benzo-1,4-oxazin-2-one **6a** and catechol derivative **5a** from the ternary mixture of compounds **1**, 2a and **3a**.

Table 24. Synthesis of 1,4-benzoxazine derivatives by NOL/LT.

Figure 5.7 Heterogeneous multicomponent bio-chemo multienzymes cascade synthesis of catechols **8a-c** from the ternary mixture of compounds **1**, **2a** and **7a-c**. The yield was evaluated on the basis of mmol of the recovered product. Traces amount of tyrosol octanoate **4a** (1-2%) were detected in the reaction mixture**.**

Acknowledgments

Ringrazio il mio tutor, il prof. Saladino, per il sostegno, la fiducia e i consigli dati in tutti i miei progetti, essendo così un aiuto fondamentale per continuare a credere nelle mie capacità e non mollare nemmeno nelle piccole sconfitte.
Ringrazio tutto il gruppo di laboratorio, in particolare Bruno, Lorenzo e Davide, che in questi anni mi hanno sempre consigliata e ognuno a proprio modo mi ha insegnata a crescere.
Un ringraziamento ad Eliana, per avermi sempre spronata e creduto in me, nelle mie capacità e nella mia voglia di imparare.
Un grazie di cuore va a Valeria per aver condiviso, anche se a distanza, questo lungo percorso insieme, tra gioie e dolori, supportandomi in ogni scelta.
Un grazie importante va a tutti i miei amici, lontani e vicini che ci sono sempre stati e hanno sempre creduto in me e nelle mie scelte.
Un grazie speciale va alle amiche di una vita, Laura, Veronika e Serafina, che nonostante la lontananza sono sempre state presenti non facendomi mai sentire sola.
Un grazie molto importante va ad Alessio, che mi sostiene con il suo amore in tutte le mie scelte e i miei traguardi.
Il ringraziamento più grande e importante va ai miei genitori, perché se sono qui e ho raggiunto questo importante traguardo della mia vita è solo grazie a loro e ai loro sacrifici e che nonostante la lontananza non mi hanno mai fatto mancare nulla.
Infine, ringrazio me stessa, che nonostante le difficoltà, gli sconforti e le sconfitte, non ho mai mollato, avendo sempre fiducia in quello che faccio.

List of papers

- Tomaino E., Capecchi E., Ubertini V., Piccinino D., Bizzarri B. M., Saladino R. Synthesis of benzoxazines by heterogeneous multicomponent bio-chemo multienzymes cascade reaction. **2023**, https://doi.org/10.1021/acs.joc.3c02314.

- Piccinino D., Ubertini V., Capecchi E., Tomaino E., Gigli V., Saladino R. Synthesis of Bioactive Hydroxytyrosol Esters via Multienzyme Cascade on Electroactive Melanin Lignin Nanoparticles: A One-Pot Approach without Extra Reducing Agents. ChemCatChem **2023**, e202300533. https://doi.org/10.1002/cctc.202300533

- Capecchi E., Piccinino D., Nascimben C., Tomaino E., Ceccotti Vlas N., Gabbellone S., Saladino R. Biosynthesis of Novel Ascorbic Acid Esters and Their Encapsulation in Lignin Nanoparticles as Carriers and Stabilizing Systems. Int. J. Mol. Sci. **2023**, 24(10), 9044. https://doi.org/10.3390/ijms24109044

- Piccinino D., Capecchi E., Trifero V., Tomaino E., Marconi C., Del Giudice A., Galantini L., Poponi S., Ruggieri A., Saladino R. Lignin Nanoparticles as Sustainable Photoprotective Carriers for Sunscreen Filters. ACS Omega **2022**, 7, 42, 37070–37077. https://doi.org/10.1021/acsomega.2c02133

- Capecchi E., Tomaino E., Piccinino D., Kidibule P. E., Fernandez-Lobato M., Spinelli D., Pogni R., Cabado A., Lago J., Saladino R. Nanoparticles of lignin and saccharides from fishery wastes as sustainable UV-shielding, antioxidant and antimicrobial bio-fillers. Biomacromolecules, **2022**, 00236a. https://doi.org/10.1021/acs.biomac.2c00236

- Tomaino E., Capecchi E., Piccinino D., Saladino R. Lignin nanoparticles support lipase-tyrosinase enzymatic cascade in the synthesis of lipophilic hydroxytyrosol ester derivatives. ChemCatChem, **2022**, e202200380. https://doi.org/10.1002/cctc.202200380

- Piccinino D., Capecchi E., Tomaino E., Gabellone S., Gigli V., Avitabile D., Saladino R. Nano-structured lignin as green antioxidant and UV shielding ingredient for sunscreen applications. Antioxidants, **2021**,10, 274. https://doi.org/10.3390/antiox10020274

- Capecchi E., Piccinino D., Tomaino E., Bizzarri B. M., Polli F., Antiochia R., Mazzei F., Saladino R. Lignin nanoparticles are renewable and functional platforms for the concanavalin a oriented immobilization of glucose oxidase–peroxidase in cascade bio-sensing. RSC Adv., **2020**, 10, 29031. DOI https://doi.org/10.1039/D0RA04485G

Patent

- Eliana Capecchi, Elisabetta Tomaino, Davide Piccinino, Rebecca Pogni, Daniele Spinelli, Stefano Poponi, Alessandro Ruggeri, Raffaele Saladino. Preparazione di particelle composite di lignina e chitosano con attività antiossidante e UV-schermante e loro applicazione nel campo delle bioplastiche. Febbraio 2022. ID: 102022000002792.

- Davide Piccinino, Capecchi Eliana, Elisabetta Tomaino, Daniele Avitabile, Stefano Poponi, Alessandro Ruggeri, Raffaele Saladino. Micro- e nano- particelle fotostabili di lignina contenenti filtri chimici UV e sostanze antiossidanti e loro uso in campo cosmetico e cosmeceutico. Marzo 2022, ID: 102022000004040.

European Research projects

- 2020-2022- European project: FISH chitinolytic biowastes FOR FISH active and sustainable packaging material' (**FISH 4 FISH**).

CHAPTER 1

INTRODUCTION

1.1 Green chemistry and Circular economy

The convergence of green chemistry and circular economy represents a fundamental paradigm in the development of sustainability and environmental protection. Green chemistry's steadfast commitment to developing chemical processes and products that minimize harm to ecosystems and human health[1] providing robust pillars for the circular economy strategy and optimizing resource efficiency.[2](**Figure 1.1)**

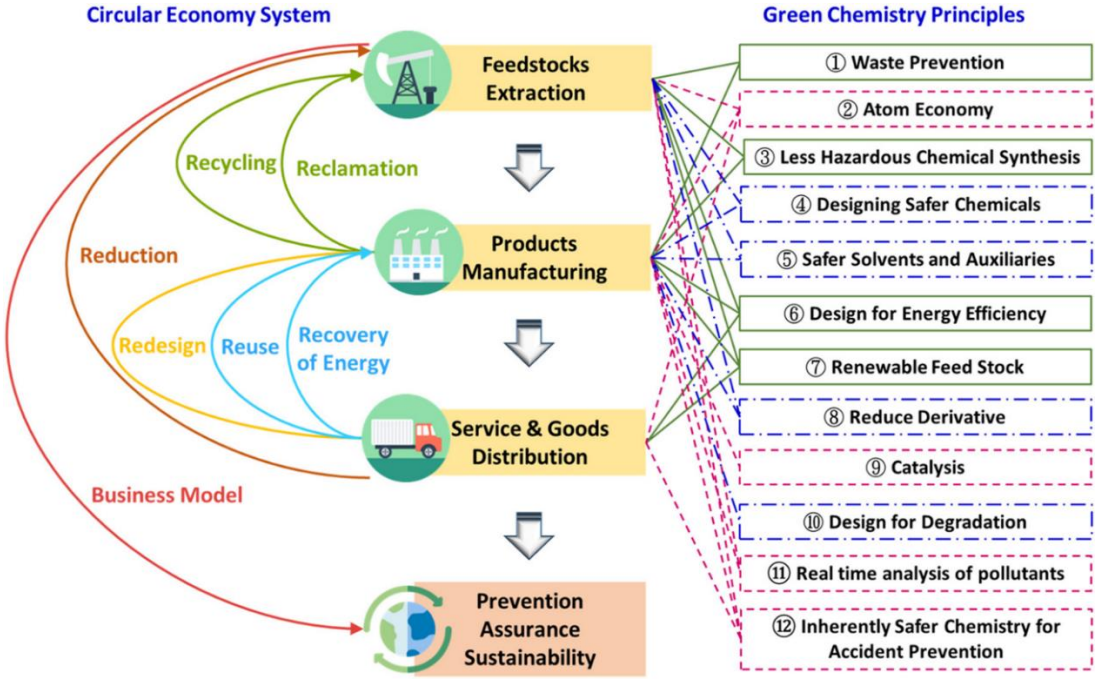


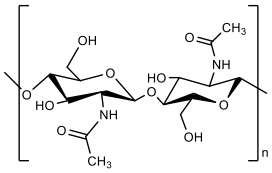
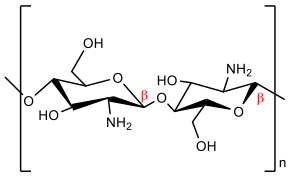
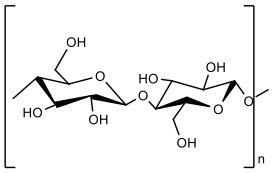
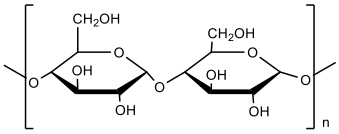
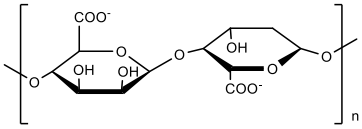
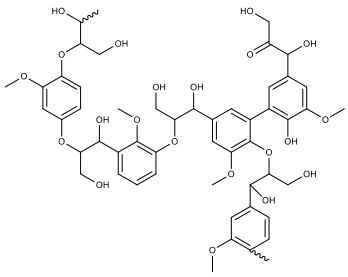
Figure 1.1. Convergence of Circular economy and Green chemistry.

The 12 fundamental principles of green chemistry[3] work as a reference for the design of novel materials and manufacturing processes, exerting far-reaching implications not only for human well-being and environmental preservation, but also for the lifecycle of products.[1,4] Recently, green chemistry has been associated to circular economy, moving away from the traditional linear economy model[5] which is characterized by a take-produce-dispose approach,[6] with generation of significant amount of wastes.[7] In addition, linear economy is responsible for the uncontrolled use of non-renewable resources like fossil fuels.[1] In contrast, circular economy approach emphasizes the principles of reuse, recycling, and resource efficiency,[8,9] by developing closed-loop production systems able to optimize resource utilization, thereby reducing waste and pollution.[1]
Thus, the association between green chemistry and circular economy furnish a potent tool for the design of ecologically friendly and economically sustainable processes at the global scale.

1.2 Chemistry of renewable biopolymers

The increasing focus on renewable biopolymers as a viable alternative to mitigate environmental pollution of materials deriving from conventional fossil fuels is highlighted by several industrial applications.[10] Renewable biopolymers include natural polyphenols such as lignin, alginate, cellulose, starch, chitin, and chitosan, derived from both industrial and domestic wastes provide environmental benefits including biodegradability, biocompatibility, non-toxicity, and cost-effectiveness,[11,12] and directly contribute to an increase in quality of life.[13-15] (**Table 1.2)**

Table 1. Summary of chemical structures and advantages of various biopolymers

Renewable biopolymers	Chemical structure	Advantages
Chitin		Non-toxic, biodegradability, abundance, and renewability
Chitosan		Natural cationic copolymer, excellent biocompatibility, low toxicity, biodegradability, and antibacterial activity
Cellulose		Biocompatibility, low density, non-toxic, low cost, biodegradable and renewable.
Starch		Non-toxic, biodegradability, abundance, and renewability.
Alginate		Biocompatible, easily functionalizable, good cell recognition, biocompatible.
Lignin		Inexpensive and renewable, high carbon content, biocompatible and renewable.

The concept of biorefinery has emerged as an appealing strategy, wherein biomass from wastes can be subjected to sustainable transformation in order to yield high-value added bioproducts.[16] For this reason, biorefineries are of pivotal relevance for circular economy.[17]
The intricate nature of biopolymers, governed by the complex molecular structure and functional properties, has paved the way for diverse commercial applications. However, the efficacy of these materials is strictly dependent from the origin, purification process, and processing methods.[18,19] Additionally, biopolymers serve as exceptional reservoirs of bioactive compounds, recognized for their well-established antioxidant and antimicrobial effects.[20] Among them, polyphenols are well recognized bioactive compounds that can be categorized into distinct classes of secondary metabolites, including flavonoids, phenolic acids, lignans, tannins, and stilbenes.[21]
Nowadays, great interest has been devoted on development of economically advantageous value-added polymers derived from lignocellulosic biomass wastes. Lignocellulosic biomass is primarily composed of cellulose microfibrils (45-60%), hemicellulose (35-25%) and lignin (15-2%).[22]
This latter demonstrated to be an environmentally and renewable benign building block for manufacturing innovative biomaterials.[22]

1.2.1 Lignin properties and applications

Lignin, the second most abundant natural polymer after cellulose, is a component of cell walls of vascular plants,[23] forming lignin-carbohydrate complexes (LCC) with cellulose and hemicellulose, a complex system that is of crucial importance for water and solute transport in the plant.[24,25] (**Figure 1.2**) Beyond its structural function, lignin plays key roles in supporting plant growth, acting as a defence barrier against microbial invasions, and mitigating environmental stress.[25]

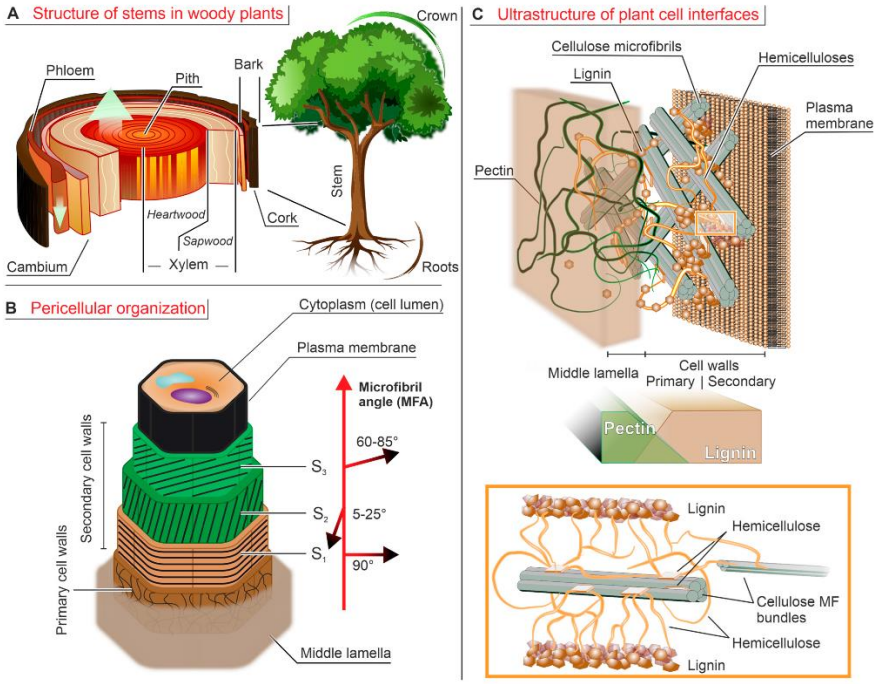


Figure 1.2 (A). Cross-section of a wood trunk. (**B).** A multi-layer structure wraps around the plant cell cytoplasm (the lumen), starting with the plasma membrane, developing with three layers (S1-S2-S3) of lignin-rich secondary cell walls and ending with the more external primary walls that are surrounded by the pectin-rich middle lamella, which also provides connection to adjacent cells. (**C**)

cellulose microfibrils (MF, gray rods) embedded in a matrix of hemicelluloses (in orange), pectin (in green, only present in the primary walls) and lignin microparticles (lignin–carbohydrate complexes, LCC).

Lignin is deprived of any ordered structure, being composed by different types of phenyl-propanoic units.[26]

The biosynthesis of lignin begins with the oxidative radical polymerization of three major monolignols: *p*-coumaryl alcohol (4-hydroxycinnamyl alcohol), coniferyl alcohol (3-methoxy-4-hydroxycinnamyl alcohol), and sinapyl alcohol (3,5-dimethoxy-4 alcohol), that are commonly referred as *p*-hydroxyphenyl (H), guaiacyl (G) and syringyl (S) units.[27,28] Monolignols have a common molecular motif and differ from each other for the substitution pattern on the aromatic moiety.[26] They are produced in the cell by the shikimate pathway, involving the deamination of phenylalanine and tyrosine by the action of phenylalanine ammonia lyase (PAL),[29,30] followed by cascade hydroxylation and *O*-methylation reactions, and reduction of the carboxylic acid group to alcohol.[31] During lignification, monolignols are transported from the cytoplasm to the apoplast[32] where laccases and peroxidases catalyse oxidative coupling processes, generating phenoxy radical intermediates.[33] By resonance, the radical are delocalized in different position of the molecule and coupling reactions at any of these positions lead to β-O-4, β-5, 5-5, β-1 and β-β sub-units.[34] The biosynthetic mechanism results in an heterogeneous polymer lacking regular and ordered repeating units, making it particularly recalcitrant and difficult to depolymerize. The composition and structure of lignin vary significantly on the basis of the natural source of lignocellulosic biomass. For example, hardwood predominantly comprises S and G units, softwood predominantly comprises G units, and grass contains small amounts of H.[35] **(Figure 1.3)**

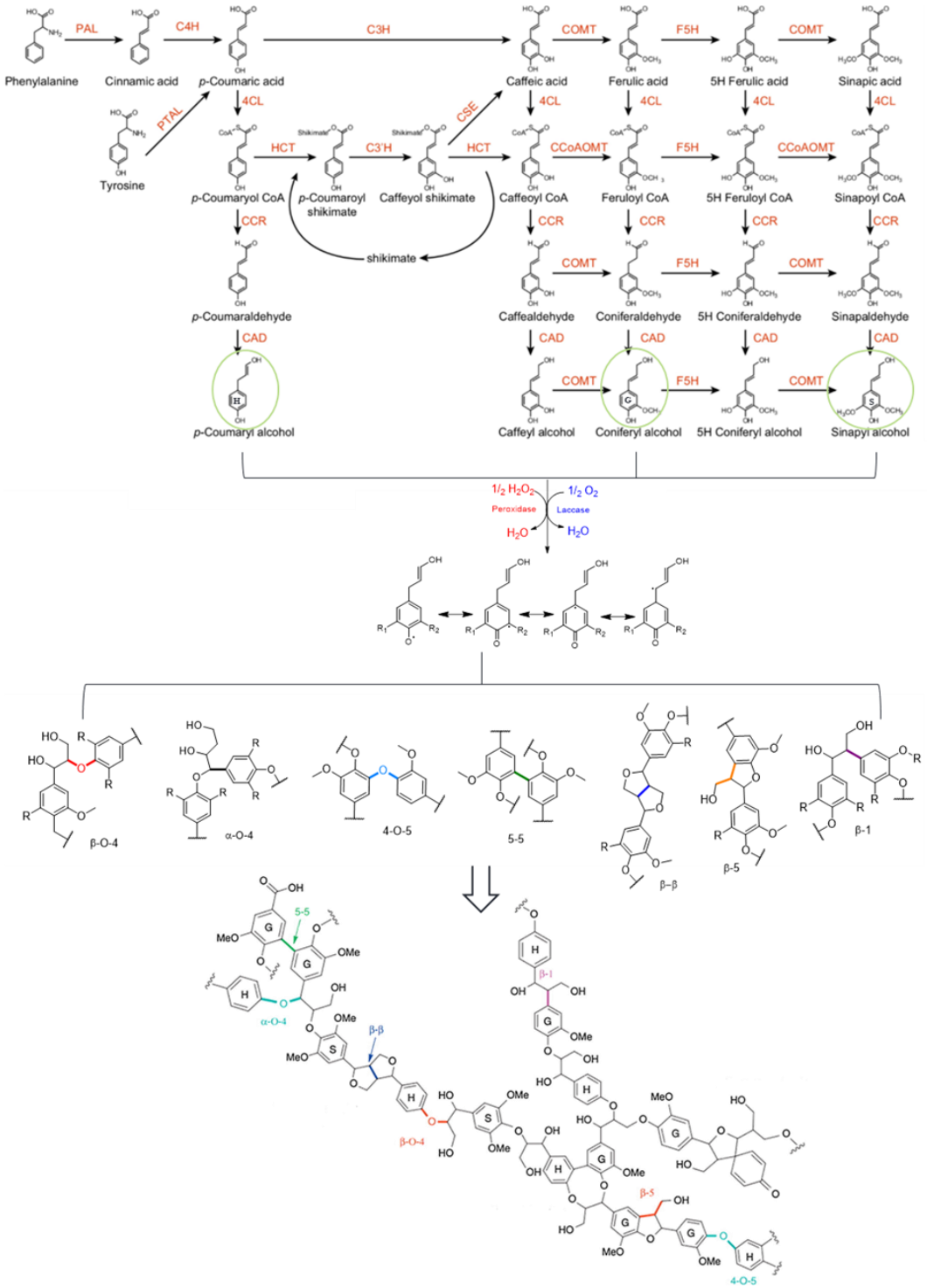


Figure 1.3. In the upper part, the lignin biosynthetic pathway. In the bottom part, the major structural unit in the polymer and the structure of lignin.

The properties of lignin, including colour, molecular weight, functional group content, and glass transition temperature (T*g*) are influenced by extraction source and process,[36] they encompass the production of Kraft lignin (containing sulfur), sulfonated lignin, soda lignin (sulfur-free, commonly extracted from grass), and organosolv lignin.[37] **(Figure 1.4)**

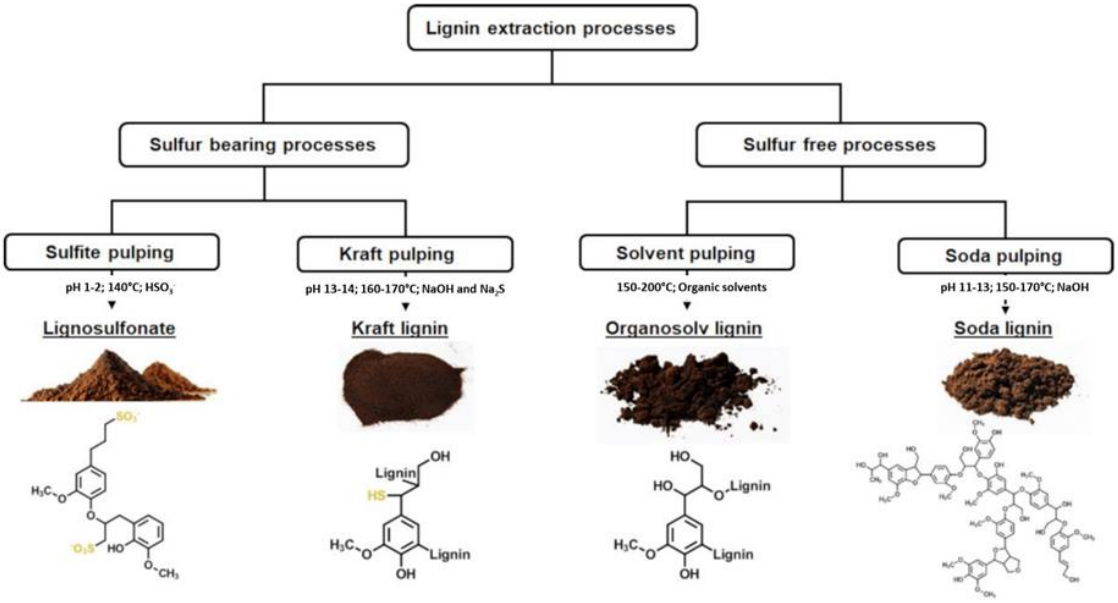


Figure 1.4 Main properties of common technical lignin.

In addition, lignin can be modified by the following procedures: (1) depolymerization or fragmentation; (2) production of graft copolymers; and (3) chemical modification of the structure.[38,39] these procedures involve the enhancement of the reactivity and efficiency by hydroxyalkylation, amination, nitration, sulfo-methylation, alkylation, esterification, ring-opening polymerization,[40] pyrolysis and hydrolysis.[41] Beyond its intrinsic properties, lignin emerges as a promising feedstock for high-value materials in various industries.[42] After these functionalization procedures lignin improve its versatility and sustainability,[26,43,44] associated with the improvement of specific chemical and physical properties, such as antioxidant properties[45] and electron transfer properties[46,47] useful in the design of UV screen and biosensors.[50,51] In addition to its roles in energy and materials, lignin emerges as a renewable alternative in the context of bioplastics[50] as well as for waste treatment.[51] This comprehensive exploration underscores the diverse applications and transformational potential of high-value lignin-derived materials across wide range of applications.

References

1- Ncube A., Mtetwa S., Bukhari M., Fiorentino G., Passaro R. Circular Economy and Green Chemistry: The Need for Radical Innovative Approaches in the Design for New Products. *Energies* **2023**, *16*, 1752.

2- Mancini E., Raggi A. A review of circularity and sustainability in anaerobic digestion processes. *Journal of Environmental Management* **2021,** 291,112695.

3- Anastas Paul T. Green Chemistry and the Role of Analytical Methodology Development. *Critical Reviews in Analytical Chemistry*, **1999,** 29:3, 167-175.

4- Mesa J. , González-Quiroga A., Maury H. Developing an indicator for material selection based on durability and environmental footprint: A Circular Economy perspective. *Resources, Conservation and Recycling* **2020,** 160, 104887.

5- Stahel W. R., and Reday G. The Potential for Substituting Manpower for Energy. *Research Contract* No. 76/l3-V. 343/78-EN, *Programme of Research and Actions on the Development of the Labour Market*, **1976.**

6- Morseletto, P. Sometimes linear, sometimes circular: States of the economy and transitions to the future. *Journal of Cleaner Production* **2023,** 136138.

7- Yang M., Chen L., Wang J., Msigwa G., Osman A. I., Fawzy S., DW Rooney Yap P. S. Circular economy strategies for combating climate change and other environmental issues. *Environmental Chemistry Letters* **2023,** 21(1), 55-80.

8- Walker A. M., Opferkuch K., Roos Lindgreen E., Raggi A., Simboli A., Vermeulen W. J., S Caeiro Salomone R. What is the relation between circular economy and sustainability? Answers from frontrunner companies engaged with circular economy practices. *Circular Economy and Sustainability* **2022,** 2(2), 731-758.

9- Stahel W. The circular economy. *Nature* **2016**, 531, 435–438.

10- Iravani S., S. Varma R. Greener synthesis of lignin nanoparticles and their applications. *Green Chem*istry **2020**, 22, 612-636.

11- Lai G., Liu X., Li S., Xu Y., Zheng Y., Guan J., Gao R., Wei Z., Wang Z., Cui S. Development of chemical admixtures for green and environmentally friendly concrete: A review. *Journal of Cleaner Production* **2023,** 389, 136116.

12- Zidanes U. L., das Chagas C.M., Lorenço M. S., da Silva Araujo E., Dias M. C., Setter C., Leite Braz R., Akira Mori F. Utilization of rice production residues as a reinforcing agent in bioadhesives based on polyphenols extracted from the bark of trees from the *Brazilian Cerrado* biome. *International Journal of Biological Macromolecules* **2024**, 254, 127813.

13- Wang X., Tarahomi M., Sheibani R., Xia C., Wang W. Progresses in lignin, cellulose, starch, chitosan, chitin, alginate, and gum/carbon nanotube (nano)composites for environmental applications: A review. *International Journal of Biological Macromolecules* **2023**, 24, 124472.

14- Kartik A., Akhil D., Lakshmi D., Gopinath K. P., Arun J., Sivaramakrishnan R., Pugazhendhi A. A critical review on production of biopolymers from algae biomass and their applications. *Bioresource Technology* **2021**, 329, 124868.

15- Culaba A. B., Mayol A. P., San Juan J. L. G., Ubando A. T., Bandala A. A., Concepcion II R. S., Alipio M., Chen W-H., Show P. L., Chang Jo-Shu. Design of biorefineries towards carbon neutrality: A critical review. *Bioresource Technology* **2023,** 369, 128256.

16- Duan Y., Tarafdar A., Kumar V., Ganeshan P., Rajendran K., Shekhar Giri B., Gomez-García R., Li H., Zhang Z., Sindhu R., Binod P., Pandey A., Taherzadeh M.J., Sarsaiya S., Jain A., Kumar Awasthi M. Sustainable biorefinery approaches towards circular economy for conversion of biowaste to value added materials and future perspectives. *Fuel* **2022,** 325, 124846.

17- Ortiz-Sanchez M., Solarte-Toro J. C., Inocencio-García P. J., Cardona Alzate C. A. Sustainability analysis of orange peel biorefineries. *Enzyme and Microbial Technology* **2024**, 172, 110327.

18- Moradali M.F., Rehm B.H.A. Bacterial biopolymers: from pathogenesis to advanced materials. *Nat Rev Microbiol* **2020**), 18, 195–210.

19- Ling S., Chen W., Fan Y., Zheng K., Jin K., Yu H., Buehler M. J., Kaplan D. L. Biopolymer nanofibrils: Structure, modelling, preparation, and applications. *Progress in Polymer Science* **2018,** 85, 1–56.

20- Boateng I. D., Clark K. Trends in extracting Agro-byproducts' phenolics using non-thermal technologies and their combinative effect: Mechanisms, potentials, drawbacks, and safety evaluation. *Food Chemistry* **2024**, 437, 1, 137841.

21- Lang Y., Gao N., Zang Z., Meng X., Lin Y., Yang S., Yang Y., Jin Z., Li B. Classification and antioxidant assays of polyphenols: a review. *Journal of Future Foods* **2024**, 4, 3, 193-204.

22- Mennani M., Kasbaji M., Benhamou A. A., Boussetta A., Kassab Z., El Achaby M., Grimi N., Moubarik A. The potential of lignin-functionalized metal catalysts - A systematic review. *Renewable and Sustainable Energy Reviews* **2024,** 189, 113936.

23- Lahive C. W., Kamer P. C. J., Lancefield C. S., Deuss P. J. An Introduction to Model Compounds of Lignin Linking Motifs; Synthesis and Selection Considerations for Reactivity Studies. *ChemSusChem* **2020**, 13, 17, 4238-4265.

24- Ragauskas A.J.; Beckham G.T.; Biddy M.J.; Chandra R.; Chen F.; Davis M.F., Davison B.H.; Dixon R.A.; Gilna P.; Keller M. Lignin valorization: Improving lignin processing in the biorefinery. *Science* **2014**, 344, 1246843.

25- Rinaldi R., Jastrzebski R., Clough M.T., Ralph J., Kennema M., Bruijnincx P.C., Weckhuysen B.M. Paving the way for lignin valorisation: recent advances in bioengineering, biorefining and catalysis. *Angewandte Chemie International Edition* **2016**, *55*(29), 8164-8215.

26- Ponnusamy V. K., Nguyen D. D., Dharmaraja J., Shobana S., Banu J. R., Saratale R. G., Chang S. W., Kumar G. A review on lignin structure, pretreatments, fermentation reactions and biorefinery potential. *Bioresource Technology* **2019,** 271, 462-472.
27- Boerjan W.; Ralph J.; Baucher M. Lignin biosynthesis. *Annu. Rev. Plant Biol*. **2003**, 54, 519– 546.
28- Ralph J.; Lundquist K.; Brunow G.; Lu F.; Kim H.; Schatz P. F.; Marita J. M.; Hatfield R. D.; Ralph S. A.; Christensen J. H.; Boerjan W. Lignins: natural polymers from oxidative coupling of 4-hydroxyphenylpropanoids. *Phytochem. Rev.* **2004**, 3, 29– 60.
29- Vanholme R., Demedts B., Morreel K., Ralph J., Boerjan W. Lignin biosynthesis and structure. *Plant Physiol*. **2010,** 153, 895–905.
30- Davin L. B. et al. Dissection of lignin macromolecular configuration and assembly: comparison to related biochemical processes in allyl/propenyl phenol and lignan biosynthesis. *Nat. Prod. Rep.* **2008,** 25, 1015–1090.
31- Vanholme R.; De Meester B.; Ralph J.; Boerjan W. Lignin biosynthesis and its integration into metabolism. *Curr. Opin. Biotechnol.* **2019**, 56, 230– 239.
32- Xin A.; Herburger K. Mini Review: Transport of Hydrophobic Polymers Into the Plant Apoplast. *Front. Plant Sci.* **2021**, 11, 590990.
33- del Río J. C., Rencoret J., Gutiérrez A., Elder T., Kim H., Ralph J. Lignin Monomers from beyond the Canonical Monolignol Biosynthetic Pathway: Another Brick in the Wall. *ACS Sustainable Chemistry & Engineering* **2020,** 8 (13), 4997-5012.
34- Balk M.; Sofia P.; Neffe A.T.; Tirelli N. Lignin, the Lignification Process, and Advanced, Lignin-Based Materials. *Int. J. Mol. Sci.* **2023**, 24, 11668.
35- Lourenço A.; Rencoret J.; Chemetova C.; Gominho J.; Gutierrez A.; del Río J. C.; Pereira H. Lignin composition and structure differs between xylem, phloem and phellem in Quercus suber L. *Front. Plant Sci.* **2016,** 7, 1612.
36- Zhang H., Fu S., Chen Y. Basic understanding of the colour distinction of lignin and the proper selection of lignin in color-depended utilizations. *International Journal of Biological Macromolecules* **2020**, 147, 607-615.
37- Tanis M.H.; Wallberg O.; Galbe M.; Al-Rudainy B. Lignin Extraction by Using Two-Step Fractionation: A Review. *Molecules* **2024**, 29, 98.
38- Figueiredo P., Lintinen K., Hirvonen J. T., Kostiainen M. A., Santos H. A. Properties and chemical modifications of lignin: Towards lignin-based nanomaterials for biomedical applications. *Prog. Mater. Sci.* **2018**, 93, 233.
39- Laurichesse S.; Avérous L. Chemical modification of lignins: Towards biobased polymers. *Prog. Polym. Sci.* **2014**, 39, 1266–1290.
40- Matyjaszewski K.; Tsarevsky N.V. Macromolecular engineering by atom transfer radical polymerization. J. Am. *Chem. Soc.* **2014**, 136, 6513–6533.
41- Pandey M.P.; Kim C.S. Lignin depolymerization and conversion: A review of thermochemical methods. *Chem. Eng. Technol.* **2011**, 34, 29–41.
42- Yao L., Yang H., Meng X., Ragauskas A. J. Toward a Fundamental Understanding of the Role of Lignin in the Biorefinery Process. *Front. Energy Res.* **2022**, 9, 804086.
43- Shuai L.; Amiri M. T.; Questell-Santiago Y. M.; Héroguel F.; Li Y.; Kim H.; Meilan R.; Chapple C.; Ralph J.; Luterbacher J. S. Formaldehyde stabilization facilitates lignin monomer production during biomass depolymerization. *Science* **2016**, 354, 329– 333.
44- Li Y.; Shuai L.; Kim H.; Motagamwala A. H.; Mobley J. K.; Yue F.; Tobimatsu Y.; Havkin-Frenkel D.; Chen F.; Dixon R. A.; Luterbacher J. S.; Dumesic J. A.; Ralph J. An "ideal lignin" facilitates full biomass utilization. *Sci. Adv.* **2018**, 4 (9), eaau2968.
45- Zhang Y., Naebe M. Lignin: A Review on Structure, Properties, and Applications as a Light-Colored UV Absorber. *ACS Sustainable Chemistry & Engineering* **2021,** 9(4), 1427–1442.
46- Förster H. UV/VIS Spectroscopy in Characterization I. *Mol.Sieves* **2004**, 4, 337−426.
47- Baloch M., Alberro M., Labidi J. Electrochemical Activity of Lignin Based Composite Membranes. *Polymers (*Basel) **2021**,13(4):643.
48- Durmaz E.; Sertkaya S.; Yilmaz H.; Olgun C.; Ozcelik O.; Tozluoglu A.; Candan Z. Lignocellulosic Bionanomaterials for Biosensor Applications. *Micromachines* **2023**, 14, 1450.
49- Frommhagen M., Mutte S. K., Westphal A. H., Koetsier M. J., Hinz S. W. A., Visser J., Vincken J. P., Weijers D., Van Berkel W. J. H., Gruppen H., M. A. Kabel, *Biotechnol. Biofuels* **2017**, 10, 1.
50- Yang J.; Ching Y.C.; Chuah C.H. Applications of Lignocellulosic Fibers and Lignin in Bioplastics: A Review. *Polymers* **2019**, 11, 751.
51- Vasić V.; Kukić D.; Šćiban M.; Đurišić-Mladenović N.; Velić N.; Pajin B.; Crespo J.; Farre M.; Šereš Z. Lignocellulose-Based Biosorbents for the Removal of Contaminants of Emerging Concern (CECs) from Water: A Review. *Water* **2023**, 15, 1853.

CHAPTER 2

BIO-NANOTECHNOLOGY APPLICATIONS OF LIGNIN

2.1 Innovative bio-nanotechnology

Bio-nanotechnology is based upon the exploitation of nano-sized materials (e.g., nanoparticles, nanotubes, nanomembranes, nanowires, nanofibers and so on) ranging from 1 to 1000 nm.[52-54]

The preparation of nanomaterials is driven by the pursuit of distinctive properties that emerge at nanoscale level.[55] This phenomenon can be attributed to the 'quantum effect,' which often make the characteristics of nanomaterials different from their macroscale counterpart. [56,57]

In general, organic and inorganic nanoparticles consist of three main levels:[58] (**Figure 2.1**)

a- Superficial layer, that can be functionalized with small molecules, ions and polymers.
b- Shell layer aimed stabilize the superficial layer.
c- The core, that can be functionalized with hydrophobic drugs (entrapment and drug delivery).

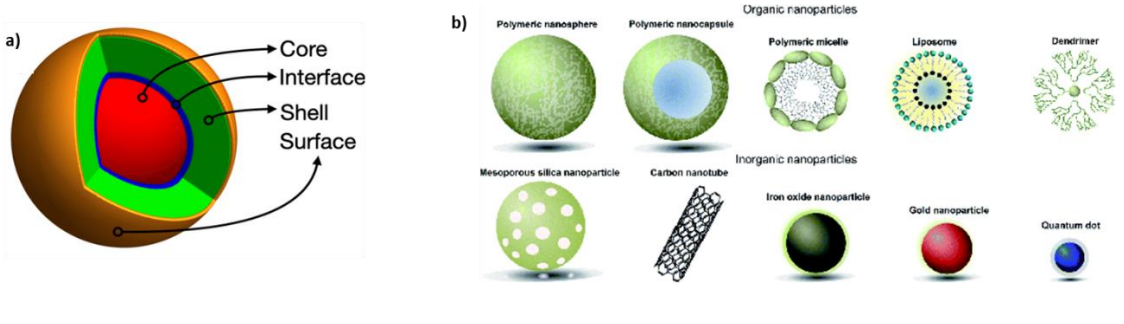


Figure 2.1 a) The layers of nanoparticles**. b)** Types of nanoparticles**.**

There are different type of nanodevices, they include nanoparticles (NPs) or nanowires, quantum dots (QDs), and nanotubes. These devices are characterized by electronic, optical, catalytic, semiconductor and magnetic properties, which make them applicable in various technological fields.[56,59] For instance, silver nanoparticles (AgNPs) have been applied in biomedical and industrial applications,[56] while gold nanoparticles (AuNPs) and titanium dioxide nanoparticles (TiO_2NPs) are employed in diagnostic tools and in the wastewater treatment. [60-62] In the medical fields, nanomaterials offer an efficient entry for drug delivery, offering an advantageous alternative to the side effects associated with conventional therapies (chemotherapy, radiotherapy, surgery).[63]

Despite their potential benefits, the preparation of nanoparticle is still expensive and, in principle, subject to produce by-products.[52] In this context, green and sustainable approaches represent a valuable alternative for design new biocompatible, biodegradable and cost-effective nanomaterials with increased biological properties, comprising electrochemical responsiveness, antioxidant and antimicrobial effects.[64-68]

2.2 Lignin nanoparticles

Lignin nanoparticles (LNPs) are environmentally friendly and cost-effective alternative to traditional organic materials and are characterized by improved chemical and physical properties compared to their native counterpart.[10,69,70]

In contrast to amorphous lignin, LNPs allow a specific organization of lignin side-chains, affording particle with tuneable shapes and dimensions.[38] Typically, LNPs show

dimensions ranging from 1 to 1000 nm[38] and exhibit a ζ–potential value less than -40mV attributed to the abundance of hydroxylic, carboxylic phenolic and aliphatic groups on the surface, imparting a negative superficial charge. The morphology of LNPs includes spheres,[69] clusters, nearly spherical structure,[71] aggregates,[69] hollow spheres, and cuboids or irregular shapes (**Figure 2.2**). The specific morphology is of paramount importance for the performance of LNPs.[72] For instance, irregularly shaped LNPs may compromise interactions with other materials,[73] while LNPs with defined spherical morphology may play a crucial role in stabilizing Pickering emulsions and find applications in biology, particularly as carriers for hydrophobic substances targeting specific cells.[74,72]

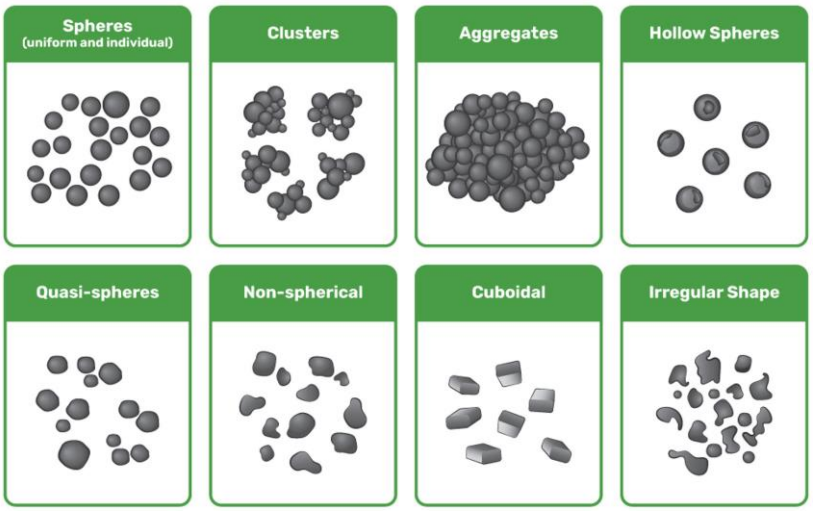


Figure 2.2. Representation of the different shapes of LNPs.

Various strategies, including physical and chemical methods (ultrasonication, dialysis, interfacial crosslinking and nanoprecipitation with antisolvent) are useful for the synthesis of LNPs with tuneable properties, such as porosity and hydrophobicity (**Figure 2.3**)[38,74] Among them, nanoprecipitation with antisolvent has proven to be the most effective approach for the production of large amount of LNPs with regular spherical shape.[75] In this latter case, lignin is solubilized in an appropriate organic solvent (DMSO, THF, or ethanol) and then poured into water to yield aggregation, instantaneously. The resulting LNPs exhibit uniform dimensions, smooth surfaces, and regular spherical shape. These properties are crucial for achieving high colloidal stability.[76,73]

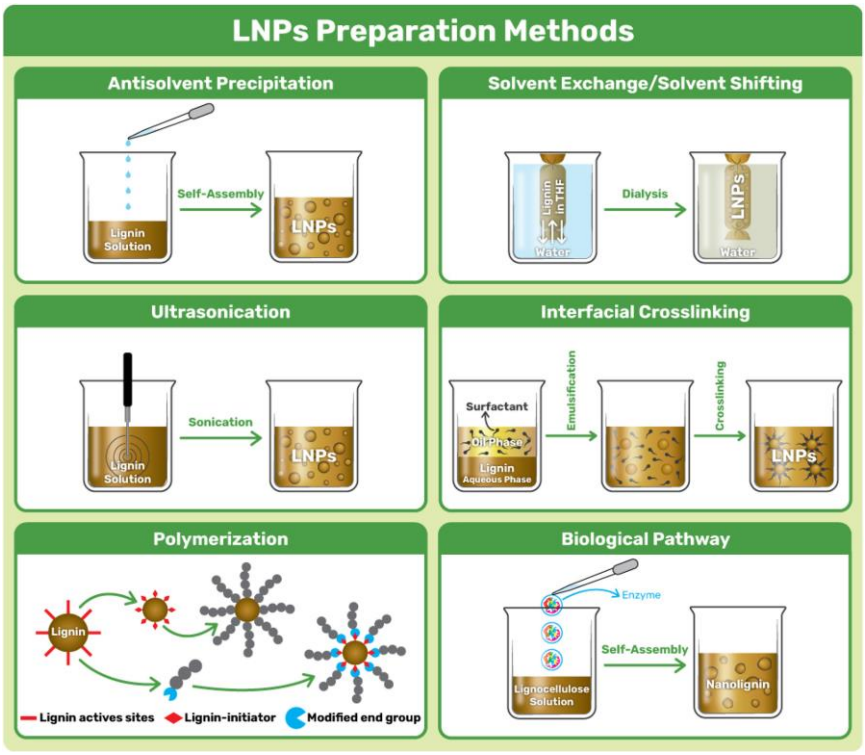


Figure 2.3. LNPs preparation methods.

The nanoprecipitation protocol is driven by non-covalent forces, including hydrogen bonds, hydrophobic interactions and π-π stacking interactions, which are influenced by the nature of the organic solvent and lignin source.[77] The π-π stacking interactions, that control the disposition of aromatic groups,[71] impact the charge transfer processes and the spectral properties,[78] leading to H-type and J-type aggregations based on the inclination angle between the molecular axis connecting the chromophore and its dipole moment.[79] In particular, when the value of the angle is lower than 54,7°C, the aromatic groups produce J-type aggregates characterized by bathochromic shift ('redshift' of UV spectra and fluorescent). The 'redshift' favours the occurrence of electron and charge transfer processes[80,81] providing new redox properties. When the angle is higher than 54,7°C, the aromatic groups make H-type aggregates that have a hypsochromic shift towards the M band.[82]

Overall, the characterization of LNPs involves the determination of the average particle size (z-average), polydispersity index (PDI), ζ-potential representing the superficial charge, static light scattering (SLS), dynamic light scattering (DLS), and morphological characterization, mainly acquired by scanning electron microscopy (SEM), transmission electron microscopy (TEM) and atomic force microscopy (ATM).[76]

Researchers have observed that the conversion of lignin into nanoparticles enhances homogeneity, dispersibility, surface area, antioxidant activity and permeability.[83]

2.2.1 Lignin nanoparticles valorisation and applications

Lignin nanoparticles are versatile platforms for the development of functional nano-biomaterials, offering a structural and morphological control of lignin at nanoscale level.[84] The distinctive chemical composition of LNPs controls a range of functionalities,

encompassing ultraviolet (UV) protection,[85] antioxidant properties, antimicrobial activity,[86] biocompatibility,[87] and pollution-absorbing capabilities.[88,89] (**Figure 2.4**)

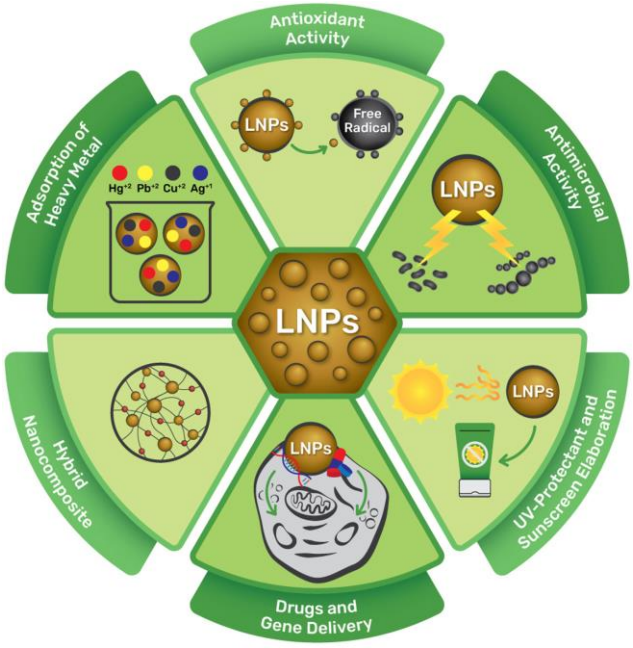


Figure 2.4 Different applications of LNPs.

Consequently, LNPs hold significant promise for applications in cosmetics,[90] drug delivery,[91] and pollution treatment.[92] Owing to their hydrophobic core (involving the hydrophobic functional groups), and their hydrophilic shell (derived from the hydrophilic functional groups), LNPs emerge as a promising biocompatible tool for drug delivery in environments characterized by high polarity, such as water.[93,38] In the field of biomedicine, LNPs can diffuse through biological membranes.[94] Numerous investigations have been undertaken to assess the biocompatibility of lignin nanoparticles across various cell lines, including murine macrophages,[95] human breast adenocarcinoma (MCF-7), and human alveolar epithelial adenocarcinoma (A549). Notably, irrespective to the nature of cell-line, LNPs showed high biocompatibility.[96]
In addition, the in vivo genotoxic effects of lignin nanoparticles have been analysed through viability and phenotypic analyses conducted on *Drosophila melanogaster* larvae and adults. The outcomes of these tests revealed absence of genotoxicity, thereby reinforcing the favourable biocompatible profile of LNPs in the context of *in vivo* systems.[96]

2.2.2 Lignin nanoparticles functionalization

The functionalization of LNPs could improve technological applications. Whitin this context, the adsorption of water-soluble polymers,[97] proteins[98] and other biopolymers on the surface of LNPs provides useful hybrid nanomaterials.[98,99] The interactions between the lignin surface and proteins are influenced by the linear form of peptides and the 3D-folding of proteins.[100] Notably, the interactions between lignin and linear peptides is influenced by the nature of the amino acids in the peptide sequence.[101] Peptides containing histidine, phenylalanine, proline and serine residues showed the highest affinity with LNPs surface. More complex 3D-folding structures of proteins can impact

on the adsorption of proteins on lignin nanoparticles.[98] In this case, the principal interactions identified between lignin and proteins include coulombic forces and hydrogen bonds.[102] Additionally, hydrophobic forces play a crucial role in enhancing protein adsorption on the lignin surface through π-π interaction between the aromatic portion of lignin and the hydrophobic and aromatic side-chains of proteins. (**Figure 2.5**)

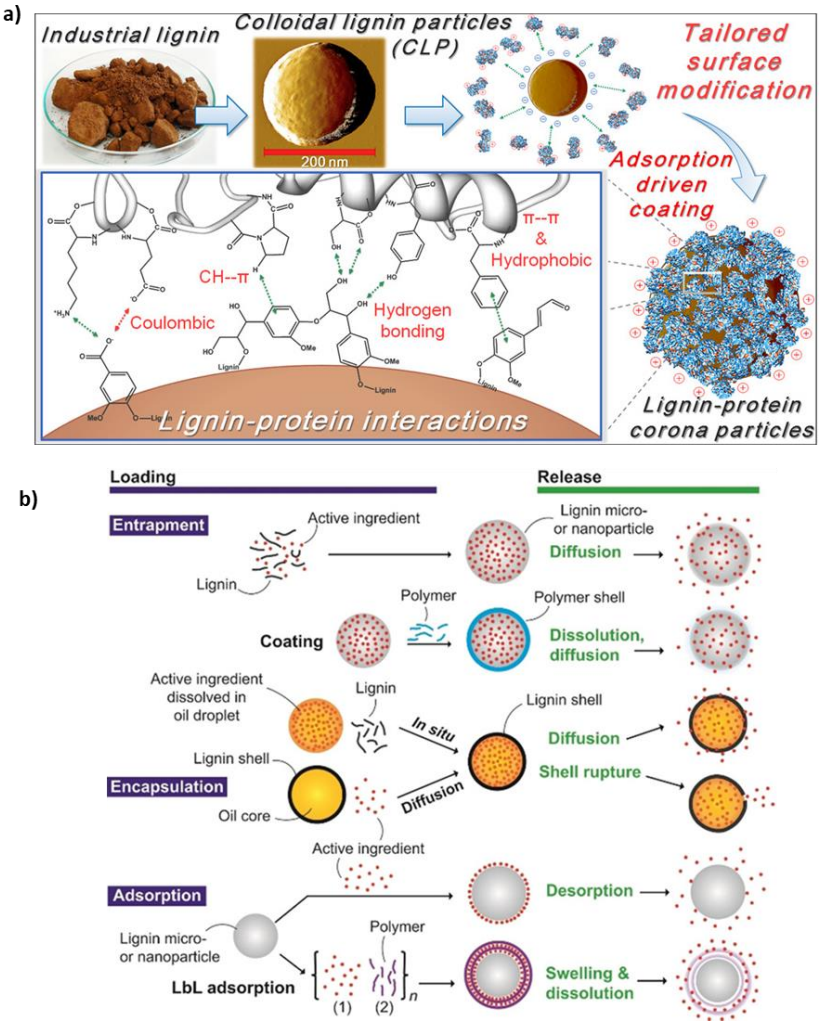


Figure 2.5 a) Main chemical interactions between lignin nanoparticles and proteins; **b)** General methods for loading and releasing active substances from various lignin-based particulate and capsule carriers.

Among the different technologies applied for the functionalization of LNPs (**Figure 2.5**), the layer by layer (LbL) technology, involving the sequential deposition of polyelectrolytes with opposite electric charge, received a great interest in the last years.[103] This technique, considered an auto-assembly technology, facilitates the development of hybrid nanomaterials.[104,105] In the LbL technique, the negative charge of lignin nanoparticles is overcompensated by the deposition of a cationic polyelectrolyte layer. The stratification of various layers, both positive and negative, enhances the stability of the overall LbL system.[106,107]

In the case of lignin nanoparticles which are dispersed in water, the introduction of cationic polyelectrolyte results in a reversal of the negative surface charge, shifting the zeta potential value from negative to positive.[74] In addition, lignin nanoparticles coated with a cationic polymer enhances colloidal system stability, imparting greater thermal stability again pH's modifications.[38] Recently, the LbL technology has been extended to the use of natural cationic polyelectrolytes such as chitosan and cationic lignin

(CATLIG).[108-110] Notably, chitosan is derived from the deacetylation of chitin from fish industry wastes,[111] while CATLIG is produced from kraft lignin that is a waste from the industrial production of pulp.[110]
By selecting an appropriate functionalization method, the properties of lignin nanoparticles can be optimized to facilitate the efficient production of nanocomposites with specific attributes, rendering them suitable for diverse applications.[109]

2.2.3 Lignin nanoparticles as functional supports for enzyme immobilization

Enzymes, natural protein-based biocatalysts, exhibit remarkable catalytic capabilities under mild biological conditions, demonstrating high specificity, selectivity, and low toxicity while significantly accelerating reaction rates.[112,113] However, their practical applications are hindered by the low stability under adverse experimental conditions.[114] Enzymatic immobilization offers a solution to solve this problem by enhancing catalytic performance and stability under challenging conditions (such as varying pH, temperature, and solvents), and facilitating recyclability without compromising activity.[115-117]
Nanomaterials are in principle excellent functional platforms for enzyme immobilization, providing a large surface area for effective enzyme loading.[118] Five main methods are employed for enzyme immobilization: adsorption, covalent immobilization, entrapment, encapsulation, and cross-linking. Adsorption (I) is the most simple method based on the adsorption of the enzymes on the surface of the matrix through hydrophobic interactions, hydrogen bonds, Van der Waals forces,[119] and electrostatic bonding.[120] Covalent immobilization (II) is based on the formation of stable covalent bonds between the enzyme and support, in order to prevent leaching process.[121] Entrapment (III) involves the immobilization of the enzymes within a polymeric network, allowing substrate and product diffusion.[120] Encapsulation (IV) is based on the entrapment of the enzymes in semi-permeable membranes, enabling movement within limited space.[122] Cross-linking (V) creates covalent bonds between enzyme molecules an the support.[122,123] The appropriate choice of both immobilization technique and support properties (roughness, hydrophobicity, porosity) is crucial for design efficient biotransformations,[122] since they can influence the enzyme conformation and activity.[124,125]
In this context, lignin nanoparticles emerge as an electroactive, sustainable, and efficient platform for enzyme immobilization.[126] For example, the low solubility of lignin nanoparticles in water facilitates the immobilization of water-soluble enzymes, overcoming recovery and separation challenges. In addition, lignin nanoparticles show advantages such as low cost, biocompatibility, and biodegradability.[127,128] Numerous studies showed the beneficial effect of lignin nanoparticles in the immobilization of several enzymes and applications, such as lipases for the synthesis of ester derivatives,[126,129] phospholipase D (PLD) useful to obtain phospholipids of commercial interest[133] tyrosinase for the synthesis of catechol and bioinks and[130,131] laccase for the selective oxidation of alcohols.[132] In these latter cases, tyrosinase and laccase were efficiently immobilized on lignin nanoparticles following the LbL protocol. In addition, amperometric analysis highlighted the occurrence of specific boosting effect in the case of immobilized laccase by both long-range electron transfer (pseudo-DET) and mediated electron transfer (MET) mechanisms. Similarly, lignin nanoparticles boosted the activity of tyrosinase by the occurrence of long-range electron transfer mechanisms.[127] This

underscores lignin nanoparticles as versatile and eco-friendly immobilization support for the immobilization of enzymes opening new strategies on the nano-biocatalysis field.

2.2.4 Multienzyme cascade immobilization

The multienzyme cascade reactions are prevalent in nature. In these systems, enzymes are organized in a cascade framework, leading to highly efficient catalysis.[134-137] Enzymatic cascades perform multi-step reactions by the fast transport of the reaction intermediates between different enzymes, reducing their diffusion in solution.[138]
Inspired by natural cascade processes, different strategies have been developed to co-immobilize enzymes at the nanoscale level[139] assuring the retention of the enzyme stability and original kinetic parameters.[140-142] The immobilization of multi-enzymes takes care to optimize the spatial organization of overall system to create 'architectures' that improve the activity, selectivity, stability, and reusability of the cascade. [143,144]
Since support materials can strongly influence enzyme properties, the ideal approach requires appropriate materials compatible with the enzymes to be immobilized in order to ensure overall activity of the system.[134,136] As a general approach, the co-immobilization method encompass the following five chemical approaches: (a) random co-immobilization, (b) sequential immobilization, (c) positional immobilization, (d) site-specific co-immobilization, and (e) cross-linking without a scaffold.[145-147] (**Figure 2.6**)

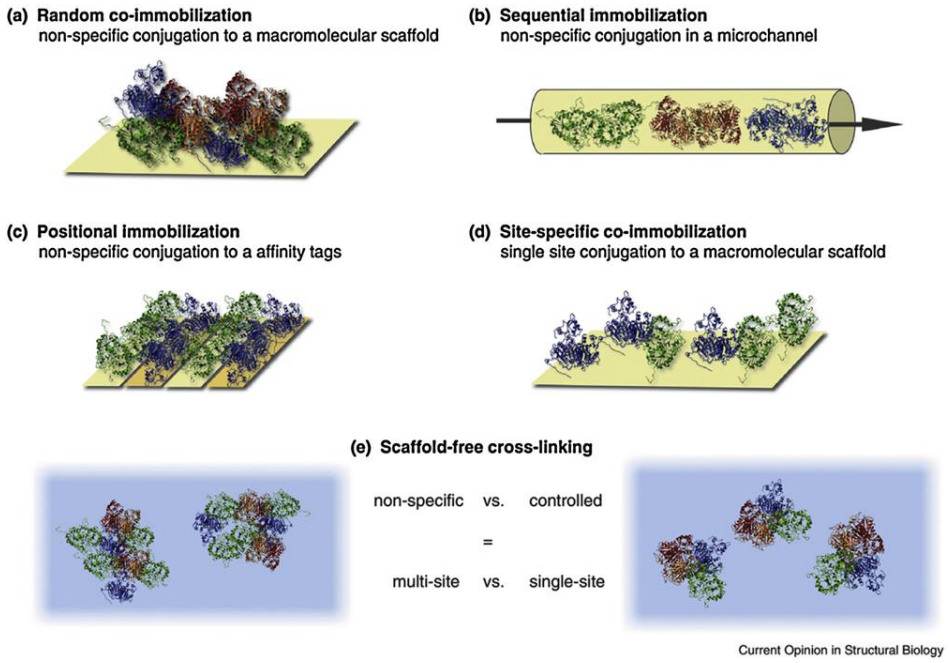


Figure 2.6. Five chemical approaches to construct multienzymatic complex.

Random co-immobilization methods require no-specific conjugation of the enzymes to the supports that negatively affect the overall catalytic activity. On the other hand, an ideal co-immobilization involves controlled and oriented enzyme co-immobilization.[147]
In fact, a correct orientation favours the occurrence of substrate channelling and tunnelling effects when enzymes are within distances of ~1 nm to ~10 nm.[150] This optimal distance limits the diffusion of the intermediates into the bulk medium and prevents rapid intermediate consumption in highly concentrated active site clusters.[148]

The use of natural lectins, such as Concanavalin A (Con A), has been reported for eco-friendly co-immobilization of enzymes. Con A is a carbohydrate-binding protein capable to bind specifically glycoproteins, providing optimal spacing for oriented immobilization[149] by formation of complexes with metal atoms (Mn^+ and Ca^+).[150]
Multienzyme complexes find applications in various fields, including biology, chemistry, bioengineering, and materials science.[141] Bio-nanocatalytic cascade systems could open novel routes to develop artificial metabolic pathways, offering sustainable approaches for chemical and biological synthesis.[139] In the context of green chemistry, one-pot multienzyme cascade reactions represent a promising alternative to avoid traditional unsustainable multi-step synthesis.[151]

References

52- Khan F.; Shariq M.; Asif M.; Siddiqui M.A.; Malan P.; Ahmad F. Green Nanotechnology: Plant-Mediated Nanoparticle Synthesis and Application. *Nanomaterials* **2022**, 12, 673.

53- Muneeswaran T., Maruthupandy M., Vennila T., Sundararaju S., Franck Quero. Nano-biomaterials for therapeutic and diagnostic applications. *Applications of Multifunctional Nanomaterials, Micro and Nano Technologies* **2023**, 27, 617-649.

54- Shahcheraghi N., Golchin H., Sadri Z. et al. Nano-biotechnology, an applicable approach for sustainable future. *3 Biotech* **2022,** 12, 65.

55- Pinem M.P.; Wardhono E.Y.; Nadaud F.; Clausse D.; Saleh K.; Guenin E. Nanofluid to Nanocomposite Film: Chitosan and Cellulose-Based Edible Packaging. *Nanomaterials* **2020**, 10, 660.

56- Willner I.; Willner B. Biomolecule-based nanomaterials and nanostructures. *Nano Lett.* **2010**, 10, 3805–3815.

57- Iravani S.; Korbekandi H.; Mirmohammadi S.V.; Zolfaghari B. Synthesis of silver nanoparticles: Chemical, physical and biological methods. *Res. Pharm. Sci.* **2014**, 9 (6), 385-406.

58- Sander M. S., Tan L. S. Nanoparticle arrays on surfaces fabricated using anodic alumina films as templates. *Advanced functional materials* **2003,** 13(5), 393-397.

59- Khan I., Saeed K., Khan I. Nanoparticles: Properties, applications and toxicities. *Arabian Journal of Chemistry* **2019**, 12, 908-931.

60- El-Khawaga A. M., Zidan A., Abd El-Mageed A. I. A. Preparation methods of different nanomaterials for various potential applications: A review. *Journal of Molecular Structure* **2023,** 1281, 135148.

61- Jiang H., Manolache S., Wong A. C. L., Denes F. S. Plasma-enhanced deposition of silver nanoparticles onto polymer and metal surfaces for the generation of antimicrobial characteristics. *Journal of Applied Polymer Science* **2004**, 93(3), 1411-1422.

62- Aromal S. A., Philip D. Green synthesis of gold nanoparticles using Trigonella foenum-graecum and its size-dependent catalytic activity. *Spectrochimica acta Part A: molecular and biomolecular spectroscopy* **2012**, 97, 1-5.

63- Yapaoz M. A., Attar A. Salvia officinalis-derived rutile TiO_2NPs: production, characterization, antibacterial evaluation and its effect on decolorization. *Materials Research Express* **2019**, 6(5), 055039.

64- Mahmoud W. M., Rastogi T., Kümmerer K. Application of titanium dioxide nanoparticles as a photocatalyst for the removal of micropollutants such as pharmaceuticals from water. *Current Opinion in Green and Sustainable Chemistry* **2017**, 6, 1-10.

65- Hager S., Fittler F.J., Wagner E., Bros M. Nucleic acid-based approaches for tumour therapy. *Cells* **2020**, 9(9):2061.

66- Verma SK, Suar M., Mishra YK. Editorial: Green Perspective of Nano-Biotechnology: Nanotoxicity Horizon to Biomedical Applications. *Front. Bioeng. Biotechnol* **2022**, 10, 919226.

67- Zhang Z., Terrasson V., Guénin E. Lignin Nanoparticles and Their Nanocomposites. *Nanomaterials* **2021**, 11, 1336.

68- Ates B., Koytepe S., Ulu A., Gurses C., Thakur V. K. Chemistry, Structures, and Advanced Applications of Nanocomposites from Biorenewable Resources. *Chemical Reviews.* **2020**, 120, 17, 9304–9362.

69- Iravani S., Varma R. S. Plant-Derived Edible Nanoparticles and miRNAs: Emerging Frontier for Therapeutics and Targeted Drug-Delivery. *ACS Sustainable Chemistry & Engineering* **2019**, 7(9), 8055–8069.

70- Chauhan P. S. Lignin nanoparticles: Eco-friendly and versatile tool for new era. *Bioresource Technology Reports* **2020**, 9,1003.

71- Figueiredo P., Lahtinen M. H., Agustin M. B., de Carvalho D. M., Hirvonen S.-P., Penttilä P. A., Mikkonen K. S. Green Fabrication Approaches of Lignin Nanoparticles from Different Technical Lignins: A Comparison Study. **2021**, 14, 21, 4718-4730.

72- Pylypchuk IV, Karlsson M., Lindén PA, Lindström ME, Elder T, Sevastyanova O, Lawoko M. Molecular understanding of the morphology and properties of lignin nanoparticles: unravelling the potential for tailored applications. *Green Chem.* **2023,** 12;25(11):4415-4428.

73- Sipponen M.K., Lange H., Ago M., Crestini C., Understanding lignin aggregation processes. A case study: budesonide entrapment and stimuli-controlled release from lignin nanoparticles. *ACS Sustain. Chem. Eng.* **2018**, 6, 9342–9351.

74- Sharma S., Kachhia P., Shukla V., Patel A., Rathod V., Narra M. Valorization of lignin into nanoparticles and nanogel: Characterization and application. *Bioresource Technology Reports.* **2022**, 18, 101041

75- Domínguez-Robles J., Tamminen T., Liitiä T., Peresin M. S., Rodríguez A., Jääskeläinen A. S. Aqueous acetone fractionation of kraft, organosolv and soda lignins. *Int. J. Biol. Macromol.* **2018**, 106, 979.

76- Österberg M., Sipponen M. H., Mattos B. D., Rojas O. J. Spherical lignin particles: a review on their sustainability and applications. *Green Chem.* **2020**, 22, 2712.

77- Lievonen M., Valle-Delgado J. J., Mattinen M. L., Hult, Lintinen E. L. K., Kostiainen M. A., A. Paananen, G. R. Szilvay, H. Setälä, M. Österberg. A simple process for lignin nanoparticle preparation. *Green Chem.* **2016**, 18, 1416.

78- Schneider W. D. H., Pinheiro Dillon A. J., Camassola M. Lignin nanoparticles enter the scene: A promising versatile green tool for multiple applications. *Biotechnology Advances* **2021**, 47 107685.

79- Mikulski D., Eder K., Molski M. Quantum-chemical study on stacking interactions between bioactive polyphenols (trans-resveratrol, trans-piceatannol) and ribonucleosides. Insight into minimum energy geometries of π–π stacked systems. *Computational and Theoretical Chemistry* **2014**, 1046, 118–125.

80- Mishra P.K.; Ekielski A. The Self-Assembly of Lignin and Its Application in Nanoparticle Synthesis: A Short Review. *Nanomaterials* **2019,** 9, 243.
81- DiLabio G. A., Johnson E. R. Lone Pair−π and π−π Interactions Play an Important Role in Proton-Coupled Electron Transfer Reactions. *Journal of the American Chemical Society* **2007**, 129(19), 6199–6203.
82- Batra A., Kladnik G., Vázquez H., Meisner J. S., Floreano L., Nuckolls C., Venkataraman L. Quantifying through-space charge transfer dynamics in π-coupled molecular systems. *Nature Communications* **2012**, 3, 1086.
83- McRae E. G., M. Kasha. "Physical processes in radiation biology." by L. Augenstein, R. Mason and B. Rosenberg *(Academic Press, New York, 1964*) **1964,** 3, 23-42.
84- Xiong F., Han Y., Wang S., Li G., Qin T., Chen Y., Chu F., Preparation and formation mechanism of size-controlled lignin nanospheres by self-assembly. *Ind. Crop. Prod.* **2017**, 100, 146–152.
85- Kai X., Can J., Gui-feng L., Gilkes N., Saddler J.N. Preparation and characterization of lignin nanoparticles with controllable size by nanoprecipitation method. *Chem. Ind. For. Prod.* **2015,** 5, 85–92.
86- Kim G., Park J., Kim B. M., Kim J., Kim K.-J., Park J. Influence of nanoprecipitation techniques on lignin nanoparticle structure. *Colloids and Surfaces A: Physicochemical and Engineering* Aspects **2024**, 682, 132803.
87- Yearla S. R., Padmasree K. Preparation and characterisation of lignin nanoparticles: evaluation of their potential as antioxidants and UV protectants. *Journal of Experimental Nanoscience* **2016**, 11(4), 289-302.
88- Yang W., Fortunati E., Gao D., Balestra G. M., Giovanale G., He X., Torre L., Kenny J.M., Puglia D. Valorization of acid isolated high yield lignin nanoparticles as innovative antioxidant/antimicrobial organic materials. *ACS Sustainable Chemistry & Engineering* **2018**, 6(3), 3502-3514.
89- Du B., Li W., Bai Y., Pan Z., Wang Q., Wang X., Ding H., Lv G., Zhou J. Fabrication of uniform lignin nanoparticles with tuneable size for potential wound healing application. *International Journal of Biological Macromolecules* **2022**, 214 170–180.
90- Li Y., Wu M., Wang B., Wu Y., Ma M., Zhang X. Synthesis of magnetic lignin-based hollow microspheres: a highly adsorptive and reusable adsorbent derived from renewable resources. *ACS Sustainable Chemistry & Engineering* **2016**, 4(10), 5523-5532.
91- Ma Y. Z., Zheng D. F., Mo Z. Y., Dong R. J., Qiu X. Q. Magnetic lignin-based carbon nanoparticles and the adsorption for removal of methyl orange. *Colloids and Surfaces A: Physicochemical and Engineering Aspects* **2018**, 559, 226-234.
92- Qian Y., Zhong X., Li Y., Qiu X. Fabrication of uniform lignin colloidal spheres for developing natural broad-spectrum sunscreens with high sun protection factor. *Industrial Crops and Products* **2017**, 101, 54-60.
93- Ali D. A., Mehanna M. M. Role of lignin-based nanoparticles in anticancer drug delivery and bioimaging: An up-to-date review. *International Journal of Biological Macromolecules* **2022**, 221, 934-953.
94- Agustin M. B., Lehtonen M., Kemell M., Lahtinen P., Oliaei E., Mikkonen K. S. Lignin nanoparticle-decorated nanocellulose cryogels as adsorbents for pharmaceutical pollutants. *Journal of Environmental Management* **2023**, 330, 117210.
95- Alqahtani M.S.; Alqahtani A.; Al-Thabit A.; Roni M.; Syed R. Novel lignin nanoparticles for oral drug delivery. *J. Mater. Chem. B* **2019**, 7, 446.
96- Ajdary M., Moosavi M. A., Rahmati M., Falahati M., Mahboubi M., Mandegary A., Varma R. S. Health concerns of various nanoparticles: a review of their in vitro and in vivo toxicity. *Nanomaterials* **2018**, (9), 634.
97- Imlimthan S., Correia A., Figueiredo P., Lintinen K., Balasubramanian V., Airaksinen A. J., Sarparanta M. Systematic in vitro biocompatibility studies of multimodal cellulose nanocrystal and lignin nanoparticles. *Journal of Biomedical Materials Research Part A* **2019**,108(3), 770-783.
98- Siddiqui L., Bag J., Seetha Mittal D., Leekha A., Mishra H, Talegaonkar S. Assessing the potential of lignin nanoparticles as drug carrier: Synthesis, cytotoxicity and genotoxicity studies. *International Journal of Biological Macromolecules* **2020**, 152, 786–802.
99- Moreno A.; Sipponen M. H. Lignin-Based Smart Materials: A Roadmap to Processing and Synthesis for Current and Future Applications. *Mater. Horiz.* **2020**, 7, 2237– 2257
100- Leskinen T., Witos J., Valle-Delgado J. J., Lintinen K., Kostiainen M., Wiedmer S. K., Mattinen M. L. Adsorption of proteins on colloidal lignin particles for advanced biomaterials. *Biomacromolecules* **2017**, 18(9), 2767-2776.
101- Bai F, Dong T, Chen W, Wang J, Li X. Nanocellulose Hybrid Lignin Complex Reinforces Cellulose to Form a Strong, Water-Stable Lignin-Cellulose Composite Usable as a Plastic Replacement. *Nanomaterials* **2021**, 11(12), 3426.
102- Peng Z., Peralta M. D. R., Cox D. L., Toney M. D. Bottom-up synthesis of protein-based nanomaterials from engineered β-solenoid proteins. *PLOS ONE* **2020**, 15(2), e0229319.
103- Yamaguchi A., Isozaki K., Nakamura M., Takaya H., Watanabe T. Discovery of 12-mer peptides that bind to wood lignin. *Scientific Reports* **2016,** 6(1).
104- Richter A. P., Bharti B., Armstrong H. B., Brown J. S., Plemmons D., Paunov V. N., Velev O. D. Synthesis and characterization of biodegradable lignin nanoparticles with tunable surface properties. *Langmuir* **2016**, 32(25), 6468-6477.
105- Ball V.; Bernsmann F.; Betscha C.; Maechling C.; Kauffmann S.; Senger B.; Voegel J.C.; Schaaf P.; Benkirane-Jessel N. Polyelectrolyte multilayer films built from poly(L-lysine) and a two-component anionic polysaccharide blend. *Langmuir* **2009**, 25, 3593-6000.
106- Cuomo F.; Lopez F.; Ceglie A. Templated globules — applications and perspectives. *Adv. Colloid Interface Sci.* **2014**, 205, 124–133.

107- Luo H.; Shen Q.; Ye F.; Cheng Y.F.; Mezgebe M.; Qin R.J. Structure and properties of layer-by-layer self-assembled chitosan/lignosulfonate multilayer film. *Mater. Sci. Eng. C.* **2012**, 32, 2001–2006.
108- Shutava T.; Prouty M.; Kommireddy D.; Lvov Y. pH Responsive Decomposable Layer-by-Layer Nanofilms and Capsules on the Basis of Tannic Acid. *Macromolecules* **2005**, 38, 2850– 2858.
109- Zou T., Sipponen M. H., Österberg M. Natural shape-retaining microcapsules with shells made of chitosan-coated colloidal lignin particles. *Frontiers in chemistry* **2019**, 7, 370.
110- Sipponen M. H., Smyth M., Leskinen T., Johansson L. S., Österberg M. All-lignin approach to prepare cationic colloidal lignin particles: stabilization of durable Pickering emulsions. *Green Chemistry* **2017**, 19(24), 5831-5840.
111- Wang W, Meng Q, Li Q, Liu J, Zhou M, Jin Z, Zhao K. Chitosan Derivatives and Their Application in Biomedicine. *Int J Mol Sci.* **2020**,12;21(2):487.
112- Dey N., Kumar G., A.S. Vickram, Monisha Mohan, Reeta Rani Singhania, Anil Kumar Patel, Cheng-Di Dong, K. Anbarasu, S. Thanigaivel, Vinoth Kumar Ponnusamy. Nanotechnology-assisted production of value-added biopotent energy-yielding products from lignocellulosic biomass refinery – A review. *Bioresource Technology* **2022**, 344 126171.
113- Zhang H., Nie M., Gu Z., Xin Y., Zhang L., Li Y., Shi G. Preparation of water-insoluble lignin nanoparticles by deep eutectic solvent and its application as a versatile and biocompatible support for the immobilization of α-amylase. *International Journal of Biological Macromolecules* **2023**, 249, 125975.
114- Madhavan A, Sindhu R, Binod P, Sukumaran RK, Pandey. A Strategies for design of improved biocatalysts for industrial applications. *Biores Technol* **2017**, 245, 1304–1313.
115- Nguyen H. H, Lee S. H., Ui Lee J., Cesar D. Fermin, Kim M. Immobilized Enzymes in Biosensor Applications. *Materials* **2019**, 12, 121.
116- Sirisha V.L., Jain A., Jain A. Enzyme Immobilization: An Overview on Methods, Support Material, and Applications of Immobilized Enzymes. *Advances in Food and Nutrition Research* **2016**, 179-211.
117- Puri M., Barrow C. J., Verma, M. L. Enzyme immobilization on nanomaterials for biofuel production. *Trends in Biotechnology* **2013**, 31(4), 215-216.
118- Gupta M. N., Kaloti M., Kapoor M., Solanki K. Nanomaterials as matrices for enzyme immobilization. *Artificial Cells, Blood Substitutes, and Biotechnology* **2011**, 39(2), 98-109.
119- Nisha S, Karthick AS, Gobi N. A review on methods, application and properties of immobilized enzyme. *Chem Sci Rev Lett* **2012**, 1(3),148–155.
120- Nguyen H. H., Kim M. An Overview of Techniques in Enzyme Immobilization. *Appl. Sci. Converg. Technol.* **2017**, 26(6): 157-163
121- Bai Y, Huang H, Meng K, Shi P., Yang P., Luo H., Luo C., Feng Y., Zhang W., Yao B. Identification of an acidic α-amylase from Alicyclobacillus sp. A4 and assessment of its application in the starch industry. *Food Chem* **2012,** 131(4):1473–1478.
122- Singh A., Negi M. S., Dubey A., Kumar V., Verma A. K. Methods of Enzyme Immobilization and Its Applications in Food Industry. *Enzymes in Food Technology* **2018**, 103–124.
123- Datta S, Christena LR, Rajaram YRS. Enzyme immobilization: an overview on techniques and support materials. *3 Biotech* **2013**, 3(1):1–9.
124- Fischer N. O., McIntosh C. M., Simard J. M., Rotello V. M. Inhibition of chymotrypsin through surface binding using nanoparticle-based receptors. *Proc. Natl. Acad. Sci. U. S. A* **2002**, 99, 5018–5023.
125- Aissaoui N., Bergaoui L., Boujday S., Lambert J. F., Methivier C., Landoulsi J. Enzyme immobilization on silane-modified surface through short linkers: fate of interfacial phases and impact on catalytic activity. *Langmuir* **2014**, 30(14), 4066-4077.
126- Sipponen M. H., Farooq M., Koivisto J., Pellis A., Seitsonen J., Österberg M. Spatially confined lignin nanospheres for biocatalytic ester synthesis in aqueous media. *Nature communications* **2018**, 9:2300.
127- Westereng B.; Cannella D.; Agger J.W.; Jørgensen H.; Andersen M.L.; Eijsink V.G.H.; Felby C. Enzymatic cellulose oxidation is linked to lignin by long-range electron transfer. *Sci. Rep.* **2015**, 5, 18561.
128- Li R., Huang D., Lei L., Chen S., Chen Y., Wang G., Chen H. Lignin and metal–organic frameworks: mutual partners on the road to sustainability. *Journal of Materials Chemistry A* **2023**, 11(6), 2595-2617.
129- Huan Zhang, Rui Zhu, Yi Shi, Xin Yu, Liang Zhang, Youran Li, Guiyang Shi. Lipase immobilization using scalable and biocompatible lignin-based material as a carrier. *Industrial Crops and Products* **2023**, 193, 116241.
130- Capecchi E., Piccinino D., Delfino I., Bollella P., Antiochia R., Saladino R., Functionalized Tyrosinase-Lignin Nanoparticles as Sustainable Catalysts for the Oxidation of Phenols. *Nanomaterials* **2018**, 8(6),438.
131- Capecchi E., Piccinino D., Bizzarri B. M., Avitabile D., Pelosi C., Colantonio C., Calabro G., Saladino R. Enzyme-Lignin Nanocapsules Are Sustainable Catalysts and Vehicles for the Preparation of Unique Polyvalent Bioinks. *Biomacromolecules* **2019**, 20, 1975−1988.
132- Piccinino D., Capecchi E., Botta L., Bollella P., Antiochia R., Crucianelli M., Saladino R. Layer by layer supported laccase on lignin nanoparticles catalyzes the selective oxidation of alcohols to aldehydes. *Catal. Sci. Technol*. **2019**, 9, 4125-4134.
133- Rossato L. A. M., Morsali M., Ruffini E., Bertuzzi P., Serra S., D'Arrigo P., Sipponen M.. Phospholipase D Immobilization on Lignin Nanoparticles for Enzymatic Transformation of Phospholipids. *ChemSusChem* **2023**, e202300803.
134- Lopez-Gallego F. On-pot and cell-free biocatalysis using co-immobilized enzymes on advanced materials. *Methods Enzymol*. **2019**; 617:385-411.

135- Jia F., Mallapragada S. K., Narasimhan B. Multienzyme Immobilization and Colocalization on Nanoparticles Enabled by DNA Hybridization. *Ind. Eng. Chem. Res* **2015**, 54, 42, 10212-10220.
136- Hwang E. T., Lee S. Multienzymatic Cascade Reactions via Enzyme Complex by Immobilization. *ACS Catal.* **2019**, 9, 4402−4425.
137- Yu X., Zhang Z., Li J., Su Y., Gao M., Jin T., Chen G. Co-immobilization of multi-enzyme on reversibly soluble polymers in cascade catalysis for the one-pot conversion of gluconic acid from corn straw. *Bioresource Technology* **2021**, 321, 124509.
138- Zhang Y.-H. P. Substrate Channeling and Enzyme Complexes for Biotechnological Applications. *Biotechnol. Adv.* **2011**, 29 (6), 715−725.
139- Giannakopoulou A., Patila M., Spyrou K., Chalmpes N., Zarafeta D., Skretas G., Gournis D., Stamatis H. Development of a Four-Enzyme Magnetic Nanobiocatalyst for Multi-Step Cascade Reactions. *Catalysts* **2019**, 9, 995.
140- AAdT J., Ladeira YFX, França AdS, Souza Romad, Moraes AH, Wojcieszak R, Itabaiana I Jr., Miranda ASd. Multicatalytic Hybrid Materials for Biocatalytic and Chemoenzymatic Cascades—Strategies for Multicatalyst (Enzyme) Co-Immobilization. *Catalysts* **2021**; 11(8):936.
141- Tan Z., Cheng H., Chen G., Ju F., Lucas J. F., Zdarta J., Jesionowski T., Bilal M. Designing multifunctional biocatalytic cascade system by multi-enzyme co-immobilization on biopolymers and nanostructured materials. International Journal of Biological *Macromolecules* **2023**, 227, 535-550.
142- Rocha-Martin J., Velasco-Lozano S., Guisa´n J. M., Lo´pez-Gallego F. Oxidation of phenolic compounds catalyzed by immobilized multi-enzyme systems with integrated hydrogen peroxide production. *Green Chemistry* **2014**, 16(1), 303–311.
143- Poshyvailo L., von Lieres E., Kondrat S. Does metabolite channeling accelerate enzyme-catalyzed cascade reactions? *PLoS ONE* **2017**, 12(2): e0172673.
144- Pei R., Liu J., Jing C., Zhang M. A Multienzyme Cascade Pathway Immobilized in a Hydrogen-Bonded Organic Framework for the Conversion of CO_2. *Small* **2023**, 2306117.
145- Ji Q., Wang B., Tan J., Zhu L., Li L. Immobilized multienzymatic systems for catalysis of cascade reactions. *Process Biochemistry* **2016**, 51, 1193–1203.
146- Kuzmak A., Carmali S., von Lieres E., Alan J. Russell, Svyatoslav Kondrat. Can enzyme proximity accelerate cascade reactions? *Scientific Reports* **2019**, 9:455.
147- Xu K, Chen X, Zheng R, Zheng Y. Immobilization of Multi-Enzymes on Support Materials for Efficient Biocatalysis. *Front Bioeng Biotechnol*. **2020**, 30; 8:660.
148- Wheeldon, I., Minteer, S., Banta, S. et al. Substrate channelling as an approach to cascade reactions. *Nature Chem* **2016**, 8, 299–309
149- You Yong, Rui Su, Xuerun Liu, Weina Xu, Yifei Zhang, Rui Wang, Pingkai Ouyang, Jianzhong Wu, Jun Ge, Zheng Liu. Lectin corona enhances enzymatic catalysis on the surface of magnetic nanoparticles. *Biochemical Engineering Journal* **2018**, 129, 26-32.
150- R. Victor Rebois, Peter Schuck and John K. Northup. Elucidating Kinetic and Thermodynamic Constants for Interaction of G Protein Subunits and Receptors by Surface Plasmon Resonance Spectroscopy. *Methods in Enzymology* **2002**, 344.
151- Losada-Garcia N, Cabrera Z, Urrutia P, Garcia-Sanz C, Andreu A, Palomo JM. Recent Advances in Enzymatic and Chemoenzymatic Cascade Processes. *Catalysts* **2020**; 10(11):1258.

CHAPTER 3

ADVANCED MATERIAL SCIENCES APPLICATIONS OF LIGNIN NANOPARTICLES: THE BIOPLASTIC CASE

3.1 Nanoparticles of Lignins and Saccharides from Fishery Wastes as Sustainable UV-Shielding, Antioxidant, and Antimicrobial Biofillers

3.1.1 Aim of work

Lignin is the most abundant polyphenol in nature.[27] It is characterized by its amorphous structure and variable elemental composition depending on origin and isolation technologies.[152] Lignin is recovered in a large amount as a waste from pulp and paper and biorefinery processes,[153] serving as renewable compounds in Green Chemistry and Circular Economy.[154] Biofillers from lignin have been reported[155−158] and their role in the control of thermal stability, printability, and flexural capability of advanced materials deeply investigated.[159−165] Organosolv lignin biofillers are ingredients in 3Dprinting technologies,[166] as well as in rubber,[167] ink,[168] and adhesive applications.[169,170] The self-assembly of lignin into ordered nanoparticles (LNPs) improves chemical, physical, and rheological properties due to the emergence of interactions between the aromatic subunits of the polymer.[171] Chitosan (CH) and chitooligosaccharides (COSs) are biodegradable and biocompatible natural compounds characterized by antimicrobial and anti-inflammatory activities.[172−183] Blends of LNPs and CH are reported in the decontamination of water[184] and in the synthesis of hydrogel[185,186] and food packaging materials.[187] The preparation of nanoparticles of chitosan and lignin has been reported under different experimental conditions, including microfluidic electrostatic assembly,[188] layer-by-layer,[109] nanoprecipitation,[189] Pickering emulsion polymerization,[190,191] solvent casting,[187] hydrothermal methods,[192] and sonochemistry,[186] focusing on the application as a pH responsive delivery device, composite sorbent, packaging ingredient, and UV absorber. These synthetic procedures always involved the use of high-molecular-weight chitosans (from 100 to 400 KDa) characterized by high deacetylation degree (>80%), the only exception being reported in the case of methacrylated lignin, in which chitosan oligomers were also applied.[193] A comparative study on the effect of the molecular weight and of the deacetylation degree of chitosan and chitosan oligomers in the chemo-physical, biological, and rheological properties of lignin/chitosan nanoparticles is not available. Here, we report the preparation and structural characterization of lignin and saccharide nanoparticles by applying nanoprecipitation technology. Kraft lignin (KL) and organosolv lignin (OL) were used in association with CH and COSs with different values of molecular weight and deacetylation degree recovered from fishery wastes. The stability, aggregation state, and biological properties of novel nanoparticles were influenced by the structure of the saccharide and the optimal conditions consisting of the use of low-molecular-weight and highly deacetylated molecules. As a general trend, nanoparticles containing COSs showed higher antioxidant, UV-shielding, and antimicrobial activities than the high-molecular-weight CH counterpart and were characterized by the presence of a hypsochromic effect due to the formation of aggregates of H-type, highlighting the emergence of specific interactions and synergistic effects between the polyphenol and saccharide components.

3.1.2 Experimental part

Materials
Organosolv lignin (OL) and Kraft lignin (KL) were obtained from Chemical Point and Stora Enso, respectively. Chitosan from fishery wastes (CH1−4) was prepared by ANFACOCECOPESCA, and commercial chitosan (CH5−7) was purchased from Acros Organics and Sigma-Aldrich. Chitooligosaccarides (COS1−10) were produced with endochitinase Chit33 from Trichoderma harzianum expressed in Pichia pastoris; the detailed protocol for the production of Chit33 is given in the Supporting Information, S1. 3,5-Dinitrosalicylic acid (DNSA) and 2,2′-diphenylpicrylhydrazyl (DPPH) were supplied by TCI chemicals and used without further purification.

Preparation of CH1−4 from Fishery Wastes
The chitosan samples CH1−4 were obtained from crustacean's exoskeletons of big size that were initially disinfected following autoclaving for 3 min at 121 °C. The shells were mashed and dried in a forced air-drying oven for 48 h at 60 °C. Once dried, they were crushed in a STEPHAN for 4 min, and fractions were selected using a 2 mm mesh size sieve. Deproteinization was performed with a NaOH solution (4% in deionized water, 1:5 w/v ratio). The mixture was incubated in an orbital shaker (200 rpm) for 3 h at 65 °C, followed by vacuum filtration and washing until the pH of the extract became neutral, and finally dried at 60 °C. The dried material was treated with 2.5 M HCl (1:10 w/v) under orbital agitation for 3 h at 25 °C. After this time, it was filtered under vacuum and washed until the pH of the extract was neutral and then dried at 60 °C. Depigmentation was performed by treatment with ethanol (1:10 w/v ratio). The mixture was kept under orbital agitation for 3 h at 30 °C. Subsequently, the material was filtered and washed until neutral and dried at 60 °C. Deacetylation was performed by treatment of the sample with NaOH (1:10 w/v ratio). The mixture was kept under orbital agitation for 24 h at 80 °C, followed by filtration and washing until neutrality and dried at 60 °C. Structural characterization of samples consisted in the evaluation of the deacetylation degree (DD) and the determination of the molecular weight (MW). For the analysis, the sample was treated with HCl (1 M) at 80 °C until the material dissolved. The DD was estimated using the potentiometer titration method starting from chitosan (500 mg) dissolved in HCl (50 mL; 0.3 M) at 25 °C. The solution was titrated with NaOH (0.1 M) until a change of 2 pH units was detected. The DD was calculated from the following formula:

$$DD(\%) = 16.1((V_2 - V_1)/w)*M$$

where M is the molarity of the NaOH solution, V_2-V_1 is the difference in the volume of added NaOH required for the change of 2 pH units, w is the weight of chitosan, and 16.1 is a value related to the equivalent weight of chitosan. The formula used for the estimation of the intrinsic viscosity was $[\eta] = KMv\Lambda\alpha$. Measurements of the intrinsic viscosity η were performed by the analysis of solutions with different concentrations (acetic acid and sodium acetate) using the AR/1000 rheometer (TA Instruments, Waters LLC). It uses a cone−plate system in aluminium of 60 mm in diameter and angle 2°1′2″ equipped with a Peltier system of temperature control, which must be fixed at 25 °C to measure the viscosity. The intrinsic viscosity was obtained by the representation of the reduced and inherent viscosity of the chitosan with the best and worst degree of deacetylation, taking into account the average of the ordinates at the origin. From this value, and through the molecular weight equation, the K and α parameters were calculated to be 0.074 and 0.76, respectively.

Preparation of CH1−7/KLNPs and CH1−7/OLNPs

The CH1−7/KLNPs and CH1−7/OLNPs were prepared by the nanoprecipitation procedure[194,195] using acetic acid (1.0% water solution) as an antisolvent and tetrahydrofuran (THF) as a primary solvent. As a general procedure, lignin (12 g) in THF (0.5 L) was rapidly added to CH (20 g) in acetic acid (1.5 L) under gentle mechanical stirring at 25 °C. CH1−7/KLNPs and CH1−7/OLNPs were isolated after evaporation of THF under reduced pressure, followed by washing with acetic acid (3.0% water solution), centrifugation (12 100 rpm for 10 min 2×), and freeze-drying for 24 h.

Preparation of COS1−10

Chitooligosaccharides (COS1−10) characterized by different values of DD and MW were prepared by enzymatic treatment of CH1−4 with endochitinase Chit33 from Trichoderma harzianum expressed in Pichia pastoris. CH1−4 (4% w/w) were dissolved in acetic acid 0.1 M (1 L) under gentle magnetic stirring overnight. CH solutions were dialyzed against distilled water until pH 5 was reached. The solutions of CH1−4 were then treated with endochitinase Chit33. The initial chitinase activity was determined by the detection of reducing sugars obtained from chitinolytic materials. Reactions were performed by Chit33 (40 total units) in a 3.0 L flask at 45 °C and 200 rpm for 5 days. Reactions were stopped at 80 °C for 10 min, and a few drops of NaOH (10 M) were added until pH 9 was achieved to facilitate the separation of reaction products from the nondigested CH by centrifugation (4000g for 10 min). After the centrifugation step, the supernatant was clarified by filtration (0−45 μm and 0.22 μm membranes). COS (3−10, 10−30 kDa, and more than 30 kDa) were separated according to their size using 3000, 10 000, and 30 000 MWCO PES membranes using a Vivaflow 50 system and dialyzed against distilled water to a neutral pH value. All fractions were freeze-dried.

Preparation of COS1−10/OLNPs

COS1−10/OLNPs were prepared by the nanoprecipitation process. In particular, OL (12 g) in THF (0.5 L) was rapidly added to the appropriate COS1−10 (20 g) in deionized water (1.5 L) at 25°C under gentle stirring. COS1−10/OLNPs formed instantaneously and were isolated after evaporation of THF under reduced pressure, centrifugation (12 100 rpm for 10 min), and freeze-drying.

3,5-Dinitrosalicylic Acid Colorimetric Assay

The amount of residual CH1−7 and COS1−10 was evaluated spectrophotometrically through the 3,5-dinitrosalicylic acid (DNSA) colorimetric assay using CH5 as standard for the calibration curve (concentration range between 100 μg/mL and 1000 μg/mL).[196] The stock solution was prepared by adding DNSA (0.5 g) and sodium potassium tartrate (15 g) to NaOH solution (0.3 M, 60 mL). Before the spectrophotometric analysis, the sample was treated with $NaNO_2$ (0.5 M, 0.1 mL) at 80 °C for 45 min to obtain the reducing sugar forms. At the end of the reduction, the DNSA solution (1 mL) was added to the reaction mixture. The amount of the saccharide was evaluated by the calibration curve of CH5 by measuring the absorbance at 540 nm.

Differential Scanning Calorimetry (DSC) Analysis

The melting point values were measured by differential scanning calorimetry (DSC) in a DSC822e apparatus from METTLER TOLEDO (Columbus, Ohio). All of the samples were heated from 0 °C up to 350 °C at 10 °C/min under a N_2 atmosphere (flow rate of 80 mL/min).

Field Emission Scanning Electron Microscopy (FESEM)
The field emission scanning electron microscopy (FESEM) of CH/OLNPs and COS/OLNPs was performed on an FESEM ZEISS GeminiSEM500 operated at 5 kV after 20 μL (with deionized water) of sample dispersion was dropped on specimen stubs, air dried, and coated with gold by sputtering with an AGAR (Auto Sputter Coater). Before the observations, the sample received a deposition of chromium thin film (5 nm) by sputter coating using a QUORUM Q 150T ES plus coater.

FTIR ATR Analysis
Attenuated total reflection Fourier transform infrared (ATR-IR) spectroscopic analysis was performed using a PerkinElmer (Spectrum One) spectrometer (UATR unit cell), averaging 32 scans (resolution of 4 cm^{-1}).

Dynamic Light Scattering (DLS) and ζ Potential Analysis
The hydrodynamic diameter and ζ-potential were measured with DLS by suspending a freshly prepared sample in H_2O using a Zetasizer Nano ZS (Malvern Instruments, Malvern, U.K.) apparatus equipped with a He−Ne laser (633 nm, a fixed scattering angle of 173°, 25 °C). Measurements were performed in triplicate at room temperature (T = 25°C).

Antioxidant Activity
The antioxidant activity was determined spectrophotometrically using the 2,2′-diphenyl picrylhydrazyl (DPPH) radical scavenging assay. The DPPH solution shows a strong absorption band at 517 nm (deep violet colour). Briefly, the stock solution of the sample was diluted to a dilution series (six different concentrations in the range of 5−500 μg/mL, ethanol/water (6:1)). The decrease in the absorbance measured at 517 nm was determined by adding an aliquot of each dilution (0.5 mL) in a freshly prepared solution of DPPH (0.25 mM) in 2.5 mL of methanol at 37 °C in the dark for 30 min. The kinetics of the process was analyzed for each concentration tested, and the rate of DPPH remaining at a steady state was estimated. The radical scavenging activity was expressed as the IC_{50} value (defined as the concentration of the substrate in μg/mL that causes a 50% loss of DPPH activity).

UV Shielding Assay
The UV absorption properties were determined with a Cary UV 60 spectrophotometer using the same concentration of nanoparticles (0.1 mg/mL) in deionized H_2O (3.0 mL), working in the range between 190 and 600 nm at 25 °C under gentle stirring.

Antimicrobial Activities of COS1−10/OLNPs
For evaluation of the doubling time, Escherichia coli and Staphylococcus aureus were cultured separately in sterilized Luria−Bertani (LB) broth medium (30 mL) and kept in a shaker incubator at 37 °C for 16 h. The cultures (0.01 mL) were transferred to 96-well plates containing COS1−10/OLNPs (0.02 mg) in deionized water (0.01 mL) and LB (183.3 μL) and maintained at 37 °C with only 5 s of agitation periods prior to each of the growth monitoring at OD600, which were every 15 min. The cultures were normalized to an initial growth of 0.05 OD600. Wells containing microorganisms alone and OLNPs were used as a control. The procedures to determine the growth rate were the same as explained previously.[197] The minimum inhibitory concentrations (MICs, mg/mL) were measured by growing microorganisms in the presence of different concentrations of COS/OLNPs (from 0 to 6.4 mg/mL). MIC_{50} values were defined as the lowest concentration of the sample at which 50% of the bacterial growth was inhibited.

3.1.3 Results and discussions

Preparation of Nanoparticles Containing Lignins and Saccharides.
Commercially available KL[198,199] and OL[200,201] were selected as the lignin component. KL is a byproduct of the Kraft chemical pulping process covering c.a. 95% of the overall pulp wastes.[202,203] OL is derived from organic solvent bleaching of the lignocellulosic material at high temperatures.[204−207] OL and KL are structurally modified with respect to the native counterpart.[206] KL is subjected to severe chemical modifications, including the cleavage of β-O-4 subunits[208] and the incorporation of sulfur atoms.[209,210] Conversely, OL is a sulfur-free lignin with a high amount of β-O-4 subunits and long and flexible aliphatic side-chains. These latter subunits influence the performance of lignin biofillers by tuning the mechanical stiffness, thermochemical, and flexible module properties.[211] Initially, nanoparticles were prepared by nanoprecipitation starting from lignins and selected CH from fishery wastes (CH1−4/KLNPs and CH1−4/OLNPs) or alternatively from a commercial source (CH5−7/KLNPs and CH5−7/OLNPs),[194,195] using acetic acid (1.0% water solution) as an antisolvent and tetrahydrofuran (THF) as a primary solvent (**Figure 1**). The deacetylation degree (DD), average molecular weight (MW), and melting point (M_p) of CHs are presented in **Table 2**. As a general procedure, lignin (12 g) in THF (0.5 L) was rapidly added to CH (20 g) in acetic acid (1.0% water solution, 1.5 L) under gentle mechanical stirring at 25 °C (**Figure 3.1**, Panel A, B). Nanoparticles formed instantaneously as a colloidal suspension (**Figure 3.1**, Panel C). CH/KLNPs and CH/OLNPs were isolated after the evaporation of THF under reduced pressure, followed by washing with acetic acid (3.0% water solution), centrifugation (12 100 rpm for 10 min 2×), and freeze-drying (**Figure 3.1**, Panel D). As a general trend, CH/KLNPs were brighter than the CH/OLNP counterpart (**Figure 3.2**, Panel A versus Panel B). CH/OLNPs were obtained in yield (total amount in weight of nanoparticles with respect to the initial amount of lignin and CH) higher than CH/KLNPs (**Table 2**, entries 10−16 versus entries 3−9). Commercially available chitosan (from CH5 to CH7) and chitosan from fishery waste (from CH1 to CH4) showed a similar yield. Irrespective of the experimental conditions, the highest yield was always observed in the case of CH1 (**Table 2**, entries 6 and 13, respectively).

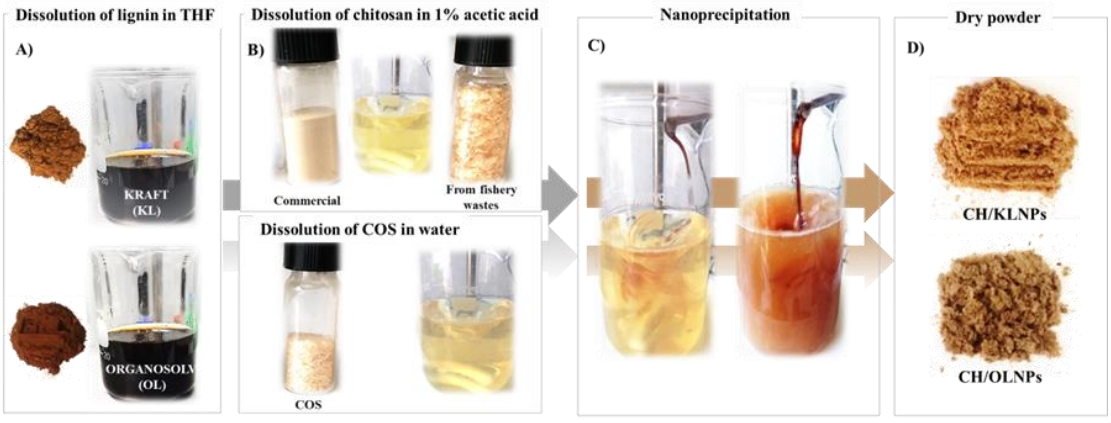


Figure 3.1 Schematic representation of the nanoprecipitation for the preparation of mixed lignin nanoparticles bearing chitosan (CH/LNPs) and chito-oligosaccharides (COS/OLNPs). Panel A: dissolution of Kraft lignin in THF (the upper part) and Organosolv lignin (bottom part). Panel B: dissolution of CH and COS in acetic acid (upper part) and in deionized water (bottom part), respectively. Panel C: nanoprecipitation procedure at two different times (few seconds). Panel D: CH/KLNPs and CH/OLNPs obtained after freeze-dry.



Figure 3.2. Pictures of CH/KLNPs (Panel A) and CH/OLNPs (Panel B) obtained from the nanoprecipitation process and classified depending on the CH type. Samples 1 and 8: commercial medium molecular weight CH. Samples 2 and 9: commercial low molecular weight CH. Samples 2 and 9: commercial low molecular weight CH. Samples 3 and 10: commercial shrimp CH. Samples 4 and 11: CH from fishery waste with 57-80% de-acetylation degree. Samples 5 and 12: CH from fishery waste with 57%-70% de-acetylation degree. Samples 6 and 13: CH from fishery waste with 64% de-acetylation degree. Samples 7 and 14: CH from fishery waste with 30% de-acetylation degree.

The melting point of CH/OLNPs and CH/KLNPs was evaluated by differential scanning calorimetry (DSC), using native OLNPs and KLNPs as references (**Table 2**). The original DSC curves are reported in Supporting Information S2 (Figures S2.1 and Figure S2.2, respectively). As a general trend, the presence of the saccharide increased the melting point of nanoparticles with respect to reference (**Table 2**). In addition, nanoparticles prepared from OL showed a melting point higher than KLNPs at parity of the type of CH (**Table 2**, entries 3-9 versus entries 10-16). This thermochemical behaviour was consistent with data previously reported for KL and OL.[212,213] In the case of KL samples, commercially available chitosan generally improved the melting point of nanoparticles with respect to fishery-waste counterpart (**Table 2**, entries 3-5 versus entries 6-9), with the only exception of CH4 which showed the highest value of melting point. Conversely, commercially available chitosan and chitosan from fishery waste showed comparable value of melting point when aggregated with OL (**Table 2**, entries 10-12 versus entries 13-16), reflecting the different properties and elemental composition of the two lignin samples. CH/OLNPs showed melting point values compatible with that of common bio-plastics, such as poly(lactic acid) (PLA:120-175 °C),[214] poly(butylene succinate) (PBS: 107 °C),[215] poly(butylene succinate adipate) (PBSA: 83,7 °C)[216] and poly(butylene adipate terephthalate) (PBAT: 120 °C), making them useful bio-filler for advanced blends.[217] The relative amount of CH and lignin embedded into nanoparticles was evaluated by 3, 5-dinitrosalicylic acid (DNSA) colorimetric assay.[196,218] The type of lignin, and the molecular weight and DD of the saccharide affected the amount of the two components (**Table 2**). CH aggregated with OL better than KL (**Table 2**, entries 10-16 versus entries 3-9), and the amount of embedded saccharide increased by increasing the value of DD (**Table 2**, entries 3, 6 and entries 10, 13 versus entries 8, 9 and entries 15, 16). Commercially available chitosan and chitosan from fishery waste showed comparable amount of embedded saccharide in KL samples (**Table 2**, entries 3-5 versus entries 6-9). A similar trend was observed for OL samples (**Table 2**, entries 10-12 versus entries 13-16). In both cases, CH1 was aggregated into lignin in the highest amount. FT-IR analysis of CH/OLNPs confirmed the presence of lignin and saccharide components into nanoparticles (**Figure 3.3**). The amide I band (1640 cm^{-1}) and amide II band (1585 cm^{-1}), and bands at 1066 cm^{-1} and 1028 cm^{-1}, characteristic of the C-O stretching of CH, were clearly identified in the spectra besides to typical bands of lignin at 1614 cm^{-1}

(aromatic bending vibration),[219] 1462 cm^{-1} (C–H deformations), 1332 cm^{-1} (C=O stretching), and 1116 cm^{-1} (aromatic C–H in plane deformation).[220] FT-IR of original CH and OL samples are in Supporting Information S3.

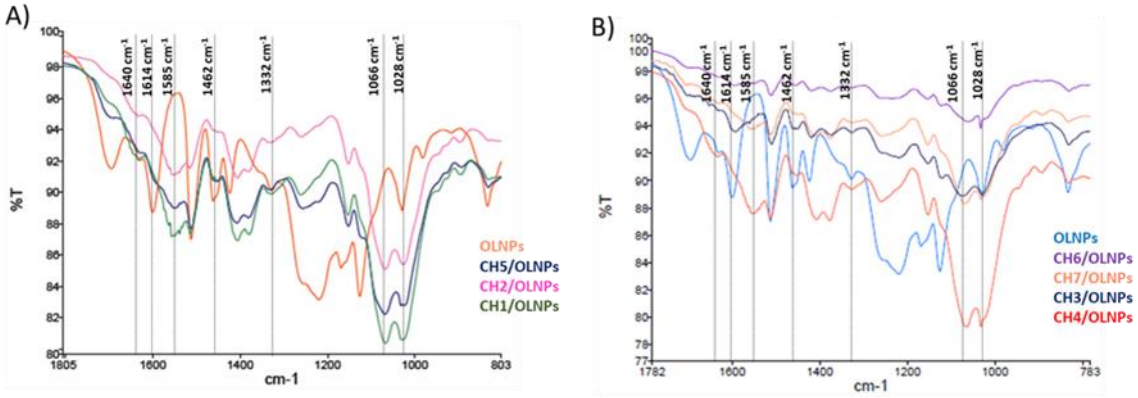


Figure 3.3. FT-IR spectra of CH/OLNPs. Panel A: CH/OLNPs bearing CH with high DD value. Panel B: CH/OLNPs bearing CH with low DD value.

Chito-oligosaccharides with different values of DD and MW were prepared by enzymatic treatment of CH1-4 with endo-chitinase Chit33 from Trichoderma harzianum expressed in Pichia pastoris.[178] Briefly, CH (4% w/w) was solubilized in acetic acid 0.1M (1.0 L) and dialyzed against water until pH 5 was reached. After the dialysis, CH was treated with Chit33 (40 units) in 3.0 L flask at 45 °C for 5 days. Reactions were stopped increasing the temperature (80 °C for 10 min), followed by addition of NaOH (30 mL; 10 M, pH 9), centrifugation (4000 x g for 10 min) and filtration (0-45 µm and 0.22 µm). COS1-10 (**Table 2**, entries 17-26) were isolated using PES membranes (3000, 10000 and 30000 MWCO), dialyzed against distilled water to neutral pH and freeze dry. The hydrolytic activity of Chit33 and DD and yield values of COS1-10 (defined with respect to the total amount of recovered COS) are reported in **Table 2** COS1-10 were applied for the preparation of nanoparticles selecting OL on the basis of previously reported melting point and aggregation data. OL (12 g) in THF (0.5 L) was rapidly added to the appropriate COS (20 g) in deionized water (1.5 L) at 25 °C under gentle stirring. Acetic acid was not required as anti-solvent due to the high solubility of COS in water. Nanoparticles COS1-10/OLNPs formed instantaneously (**Figure 3.1**, Panel C) and were recovered by centrifugation (12100 rpm for 10 minutes) and freeze dry (**Table 2**; entries 17-26). The melting point of COS1-10/OLNPs increased by lowering the MW of the saccharide (see for example **Table 2**, entry 19 and entry 25 versus entry 21, and entry 26, the original DSC curves of COS1-10/OLNPs are in Supporting information S2; Figures S2.3) and was of the same order of magnitude than CH/OLNPs. In addition, low molecular weight COS aggregated more efficiently into nanoparticles (**Table 2**, entries 17, 19, 22 and 25 versus entries 18, 21, 24 and 26).

Table 2. Yield, ratio of components, melting point and DPPH scavenging activity (IC_{50}, μg/mL) of CH/KLNPs, CH/OLNPs and COS/OLNPs.

Entry	Lignin	CH	COS	DD%	Mw (KDa)	Mp (°C)[g]	Yield[c]	Ratio[d]	DPPH IC_{50} [μg/mL]
1	KL	-	-	-	6-7	59.46	96%	-	-
2	OL	-	-	-	1.51	67.78	96%	-	14.08
3	KL	CH5[a]	-	90	100-300	60.00	86%	1.29	-
4	KL	CH6[a]	-	75-85	50-190	59.10	83%	1.21	-
5	KL	CH7[a]	-	75	50-190	62.00	82%	1.20	-
6	KL	CH1[b]	-	57-80	53-64	45.30	88%	1.32	-
7	KL	CH2[b]	-	57-70	90	55.16	86%	1.30	-
8	KL	CH3[b]	-	64	171	57.30	82%	1.20	-
9	KL	CH4[b]	-	30	190	74.24	79%	1.15	-
10	OL	CH5[a]	-	90	100-300	66.50	88%	1.35	15.00 (43.44)[h]
11	OL	CH6[a]	-	75-85	50-190	59.70	85%	1.27	14.15 (42.53)[h]
12	OL	CH7[a]	-	75	50-190	67.09	84%	1.22	18.00 (45.32)[h]
13	OL	CH1[b]	-	57-80	53-64	77.01	92%	1.40	14.08 (42.34)[h]
14	OL	CH2[b]	-	57-70	90	60.00	88%	1.35	17.60 (42.46)[h]
15	OL	CH3[b]	-	64	171	66.97	83%	1.19	17.20 (43.72)[h]
16	OL	CH4[b]	-	30	190	66.97	81%	1.16	16.40 (41.52)[h]
17	OL	CH2	COS1 (33.3)[e][29.3][f]	57-70	3-10	67.22	95%	1.54	11.87 (39.44)[i]
18	OL	CH2	COS2 (14.6)[e][29.3][f]	57-70	>30	68.90	94%	1.52	12.80 (24.65)[i]
19	OL	CH1	COS3 (23.1)[e][39.0][f]	57-80	3-10	74.50	96%	1.56	11.08 (41.08)[i]
20	OL	CH1	COS4 (31.1)[e][39.0][f]	57-80	10-30	62.29	95%	1.51	12.05 (22.93)[i]
21	OL	CH1	COS5 (27.3)[e][39.0][f]	57-80	>30	60.50	92%	1.53	12.69 (24.05)[i]
22	OL	CH3	COS6 (46.2)[e][33.6][f]	64	3-10	63.99	95%	1.55	11.80 (20.54)[i]
23	OL	CH3	COS7 (31.1)[e][33.6][f]	64	10-30	61.53	93%	1.52	12.64 (20.12)[i]
24	OL	CH3	COS8 (33.3)[e][33.6][f]	64	>30	60.09	91%	1.49	11.80 (23.48)[i]
25	OL	CH4	COS9 (33.3)[e][58.4][f]	30	3-10	72.22	94%	1.55	11.64 (32.80)[i]
26	OL	CH4	COS10 (14.6)[e][58.4][f]	30	>30	61.03	89%	1.52	13.90 (49.30)[i]

[a] CH commercial sample. [b] CH fishery waste sample. [c] The yield was calculated as amount of recovered nanoparticles with respect to initial amount of lignin and saccharide. [d] The ratio is defined as gram of saccharide per gram of lignin. [e] Total yield expressed as %w/w of COS recovered from initial CH. [f] Percentage of hydrolytic activity for each type of CH with respect to 100% of hydrolytic activity (2.8U/mL) against chitin as reference. [g] Melting point calculated by DSC analysis. [h] IC_{50} [μg/mL] calculated by DPPH scavenging assay of CH1-7. [i] IC_{50} [μg/mL] calculated by DPPH scavenging assay of COS 1-10.

Morphological and dimensional analysis.

Scanning electron microscopy (SEM) images of CH/OLNPs are reported in **Figure 3.4** (Panel A). The SEM images of CH/KLNPs are reported in Supporting information S4; Figures S4.1. Nanoparticles showed a regular spherical shape with roughly aggregate of small clumps on the surface more pronounced in the case of samples bearing CH with high value of DD (**Figure 3.4**, Panel A; the second and third column, respectively). These clumps are fingerprint of the saccharide[221-223] and were not visible on the surface of nanoparticles produced from lignin alone (**Figure 3.4**, Panel A; first column). In addition, the presence of high DD chitosan (CH5/OLNPs and CH1/OLNPs, respectively) afforded nanoparticles with a lower aggregation state than CH4/OLNPs. The presence of holes on the surface of nanoparticles was explained taking into account the rush out effect of the solvent during the drying procedure.[224] COS3/OLNPs, COS9/OLNPs, COS5/OLNPs and COS10/OLNPs, were selected in order to cover different values of molecular weight and DD, and showed a morphology similar to CH/OLNPs (**Figure 3.4**, Panel C).

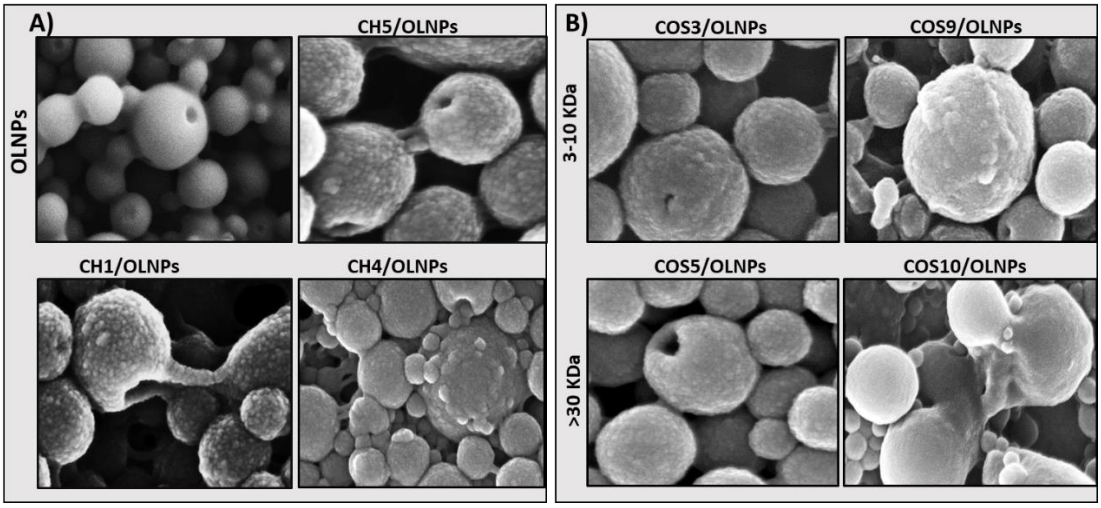


Figure 3.4. SEM images of CH/OLNPs and COS/OLNPs. Panel A: CH/OLNPs bearing CH with high DD (CH5/OLNPs and CH1/OLNPs) and low DD (CH4/OLNPs), respectively. Panel B: COS/OLNPs bearing COS with high DD (COS3/OLNPs and COS5/OLNPs) and low DD (COS9/OLNPs and COS10/OLNPs), respectively.

Dynamic light scattering (DLS) and zeta-potential values of CH1/OLNPs, CH4/OLNPs, CH5/OLNPs are reported in **Table 3** (entries 1-4) and the DLS and zeta-potential values of CH1/KLNPs, CH4/KLNPs, CH5/KLNPs are reported in Supporting information S4 (Table SI 4.2). CH/OLNPs inverted the zeta potential value with respect to OLNPs, probably due to the over-balancing of the original negative charge of lignin by the positive charge of the saccharide (**Table 3**, entries 2-4 versus entry 1).[109] CH5/OLNPs showed average diameter of the same order of magnitude than OLNPs, whilst CH1/OLNPs and CH4/OLNPs were larger than the reference, CH4/OLNPs having the highest value of poly-dispersion index (PDI). The presence of COS into nanoparticles do not revert the

zeta potential, COS/OLNPs showing negative values in the range between -26 mV and -54 mV (**Table 3**, entries 5-8), probably as a consequence of the absence of acetic acid as anti-solvent in their preparation. In addition, COS with low MW values favoured lower values of PDI (**Table 3**, entries 5-7).

Table 3. DLS and ζ-potential of CH/OLNPs and COS/OLNPs.

Entry	Sample	Size(nm)	PDI[b]	ζ-Potential (mV)
1	OLNPs	160	0,29	-45
2	CH1/OLNPs	566	0,46	+63
3	CH4/OLNPs	531	0,54	+48
4	CH5/OLNPs	149	0,18	+26
5	COS3/OLNPs (3-10 KDa)[a]	368	0,17	-39
6	COS5/OLNPs (>30 KDa)[a]	373	0,50	-26
7	COS9/OLNPs (3-10 KDa)[a]	218	0,20	-54
8	COS10/OLNPs (>30 KDa)[a]	594	0,49	-50

[a]Molecular Weight of COS. [b]Polydispersion index.

Antioxidant activity.

The antioxidant activity of CH/OLNPs and COS/OLNPs was evaluated by 2, 2'-diphenyl picrylhydrazyl (DPPH) radical scavenging assay (**Table 2**). The antioxidant activity of OLNPs, CH1-7, and COS1-10 alone were used as references (**Table 2**). Briefly, the appropriate sample was diluted at six different concentrations (in the range between 5.0 μg/mL and 500 μg/mL) and analysed by UV-visible spectrophotometry in ethanol-water mixture (60% v/v). The decrease in absorbance was determined at λ_{max} 517 nm by adding an aliquot of each sample (0.5 mL) in freshly prepared methanol solution of DPPH (2.5 mL, 0.25 mM) at 37 °C in the dark for 30 min. The kinetic of the process was evaluated for each concentration and the rate of DPPH remaining at the steady state estimated. The radical scavenging activity was expressed as the IC_{50} value (defined as the concentration of substrate in μg/mL that causes 50% loss of DPPH activity) as follow:

$$[(Abs_{control}-Abs_{sample})/Abs_{control}]x\ 100$$

Where '$Abs_{control}$' is the absorbance of the control. CH/OLNPs showed antioxidant activity lower, or of the same order of magnitude, than OLNPs (**Table 2**, entries 10-16), in CH/OLNPs both types of chitosan showed comparable antioxidant activity (**Table 2**, entries 10-12 versus entries 13-16), CH1/OLNPs showing the highest antioxidant activity (lowest value of IC_{50}). Conversely, COS/OLNPs were antioxidant more effective than OLNPs and COS alone, showing IC_{50} value similar to commercially available hydroxy benzyl toluene (BHT).[225] The occurrence of a synergistic effect between the lignin and saccharide components was evaluated by comparing the IC_{50} value of COS/OLNPs with that of the mixture of COS and OLNPs taken in the same relative amount they are embedded into nanoparticles. The ratio between these values is a measure of the occurrence of synergistic effect (ratio < 0.5) or, in alternative, simple additive effect (ratio >0.5)[226,227] between the two components. COS1/OLNPs, COS3/OLNPs and COS9/OLNPs showed a synergistic effect (**Table 4**), highlighting the beneficial role of low MW COS in the overall antioxidant activity.

Table 4. Determination of synergistic or additive antioxidant effect of lignin and saccharide for COS/OLNPs.

Entry	COS+OLNPs	IC_{50} [μg/mL][a]	Ratio (%)[b] (IC50 COSn/OLNPs: IC50COSn+OLNPs)	Effects [c]
1	COS1+OLNPs	25.00	0.47	Synergistic
2	COS2+OLNPs	13.57	0.94	Additive
3	COS3+OLNPs	27.00	0.41	Synergistic
4	COS4+OLNPs	12.10	0.99	Additive
5	COS5+OLNPs	13.04	0.97	Additive
6	COS6+OLNPs	12.70	0.93	Additive
7	COS7+OLNPs	12.75	0.99	Additive
8	COS8+OLNPs	12.10	0.97	Additive
9	COS9+OLNPs	24.20	0.48	Synergistic
10	COS10+OLNPs	21.40	0.66	Additive

[a] DPPH scavenging activity (μg/mL) of the mixture between COSn and OLNPs. [b] Ratio (%) between the IC_{50} value of **COS/OLNPs** (Table 1) and the IC_{50} value of the mixture of the two components. [c] Synergistic effect (ratio < 0.5) or, in alternative, simple additive effect (ratio > 0.5).

UV absorption properties.

The UV-absorption properties were determined by UV-visible analysis in the range between 210 nm and 600 nm (**Figure 3.5**, panel A-C and Supporting information S5, Figure S5). CH/OLNPs and CH/KLNPs showed UV-absorption capacity lower than OLNPs and KLNPs, respectively (**Figure 3.5**, Panel A and Supporting information S5; Figure S5, respectively), probably due to a detrimental effect exerted by chitosan in the supramolecular organization of the aromatic subunits of lignin. In a similar way, COS/OLNPs with high MW showed a decreased UV absorption capacity with respect to OLNPs (**Figure 3.5**, Panel B). Conversely, COS3/OLNPs, COS6/OLNPs and COS9/OLNPs, characterized by a low value of MW, showed UV-absorption capacity of the same order of magnitude (COS6/OLNPs), or higher than (COS3/OLNPs) OLNPs, respectively (**Figure 3.5**, Panel C). Note that, in the case of COS3/OLNPs, the UV-visible spectrum was characterized by hypsochromic shift of the λ_{max} with respect to native OLNPs, probably associated to the formation of H-aggregation state.[228]

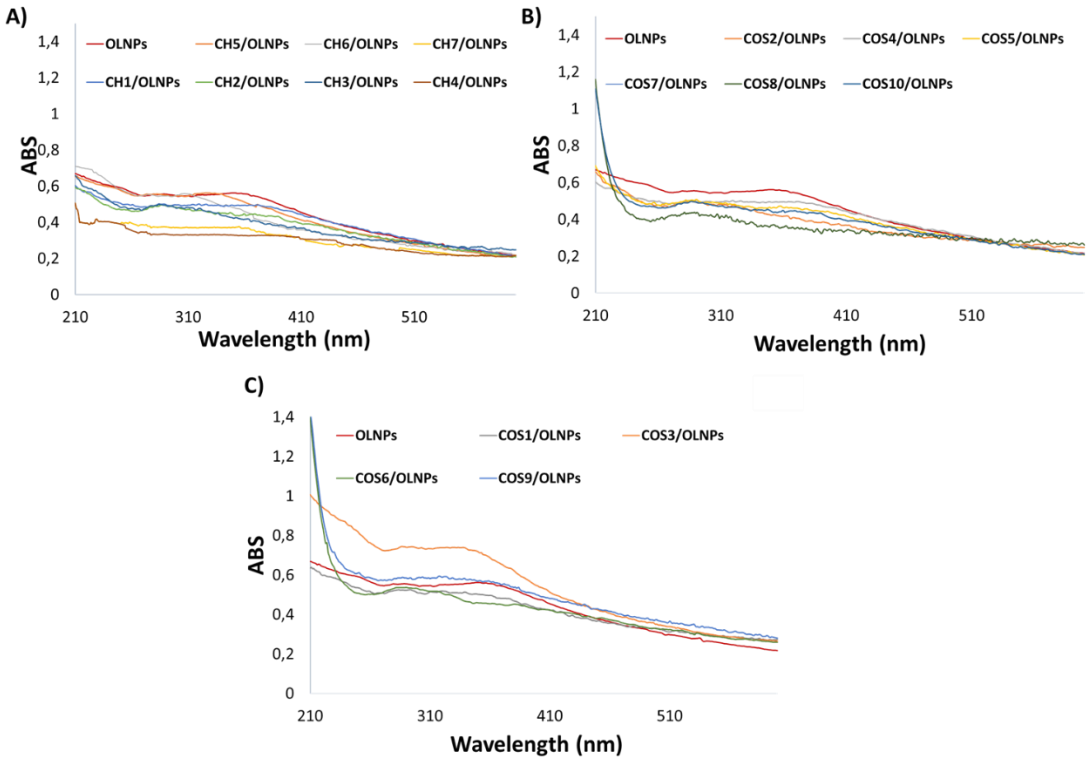


Figure 3.5. UV-absorbing capacity of CH/OLNPs and COS/OLNPs. Panel A: CH/OLNPs. Panel B: COS/OLNPs characterized by high MW saccharides. Panel C: COS/OLNPs characterized by low MW saccharides.

Antimicrobial Activity.

The antimicrobial activity of COS/OLNPs was determined against common foodborne pathogens, Gram-positive (Staphylococcus aureus) and Gram-negative (Escherichia coli), by evaluation of the bacteria doubling time when they were grown in nutrient broth (**Figure 3.6**, Panel A). As a general trend, low molecular weight COS/OLNPs were more active than CH/OLNPs and CH/KLNPs (Supporting information S6, Figure S6). This result is in accordance with data previously reported about the antimicrobial activity of free COS when compared with that of chitosan.[229] COS1/OLNPs, COS10/OLNPs and COS5/OLNPs showed the highest activity against E. coli, while COS1/OLNPs, COS7/OLNPs and COS3/OLNPs were more effective against S. *aureus*. On the basis of these data, we were not able to find a specific correlation between molecular weight/de-acetylation degree and inhibition in the case of E. *coli*, while S. *aureus* was selectively inhibited by low molecular weight and high de-acetylated COS. The minimum inhibitory concentration (MIC_{50}) is reported in **Figure 3.6** (Panel B). Among the samples tested, COS1/OLNPs was more active against E. *coli*, while COS7/OLNPs against S. *aureus*.

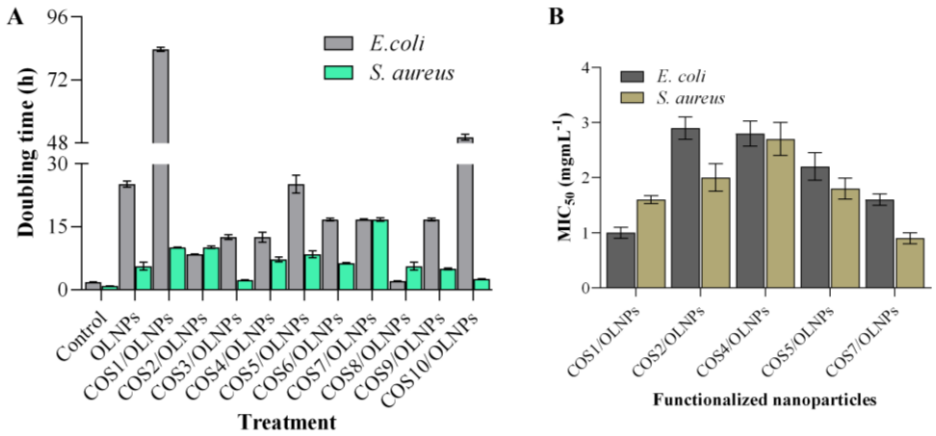


Figure 3.6. Antibacterial activity of COS1-10/OLNPs. Panel A: doubling time for the referred Gram-negative and Gram-positive bacteria. Panel B: minimum inhibitory concentration (MIC50) of COS1/OLNPs, COS2/OLNPs, COS4/OLNPs, COS5/OLNPs and COS7/OLNPs evaluated against E. coli and S. aureus. All the data included the standard error of the mean of three independent assays.

References

152- Poveda-Giraldo, J. A.; Solarte-Toro, J. C.; Cardona Alzate, C. A. The potential use of lignin as a platform product in biorefineries: A review. *Renewable Sustainable Energy Rev.* **2021**, 138, No. 110688.

153- Luzi, F.; Torre, L.; Kenny, J.; Puglia, D. Bio- and Fossil-Based Polymeric Blends and Nanocomposites for Packaging: Structure−Property Relationship. *Materials* **2019**, 12, 471.

154- Dessbesell, L.; Paleologou, M.; Leitch, M.; Pulkki, R.; Xu, C. Global lignin supply overview and kraft lignin potential as an alternative for petroleum-based polymers. *Renewable Sustainable Energy Rev.* **2020**, 123, No. 109768.

155- Hahladakis, J. N.; Velis, C. A.; Weber, R.; Iacovidou, E.; Purnell, P. An overview of chemical additives present in plastics: Migration, release, fate and environmental impact during their use, disposal and recycling. *J. Hazard. Mater.* **2018**, 344, 179−199.

156- Rhim, J. W.; Park, H. M.; Ha, C. S. Bio-nanocomposites for food packaging applications. *Prog. Polym. Sci.* **2013**, 38, 1629−1652.

157- Lambert, S.; Wagner, M. Environmental performance of biobased and biodegradable plastics: the road ahead. *Chem. Soc. Rev.* **2017**, 46, 6855−6871.

158- Mohamad Aini, N. A.; Othman, N.; Hussin, M. H.; Sahakaro, K.; Hayeemasae, N. Lignin as Alternative Reinforcing Filler in the Rubber Industry: A Review. *Front. Mater.* **2020**, 6, 329.

159- Pucciariello, R.; Villani, V.; Bonini, C.; D'Auria, M.; Vetere, T. Physical properties of straw lignin-based polymer blends. *Polymer* **2004**, 45, 4159−4169.

160- Nguyen, N. A.; Bowland, C. C.; Naskar, A. K. A general method to improve 3D-printability and inter-layer adhesion in lignin-based composites. *Appl. Mater. Today* **2018**, 12, 138−152.

161- Cao, Q.; Wu, Q.; Dai, L.; Shen, X.; Si, C. A well-defined lignin-based filler for tuning the mechanical properties of polymethyl methacrylate. *Green Chem.* **2021**, 23, 2329−2335.

162- Reza Barzegari, M.; Alemdar, A.; Zhang, Y.; Rodrigue, D. Mechanical and rheological behavior of highly filled polystyrene with lignin. *Polym. Compos*. **2012**, 33, 353−361.

163- Barzegari, M. R.; Alemdar, A.; Zhang, Y.; Rodrigue, D. Thermal Analysis of Highly Filled Composites of Polystyrene with Lignin. Polym. *Polym. Compos*. **2013**, 21, 357−366.

164- El-Zawawy, W. K.; Ibrahim, M. M.; Belgacem, M. N.; Dufresne, A. Characterization of the effects of lignin and lignin complex particles as filler on a polystyrene film. *Mater. Chem. Phys*. **2011**, 131, 348−357.

165- Hu, L.; Stevanovic, T.; Rodrigue, D. Unmodified and esterified Kraft lignin-filled polyethylene composites: Compatibilization by free-radical grafting. *J. Appl. Polym. Sci*. **2014**, 132.

166- Ebers, L.-S.; Arya, A.; Bowland, C. C.; Glasser, W. G.; Chmely, S. C.; Naskar, A. K.; Laborie, M. P. 3D printing of lignin: Challenges, opportunities and roads onward. *Biopolymers* **2021**, 112, 6.

167- Nguyen, N. A.; Meek, K. M.; Bowland, C. C.; Barnes, S. H.; Naskar, A. K. An Acrylonitrile−Butadiene−Lignin Renewable Skin with Programmable and Switchable Electrical Conductivity for Stress/Strain-Sensing Applications. *Macromolecules* **2018**, 51, 115−127.

168- Belgacem, M. N.; Blayo, A.; Gandini, A. Organosolv lignin as a filler in inks, varnishes and paints. *Ind. Crops Prod.* **2003**, 18, 145−153.

169- Khan, T. A.; Lee, J. H.; Kim, H. J. Lignin-Based Adhesives and Coatings. In Lignocellulose for Future Bioeconomy, **2019**; Vol. 17, pp 153−206.

170- Kalami, S.; Arefmanesh, M.; Master, E.; Nejad, M. Replacing 100% of phenol in phenolic adhesive formulations with lignin. *J. Appl. Polym. Sci.* **2017**, 134, 45124.

171- Piccinino D.; Capecchi E.; Tomaino E.; Gabellone S.; Gigli, V.; Avitabile, D.; Saladino, R. Nano-Structured Lignin as Green Antioxidant and UV Shielding Ingredient for Sunscreen Applications. *Antioxidants* **2021**, 10, 274.

172- Polinarski, M. A.; Beal, A. L. B.; Silva, F. E. B.; Bernardi-Wenzel, J.; Burin, G. R. M.; Muniz, G. I. B.; Alves, H. J. New Perspectives of Using Chitosan, Silver, and Chitosan−Silver Nanoparticles against Multidrug-Resistant Bacteria. *Part. Syst. Charact.* **2021**, 38, No. 2100009.

173- Liu, H.; Du, Y.; Wang, X.; Sun, L. Chitosan kills bacteria through cell membrane damage. *Int. J. Food Microbiol.* **2004**, 95, 147−155.

174- Goy, R. C.; Morais, S. T. B.; Assis, O. B. G. Evaluation of the antimicrobial activity of chitosan and its quaternized derivative on E. coli and S. aureus growth. *Rev. Bras. Farmacogn*. **2016,** 26, 122−127.

175- Liaqat, F.; Eltem, R. Chitooligosaccharides and their biological activities: A comprehensive review. *Carbohydr. Polym*. **2018**, 184, 243−259.

176- Silva, N. S. d.; Araújo, N. K.; Daniele Silva, A.; Oliveira, J. W.; Medeiros, J. M.; Araújo, R.; M Fernandes-Pedrosa, M.; et al. Antimicrobial Activity of Chitosan Oligosaccharides with Special Attention to Antiparasitic Potential. *Mar. Drugs* **2021**, 19, 110.

177- Tripathi, S.; Mehrotra, G. K.; Dutta, P. K. Chitosan based antimicrobial films for food packaging applications. *Polymers* **2021**, 8, 93.

178- Kidibule, P. E.; Santos-Moriano, P.; Plou, F. J.; Fernández-Lobato, M. Endo-chitinase Chit33 specificity on different chitinolytic materials allows the production of unexplored chitooligosaccharides with antioxidant activity. *Biotechnol. Rep.* **2020**, 27, e00500.

179- Behera, H. T.; Mojumdar, A.; Das, S. R.; Jema, S.; Ray, L. Production of N-acetyl chitooligosaccharide by novel Streptomyces chilikensis strain RC1830 and its evaluation for anti-radical, antiinflammatory, anti-proliferative and cell migration potential. *Bioresour. Technol. Rep*. **2020**, 11, No. 100428.
180- Kumar, A. The virtuous potential of chitosan oligosaccharide for promising biomedical applications. *Mater. Res.* **2020**, 35, 1225.
181- Abd El-Hack, M. E.; El-Saadony, M. T.; Shafi, M. E.; Zabermawi, N. M.; Arif, M.; Batiha, G. E.; Al-Sagheer, A. A.; et al. Antimicrobial and antioxidant properties of chitosan and its derivatives and their applications: A review. *Int. J. Biol. Macromol.* **2020**, 164, 2726−2744.
182- Eom, T. K.; Senevirathne, M.; Kim, S. K. Synthesis of phenolic acid conjugated chitooligosaccharides and evaluation of their antioxidant activity. *Environ. Toxicol. Pharmacol*. **2012**, 34, 519−527.
183- Asif, T.; Javed, U.; Zafar, S. B.; Ansari, A.; Qader, S. A.; Aman, A. Bioconversion of Colloidal Chitin Using Novel Chitinase from Glutamicibacter uratoxydans Exhibiting Anti-fungal Potential by Hydrolyzing Chitin Within Fungal Cell Wall. *Waste Biomass Valorization* **2020**, 11, 4129−4143.
184- Sohni, S.; Hashim, R.; Nidaullah, H.; Lamaming, J.; Sulaiman, O. Chitosan/nano-lignin based composite as a new sorbent for enhanced removal of dye pollution from aqueous solutions. *Int. J. Biol. Macromol*. **2019**, 132, 1304−1317.
185- Yang, W.; Fortunati, E.; Bertoglio, F.; Owczarek, J. S.; Bruni, G.; Kozanecki, M.; Puglia, D.; et al. Polyvinyl alcohol/chitosan hydrogels with enhanced antioxidant and antibacterial properties induced by lignin nanoparticles. *Carbohydr. Polym.* **2018**, 181, 275−284.
186- Ingtipi, K.; Moholkar, V. S. Sonochemically Synthesized Lignin Nanoparticles and its Application in the Development of Nanocomposite Hydrogel. *Mater. Today: Proc.* **2019**, *17*, 362−370.
187- Yang, W.; Owczarek, J. S.; Fortunati, E.; Kozanecki, M.; Mazzaglia, A.; Balestra, G. M.; Puglia, D.; et al. Antioxidant and antibacterial lignin nanoparticles in polyvinyl alcohol/chitosan films for active packaging. *Ind. Crops Prod*. **2016**, 94, 800−811.
188- Chai, Y.; Wang, Y.; Li, B.; Qi, W.; Su, R.; He, Z. Microfluidic Synthesis of Lignin/Chitosan Nanoparticles for the pH-Responsive Delivery of Anticancer Drugs. *Langmuir* **2021**, 37, 7219−7226.
189- Liu, Jinrong.; Moreno, Adrian.; Chang, Jian.; Morsali, Mohammad.; Yuan, Jiayin.; Mika, H. Sipponen Fully Biobased Photothermal Films and Coatings for Indoor Ultraviolet Radiation and Heat Management. *ACS Appl. Mater. Interfaces* **2022**, 14, 12693−12702.
190- Moreno, A.; Morsali, M.; Liu, J.; Sipponen, M. H. Access to tough and transparent nanocomposites via Pickering emulsion polymerization using biocatalytic hybrid lignin nanoparticles as functional surfactants. *Green Chem*. **2021**, 23, 3001−3014.
191- Moreno, A.; Sipponen, M. H. Biocatalytic nanoparticles for the stabilization of degassed single electron transfer-living radical pickering emulsion polymerizations. *Nat. Commun*. **2020**, 11, No. 5599.
192- Khan, A.; Goepel, M.; Lisowski, W.; Łomot, D.; Lisovytskiy, D.; Mazurkiewicz-Pawlicka, M.; Glaser, R.; Colmenares, J. C. Titania/chitosan−lignin nanocomposite as an efficient photocatalyst for the selective oxidation of benzyl alcohol under UV and visible light. *RSC Adv.* **2021**, 11, 34996.
193- Sánchez-Hernández, E.; Langa-Lomba, N.; González-García, V.; Casanova-Gascón, J.; Martín-Gil, J.; Santiago-Aliste, A.; Torres-Sánchez, S.; Martín-Ramos, P. Lignin−Chitosan Nanocarriers for the Delivery of Bioactive Natural Products against Wood-Decay Phytopathogens. *Agronomy* **2022**, 12, 461.
194- Piccinino, D.; Capecchi, E.; Delfino, I.; Crucianelli, M.; Conte, N.; Avitabile, D.; Saladino, R. Green and Scalable Preparation of Colloidal Suspension of Lignin Nanoparticles and Its Application in Eco-friendly Sunscreen Formulations. *ACS Omega* **2021**, 6, 21444−21456.
195- Leskinen, T.; Smyth, M.; Xiao, Y.; Lintinen, K.; Mattinen, M. L.; Kostiainen, M. A.; Oinas, P.; Österberg, M. Scaling Up Production of Colloidal Lignin Particles. *Nord. Pulp Pap. Res. J.* **2017**, 32, 586−596.
196- Mojumdar, A.; Upadhyay, A. K.; Raina, V.; Ray, L. A simple and rapid colorimetric method for the estimation of chitosan produced by microbial degradation of chitin waste. *J. Microbiol. Methods.* **2019**, 158, 66−70.
197- Gomes, L. C.; Faria, S. I.; Valcarcel, J.; Vázquez, J. A.; Cerqueira, M. A.; Pastrana, L.; Bourbon, A. I.; Mergulhão, F. J. The Effect of Molecular Weight on the Antimicrobial Activity of Chitosan from Loligo opalescens for Food Packaging Applications. *Mar. Drugs* **2021**, 19, 384.
198- Crestini, C.; Lange, H.; Sette, M.; Argyropoulos, D. S. On the structure of softwood kraft lignin. *Green Chem.* **2017**, 19, 4104−4121.
199- Sewsynker-Sukai, Y.; Naomi David, A.; Gueguim Kana, E. B. Recent developments in the application of kraft pulping alkaline chemicals for lignocellulosic pretreatment: Potential beneficiation of green liquor dregs waste. *Bioresour. Technol.* **2020**, 306, No. 123225.
200- Trubetskaya, A.; Lange, H.; Wittgens, B.; Brunsvik, A.; Crestini, C.; Rova, U.; Matsakas, L.; et al. Structural and Thermal Characterization of Novel Organosolv Lignins from Wood and Herbaceous Sources. *Processes* **2020**, 8, 860.
201- Vishtal, A.; Kraslawski, A. Challenges in industrial applications of technical lignins. *BioResources* **2011**, 6, 3547−3568.
202- Jardim, J. M.; Hart, P. W.; Lucia, L. A.; Jameel, H.; Chang, H. The Effect of the Kraft Pulping Process, Wood Species, and pH on Lignin Recovery from Black Liquor. *Fibers* **2022**, 10, 16.
203- Becker, J.; Wittmann, C. A field of dreams: Lignin valorization into chemicals, materials, fuels, and health-care products. *Biotechnol. Adv.* **2019**, 37, No. 107360.
204- Kalogiannis, K. G.; Matsakas, L.; Lappas, A. A.; Rova, U.; Christakopoulos, P. Aromatics from Beechwood Organosolv Lignin through Thermal and Catalytic Pyrolysis. *Energies* **2019**, 12, 1606.

205- Wyman, C. E.; Dale, B. E.; Elander, R. T.; Holtzapple, M.; Ladisch, M. R.; Lee, Y. Y. Coordinated development of leading biomass pretreatment technologies. *Bioresour. Technol.* **2005**, 96, 1959−1966.
206- Constant, S.; Wienk, H. L. J.; Frissen, A. E.; Peinder, P.; Boelens, R.; Bruijnincx, D. S.; P, C. A.; et al. New insights into the structure and composition of technical lignins: a comparative characterisation study. *Green Chem*. **2016**, 18, 2651−2665.
207- Mesfun, S.; Matsakas, L.; Rova, U.; Christakopoulos, P. Technoeconomic Assessment of Hybrid Organosolv−Steam Explosion Pretreatment of Woody Biomass. *Energies* **2019**, 12, 4206.
208- Lancefield, C. S.; Wienk, H. L. J.; Boelens, R.; Weckhuysen, B. M.; Bruijnincx, P. C. A. Identification of a diagnostic structural motif reveals a new reaction intermediate and condensation pathway in kraft lignin formation. *Chem. Sci.* **2018**, 9, 6348−6360.
209- Erdtman, H. Lignins: Occurrence, formation, structure and reactions. *J. Polym. Sci., Part B: Polym. Lett.* **1971,** 10, 228−230.
210- Gellerstedt, G. Softwood kraft lignin: Raw material for the future. *Ind. Crops Prod*. **2015**, 77, 845−854.
211- Nguyen, N. A.; Barnes, S. H.; Bowland, C. C.; Meek, K. M.; Littrell, K. C.; Keum, J. K.; Naskar, A. K. A path for lignin valorization via additive manufacturing of high-performance sustainable composites with enhanced 3D printability. *Sci. Adv.* **2018**, 4, 12.
212- Bhattacharyya, S.; Matsakas, L.; Rova, U.; Christakopoulos, P. Melt Stable Functionalized Organosolv and Kraft Lignin Thermoplastic. *Processes* **2020**, 8, 1108.
213- Mimini, V.; Sykacek, E.; Syed Hashim, S. N. A.; Holzweber, J.; Hettegger, H.; Fackler, K.; Rosenau, T.; et al. Compatibility of Kraft Lignin, Organosolv Lignin and Lignosulfonate With PLA in 3D Printing. *J. Wood Chem. Technol.* **2019**, 39, 14−30.
214- Chen, C. C.; Chueh, J. Y.; Tseng, H.; Huang, H. M.; Lee, S. Y. Preparation and characterization of biodegradable PLA polymeric blends. *Biomaterials* **2003**, 24, 1167−1173.
215- Rafiqah, S. A.; Khalina, A.; Harmaen, A. S.; Tawakkal, I. A.; Zaman, K.; Asim, M.; Nurrazi, M.; Lee, C. H. A Review on Properties and Application of Bio-Based Poly(Butylene Succinate). *Polymers* **2021**, 13, 1436.
216- Correlo, V. M.; Boesel, L. F.; Bhattacharya, M.; Mano, J. F.; Neves, N. M.; Reis, R. L. Properties of melt processed chitosan and aliphatic polyester blends. *Mater. Sci. Eng.* **2005**, 403, 57−68.
217- Wei, B.; Zhao, Y.; Wei, Y.; Yao, J.; Chen, X.; Shao, Z. Morphology and Properties of a New Biodegradable Material Prepared from Zein and Poly(butylene adipate-terephthalate) by Reactive Blending. *ACS Omega* **2019**, 4, 5609−5616.
218- Preety; Sharma, S.; Hooda, V. Purification and Analytical Application of Vigna mungo Chitinase for Determination of Total Fungal Load of Stored Cereals. *Appl. Biochem. Biotechnol.* **2018**, 186, 12−26.
219- Gieroba, B.; Sroka-Bartnicka, A.; Kazimierczak, P.; Kalisz, G.; Lewalska-Graczyk, A.; Vivcharenko, V.; Przekora, A.; et al. Spectroscopic studies on the temperature-dependent molecular arrangements in hybrid chitosan/1,3-β-D-glucan polymeric matrices. Int. J. Biol. *Macromol.* **2020**, 159, 911−921.
220- Nikpour, M. R.; Rabiee, S. M.; Jahanshahi, M. Synthesis and characterization of hydroxyapatite/chitosan nanocomposite materials for medical engineering applications. *Composites, Part B* **2012**, 43, 1881−1886.
221- Perchyonok, V. T.; Souza, J.; Küll, M. F.; Suzuki, T. Y. U.; Maluly-Proni, A. T.; Santos, P. H. Color stability and surface roughness of chitosan- and nanodiamond-modified bisacrylic resin. *Braz. Oral Res.* **2019**, 33, 24.
222- Cárdenas, G.; Anaya, P.; Del Rio, R.; Schrebler, R.; Von Plessing, C.; Schneider, M. Scanning electron microscopy and atomic force microscopy of chitosan composite films. J. Chil. *Chem. Soc* **2010**, 55, 352−354.
223- Fernández-Martín, F.; Arancibia, M.; López-Caballero, E.; Gómez-Guillén, C.; Montero, P.; Fernández-García, M. Preparation and Molecular Characterization of Chitosans Obtained from Shrimp (Litopenaeus vannamei) Shells. J. *Food Sci.* **2014**, 79, E1722−E1731.
224- Li, H.; Deng, Y.; Liu, B.; Ren, Y.; Liang, J.; Qian, Y.; Zheng, D.; et al. Preparation of Nanocapsules via the Self-Assembly of Kraft Lignin: A Totally Green Process with Renewable Resources. *ACS Sustainable Chem. Eng.* **2016**, 4, 1946−195.
225- Piccinino, D.; Capecchi, E.; Botta, L.; Bizzarri, B. M.; Bollella, P.; Antiochia, R.; Saladino, R. Layer-by-Layer Preparation of Microcapsules and Nanocapsules of Mixed Polyphenols with High Antioxidant and UV-Shielding Properties. *Biomacromolecules* **2018**, 19, 3883−3893.
226- Hsieh, M. H.; Hsieh, M. J.; Wu, C. R.; Peng, W. H.; Hsieh, M. T.; Hsieh, C. C. The Synergistic Effect of Antioxidant Interaction between Luteolin and Chlorogenic Acid in Lonicera japonica. *BioRxiv*, **2018**, 418319.
227- Xu, X.; Li, F.; Zhang, X.; Li, P.; Zhang, X.; Wu, Z.; Li, D. In Vitro Synergistic Antioxidant Activity and Identification of Antioxidant Components from Astragalus membranaceus and Paeonia lactiflora. *PLoS One* **2014**, 9, e96780.
228- Deng, Y.; Feng, X.; Yang, D.; Yi, C.; Qiu, X. Pi-Pi stacking of the aromatic groups in lignosulfonates. *BioResources* **2012**, 7, 1145−1156.
229- Benhabiles, M. S.; Salah, R.; Lounici, H.; Drouichea, N.; Goosen, M. F. A.; Mameri, N. Antibacterial activity of chitin, chitosan and its oligomers prepared from shrimp shell waste. *Food Hydrocolloids* **2012**, 29, 48−56

CHAPTER 4

COSMECEUTICAL APPLICATIONS OF LIGNIN NANOPARTICLES

4.1 Nano-Structured Lignin as Green Antioxidant and UV Shielding Ingredient for Sunscreen Applications (Review)

4.1.1 Aim of work

Drawbacks of Current Antioxidant and UV Shielding Ingredients in Sunscreen Formulations.

The harmful consequences of prolonged exposure of human skin to sunlight have long been explored.[230] UV radiation (190–400 nm) is the main cause of generation of radical reactive oxygen and nitrogen-centered species and related oxidative stress. Radicals are responsible for lipid peroxidation and degradation of elastin and collagen, promoting both loss of skin elasticity and aging.[231] In addition, they react with DNA promoting apoptosis, genetic mutation, and cancer.[232] In this latter case, the radical damage is related to melanoma, the most aggressive form of skin cancer, arising from melanocytes resistant to chemotherapy.[233,234] Sunscreen formulations are designed to protect the skin from solar radiation and possibly from melanoma. They contain active ingredients capable of absorbing (organic chemical filters, OCFs) or reflecting (physical mineral filters, PMFs) the UV radiation. PMFs are generally used as nanoparticles since the nanoscale improves the reflectance activity, as well as the consumer cosmetic acceptance.[235] In a typical high sun protection factor (SPF) sunscreen, the final concentration of PMFs and OCFs can reach 45% by weight.[236] In addition, UV boosters are used to further increase the SPF by physical effect, tuning the ratio between the UV shielding efficiency and the total UV filter concentration.[237] UV boosters are usually composed of plastic micro-sized spheres from petroleum origin, such as styrene/acrylate copolymers, that are well recognized as a waste in water pollution.[238] High amounts of PMFs, OCFs, and UV boosters, are detected in marine environments[235] as a consequence of their release from cosmetics, producing submicronic aggregates in freshwater, or alternatively, sediment settles in seawater.[239] Consequently, the growing consumption of sunscreens has gradually led to a significant increase in coastal pollution with a deleterious impact on marine organisms.[240] 3-Benzylidene-camphor (3-BC) and 3-(4-methyl benzylidene)camphor (4-MBC), which belong in the OCFs family, induce severe and fast coral bleaching, altering the symbiosis between coral and zooxanthellae, and inhibiting the reproduction of both oligochaete Lumbriculus variegatus[238] and marine phytoplankton.[241] Moreover, they are concentrated in tissues of aquatic organisms (mussels, crustaceans, eels, fishes, marine mammals, and pelagic birds) due to the high lipophilicity.[242] In a similar way, PMFs are harmful to marine ecosystems. Zinc oxide nanoparticles contributed significantly to the whitening of the Acropora spp.[243], and titanium oxides negatively affect dinoflagellates, fish, algae, and marine invertebrates.[244] Risks for human health are also associated to UV filters[245] as a consequence of phototoxic and photoallergic responses and, in the long term, photoaging and cell damage.[246] The absorbance spectrum of OCFs changes during the UV exposure time as a consequence of structural transformation and degradation processes.[247] These processes can produce free radicals and interaction with other sunscreen ingredients and skin constituents (e.g., lipids, proteins, and nucleic acids), altering the absorbing property of the sunscreen and inducing oxidative damage.[248] Avobenzone (AVOB), that is a widely recognized OCF in commercial sunscreens, demonstrated photo instability after prolonged UV exposure to yield radical photoproducts (**Figure 4.1A**),[249] and octyl methoxycinnamate (OMC), the most used UV-B filter, is photo-unstable after exposure to sunlight, undergoing photodimerization and loss of shielding efficiency. In this latter case, the photoproducts 4-methoxy

benzaldehyde (4-MBA) and 2-ethylhexanol (2-EH) are also produced (**Figure 4.1B**).[250,251] Moreover, benzophenone-3 (BP-3), and octocrylene (OC) are able to penetrate in the epidermal nucleated layers generating in situ radical species after UV irradiation.[252]

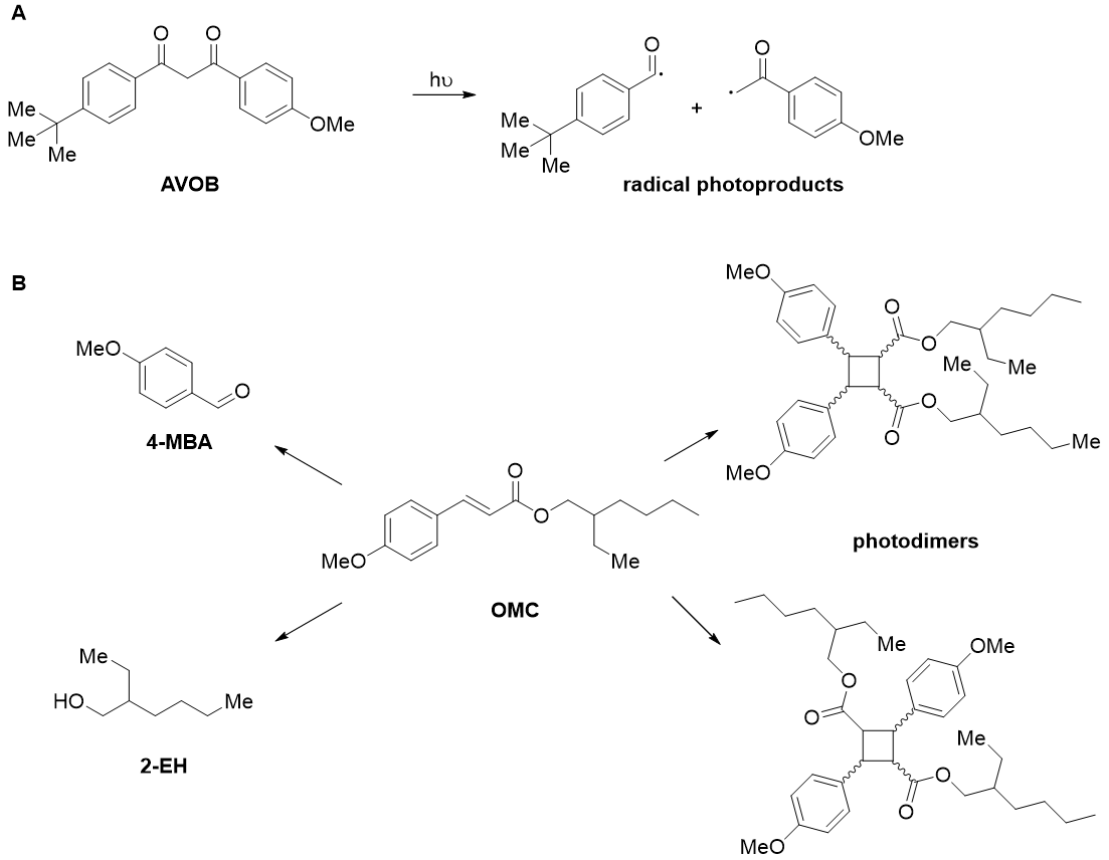


Figure 4.1. Schematic representation of photodegradation processes operative in the case of avobenzone (AVOB) (**A**) and octyl methoxycinnamate (OCM) (**B**).

Despite photodegradation and generation of radicals, OCFs cause other drawbacks for human health. For example, AVOB promotes obesogenic phenotypes in normal human epidermal keratinocytes (NHEKs), increasing the gene transcription of peroxisome proliferator-activated receptor (PPAR) and fatty acid-binding protein,[253] and affecting diabetes[254] with disruptive endocrine effects.[255] The toxic effect of some of the most representative OCFs are summarized in **Table 5**.

Table 5. Toxic effects of some of the most representative OCFs applied in sunscreen formulations.

OCFs	UV Range	Photodegradation	Toxic Effects
AVOB	357	yes	Suppression of human trophoblast cells and apoptosis mediated by mitochondrial disruption,[256] induction of obesogenic phenotypes,[257] and hormone-like activity.[258]
HS	295–315	no	Skin penetration,[259] disrupts estrogen.[260]
OMC	280–355	yes	Skin penetration, hormone like-activity; reproductive system, thyroid, and behavioral alterations in animal studies[246]
OB	270–350	yes	Estrogenic activity, alteration of sperm production in the animal associated with endometriosis in women.[261]

AVOB: avobenzone. HS: homosalate. OMC: octyl methoxycinnamate. OB: oxybenzone

Alternative UV Shielding and Antioxidant Ingredients in Sunscreen Formulations

The use of PMFs and OCFs is regulated by directives from different agencies, such as the Food and Drug Administration (FDA) and the European Chemicals Agency, in order to adequate the UV protection to minimal side effects for health.[262] The use of alternative eco-friendly and natural ingredients, deprived of toxic effects, is strongly recommended and foreseen in future formulations. The toxicity and pollution effects of actual commercial UV filters increased the interest for eco-friendly and natural alternatives.[263] Their use is considered an advantage not only for the ability to improve the SPF value in safer formulations, but also in improving the photostability of traditional UV filters.[264] Secondary metabolites of the cell, such as terpenoids and products of the shikimic acid and polyketide pathways, can play a relevant role bearing conjugated double bonds and aromatic pharmacophores with high UV absorbing and antioxidant properties.[265] They have been selected during molecular evolution by plants and microorganisms in developing defence strategies to minimize the damage of UV radiation and chemical oxidative stresses.[266-268] Sunscreen formulations containing mixtures of secondary metabolites from plants, algae, and fungi, as well as from cyanobacteria,[269] showed a higher shielding effect with respect to commercial filters. In addition, mycosporins and mycosporin-like amino acids (MAAs)[270] produced by marine phototrophs (dinoflagellates, cyanobacteria, and macro algae)[271] are able to convert radiative energy in thermal energy without generation of radical species.[272] Sunscreen formulations containing MAAs from *Porphyra umbilicals* showed a high protective effect on fibroblasts and keratinocytes exposed to UV-A.[273] Mixtures of secondary metabolites from the spent fraction of coffee grounds and green coffee oil (GCO) have a synergistic effect with traditional OCFs and increase the SPF value of sunscreen formulations (+20%).[274] The protective effect from UV-B exposure by grapes wine extract of Jacquez (namely JW-E), containing high level of proanthocyanidins, anthocyanins, and hydroxycinnamic acids, has been evaluated by three-dimensional tissue cell model of the human epidermis.[275] Finally, the water resistance of OCFs is improved by natural waxes that stabilize the SPF value of sunscreen formulations after immersion in water.[276] Waxes also increase the SPF value and improved the photostability of OCFs and PMFs after UV irradiation.[264] Despite exhibiting strong sun protection effect, most crude plant extracts are insoluble in water, thus hindering their practical applications.

4.1.2 Results and discussions

Lignin as a Novel Eco-Friendly Sunscreen Ingredient

The development of sunscreen formulations based on renewable and recyclable resources received a great interest, mainly due to circular economy and green chemistry concerns. In this context, lignin, the most abundant polyphenol in nature, is increasingly becoming one of the main protagonists since it is recovered in large amounts as a low-cost waste from pulp and paper industry and biorefinery.[24] The low environmental impact of lignin extraction and purification technologies has been reported and discussed, focusing on the expected benefits of lignin as a high added value material.[277-279] Current and potential application of lignin has been reviewed,[280-283] focusing on power fuel and syngas production (Fischer–Tropsch synthetic fuels), material science and fine-chemicals, specialties, and commodities preparation.[284,285] Lignin confers rigidity and microbiological and mechanical resistance to lignocellulosic materials.[286] In addition, it shows low-medium UV-shielding,[287] antioxidant activities[288,289] and biocompatibility.[290] The lack of toxicity of lignin has been reported by in vivo toxicity assessment in embryonic zebrafish (*Danio rerio*).[291] The efficacy of lignin as an alternative sunscreen

ingredient depends on its origin and composition, as well as from the structural order and dimensional scale.[292] The main lignin functions in sunscreen cosmetics are summarized in **Table 6**. The next paragraphs will report about these specific aspects.

Table 6. Cosmetic and cosmeceutical application of lignin.

Lignin Property	Petroleum Derived Compounds Substituted by Lignin	Ref
Antioxidant	BHT, BHA	[293]
UV booster	acrylates/c10-30 alkyl acrylate cross-polymer	[294]
Antimicrobic agent	phenoxyethanol, hydroxybenzoates and triclosan	[295]
Chelating agent	EDTA, THPE	[296]
Emulsifier and stabilizer	acrylamides salts	[297]

BHT: butylated hydroxytoluene; BHA: butylated hydroxyanisole, EDTA: ethylenediaminetetraacetic acid; THPE: tetrahydroxypropyl ethylenediamine.

Structure, Availability, and Green Application of Lignin

Lignin is an important source of phenolic compounds.[298] It is one of the main components in the plant cell wall beside cellulose, hemicellulose, pectin, and extractives. This polymer is biosynthesized by a cascade of oxidative radical couplings, involving three phenylpropanoid monomers (monolignols), namely para-hydroxyphenyl (H), syringyl (S), and guaicyl (G) alcohols (**Figure 4.2A**).[299] These compounds differ in the degree of methoxylation of the aromatic ring and are present in the polymer in a different ratio depending on the plant species considered.[286] The biosynthesis of monolignols starts in the cytoplasm, from which they are successively transported to the apoplast and delivered in different zones of the secondary area (central lamella and secondary wall of the xylem).[300,301] The physiological significance of this distribution is apparently simple: differential targeting allows for the construction of lignified cell walls with distinct biophysical properties.[302] The first step of the lignification process is the dehydrogenation of monolignols to corresponding phenoxy radicals plant cell-wall oxidases (lignin-peroxidase LiP, manganeseperoxidase MnP, hybrid LiP-MnP, versatile-peroxidase VP, and laccase).[299] Monolignols form a network of inter-unit linkages to yield relatively low molecular weight oligomers involved in the formation of stable supramolecular π-π aggregates into a complex 3D molecular architecture.[303] The main types of inter-unit linkages are the alkyl-aryl ether β-O-4, phenylcoumaran (β-5), 1,2-diaryl-propane (β-1), diaryl (5-5), diaryl ether (4-O-5), pinoresinol (β-β), and dibenzodioxin structural residues (**Figure 4.2B**). Lignin is classified into three basic types depending on the number and quality of subunits: softwood, hardwood, and grass lignin (**Table 7**). In addition, some unconventional types of structural motif, such as caffeyl lignin units (C-lignin), were also found.[304]

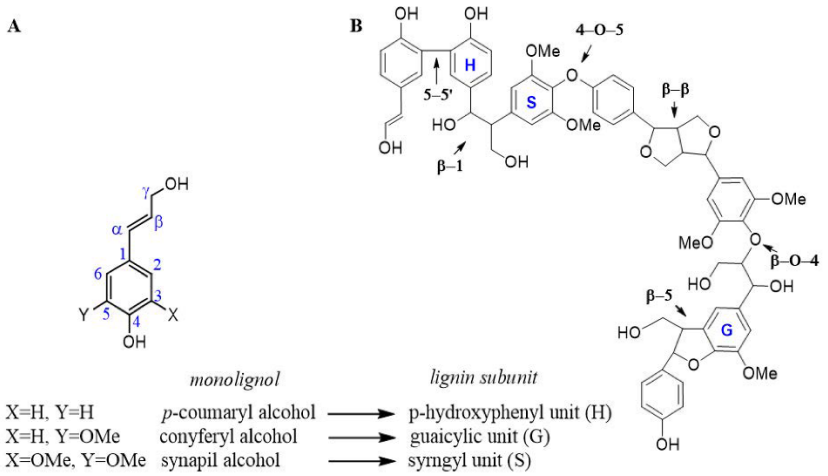


Figure 4.2. Chemical structure of the main components in lignin. (A) Monolignols; (B) representation of the main type of inter-units in lignin.

Table 7. Classification of different types of lignin depending on the amount of para-hydroxyphenyl (H), guaiacyl (G), and syringyl (S) sub-units.

Type	Grass Lignin	Softwood	Hardwood
H	5–35%	<5%	0–8%
G	35–80%	>95%	25–50%
S	20–55%	0%	% 45–75%

Proportion of different monolignols in lignin of different plants source. Adapted from [305–307].

Different technologies are available to separate wood components, and they can be classified depending on the scale of the treatment.[308] At the analytical scale (from mg to gram), milled wood lignin (MWL) is considered the most reliable model of native lignin. MWL is produced from wood chips by extraction with 1,4-dioxane and successive precipitation in water.[309] At the industrial scale (ton scale), two main types of lignin are prevailing: sulfur-containing lignin and sulfur-free lignin. Sulfur-containing lignin include lignosulfonate (LS) and kraft lignin (KL), which are produced in a strong alkaline and oxidative medium. The second category includes soda lignin (SL), organosolv lignin (OL) ionic liquid lignin (ILL), and steam-exploded lignin (SEL).[310] Sulfur-free lignins have been applied in the production of probiotics for animals due to their capacity to improve the growth of beneficial bacteria,[311,312] influencing the absorption of bile acids in the lipid metabolism.[313,314] In addition, LS is used as a binder, dispersing agent, emulsifier, and heavy metal sequestrant in the design of advanced materials and wastewater treatment, as in the case of absorption of toxic chromium, copper, cadmium, lead, zinc, nickel, cobalt, and mercury ions.[315] From the biological point of view, KL and SEL showed antioxidant activity in preserving human red blood cells.[316] This activity was associated to non-etherified phenolic hydroxyl groups, ortho-methoxy groups, and aliphatic hydroxyl groups in the side chain. In particular, ortho substituents, such as methoxy groups, stabilize phenoxy radicals by resonance and hinder their propagation. Conjugated double bonds can also improve the antiaging activity by extensive electronic delocalization. In some cases, the antioxidant activity was associated to antiviral,[317] antimicrobial, and anticancer properties.[318]

The Technology for the Self-Assembling of Lignin Nanoparticles

The low solubility of lignin represents a limit for its application in the cosmetic and cosmeceutical formulations.[319] This bias can be solved by the self-assembly of the native polymer into highly ordered lignin nanoparticles (LNPs).[78] LNPs are characterized by improved chemical and physical properties compared to the native state.[85] Their size tunability and spherical shape allowed to broaden the fields of application, encompassing drug delivery systems,[93] flame retardant[320] and reinforcing materials,[321] and waste treatment.[322] Remarkably, LNPs show improved UV shielding[85] and antioxidant properties[323] (see next paragraph). **Table 8** reports the major technologies available for the production of LNPs, the relative experimental conditions, and some of their specific applications. Briefly, the following technologies have been reported for the preparation of LNPs: (i) solvent exchange precipitation method where the starting solvent was slowly replaced by an anti-solvent by dialysis; (ii) treatment of lignin solution by adding strong acid; (iii) aerosol flow reactor equipped with collision-type jet atomizer; (iv) microchannel reactor in which the lignin solution is continuously mixed with the antisolvent; (v) CO_2 compressed fluid as antisolvent; (vi) flash-precipitation by fast adding of anti-solvent in lignin solution; and (vii) mini-emulsion between oil-phase and aqueous lignin solution under ultrasound treatment followed by polymerization with cross-linker agent. The formation of LNPs is influenced by different experimental parameters, including the physical properties of the medium (solvent, pH, temperature, stirring speed), and the chemical structure of the starting substrate (composition, molecular weight, polarity, and impurities). Among them, the pH value controls the ionization of the phenolic moieties, which in turn affect inter- and intra-molecular electrostatic interactions in the polymer. Recent studies based on light scattering analysis and pulse field gradient NMR, showed that the KL self-association process occurs below pH 9.0–11.5, the process being more efficient in water than in organic solvents.[324] In addition, a low value of temperature favours the aggregation,[325] and a combined effect of temperature and pH can finely control the particle dimension.[326] As a general trend, softwood lignins show a higher degree of aggregation with respect to the hardwood counterpart, suggesting the greater presence of efficient intermolecular HOMO-LUMO interactions.[327] The structuration process of LNPs is driven mainly by noncovalent interactions, including H-bonding, van der Waals forces, and π-π stacking aggregation between the aromatic rings of different molecules.[328] Although no studies have been carried out on the specific role played by H-bonding in the self-assembly of lignin, this is commonly cited as a relevant contributing interaction due to its directional nature.[329,330] In accordance with this hypothesis, the formation of H-bonding network affects the mechanical properties of KL gels.[331] The specific role of the Van der Waals forces in tuning the macro-syneresis of KL gel has been also reported.[332]

Table 8 Major technologies available for the production of LNPs.

Lignin	Tech.	Size (nm)	pH	Shape	Advantages	Application(s)	Limits	Ref
SL	SEP	50-250	7	S	no aggregation	drug delivery and stabilizer	toxic chemicals	[333, 334]
SL	AP	50–250	>7	I	-	drug delivery, bioplastic	-	[337, 335]
AL	AFR	30–100	<12	S	high yield	bioplastic	aggregate	[83,336,338]
AL	AP	30–100	<12	S	high stability	sunscreen	high ionic strength	[87]
AL	MR	30–100	<12	S	dispersibility	antioxidant, antimicrobial	toxic chemicals	[339, 340]

AL	SEP	30–100	<12	S	-	antioxidant, antimicrobial	toxic chemicals	[87,50]
KL	AFR	38–250	4–12	I	stability	adhesives	-	[336, 341]
KL	PCA	38–250	4–12	S	high solubility	commodities	high ionic strength	[344, 104]
KL	FP	38–250	4–12	S	UV-shielding	materials	-	[336, 342]
KL	MP	38–250	4–12	S	-	commodities	-	[336, 342]
OL	AFR	30–250	3.5–8	S	high yield	adhesives	aggregate	[336, 339,341]
OL	FP	30–250	3.5–8	S	stability	commodities	high ionic strength	[342]
OL	SEP	30–250	3.5–8	S	stability	materials	toxic chemicals	[338]

S: spherical shape. I: irregular shape. SEP: solvent exchange precipitation. AP: acid precipitation. AFR: aerosol flow reactor. MR: microchannel reactor. PCA: compressed fluid antisolvent technique. FP: flash-precipitation. MP: mini-emulsion polymerization.

Antioxidant Activity

Radical species take part in various degenerative processes, including aging and inflammatory response triggered by UV exposure.[343] For this reason, antioxidants are common ingredients in sunscreen formulations.[344] Lignin shows antioxidant activity due to the presence of the phenolic pharmacophore able to scavenge reactive radical species with formation of highly stabilized mesomeric forms. **Figure 4.3** describes the main phenolic subunits responsible for the radical scavenger activity. Phenolic hydroxyl groups, *ortho*-methoxy groups, and aliphatic hydroxyl groups play a crucial role in this activity. In particular, ortho substituents, such as the methoxy groups, stabilize phenoxy radicals by both resonance and steric hindrance effects.

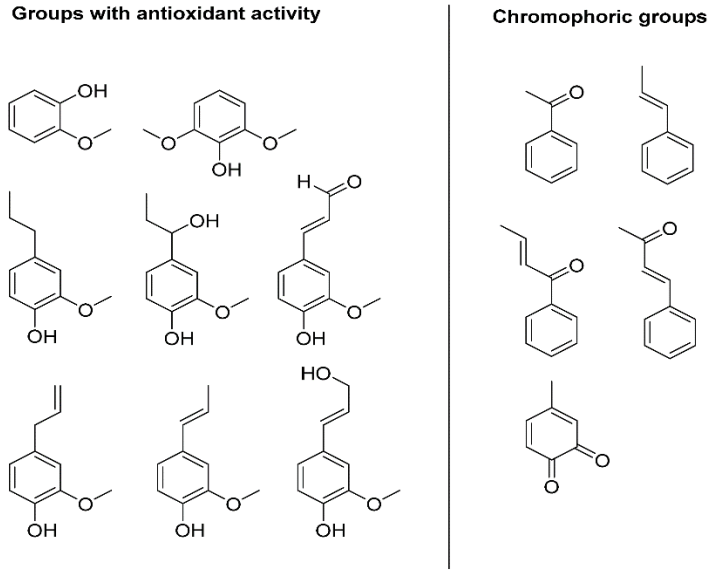
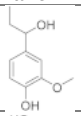
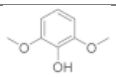
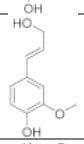
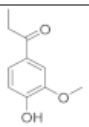
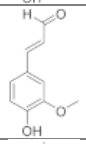
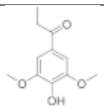
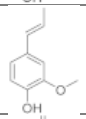
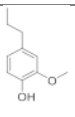
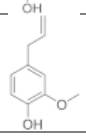


Figure 4.3. Classification and structural representation of lignin sub-units with antioxidant activity and chromophoric groups.

The demethylation process of these groups, as well as the presence of conjugated double bonds, further increase the antioxidant activity by increasing the total amount of OH and favouring extensive electronic delocalization. **Table 9** reports the antioxidant activity of

a panel of low molecular weight compounds commonly considered as simplified models of lignin, as evaluated by the DPPH assay.[327] As a general trend, the antiradical power (ARP; defined as the reverse of the dose inhibiting the 50% of the DPPH radical) and the number of reduced DPPH units (NRD; which represents the moles of DPPH reduced per mole of compound) show that syringyl-like derivatives have higher antioxidant activity than guaiacyl and para-hydroxy phenyl counterparts (**Table 9**, entry I versus entry II). In addition, lower values of ARP and NRD were observed when a carbonyl moiety was present in the phenylpropanoid side-chain (**Table 9,** entry III, IV), while the presence of a conjugated double bond system increased the antioxidant activity (**Table 9**, entry VII, VIII, IX, and X).[345] In addition to the capacity of sequestering radical species, lignin is promising to inhibit lipid peroxidation and, from a general point of view, the oxidative degradation of other cosmetic ingredients. For example, the ability of KL to inhibit the undesired radical production by PMFs (e.g., TiO_2) in sunscreen formulations has been demonstrated.[346] Interestingly, the antioxidant activity of LNPs was different order of magnitude higher than that of native lignin.[85,347] This behaviour can be explained by the higher density of phenolic and carboxylic groups on the surface of LNPs with respect to the native polymer,[348] as well as by the occurrence of favourable electron transfer processes between the ordered π-π stacked aromatic moieties.[340] In order to further increase the antioxidant activity, LNPs with mixed adsorbed polyphenols were prepared, highlighting the synergistic effects among the components.[225] The application of LNPs as UV filter or, alternatively, UV booster in broad-spectrum sunscreen formulations has been explored,[349,90,350] confirming the beneficial role of lignin when used in the nanoscale form.

Table 9. Antioxidant activity comparison of main lignin subunit.

#	Name	Structure	ARP [a]	NRD [b]	#	Name	Structure	ARP	NRD
I	Guaiacol		2.6	1.3	VI	Guaiacyl propanol-1		3.0	1.5
II	Syringol		3.6	1.8	VII	Coniferyl alcohol		4.2	2.1
III	Guacyl propanone-1		0.2	<0.1	VIII	Coniferyl aldehyde		1.9	0.97
IV	propiosyringone		0.5	0.2	IX	Isoeugenol		2.2	1
V	Propyl guaiacol		3.5	1.75	X	Eugenol		4	2

[a] ARP: antiradical power, reverse of the dose inhibiting the 50% of the DPPH radical. [b] NRD: number of reduced DPPH units, moles of DPPH reduced per mole of compound.

UV Shielding Activity

The Sun emits electromagnetic radiation in three ultraviolet (UV) wavelength areas. Rays with the shortest wavelength (UV-C, 100–290 nm) are captured by atmosphere, UV-A radiation at medium wavelength (UVA, 290–320 nm) and longer wavelength (UV-B,

320–400 nm) reach the surface of Earth. Excessive exposure to UV-B causes sunburn, while UV-A penetrates deeper into the skin. Both UV-A and UV-B are causing agents for DNA damage and cancer.[351] Lignin shows a broad absorption range in the UV region due to the presence of different chromophores and auxochromic groups (**Figure 4.3**), the maximum of absorbance being located at 283 nm.[352,353] Auxochromic groups (from ancient Greek αὐξάνω auxanō "increase" and χρῶμα chrōma "color") are groups of atoms bearing non-bonding electrons (OH, OCH_3, NH_2, CO, SH, and SCH_3) able to increase the chromophore effect. The contribution of auxochromic groups in lignin to generate a bathochromic effect (redshift phenomena) is reported[354] (**Figure 4.4**). LNPs are characterized by improved UV-shielding properties in relation to the native counterpart. For example, KL nanoparticles showed a higher absorption efficacy (up to 30%) than native KL, associated to the presence of a larger absorption band in the region of the longest wavelengths.[85,355] This effect is mainly due to the occurrence of π-π stacking interactions between the aromatic moieties, that can form two main types of aggregates, namely sandwich-type (H-orientation) and head-to-tail (J-orientation) aggregates. The J-orientation (water media) is the most efficient to decrease the energy gap for the π-π* electronic transition, thus enhancing the absorption efficacy of UV photons.[356] In addition, charge transfer complexes between electron-donating phenolic groups and electron acceptor ortho-quinones moieties can further increase the UV photo-absorbing capacity of LNPs.[357]

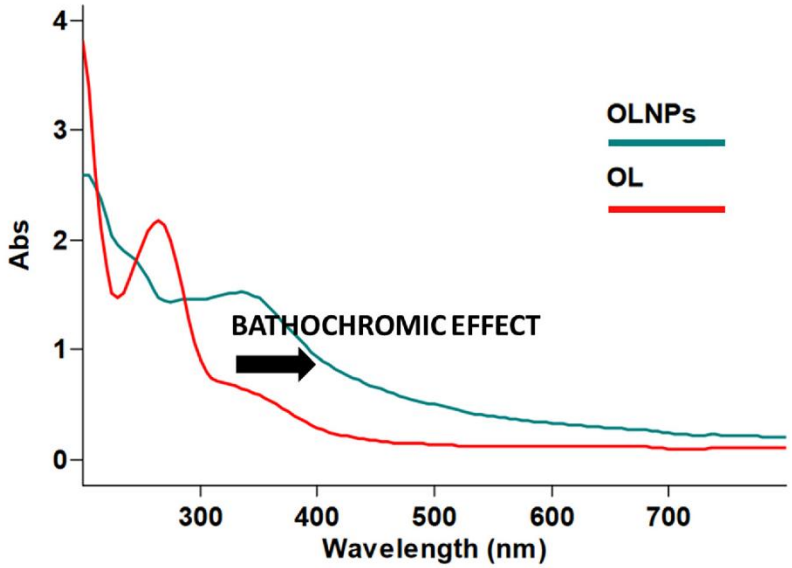


Figure 4.4. UV-VIS assay to evidence of bathochromic effect of organosolv lignin nanoparticles (OLNPs; green line) after the nanostructuration of starting technical organosolv lignin (OL; red line).

Notably, experimental data highlighted that the UV-absorbing capacity of lignin increases during the exposition to radiation as a consequence of the formation of novel chromophores, such as quinonoid units.[358] The negative charged surface of LNPs can be further functionalized by consecutive deposition of natural macromolecules or polyelectrolytes with opposite charge by the layer-by-layer technique (LbL).[130,132] In this way, mixed LNPs containing layers of other natural polyphenols, such as tannic acid, showed enhanced UV shielding properties, by occurrence of a synergistic effect between

the aggregate polymers.[339] Finally, the cavity of LNPs can be exploited for the physical encapsulation of both OCFs and PCFs to yield functionalized LNPs with UV shielding properties higher than the parent compounds. One example of this strategy is represented by the encapsulation of TiO_2 inside lignin-based colloidal nanoparticles to afford a stable UV filter deprived of undesired side-chain catalytic effect in the generation of radical species.[359]

Other Physical and Chemical Properties of LNPs Useful in Sunscreen Formulation. LNPs are characterized by a large panel of physical and chemical properties useful for the design of sunscreen formulations, encompassing emulsion stabilizer, antimicrobial, and chelating properties. These properties will be explored in the following paragraphs.

Emulsion Stabilizer Properties

The emulsions are unstable systems due to the high surface energy exerted between the two immiscible phases. For this reason, the presence of a surfactant able to reduce the surface energy is required.[360] Most surfactants derive from non-renewable precursors and are generally not biodegradable.[361] Lignin is considered an amphipathic polymer due to the presence of both hydrophilic and hydrophobic components. In addition, the presence of ionizable groups make it an efficient stabilizer by the occurrence of electrical repulsion effects.[362] A case of study for the application of LNPs as a stabilizer is represented by the production of Pickering emulsions, which were characterized by a higher deformation resistance compared to that stabilized with conventional surfactants. This effect was associated to the barrierless adsorption of the LNPs at the interfaces of two immiscible liquids, thanks to their partial wetting properties.[363] LNPs were also efficient Pickering emulsifiers to stabilize oil emulsions in water (O/W) in the formulation of sunscreen containing low soluble organic substances.[74]

Antimicrobial Properties

Lignin is characterized by antimicrobial activity as a consequence of the capacity to interact with the bacterial cell causing lysis with consequent release of the cell content. KL is effective against *Erwinia carotovora* and *Xanthomonas campestris pv. vesicatoria* (but not against *Pseudomonas syringae*), while AL showed antimicrobial activity against *Escherichia coli*, *Staphyloccocus aureus*, and *Pseudomonas*.[364] In particular, the C=C double bond and γ-methyl groups in the side chain confer to lignin a higher antimicrobial activity than phenolic and aliphatic groups.[365] Again, LNPs showed higher antimicrobial activity than the native counterpart, as a consequence of the highest contact surface area available for the interaction with the microorganisms,[352] associated to the possibility to penetrate into the bacterial cell. In addition, LNPs favoured the damage of the bacterial cell by electron transfer processes able to generate local radical species.[90] Examples of the synergy activity between silver nanoparticles[365] and lignin against Gram-positive and Gram-negative bacteria have been reported, focusing on the role of lignin as a recognizer and delivery system for the controlled release of the silver ion.[366] In this latter case, the amount of silver ions used in the treatment was 10 times lower than conventional materials, reducing the known negative impact of silver wastes on the environment. Examples of the use of lignin as a green antimicrobial ingredient in the formulation of cosmetics are reported, as in the case of the reduction or substitution of high environmental impact antimicrobial agents, such as phenoxyethanol, hydroxybenzoates, and triclosan.[295]

Chelating Properties

Chelating agents are ingredients able to complex metal ions in a stable way. These compounds play a crucial role in the stability and efficacy of cosmetics since the chelation mechanism stabilizes metal ions by preventing them from reacting with other substances and skin. The adsorbing capacity of lignin has been studied against different metal species, including chromium, copper, cadmium, lead, zinc, nickel, cobalt, and mercury.[367,368] The chelating process occurs by coordination of the metals with Lewis basic sites in lignin, such as carbonyl, carboxylic, and phenolic groups.[369] The adsorption was found to be pH dependent, being favoured by deprotonation of the active groups in lignin.[370] In this context, the use of lignin to replace commercial chelating agent characterized by a well-known environmental pollution impact (e.g., EDTA) has been reported.[371]

Colour Agreeableness of Lignin

The dark colour of lignin, that is mainly due to the harsh conditions of physical and chemical treatments (e.g., high temperature and oxidative transformations), hinders the promotion of lignin-based cosmetics on the market.[372] The principal methods to assess the lignin colour are the Munsell and CIELAB procedures.[373] The Munsell colour system determines the classification of the colour by measuring the human perceptual response, and consists in the evaluation of three independent variables, represented by the colour hue (measured in degrees on a horizontal circle), saturation (measured radially from the neutral gray axis outwards), and brightness (measured vertically on the gray axis from 0 for black and to 10 for white) parameters. This method is accurate and quantitative, but it is limited by a laborious visual matching. The CIELAB method is based on a spectrophotometer analysis in two different modes: (i) specular component included (SCI); and (ii) specular component excluded (SCE) modes. SCI is used to evaluate the actual colour using both specular and diffuse reflected light, while SCE determines the colour by excluding any specular reflected light. In the International Commission on Illumination $L^*a^*b^*$ (CIELAB) colour space, the L^* value represents a bright behaviour of a sample as follows: white when $L^* = 100$ and black when $L^* = 0$; $+a^*$ is a red shade and $-a^*$ is a green shade; $+b^*$ is a yellow shade and $-b^*$ is a blue shade. A total colour difference value (ΔE) is defined as following Equation (1):

$$\Delta E=[(\Delta L^*)2+(\Delta a^*)2+(\Delta b^*)2]/2 \quad (1)$$

where ΔL^*, Δa^*, and Δb^* are the differences in $L^*a^*b^*$ values between a reference and a sample. In order to enhance the color agreeableness of lignin, the chromophore and auxochrome groups should be blocked or cleared. This is of particular relevance in the case of sunscreen formulation. The main techniques applied to lighten lignin are described in the following paragraphs.

Drying of Lignin

Drying of lignin involves the control of the organization of the polymer structure at the morphological level by removal of the water molecules included in the sample.[374] An appropriate drying procedure can significantly reduce the dark colour of lignin without extensive structural modification of chromophores and auxochrome moieties. This procedure has been applied in the preparation of light-coloured sun creams, the control of the colour intensity depending on the specific drying method (i.e., oven, vacuum, freeze, and spray drying).[375] Oven and vacuum drying procedures favoured the formation of large particles with a glossy surface and a dark colour, while spray and freeze drying

make the lignin as a lighten coloured fine powder. In addition, a correlation between the particle size and the lignin colour was observed, small-sized particles being less coloured.

Fractionation of Lignin with Solvents

Light-coloured lignin nanoparticles (CEL-NP) have been obtained from rice husks through initial extraction of cellulolytic enzyme lignin (CEL) followed by the solvent shifting procedure.[376] The colour of CEL-NP and CEL was evaluated using the L^* a^* b^* (CIELAB) colour space method and compared with lignin from rice husks without cellulase treatment (RH) and organosolv lignin (OL), as references. The brightness (L*) and redness (a^*) values of CEL were similar to those of RH as a consequence of the low effect of cellulase activity on phenolic and quinoid chromophore groups. The L^* value of CEL was higher than that of OL and the a^* value of CEL was lesser than OL. This is because CEL was prepared under much milder conditions than OL. As expected, the nano structuration process further increased the lightness of the sample (CEL-NP). The effect of mixture of organic solvents in the lightness of lignin has been also reported.[377]

Heat Treatment

The thermal processing of lignin involves the cleavage of β-O-4 linkages and demethoxylation. Usually, this process produces condensed structures and increases the amount of chromophores groups.[378,379] As an alternative, the steam and heat treatment of wood (steam explosion procedure) for the extraction of lignin, consists in heating the starting material at temperatures between 180 °C and 220 °C and high pressure. This procedure affords an effective discoloration of lignin.[380] In this latter case, the degree of colour change (as evaluated by the DE^* value) was highly dependent from the temperature and pressure parameters.

Chemical and UV Whitening of Lignin

Traditional chemical bleaching procedures are not suitable for lignin colour reduction as their aim is to profoundly degrade the lignin structure. Softener procedures are therefore required to whiten lignin without reducing the antioxidant and UV shielding capability. Among them, sulfonation, sulphomethylation, and butane sulfonation treatments at high temperature and pressure have been shown to be effective in whitening eucalyptus lignin.[381] The reaction occurred preferentially at the C-α position of the phenylpropanoid side chain, while, when performed in the presence of formaldehyde and Na_2SO_3, the aromatic C-5 position was also modified.[382] UV irradiation combined with a long-time (20 h) H_2O_2 treatment effectively decolorizes sulfonated alkali lignin (SAL) by reducing the amounts of aromatic moieties and methoxyl and phenolic hydroxyl groups. Thanks to this treatment, SAL was successfully used as a dye dispersant.[383] Pre-treatments of the starting material can facilitate the bleaching procedure. They include autohydrolysis, steam explosion, and treatment with dilute acids. In particular, the autohydrolysis process improved the whitening of KL and decreased the excessive consumption of the sample during the overall whitening processes.[384] Selective functionalization procedures can also be applied in the whitening of lignin. For example, the acetylation of solvent-fractionated KL with acetic anhydride reduced the colour intensity of the sample without interfering with its UV absorption capability (313.5% and 145.6% in brightness and L^* value, respectively). In this latter case, the acetylation process was responsible for the inhibition of the auxochrome effect of the phenolic moieties, as a consequence of its electron withdrawing effect. Acetylation prevented demulsification processes due to the fine control of the polarity of lignin.[373] As a general trend the lightening process slightly interferes with the antioxidant and UV shielding properties.

4.2 Lignin Nanoparticles as Sustainable Photoprotective Carriers for Sunscreen Filters

4.2.1 Aim of work

UV sunscreen filters (SSFs) commonly found in commercial formulations may cause production of radical species after prolonged irradiation with a concomitant loss of cosmetic function and emergence of toxicity.[246,385,386] Photostabilizers are used to avoid these side effects by quenching the high-energy excited states of SSFs,[387] but in turn, they can be degraded with production of toxic side products.[388,389] Over the past few years, photostabilizers from renewable sources received a great interest due to green chemistry and circular economy concerns.[390] Lignin, the most abundant polyphenol in nature, is a waste recovered from pulp and paper and biorefinery processes.[391] It is characterized by different beneficial properties for cosmetic applications, including antioxidant activity,[392] sun protection factor booster,[194] antimicrobial,[393] and metal chelating effects.[394] In addition, lignin forms stable colloidal nanoparticles (LNPs) deprived of toxicity[395] and characterized by high UV absorbing capacity and radical scavenging properties[225] as a consequence of the formation of π-interaction between the aromatic subunits of the polymer.[396] Examples of application of native lignin and LNPs as sunscreens are reviewed,[397,376] and the role played by these nanodevices in the formulation of cosmetic and cosmeceutical products is deeply investigated.[293,294] These properties associated with the presence of an internal cavity make LNPs a suitable nanodevice for the encapsulation and stabilization of active substances in drug delivery[398] and Pickering emulsion technologies.[399] Here, we report that LNPs from kraft lignin are efficient and sustainable carriers for the stabilization of two common SSFs,[400] 4-tert-butyl-4′-methoxydibenzoylmethane **1** (avobenzone) and 2-ethylhexyl-3-(4-methoxyphenyl)prop-2-enoate **5** (octyl methoxycinnamate). Compound **1** is a largely applied UV-A filter whose photostability is dependent on the overall composition of the formulate.[401] Conversely, **5** is a highly active and photolabile UV-B filter.[402] Under prolonged irradiation, compound **1** is subjected to α-cleavage by a McLafferty-like retro-heteroene hydrogen rearrangement to yield tert-butylbenzene **2**, 4-tert-butyl benzoic acid **3**, and para-methoxy benzoic acid **4** (**Figure 4.5**, panel A).[403] The allergenic effect and cytotoxicity of **2–4** at the lymph node level are reported.[404] In a similar way, the prolonged irradiation of 5 causes isomerization to (Z)-cis counterpart **6**, followed by side chain degradation to 4-methoxy benzaldehyde **7** and 2-ethyl-hexanol **8**, or alternately, [2 + 2]π cycloaddition to cyclobutane dimers **9a,b** (**Figure 4.5**, panel B).[405-407]

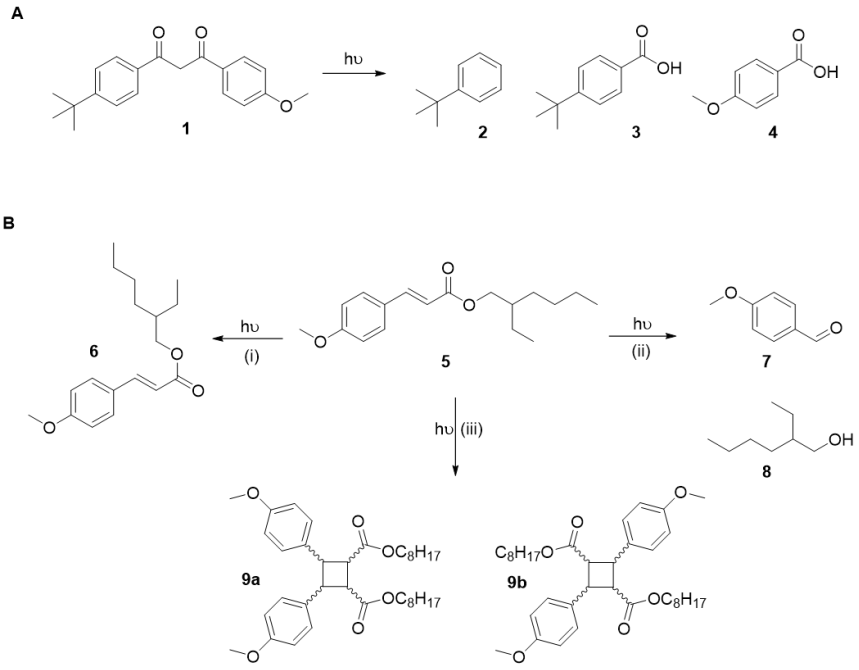


Figure 4.5. Photodegradation pathway of 1 (panel A) and 5 (panel B) after UV irradiation. (i) Z/E isomerization process; (ii) side chain cleavage; and (iii) [2 + 2]π cycloaddition.

Toxic effects of **6, 7**, and **9a,b** against cellular viability in NIH/3T3 mouse fibroblast cells are reported.[250] Antioxidants have been explored and applied as energy quenchers[408] in order to improve the photostability of **1** and **5**.[409,410] These compounds are not completely deprived of toxicity since they can generate radical oxygen species and reactive quinone derivatives.[410,411] Presently, few examples of the application of LNPs as carriers for UV filters are reported, apart from encapsulation of titanium dioxide with consequent decreased photoactivity[359] and the Pickering emulsions with SSF oils.[412] These procedures involve the formation of emulsions in which the UV filter is surrounded by LNPs, or alternately, a coating of a titanium dioxide core by layer-by-layer deposition. Otherwise, examples of encapsulation of UV filters in the internal cavity of LNPs are not reported, despite that these nanodevices are expected to improve the stability of the active ingredients by acting as a UV barrier, contemporaneously favouring their controlled release in the medium.[413] Here, we describe the encapsulation of 1 and 5 into LNPs by nanoprecipitation using eco-certified dimethyl isosorbide (DMI) as a primary solvent and deionized water as an anti-solvent. High values of loading capacity (LC) and loading efficacy (LE) were obtained. Compounds **1** and **5** were also co-encapsulated with *para*-hydroxy phenethyl alcohol **10** (hydroxytyrosol), a natural phenol from olive wastewater, characterized by high antioxidant activity and beneficial skin regenerative effects,[414] usually applied in cosmetic formulations and functional food.[415-417] Compound **10** was selected due to its well-known UV-B shielding capacity and radical quenching properties.[418] After the loading procedure, compounds **1** and **5** showed increased photostability with respect to the bare counterpart, showing a beneficial role of the lignin carrier and hydroxytyrosol in the inhibition of photodegradative pathways.

4.2.2 Experimental part

Reagents
4-Tert-butyl-4′-methoxydibenzoylmethane **1** (avobenzone), 2-ethylhexyl-3-(4-methoxyphenyl)prop-2-enoate **5** (octyl methoxycinnamate, and para-hydroxy phenethyl alcohol 10 (hydroxytyrosol) were obtained from Sigma-Aldrich and used without further purification. Kraft lignin (KL) was obtained from Sigma-Aldrich and was purified before use by standard procedures,[419] including alkali–acid treatment and continuous washing with deionized water. DMI (purity 98.0%) was purchased from TCI Europe and used without further purification.

Encapsulation Protocol and Determination of Loading Parameters
LNPs were prepared using the nanoprecipitation method. KL (100.0 mg) was dissolved in DMI:H_2O (3.0 mL, 2.5:0.5 v/v) at 50 °C for 12 h under gentle magnetic stirring. Milli-Q water (6.0 mL) was added to the KL solution and LNPs formed instantaneously. For the encapsulation procedure, the appropriate compound to be encapsulated (0.06 mmol) was dissolved in the KL solution before the addition of water. A similar procedure was repeated in the presence of a mixture of compounds (1:1 molar ratio). After the precipitation, LNPs were recovered by centrifugation (6500 rpm, 10 min). The LC and LE were evaluated using the high-performance liquid chromatography (HPLC) analysis of the supernatant obtained after centrifugation using eqs 1 and 2:

$$LC(\%): \frac{(weight\ of\ starting\ SSF - weight\ of\ unloaded\ SSF)}{wight\ of\ lignin} \times 100$$

$$LE\ (\%): \frac{(weight\ of\ starting\ SSF - weight\ of\ unloaded\ SSF)}{weight\ of\ starting\ SSF} \times 100$$

Here, LC is the percentage of the encapsulated compound with respect to starting KL, while LE represents the amount of encapsulated compound with respect to the initial concentration of SSF.

2,2'-Diphenyl picrylhydrazyl (DPPH) Radical Scavenging Activity
The antioxidant activity of LNPs was evaluated by the DPPH radical scavenging assay. The test was performed starting from different amounts of LNPs (500, 250, 100, 50, and 10 μg/mL) in H_2O (0.550 mL), which were added to a freshly prepared DPPH solution (2.45 mL, 0.7 mM in MeOH). The spectrophotometric analysis was carried out in duplicate at 25°C. The radical scavenging activity was monitored as a function of time by measuring the absorbance band of DPPH at 517 nm (λ_{max}) until the absorbance values reached a plateau. The kinetics of the process was analyzed for each concentration tested, and the amount of DPPH remaining at the steady state was estimated. This value was used to calculate the IC_{50} (concentration of the substrate that causes 50% loss of DPPH activity). Data were expressed as percentage of inhibition of DPPH activity based on the following eq 3:

$$inhibition\ of\ DPPH\ (\%): \frac{(Abs\ control - Abs\ sample)}{Abs\ control} \times 100$$

where "Abs control" is the absorbance of the DPPH solution in the absence of the sample.

Hydrodynamic Diameter and ζ-Potential Analyses
The hydrodynamic diameter and ζ-potential values were evaluated in H_2O by dynamic light scattering (DLS) using a Zetasizer Nano ZS (Malvern Instruments, Malvern, UK) apparatus equipped with a He–Ne laser (633 nm, fixed scattering angle of 173°, 25 °C). Measurements were performed in triplicate at 25 °C.

Field-Emission Scanning Electron Microscopy (FESEM)
FESEM was carried out using a ZEISS Gemini 500 (Oberkochen, Germany) at 5 kV. As a general procedure, LNPs in water (20 μL) were deposited on a coverslip coated with gold (AGAR auto sputter coater) and dehydrated in air. The coverslip was mounted on the stub with conductive carbon glue and a thin film (5.0 nm) of chromium was deposited using the Sputter Quorum Q150T ES plus to make the sample sufficiently conductive for measurement purposes.

Small-Angle X-ray Scattering (SAXS)
The measurements were performed by SAXS with a Xeuss 2.0 Q-Xoom system (Xenocs SAS, Grenoble, France) equipped with a microfocus Genix 3D X-ray source (λ = 0.1542 nm) and a two-dimensional Pilatus3 R 300K detector, which can be placed at a variable distance from the sample. The beam size was determined by the two-pinhole collimation system equipped with "scatterless" slits to be 0.5 mm × 0.5 mm. Calibration of the scattering vector q range is described in eq 4:

$$q: \frac{(4\pi * \sin\theta)}{\lambda}$$

and 2θ is the scattering angle, and the calibration was performed using silver behenate. Measurements with two different sample detector distances (26.2 and 250 cm) were performed and the overall explored q region was $0.045 < q < 17$ nm^{-1}. Samples of LNPs (concentration of the SAXS samples: 1.0 mg/mL) dispersed in a DMI:H_2O 1:3 mixture were inserted into disposable borosilicate glass capillaries with a nominal internal diameter of 0.15 cm, sealed with hot glue, and placed in the instrument sample chamber at room temperature and reduced pressure (∼0.2 mbar). The two-dimensional scattering patterns were measured for a total of 3.5 h acquisition time per sample, subtracted for the "dark" counts, and then masked, azimuthally averaged, and normalized for calculating the transmitted beam intensity, exposure time, and subtended solid angle per pixel using the FoxTrot software developed at SOLEIL. The one-dimensional I versus q profiles were then subtracted for the solvent and capillary contributions and expressed in absolute scale units (cm^{-1}) by dividing for the sample thickness estimated by scanning the capillary with the X-ray beam. The different angular ranges were merged using the SAXS utilities tool.[420]

UV–Visible Assay
LNPs (10 μg) in cyclohexane were analyzed in a quartz cuvette (3.0 mL, 1 cm path length) by a Varian Cary UV 60 scan (Crawley, UK) in the range between 250 and 800 nm with a scan speed of 400 nm/min and a bandwidth of 5 nm at 25 °C under gentle stirring. The analysis was elaborated by the UV–vis scan software.

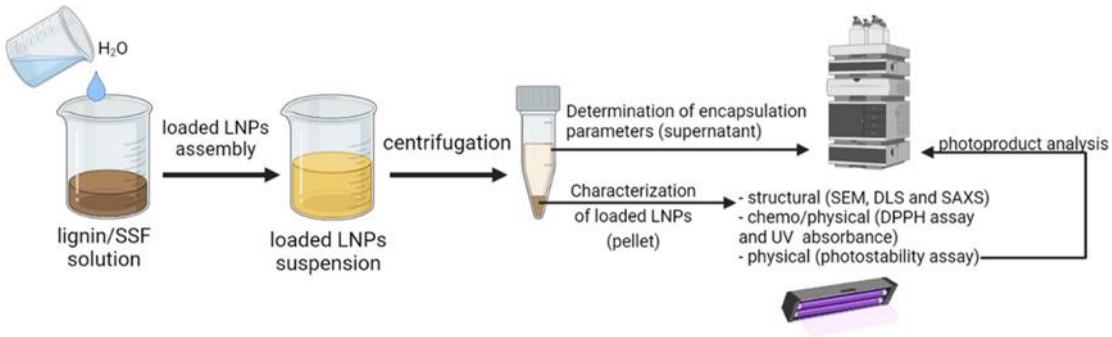
Photostability Assay
LNPs (10.0 mg) were suspended in cyclohexane (5.0 mL) in an open glass lens (10.0 cm diameter). The suspension was irradiated using a UV Hg low-pressure lamp (HAERUS 250W; 40 cm of distance to obtain 3000 mj/cm2) for 20.0 min. After the irradiation,

tetrahydrofuran (THF, 5.0 mL) was added to the crude in order to degrade LNPs, followed by filtration (25 mm, 0.22 μm syringe filter), roto-evaporation, and freeze-drying. The percentage of photodegradation was evaluated by HPLC analysis of the supernatant after the filtration step.

HPLC Analysis
The HPLC analysis was performed using an UltiMate 3000 rapid resolution system (Thermo Fisher Scientific) equipped with an Alltima C18 column (250 mm × 4.6 mm, 5 μm), an injection volume of 10 μL, a mobile phase flow rate of 1.0 mL/min, and a detector set up at 319 nm for 1, 361 nm for 5, and 280 nm for 10, respectively. The analysis was repeated in triplicate. The compounds were separated using the isocratic method using 95.0% MeOH and 5.0% ultrapure formic acid for 25 min and quantified using the calibration curve method.

4.2.3 Results and discussions

Preparation and Characterization of LNPs
LNPs were prepared by nanoprecipitation using eco-certified DMI as the primary solvent and deionized H_2O as the anti-solvent. As a general procedure, compounds **1** and **5** (0.06 mmol) were dissolved in DMI/water (3.0 mL, 2.5:0.5 v/v) in the presence of KL (100 mg) at 50 °C under gentle magnetic stirring. Deionized water (6.0 mL) was added with formation of a colloidal suspension of LNPs and contemporaneous encapsulation of the selected compound. The mixture was centrifuged (7000 rpm, 15 min), washed with deionized water (×3, 9.0 mL), and freeze-dried to yield LNPs-1 and LNPs-5, respectively (**Scheme 4.1**).



Scheme 4.1. General Procedure for the Preparation and Characterization of Loaded LNPs.

A similar procedure was applied in the presence of a mixture of **1** and **5** (1:1 molar ratio) to yield LNPs-1/5. In addition, compounds **1** and **5** were co-encapsulated with hydroxytyrosol **10** (0.06 mmol) to yield LNPs-1/10 and LNPs-5/10, respectively. LC (eq 1) and LE (eq 2) of LNPs were evaluated by HPLC analysis of the residual compound in the supernatant after the centrifugation step. Irrespective of the experimental conditions, the LNPs showed high values of LE and LC (**Table 10**), confirming the efficacy of LNPs in the encapsulation of aromatic derivatives.[421]

Table 10. Encapsulation Parameters, Hydrodynamic Diameter, ζ-Potential, and Polydispersive Index of LNPs-1, LNPs-5, LNPs-1/5, LNPs-1/10, and LNPs-5/10.

entry	Sample	compound	LE (%)	LC (%)	z-potential	Mean size (nm)	PDI[a]
1	LNPs				-34.5	225	0.101
2	LNPs-1	1	86.1	10.8	-33.7	291	0.141
3	LNPs-5	5	79.7	12.4	-32.9	286	0.139
4	LNPs-1/5	1,5	82.9	11.1	-34.1	301	0.138
5	LNPs-1/10	1,10	85.1	12.0	-36.0	302	0.134
6	LNPs-5/10	5,10	81.9	10.9	-34.2	297	0.135

[a]Polydispersive index.

Figure 4.6 shows the FESEM analysis results of LNPs-1 (panel A), LNPs-5 (panel B), and LNPs-1/5 (panel C) as selected representative samples (SEM images of empty LNPs, LNPs-1/10, and LNPs-5/10 are shown in Figure S1, Supporting Information). The samples were characterized by regular and spherical-shaped nanoparticles bearing small clumps on the surface, which appears rather rough. DLS analysis of LNPs showed the formation of monodisperse population of particles (**Figure 4.6**, bottom).

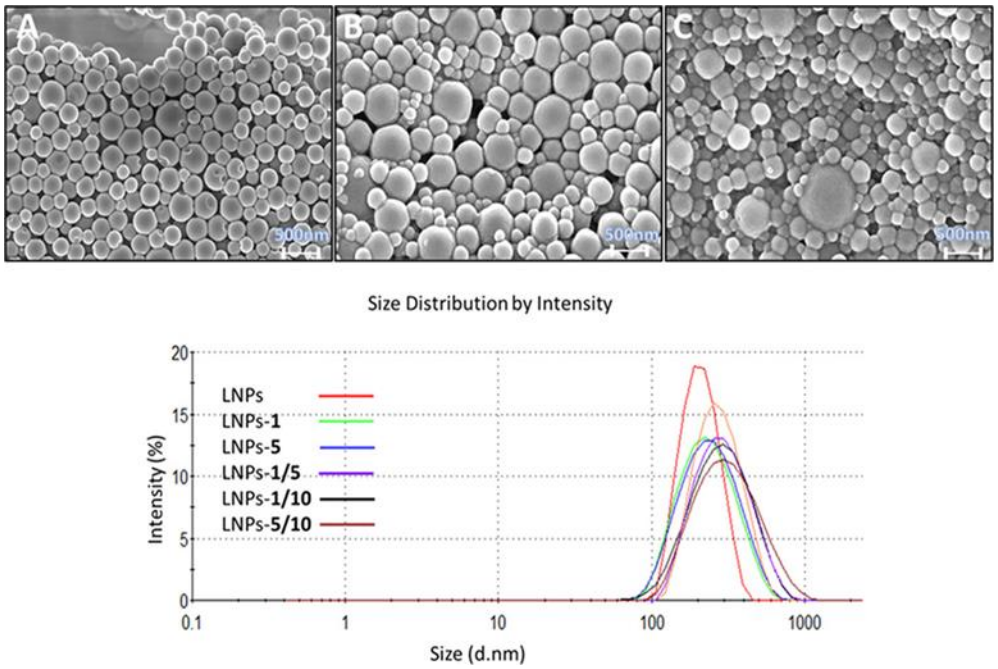


Figure 4.6. Results of (top) FESEM analysis of LNPs-1 (panel A), LNPs-5 (panel B), and LNPs-1/5 (panel C) and (bottom) DLS analysis.

The average diameter of LNPs was in the range between 286 nm (LNPs-5; entry 3, **Table 10**) and 302.3 nm (LNPs-1/10; entry 5, **Table 10**). It was higher than that previously observed for empty LNPs (entry 1, **Table 10**) in accordance with the steric hindrance of encapsulated compounds.[422] The ζ-potential value was found to be almost constant irrespective of the loaded compound (**Table 10**, entries 2–6) and of the same order of magnitude as empty LNPs (**Table 10**, entry 1), confirming the absence of significant adsorption phenomena on the surface of LNPs.

The SAXS analysis was performed in the selected cases of empty LNPs, LNPs-1, LNPs-5, and LNPs-1/5. As shown in **Figure 4.7** panel A, the four samples had almost

superimposable scattering profiles, but LNPs-1 and LNPs-1/5 showed additionally the presence of an evident diffraction peak at 3.065 nm^{-1}, corresponding to an interplanar distance of 2.05 nm, and subsequent weaker peaks (the second at 6.13 nm^{-1}) characteristic of a crystalline phase. These peaks were not observed in LNPs-5 and in empty LNPs. Considering the reported crystallinity of compound **1** (compound **5** is an oil) and comparing the observed positions of the diffraction peaks in units of 2θ (at 4.3, 8.6, 16.6, and 18.4°, Figure 3 panel B) to those reported in the literature,[423] these data suggest the presence of compound 1 in LNPs-1 and LNPs-1/5 samples, respectively, in the crystalline isoform II, reported as a metastable phase accessible from the melt of the commercially available form I.

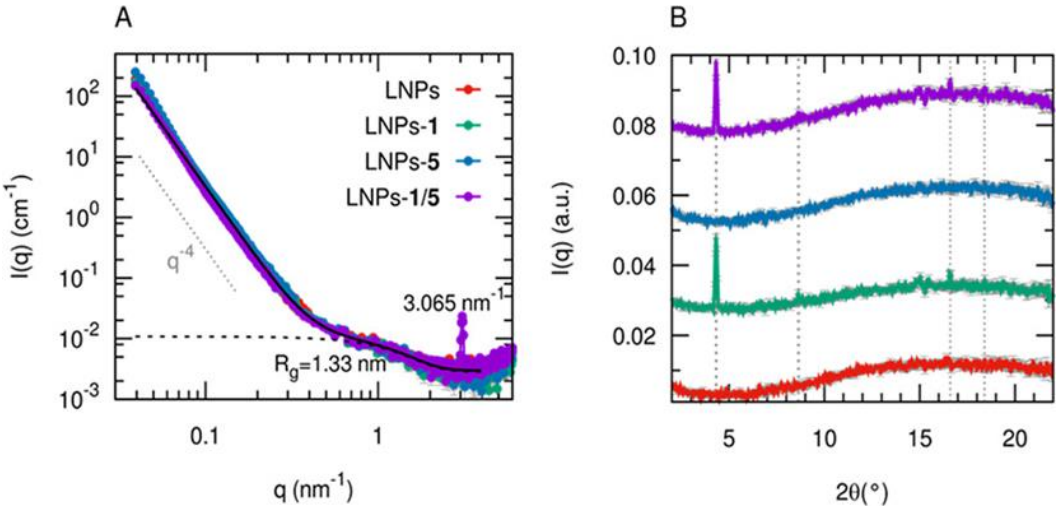


Figure 4.7. SAXS profiles of LNP samples. (A) The intensity vs q data in a double logarithmic scale are shown as colored dots and lines (LNPs, red; LNPs-1, green; LNPs-5, blue; and LNPs-1/5, purple), while the model function of the Porod law decay (c/q4, with c = 3.2 × 10^{-4} cm^{-1} nm^{-4}, reference slope indicated as dotted gray line) and the Guinier contribution (I(0)exp(−R_g2q2/3) with I(0) = 8 × 10^{-3} cm^{-1} and R_g = 1.33 nm) with a flat background (3 × 10^{-3} cm^{-1}) are shown as a solid black line. The latter contribution is also reported as a dashed black line. The most evident diffraction peak position is indicated. (B) The wider-angle scattering region presenting the diffraction peaks for samples LNPs-1 and LNPs-1/5 (q > nm^{-1}) is highlighted by plotting data as a function of 2θ rather than q. The data are vertically shifted on the intensity scale for better visualization and the peak positions are indicated by dotted gray lines.

Regarding the measured scattering signal at lower angles, in agreement with the DLS data showing LNPs with diameters of the order of 200–300 nm, the overall size of the particles in the samples lies beyond the resolution limit of the used SAXS. Therefore, the decay of the initial intensity in the scattering profiles (q <0.4 nm^{-1}) is evident on a length scale between 70 and 10 nm, following the power law (Porod law, ∼1/q4), expected for the interface between the particles and the solvent. A fit according to the Guinier law in this region provides such additional feature, related to a radius of gyration R_g of 1.33 nm, which means sizes of 3–4 nm (from the value of the radius of gyration R_g of 1.33 nm estimated from the intensity decay according to the Guinier law) such an additional feature could be interpreted as due to both the characteristic internal porosity of the self-assembled LNPs and the individual lignin units.[396,374]

UV-Shielding Capacity of LNPs

The UV-shielding capacity of LNPs-1, LNPs-5, and LNPs-1/5 was evaluated by a spectrophotometric analysis after dispersion of 10 μg of the particles in 3.0 mL of cyclohexane (250–800 nm) at 25 °C (UV-shielding data of LNPs-1/10 and LNPs-5/10 are shown in Figure S2).

Empty LNPs and compounds **1**, **5**, and **10** were used as references (**Figure 4.8**, panels A–C). LNPs-1, LNPs-5, and LNPs-1/5 showed increased absorption capacity (hyperchromic effect) and pronounced bathochromic shift with respect to references. In particular, LNPs-1 and LNPs-5 showed an appreciable red shift (Δλ of 43.7 nm and Δλ of 51.2 nm, respectively) with respect to the corresponding references **1** (364.5 nm) and **5** (310.2 nm) as reported in **Figure 4.8** panels A and B. A similar effect was observed for LNPs 1/5 (**Figure 4.8**, panel C).

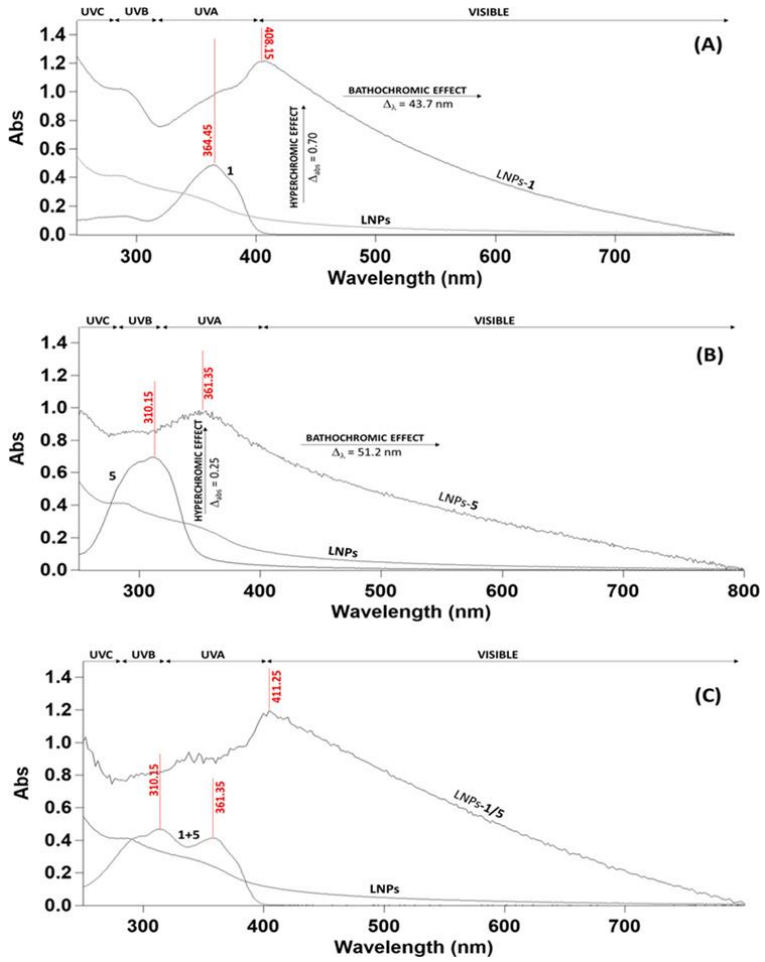


Figure 4.8. In vitro UV–vis absorbance of aqueous suspensions of LNPs-1 (panel A), LNPs-5 (panel B), and LNPs-5/10 (panel C).

This effect was probably due to the interaction between the auxo-chromic groups of KL and the chromophore moieties of compound **1** and **5**, associated with the formation of typical J-aggregation modes in lignin subunits.

Antioxidant Activity of LNPs

The antioxidant activity of LNPs-1, LNPs-5, LNPs-1/5, LNPs-1/10, and LNPs-5/10 was evaluated by measuring the radical scavenging activity against DPPH. The percentage of quenching of the DPPH radical was evaluated at different sample concentrations by

applying eq 3. The IC_{50} values (μg/mL of sample that causes 50% loss of DPPH concentration) are reported in **Figure 4.9** and Table S1. Empty LNPs and commercially available butyl-hydroxytoluene (BHT) were used as references. LNPs-5 and LNPs-1/5 showed higher antioxidant activities than LNPs-1 and references. The presence of **10** further increased the antioxidant activity, and LNPs-1/10 and LNPs-5/10 showed IC_{50} values lower than those of LNPs-1 and LNPs-5, respectively.
LNPs-5/10 showed the highest antioxidant activity. Irrespective of the sample, the antioxidant activity of LNPs was probably due to the radical scavenging properties of aromatic OH moieties, as previously reported.[349]

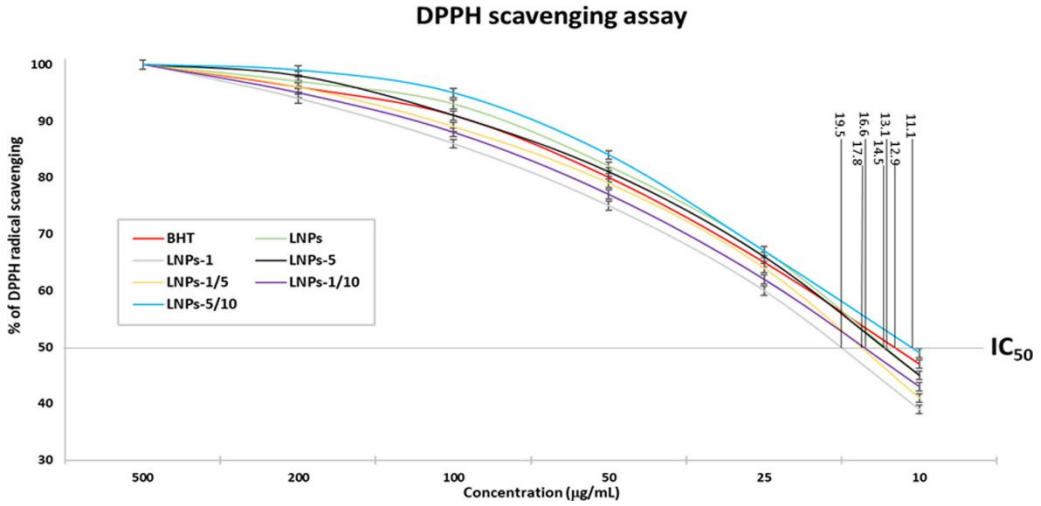


Figure 4.9. DPPH scavenging activity of loaded lignin nanoparticles presented as % of DPPH radical inhibitions and IC50 values (μg/mL).

UV Photostability of 1 and 5 after Encapsulation into LNPs
The ability of LNPs to protect **1** and **5** from UV photodegradation was evaluated by analysis of the residual amount of these compounds after irradiation. Briefly, LNPs **1** and **5** (10 mg) were suspended in 5.0 mL of cyclohexane and irradiated by a UV lamp (Hg, low pressure) for 20 min at 25 °C. The irradiation of **1** and **5** alone or their mixture (1:1 equivalent ratio) was performed under similar experimental conditions as a reference. After the irradiation of the sample, the nanoparticles were treated with THF (5.0 mL) in order to deliver the encapsulated compounds. The residual amount of 1 and **5** was determined after evaporation of the organic phase by HPLC analysis. High percentage of photodegradation was measured for **1** (72.2%) and **5** (79.1%) as references with formation of expected photoproducts **2**–**4** and **7** and **8**, respectively. The percentage of photodegradation increased for **5** (87.8%) and decreased for **1** (69.2%) during the irradiation of the mixture due to the undesired photochemical-induced isomerization of **5** by **1**.[424,425] It is worth noting that photodegradation was significantly reduced in the case of LNPs-1 (12.8%) and LNPs-5 (10.9%), confirming the photostability of the compounds after the encapsulation process (**Figure 4.10** and Table S2). A similar result was observed for LNPs-1/5 in which case the energy transfer process was limited by the presence of lignin. This enhanced photostability is of great commercial interest since both **1** and **5** are widely used as a mixture in sunscreen formulations. Finally, the photodegradation of **1** and **5** was further inhibited by the presence of 10 (LNPs-1/10 5.1% and LNPs-5/10 4.2%) as a consequence of a combined UV shielding and antioxidant effect exerted by this catechol derivative (**Figure 4.10** and Table S2).

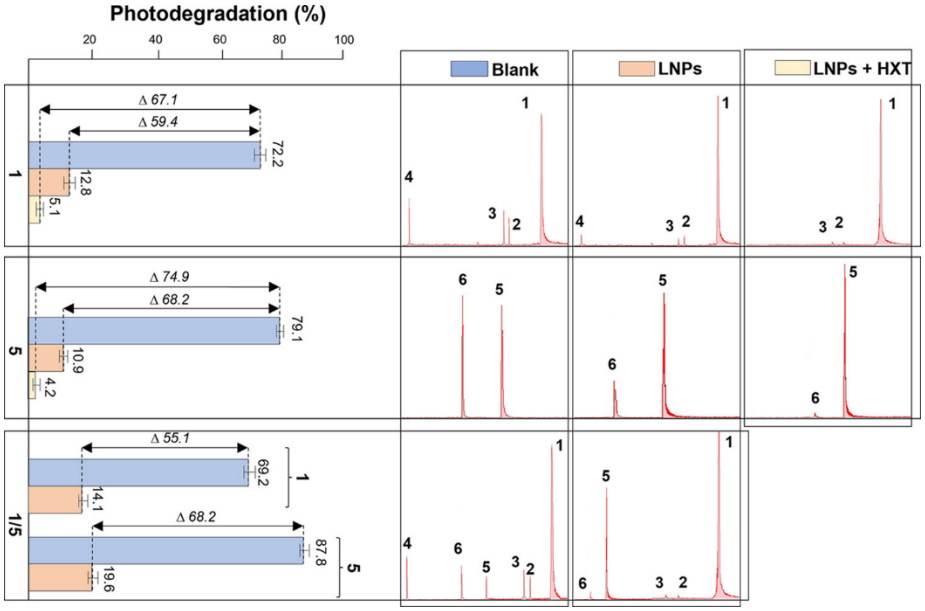
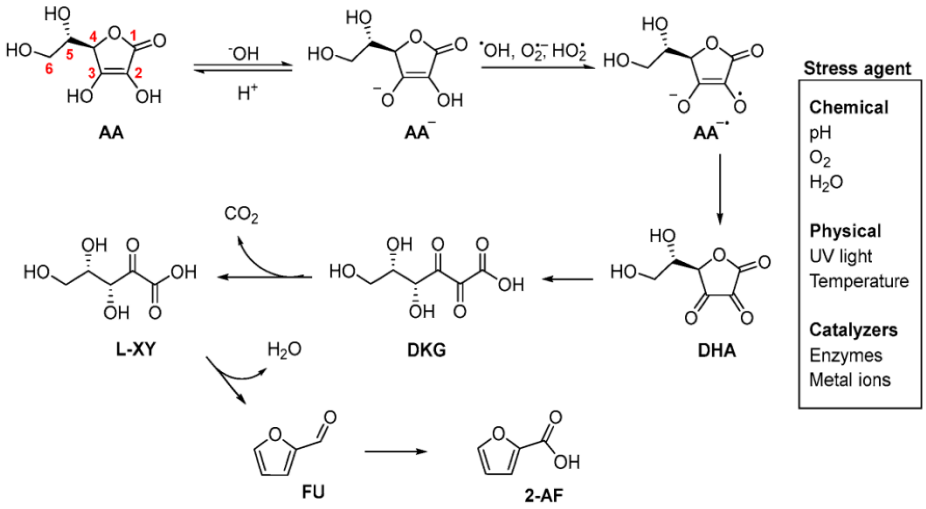


Figure 4.10. Photostability evaluation of loaded LNPs compared to the corresponding dissolved SSF.

4.3 Biosynthesis of Novel Ascorbic Acid Esters and Their Encapsulation in Lignin Nanoparticles as Carriers and Stabilizing Systems

4.3.1 Aim of work

Ascorbic acid (AA, Vitamin C) is a water-soluble vitamin produced by the metabolism of plants and animal species.[426] It is characterized by a glucose-like structure comprising six carbon atoms, two of them which are involved in the enediol moiety responsible for the reducing activity.[427] AA is used in cosmeceutical, pharmaceutical and nutraceutical applications at high concentration (up to 15% w/w) as potent antioxidant additive to contrast skin aging processes and to protect the cell against UV-induced photo-damage, promoting the differentiation of keratinocytes and decreasing the biosynthesis of melanin.[428] In addition, it showed repair tissue's activity, activation of the immune system, neo synthesis of collagens, and production of specific neurotransmitters.[429-432] Unfortunately, AA is susceptible to oxidative degradation showing low stability under both aerobic and anaerobic conditions,[433,434] with concomitant loss of biological activity and emergence of unpleasant Maillard browning side processes.[435] The degradation of AA involves the oxidation to dehydroascorbic acid (DHA), followed by nucleophilic ring-opening of the lactone ring to yield diketogulonic acid (DKG). Finally, DKG releases CO_2 and L-xylosone (L-XY), 2-furanoic acid (2-AF), and furfural (FU) (**Scheme 4.2**). This process is associated with change of the colour, smell, and gas generation, as well as loss of homogeneity of formulate.



Scheme 4.2. Degradation pathway of AA. AA: ascorbic acid; L-XY: L-xylosone, 2-AF: 2-furanoic acid; DHA: dehydroascorbic acid; DKG: di-ketogulonic acid; FU: furfural. The numbering of the carbon atoms of ascorbic acid is highlighted by the red numbers.

In order to improve the stability of AA, appropriate chemical and physical conditions have been selected for the control of solubility, viscosity, polarity of the medium and pH range, which was occasionally associated with emulsifying agents and additives.[436,437] Recent approaches to improve the stability of AA encompass the synthesis of stable derivatives or, in alternative, the protection of the molecule by encapsulation technology. In the first case, AA is alkylated with alcohols or, in alternative, esterified with carboxylic

acids.[438,439] In the second case, it was encapsulated inside micro- and nano carriers from natural (i.e., chitosan, alginate, phospholipids)[440] and synthetic (i.e., acrylic compound) [441] origins.[442]

Renewable polyphenols, such as lignin, may be applied for the encapsulation and controlled release of low stable natural substances.[93] Lignin is produced in miles scale of tons annually as a byproduct from the biorefinery and pulp industries.[443] The commercial interest for this polymer has grown in the last year in the context of green chemistry and circular economy.[444] Procedures for the large-scale preparation of lignin nanoparticles (LNPs) are reported in the literature.[194] Compared to amorphous lignin, after the nano-structuration process, LNPs showed improved antioxidant,[445] UV shielding,[353] and anti-microbial properties, as a consequence of the π–π interactions between the aromatic subunits of the polymer.[225] Examples of encapsulation of bioactive natural substances inside LNPs are reported, including the encapsulation of resveratrol[446] and curcumin.[398] LNPs have been also applied in the stabilization of photosensitive commercial UV filters[447] and in the controlled release of bioactive thymine photo-dimers useful for the activation of alert cellular pathway in damaged cells.[448] We report here the synthesis of novel ferulic acid and palmitic acid esters of 3-O-ethyl ascorbic acid by lipase B from *Candida antarctica* immobilized on LNPs and their successive encapsulation inside LNPs prepared from kraft lignin by solvent shift procedure. 3-O-ethyl ascorbic acid is a stabilized derivative of AA widely applied in cosmetic formulations,[449] due to the selective protection of the most acidic C3 hydroxyl group ($pK_a = 4.25$) in the molecule.[450] In addition, ferulic acid and palmitic acid were selected since their esters are well recognized to have high stability.[451,452] LNPs showed synergistic effect with encapsulated AA esters improving the overall antioxidant activity and stabilizing the encapsulated compounds towards pH and temperature variations. The kinetic release of AA esters from LNPs showed a Fickian-like diffusion process characterized by release of the encapsulated compounds during the first 24 h. The capability of LNPs to stabilize AA esters, associated to the synergy effect in the antioxidant activity, highly suggested LNPs as an effective carrier of AA derivatives in cosmetic and cosmeceutical formulations.

5.7.3 Experimental part

Materials

Kraft lignin (KL) was purchased from Sigma Aldrich (St. Louis, MO, USA) and used after purification by standard procedures including alkali–acid treatment and continuous washing with deionized water. Dimethyl isosorbide (DMI), ethanol, 2,2-diphenyl-1-picrylhydrazyl (DPPH), L-ascorbic acid AA, 3-O-ethylascorbate 1, ferulic acid 2, palmitic acid 3, 6-O-Palmitoyl-L-ascorbic acid **6**, diisopropyl azodicarboxylate (DIAD), triphenylphosphine (TPP), butylhydroxytoluene (BHT), *para*-4-nitrophenyl laurate (para-NPL), chitosan (non-animal derived, average Mw 50 kDa, CH), concanavalin A (Con A, from *Canavalia ensiformis*, Jack bean type VI), and Lipase B from *Candida antarctica* were purchased from Sigma Aldrich and used without further purification. Analytical grade tetrahydrofuran THF and 2-methyl tetrahydrofuran (2-MeTHF) were refluxed over Na–benzophenone under nitrogen, followed by distillation and storage over 4 Å molecular sieves. Deuterated and HPLC purity-grade solvents were purchased from VWR. ^{1}H and ^{13}C NMR spectra were obtained in $MeOD_3$ using a Bruker 400 MHZ spectrometer (Bruker, Billerica, MA, USA).

*Preparation and Kinetic Characterization of **Biocatalyst I***

Biocatalyst I was prepared as reported in reference.[453] Briefly, LNPs (5 mg, 1.0 mg mL^{-1}) obtained by nanoprecipitation from KL in Milli-Q water were added to CH (10 mg, 1.0 mg mL^{-1} in diluted acetic acid 1.0% v/v) under slow magnetic stirring (200 rpm) for 2 h at room temperature. The LNPs/CH intermediate (1.0 mg mL^{-1}) was coated with ConA (0.4 mg mL^{-1}) in sodium phosphate buffer (PBS, 1.0 mL; pH 7.3, 0.1 M) at room temperature to yield LNPs/CH/ConA. This latter intermediate (1.5 mg mL^{-1}) was dispersed in PBS (1.0 mL; 0.1 M, pH 7) and added of lipase B from *Candida antarctica* (25 U; 3.0 mg mL^{-1}) dissolved in PBS (0.1 M; pH 7) under gentle stirring (200 rpm) at 4 °C for 24 h and the suspension was centrifuged and washed two times with PBS (pH 7, 0.1 M) to afford **biocatalyst I** (overall yield 85% in weight with respect to LNPs/CH/ConA intermediate).

The enzymatic activity and kinetic parameters of **biocatalyst I** were determined by the para-NPL assay.[454] In particular, the activity of lipase was evaluated by measuring the increase in absorbance (λ_{max} 405 nm) produced during the release of *para*-nitrophenol in the hydrolysis of *para*-NPL in Tris-HCl (0.1 M, pH 7.4) at 25 °C for 15 min. In a typical experiment, biocatalyst I (1.5 mg mL^{-1} in PBS, 0.1 M, pH 7) was added to *para*-NPL solution (0.1 mL; 20 mM; $CNCH_3$: water 1:1) in Tris-HCl. The international unit of lipase activity was defined as the amount of the enzyme necessary to hydrolyze 1.0 μmol of *para*-NPL in 1.0 min at 25 °C and optimal pH. Kinetic parameters (Km and Vmax) of biocatalyst I were determined by measuring the activity of lipase (25 U) using different concentration of *para*-NPL (from 0 to 10 mM) in Tris-HCl (pH 7.4). The kinetic parameters were analyzed by Lineweaver–Burk plots and calculated in triplicate with the GraphPad Prism 9 software.

*Synthesis and Characterization of Esters **4** and **5***

3-O-ethyl-L-ascorbyl-6-ferulate **4** and 3-O-ethyl-L-ascorbyl-6-palmitate **5** were synthesized from 3-O-ethyl ascorbic acid **1** and the appropriate carboxylic acid in 2-MeTHF in the presence of **biocatalyst I.** Compound **1** (103 mg, 0.5 mmol) and the appropriate carboxylic acid (1.0 eq.) were dissolved in 2-MeTHF (5.0 mL) in the presence of **biocatalyst I** (5 U), and the mixture was gentle stirred at 50 °C for 48 h under argon atmosphere in the presence of anhydrous molecular sieves. At the end of the reaction, **biocatalyst I** was recovered by centrifugation (6000 rpm), and the organic phase was evaporated under reduced pressure. The crude was dissolved in EtOAc (5.0 mL), washed with NaCl ss, dried over anhydrous Na_2SO_4 and evaporated under high vacuum. Esters 4 and 5 were obtained after chromatographic purification by using CH_2Cl_2:MeOH 95:5 as eluent.

3-O-ethyl-L-ascorbyl-6-ferulate **4.** Yield: 38.8% mp: 175–181°C, yellow solid. Elemental analysis for $C_{18}H_{20}O_9$, expected value: C, 56.84; H, 5.30; O, 37.87; measured value: C, 56.80; H, 5.30; O, 37.83. ^{1}H NMR ($MeOD_3$, 400 MHz): δH 7.63 (1H, d, J = 16Hz, H11), 7.19 (1H, s, H10), 7.08 (1H, d, J = 6.4 Hz, H9), 6.83 (1H, d, J = 16Hz, H8), 6.34 (1H, d, J = 15.88 Hz, H7), 4.38 (1H, d, J = 3.28 Hz, H6), 4.36–4.31 (4H, m, H5 + H4), 3.90 (3H, s, H3), 3.67 (1H, d, J = 6.96 Hz, H2) 1.40 (3H, t, H1). ^{13}C NMR ($MeOD_3$, 100 MHz): δC 169.58 (C18), 162.96 (C17), 150.67 (C16), 149.09 (C15), 147.96 (C14), 145.53 (C13), 126.38 (C12), 122.59 (C11), 119.06 (C10), 115.06 (C9), 114.49 (C8), 110.27 (C7), 75.33 (C6), 69.17 (C5), 67.14 (C4), 64.40 (C3), 55.04 (23), 14.40 (C1).

3-O-ethyl-L-ascorbyl-6-palmitate **5**. Yield: and 47.1% mp: 121–129°C, bright yellow solid. Elemental analysis for $C_{24}H_{42}O_7$, expected value: C, 65.13; H, 9.57; O, 25.30; measured value: 65.10; H, 9.51; O, 25.28. ^{1}H NMR ($MeOD_3$, 400 MHz): δH 4.75 (1H, s,

H9), 4.38–4.36 (2H, m, H8), 4.29–4.18 (2H, m, H7), 4.12–4.08 (1H, m, H6), 2.40 (2H, t, H5), 1.66–1.61 (2H, t, H4), 1.40–1.37 (3H, t, H3), 1.30 (24H, m, H2), 0.93 (3H, t, H1); ^{13}C NMR ($MeOD_3$, 100 MHz): δC (ppm) 173.74 (C17), 171.74 (C16), 152.59 (C15), 118.69 (C14), 75.79 (C13), 66.66 (C12), 64.40 (C11), 62.09 (C10), 33.48 (C9), 31.69 (C8), 29.39–28.81 (C7 + C6 + C5), 24.59 (C4), 22.35 (C3), 14.4 (C2), 13.07 (C1).

Encapsulation of AA and AA Derivatives into LNPs

The encapsulation protocol was applied for AA, **1**, **4**, **5**, and **6** by the solvent shifting protocol.[205] Briefly, lignin solution were prepared adding KL (20.0 mg) in DMI (2.0 mL) at 45 °C under magnetic stirring for 24 h. Successively, the appropriate compound (0.03 mmol) was added at room temperature under magnetic stirring for 6 h. MilliQ water (6.0 mL) was added to previously solution to produce the corresponding LNPs-AA, LNPs-1, LNPs-4, LNPs-5, and LNPs-6, which were recovered by centrifugation (2000 rpm; 20 min) and freeze dry (LABCONCO, Kansas City, MO, USA, freeze time 48 h).

Determination of Loading Efficiency and Kinetic of Release of LNPs-4 and LNPs-5

The loading efficiency (LE) was evaluated by HPLC analysis of the supernatant recovered from the centrifugation step by applying the Equation (2):

$$LE\ (\%): \frac{(weight\ of\ starting\ SSF - weight\ of\ unloaded\ SSF)}{weight\ of\ starting\ SSF} \times 100$$

where LE represents the amount of encapsulated compound with respect to the initial concentration of esters **4** and **5.**

The HPLC analysis was performed by Ultimate 3000 Rapid Resolution system (ThermoFisher scientific, Waltham, MA, USA) equipped with Alltima C18 (250 mm × 4.6 mm, 5 μm) column, injection volume 10 μL, mobile phase flow rate 1.0 mL/min and a detector set up at 254 nm for ascorbic acid and compounds **1**, **5**, and **6**, and 320 nm for ester **4**. The analysis was repeated in triplicate. The compounds were separated by isocratic method using 95.0% of ultra-pure formic acid and 5.0% MeOH for 25 min and quantified by using the calibration curve method.

The profile release of LNPs-4 and LNPs-5 was evaluated suspending the sample (10.0 mg) in Na-acetate buffer (3.0 mL, pH 3.0 and 5.4) in dialysis bag (cellulose membrane, MWCO = 1.000) inserted in the acceptor compartment (25.0 mL) under slight stirring at room temperature for 24 h. At regular intervals time, aliquots (1.50 mL) were collected from the acceptor compartment with milliQ water replacing to maintain a constant volume. The aliquots were quantified by the HPLC method previously described using the calibration curve procedure. The measurements were performed in triplicate. Data were elaborated by applying the kinetic models reported in Equations (3)–(6),[455] including zero-order (3), first-order (4), Higuchi (5), and Korsmeyer–Peppas (6) models:

$$Q_0 - Q_t = k_0 t$$

$$\log C = \log C_0 - \frac{K_t}{2.303}$$

$$\frac{M_t}{M_\infty} = K_H * t^{\frac{1}{2}}$$

$$\frac{M_t}{M_\infty} = K_{KP} \ * \ t^{nKP}$$

where Q_0: the starting amount of compound dissolved in the solution; Q_t: amount of released compound at time (t); K_0: constant of zero-order release express in units of concentration/time; K: constant of first-order release presented in units of time^{-1}; C_0: starting concentration of compound; KH: constant of the Higuchi model; M_t: amount of released compound; M_∞: amount of compound in dosage form; M_t/M_∞: amount of compound released at time t ratio of released compound ratio; KP: release constant related to the Korsmeyer–Peppas model. In the Korsmeyer–Peppas "n" was found by using the portion of the release curve where $M_t/M_\infty < 0.6$.

Average Size and ζ-Potential Determination

The hydrodynamic diameter and ζ-potential values were evaluated in H_2O by dynamic light scattering (DLS) using a Zetasizer Nano ZS (Malvern Instruments, Malvern, UK) apparatus, equipped with He-Ne laser (633 nm, fixed scattering angle of 173°, 25 °C). Measurements were performed in triplicate at 25 °C.

FE-SEM Analyses

FE-SEM was carried out by ZEISS Gemini 500 (Oberkochen, Germany) at 5 kV. The appropriate compound in water (20 μL) was deposited on a coverslip coated with gold (AGAR Auto Sputter Coated) and dehydrated in air. The coverslip was mounted on the stub with conductive carbon glue and a thin film (5.0 nm) of chromium was deposited using the Sputter QUORUM Q 150T ES plus (Laughton, United Kingdom) to make the sample sufficiently conductive for measurement purposes.

Antioxidant Activity

The antioxidant activity was evaluated by the 2,2′-diphenyl picrylhydrazyl (DPPH) radical scavenging assay. The test was performed starting from different amounts of sample (500, 250, 100, 50, and 10 μg/mL) in water (0.550 mL) by addition to freshly prepared DPPH solution (2.45 mL, 0.7 mM in MeOH). The spectrophotometric analysis was carried out in duplicate at 25 °C. The radical scavenging activity was monitored as a function of time by measuring the absorbance band of DPPH at 517 nm (λ_{max}) until the absorbance value reached a plateau. The kinetic of the process was analyzed for each concentration tested, and the amount of DPPH remaining at the steady state was estimated. This value was used to calculate the IC_{50} (concentration of the substrate that causes 50% loss of DPPH activity). Data were expressed as percentage of inhibition of DPPH activity based on Equation (7):

$$inhibition\ of\ DPPH\ (\%): \frac{(Abs\ control - Abs\ sample)}{Abs\ control} \times 100$$

where "Abs control" is the absorbance of the DPPH solution in the absence of the sample. The measurements were performed in triplicate.

Thermal Stability Assay

The free and encapsulated AA esters (1.0 mg/mL) were incubated in Na-acetate aqueous (pH 3.0) solution in presence of DMI (7.0% v/v) as co-solvent into capped glass vials and placed in standard oven at 60 °C for 24 h. After incubation time, the residual compound was recovered by liquid-liquid extraction and quantified by HPLC analysis. In the case of LNPs-4 and LNPs-5 the analysis required the initial disaggregation of LNPs by

treatment with THF (5.0 mL) at room temperature under gentle magnetic stirring followed by filtration of the organic phase on 0.23 μm disc filter.

4.3.3 Results and discussions

Synthesis of 3-O-ethyl Ascorbic Acid Esters

Ascorbic acid esters have been previously synthesized by hazardous procedures for environment and human health, including Fischer esterification[456,457] and toxic acyl chlorides.[458] Alternative carbodiimide based coupling reactions, such as the use of N,N′-dicycloexhylcarbodiimide (DCC) and 1-ethyl-3-(3-dimethylaminopropyl)carbodiimide (EDC), were not completely deprived of environmental drawbacks.[459] Biocatalytic procedures involving lipase B from *Candida antarctica* furnished a greener procedure with both aromatic and aliphatic carboxylic acids even in organic solvent.[438] In this latter case, the esterification proceeded selectively at the primary alcoholic group of AA.[460] The application of lipase B from *Candida antarctica* in heterogeneous condition for the synthesis of AA esters is limited to the use of synthetic polyacrylic resin as a support.[461] Recently, we reported the immobilization of lipase M from *Mucor javanicus* on the surface of LNPs coated with chitosan and Concanavalin A, and its use for the synthesis of hydroxytyrosol esters in a cascade reaction with tyrosinase.[453] Here, we extended the application of this procedure (deprived of tyrosinase) for the immobilization of lipase B from *Candida antarctica* and the successive synthesis of 3-O-ethyl ascorbic acid esters. Briefly, the preparation of **biocatalyst I** required the following steps: (a) formation of LNPs from KL by nanoprecipitation in THF as primary solvent and water as antisolvent; (b) layer-by-layer coating of LNPs with chitosan; (c) concanavalin A deposition; and (d) immobilization of lipase. The schematic representation of the preparation of **biocatalyst I** is reported in **Figure 4.11**. The immobilization and activity of **biocatalyst I** resulted in 87% and 60%, respectively.

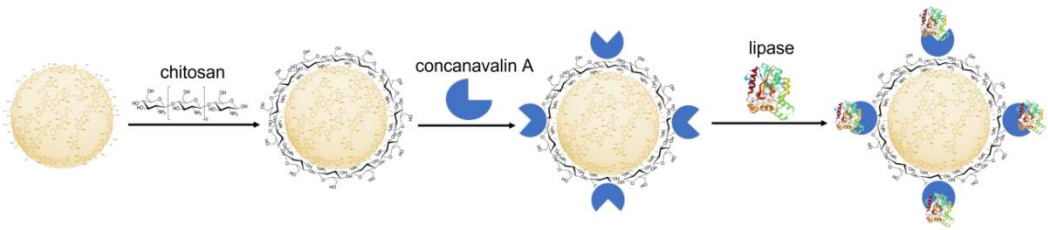


Figure 4.11. Schematic representation of preparation steps of biocatalyst I.

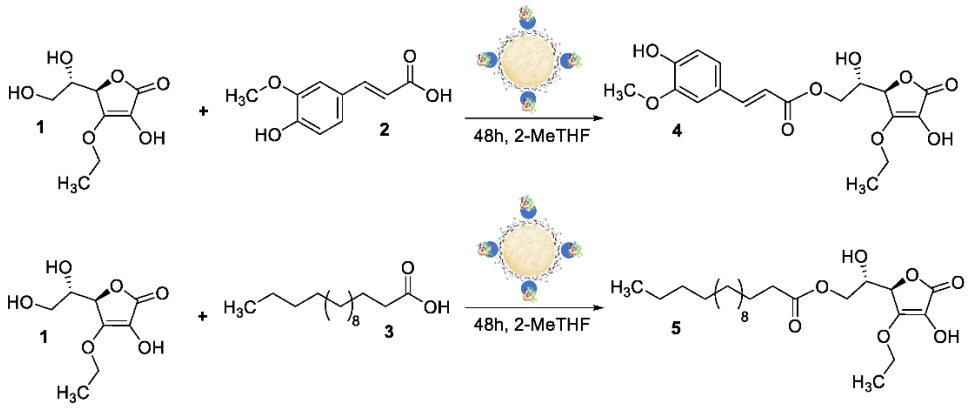
The kinetic parameters of **biocatalyst I** were determined by using the standard *para*-nitrophenyl laurate (*para*-NPL) assay and were compared with native lipase as a reference.[462] As reported in **Table 11**, **biocatalyst I** showed K_m value lower and V_{max} value higher than native lipase (**Table 11**) confirming the beneficial effect played by the immobilization process.

Table 11. Kinetic parameters of **biocatalyst I**.

Catalyst	K_m (mM) [1]	V_{max} (μmol L^{-1} s^{-1}) [2]
Free Lipase	4.2	0.24
Biocatalyst I	3.2	0.45

[1] Average error is 2–4%. [2] Average error is 1–3%.

FE-SEM image of **biocatalyst I** showed the presence of roughly aggregated on the surface on the particles in accordance with the deposition of ConA and lipase (reported in Supplementary Materials, Figure S1).
The synthesis of 3-O-ethyl ascorbic acid esters **4** and **5** was then performed starting from 3-O-ethyl ascorbic acid **1** (103 mg, 0.5 mmol) and equimolar amount of ferulic acid **2** (97.1 mg), or in alternative, palmitic acid **3** (128.2 mg), previously dissolved in 2-MeTHF (5.0 mL). 2-MeTHF was selected as reaction solvent due to the previously reported application in enzymatic transformations.[463,464] **Biocatalyst I** (5 U) was added to the solution and the mixture was gently stirred at 50 °C for 48 h under argon atmosphere in the presence of anhydrous molecular sieves (**Scheme 4.3**). 3-O-ethyl-L-ascorbyl-6-ferulate **4** and 3-O-ethyl-L-ascorbyl-6-palmitate **5** were obtained in 38.8% and 47.1% yields, respectively, beside the unreacted substrate. These yields are of the same order of magnitude as those obtained by chemical procedures, such as the Mitsunobu reaction described in Supplementary Materials Figure S2.



Scheme 4.3. Synthesis of 3-O-ethyl ascorbic acid esters 4 and 5 by using biocatalyst I in 2-MeTHF.

NMR data were in accordance with the proposed structures. In particular, the ^{1}H NMR spectrum of ester **4** and **5** showed the typical multiplet shift of CH_2 of ester bond at δ ppm 4.38 and 4.29, respectively, associated to the presence of the corresponding ^{13}C NMR signal at δ ppm 64.40 as reported in supporting information (Figures S3 and S4) The UV-vis absorbance analysis of dissolved esters **4** and **5** in comparison with **1** and **2** are reported in Supplementary Materials Figure S5.

Encapsulation of AA Derivatives and Morphological Characterization
The schematic representation for the encapsulation protocol is reported in **Figure 4.12**. Briefly, commercially available KL and esters **4** or **5** were dissolved in pure DMI[194] (primary solvent) in order to avoid the possible degradation processes due to the presence of water.[465] The solution was successively added with milliQ water (anti-solvent) at room temperature under gentle magnetic stirring with instantaneous precipitation of LNPs-4 and LNPs-5 which were fast recovered by centrifugation. Note that DMI was selected as primary solvent due to its certified eco-sustainability.[466] Ascorbic acid and compounds **1** and **6** were also encapsulated to obtain LNPs-AA, LNPs-1, and LNPs-6 as references. The encapsulation protocol was studied in different compound to LNPs ratios (ratio: 1:1, 1:5, 1:10) in order to evaluate the optimal experimental conditions.

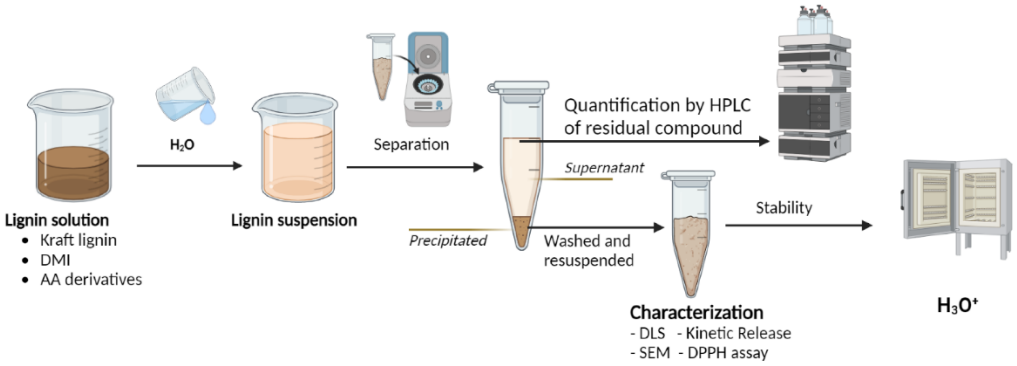
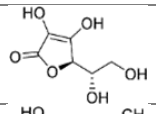
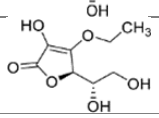
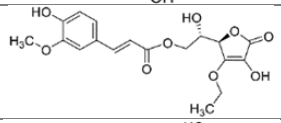
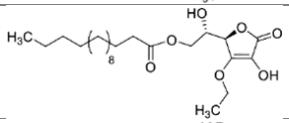
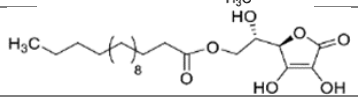


Figure 4.12. Schematic representation of the encapsulation protocol of esters **4** and **5.** DMI: dimethyl isosorbide; AA: ascorbic acid; DLS: dynamic light scattering; SEM: scanning electron microscopy.

The optimal condition corresponding to well dispersed LNPs was obtained in the 1:10 ratio, while undesired aggregates were observed under the resting experimental conditions. The loading efficiency (LE) was evaluated by HPLC analysis (original chromatograms are available in Figure S6) of the residual amounts of esters in the supernatant (see **Table 12**). LNPs-4 and LNPs-5 showed LE values higher than LNPs-AA and LNPs-1 as references. The high efficacy observed in the encapsulation of esters **4** and **5** was probably due to their high lipophilicity and steric hindrance which favoured the interaction with the hydrophobic core of LNPs.[467]

Table 12. Efficiency of loading of ascorbic acid esters and other AA derivatives into LNPs.

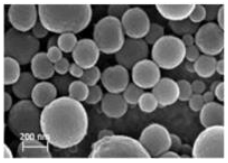
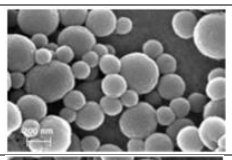
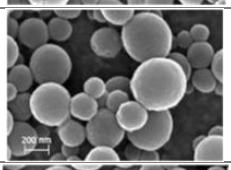
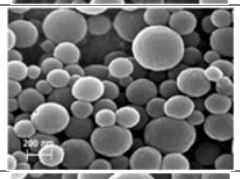
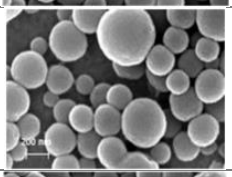
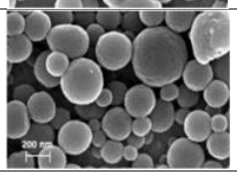
Name	LNPs	Structure	LE (% ± SD)
L-ascorbic acid (AA)	LNPs-AA		4.3 ± 0.91
3-*O*-ethyl-L-ascorbic acid (1)	LNPs-**1**		13.2 ± 1.62
3-*O*-ethyl-L-ascorbyl-6-ferulate (4)	LNPs-**4**		69.1 ± 1.91
3-*O*-ethyl-L-ascorbyl-6-palmitate (5)	LNPs-**5**		44.8 ± 3.12
L-ascorbyl-6-palmitate (6)	LNPs-6		32.8 ± 1.47

LE: loading efficiency calculated by Equation (2). SD: standard deviation; LNPs: lignin nanoparticles; AA: ascorbic acid.

In addition, π–π interactions between the aromatic moiety of the molecule and lignin subunits were probably operative in the case of ester **4**. Note that LNPs-4 and LNPs-5 also showed LE values higher LNPs-6, suggesting the beneficial role of the ethereal protection of the AA scaffold in the encapsulation procedure.

The size characterization of loaded LNPs and the empty counterpart was conducted by DLS analysis (**Table 13**). As a general trend, the average diameter of LNPs proportionally increased after the encapsulation by increasing the LE value. The PDI and Z-potential values remained similar to the empty LNPs.

Table 13. Morphology and size characterization of loaded LNPs.

Sample	Mean Size (nm ± SD)	PDI	Z-Potential (mV ± SD)	SEM Images
LNPs	221 ± 1.2	0.101	−34.5 ± 1.2	
LNPs-AA	226 ± 0.9	0.109	−34.9 ± 1.1	
LNPs-1	254 ± 1.4	0.121	−34.2 ± 0.7	
LNPs-4	314 ± 1.0	0.159	−35.4 ± 0.9	
LNPs-5	279 ± 1.1	0.111	−37.1 ± 1.4	
LNPs-6	259 ± 1.9	0.129	−36.8 ± 0.8	

PDI: polydispersion index; SD: standard deviation; LNPs: lignin nanoparticles; AA: ascorbic acid.

Release Profile and Kinetic Release Data of Esters 4 and 5 from LNPs

The release profiles of esters 4 and 5 were studied by analyzing the UV-absorption pattern of dialyzed solutions from LNPs-4 and LNPs-5 suspended in Na-acetate buffer (pH values 5.4 or 3.0) at room temperature for 24 h. The pH values were selected in order to model the microenvironment of the skin[468] and of typical anti-age serum formulations,[469] respectively (**Figure 4.13A**). As a general trend, the release of esters **4** and **5** was faster during the first 5 h, followed by a plateau. In addition, the release profile was favoured under the most acidic conditions. Ester **4** showed slight delay with respect to ester **5**, probably due to the presence of extra π–π interactions. After 24 h, esters **4** and **5** were released in 68% and 84% at pH 3.0 and in 62% and 78% at pH 5.4, respectively.

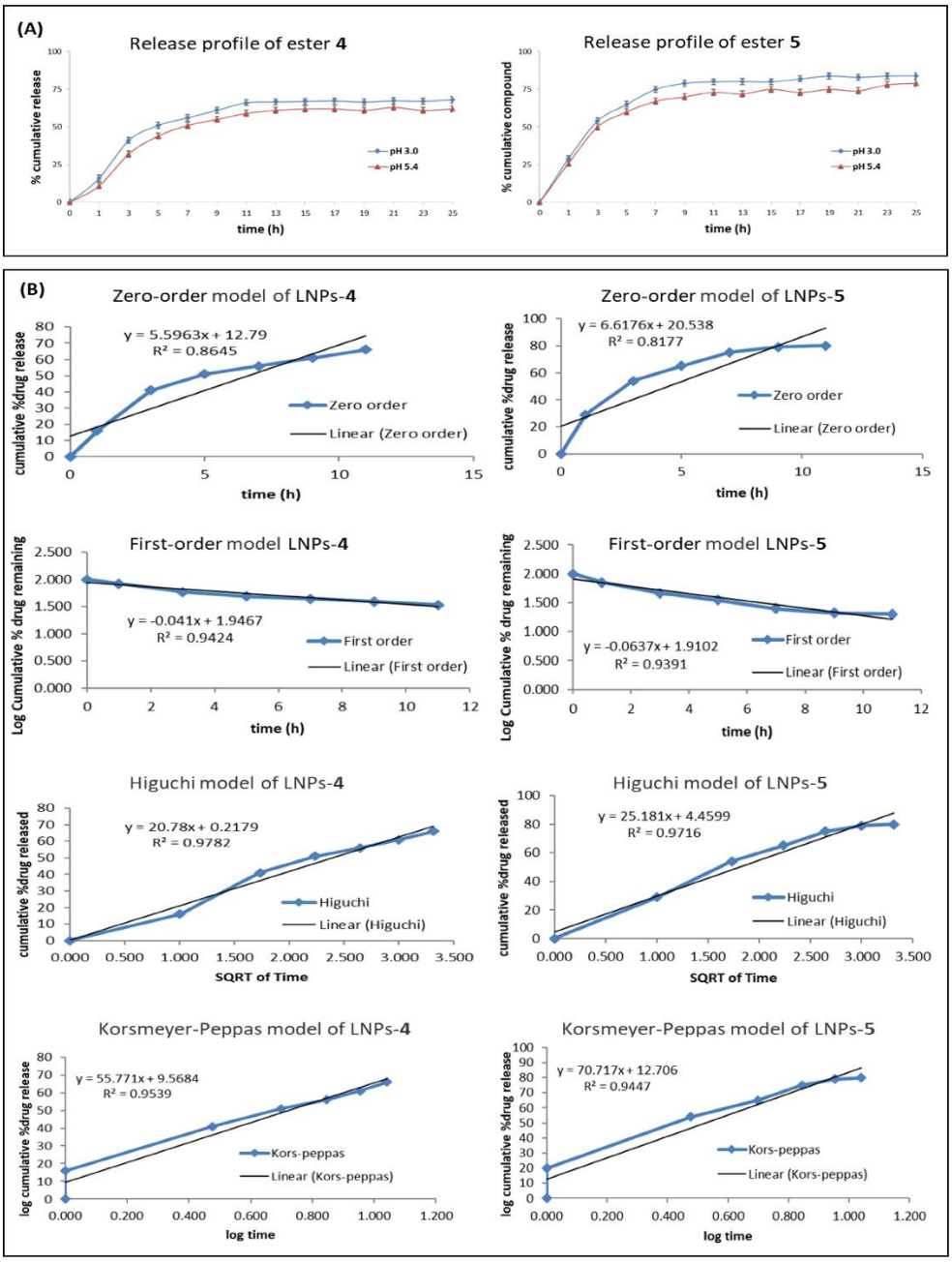


Figure 4.13 Panel (A) Release profile of esters 4 and 5 at selected pH values (pH 3.0 and pH 5.4). Panel (B) Zero-order, first-order, Higuchi and Korsmeyerñ–Peppas kinetic models for the release of esters 4 and 5 at pH 3.0.

Next, kinetic profiles of LNPs-4 and LNPs-5 were evaluated by fitting the release profiles data with zero-order, first-order, Higuchi, and Korsmeyerñ–Peppas kinetic models at pH 3.0 as a representative pH value (Section 3). The data plotting was expressed by using R^2 coefficient and linear regression (**Figure 4.13B**). The Higuchi model provided the best fit (R^2 value 0.9782 for LNPs-4 and 0.9716 for LNPs-5), confirming the presence of Fickian-like diffusion-controlled process.[470] This phenomenon is specific for host compounds which are characterized by a size significantly smaller than that of the carrier matrix and where swelling and matrix dissolution are negligible. Furthermore, first 60% ester release profile were fitted in Korsmeyer-Peppas model obtaining good fit (R^2 value 0.953 for LNPs-4 and 0.9447 for LNPs-5) and "n" index lower of 0.5, suggesting a quasi-Fickian diffusion process.[471]

Antioxidant Activity

The antioxidant activity of esters **4** and **5** was evaluated by spectrophotometric assay using 2,2-diphenyl-1-picrylhydrazyl (DPPH) as a probe. Ascorbic acid and compounds **1–2** and **6** were studied as references. The analysis was performed at different concentrations of the sample (500, 250, 100, 50, and 10 μg/mL) in milliQ water by monitoring the reduced form of DPPH at 517 nm.

The results were expressed in terms of IC_{50} (the amount of antioxidant compound required to inhibit the starting concentration of the DPPH radical by 50%) and antioxidant capacity index ACI (the inverse value of IC_{50}). Esters **4** exhibited lower IC_{50} and higher ACI values with respect to AA derivatives references (**Table 14**, entry 2–4), confirming the contribution of ferulic acid in the antioxidant activity, while ester **5** showed a similar trend to commercial analogue **6** (**Table 14**, entry 5–6).

Table 14. The antioxidant activity was expressed in IC_{50} values (μg/mL).

Entry	Compound	IC_{50} (μg/mL ± SD)	ACI
1	**AA**	6.5 ± 1.9	15.4
2	**1**	13.9 ± 2.7	7.2
3	**2**	21.7 ± 1.1	4.6
4	**4**	11.5 ± 3.8	8.7
5	**5**	17.1 ± 2.1	5.8
6	**6**	17.4 ± 1.1	5.7
8	LNPs	19.9 ± 3.4	5.0
9	LNPs-**4**	7.1 ± 2.2 (0.23) [a]	14.1
10	LNPs-**5**	12.1 ± 4.1 (0.33) [a]	8.3

IC_{50}: inhibition concentration; SD: standard deviation; ACI: antioxidant capacity index defined as the reciprocal of IC_{50}. A IC_{50} ratio obtained from Equation (1).

Next, the IC_{50} and ACI of LNPs-4 and LNPs-5 were evaluated by using empty LNPs as a reference (**Table 14**, entry 8–10). LNPs-4 and LNPs-5 showed IC_{50} values (7.1 and 12.1, respectively) lower than esters **4** and **5** alone (11.5 and 17.1, respectively). The improved antioxidant activity of esters **4** and **5** after encapsulation was probably due to the co-antioxidant effect exerted by LNPs (which showed the IC_{50} value of 19.9) in the scavenging of free radicals.[472] In order to evaluate the occurrence of a synergistic effect between lignin nanoparticles and loaded esters we applied Equation (1):

$$IC_{50}\ ratio = \frac{LNP_{sIC50}}{eLNPs_{IC50} + E_{IC50}} \times 100$$

where $LNPs_{IC50}$ is the IC_{50} value of LNPs-4 or LNPs-5, $eLNPs_{IC50}$ is the IC_{50} value of empty LNPs and E_{IC50} is the IC_{50} value of free esters **4** and **5**. The synergistic effect is represented by a ratio value < 0.5, while the simple additive effect corresponds to ratio > 0.5. LNPs-4 and LNPs-5 showed a synergistic effect occurring between lignin and loaded esters (ratio value 0.23 and 0.33, respectively) probably as a consequence of the regeneration of exhausted esters by electroactive LNPs trough hydrogen atom transfer (HAT).[473] Examples of synergistic effect between amorphous lignin and antioxidant compounds are documented,[474,475] and the role of the aromatic hydroxyl groups in the HAT mechanism discussed in detail in the case of LNPs.[476,477]

Thermal Stability

The chemical stability of esters **4** and **5** and corresponding LNPs-4 and LNPs-5 was evaluated in sodium acetate solution (pH 3.0) and DMI as co-solvent by heating the sample at 60 °C in a standard oven for 24 h in the presence of air. Sodium acetate solution was selected since pH 3 was characteristic of cosmetic formulation containing AA.[469] Ascorbic acid, compounds **1**, **6** and empty LNPs were studied as references. After the incubation time, the sample was analyzed in order to evaluate the residual amount of the original compound by HPLC analysis. In the case of LNPs-4 and LNPs-5 the analysis required the disaggregation of LNPs by treatment with THF at room temperature under gentle magnetic stirring followed by filtration of the organic phase on 0.23 μm disc filter. As expected, the almost total degradation of AA was observed after 24 h of treatment (**Figure 4.14**), while the AA derivatives **1** and **6** showed a moderate pH and thermal resistance (42.1% and 39.5%, respectively).[478] Esters **4–6** showed an improved stability as a consequence of the protection of the sensitive primary alcohol moiety in the AA scaffold. In this latter case, the contemporary protection of the enediol moiety further increased stability. Noteworthy, LNPs-4 and LNPs-5 fully retained stability after the thermal/pH treatment confirming the beneficial role exerted by the encapsulation process.

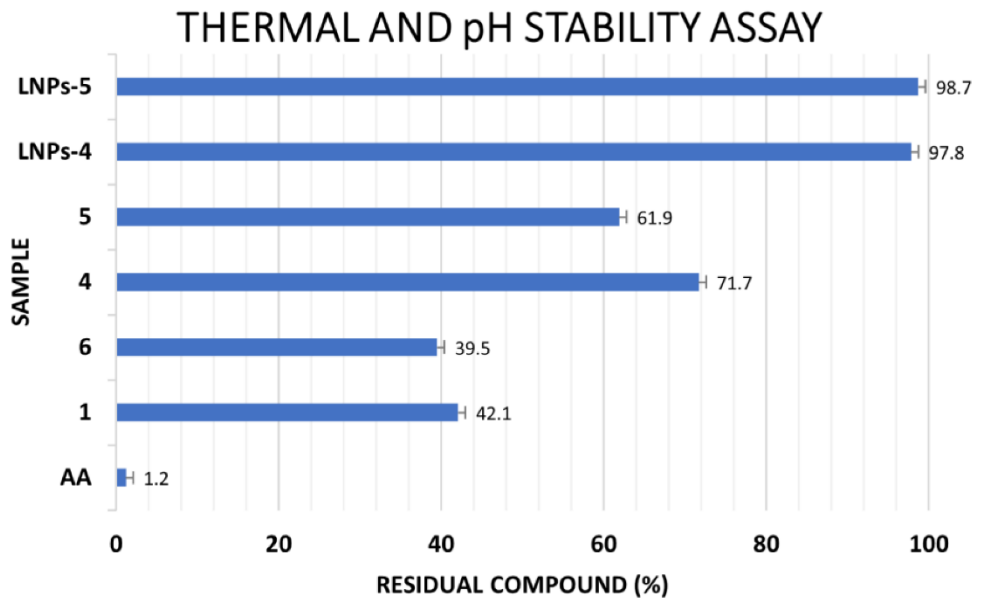


Figure 4.14. Evaluation of stability of AA derivatives under selected pH and temperature conditions.

References

230- Lehmann, P. Sun exposed skin disease. *Clin. Dermatol.* **2011**, 29, 180–188.
231- Sambandan, D.R.; Ratner, D. Sunscreens: An overview and update. J. Am. Acad. Dermatol. 2011, 64, 748–758.
232- Bessada, S.M.F.; Alves, R.C.; Oliveira, M.B.P.P. Coffee silverskin: A review on potential cosmetic applications. *Cosmetics* **2018**, 5, 1–5.
233- Kawczyk-Krupka, A.; Bugaj, A.M.; Latos, W.; Zaremba, K.; Sieroń, A. Photodynamic therapy in treatment of cutaneous and choroidal melanoma. *Photodiagn. Photodyn. Ther*. **2013**, 10, 503–509.
234- Abdul-Karim, R.M.; Cowey, C.L. Challenging the standard of care in advanced melanoma: Focus on pembrolizumab. *Cancer Manag. Res.* **2017**, 9, 433–442.
235- Rodil, R.; Moeder, M.; Altenburger, R.; Schmitt-Jansen, M. Photostability and phytotoxicity of selected sunscreen agents and their degradation mixtures in water. *Anal. Bioanal. Chem.* **2009**, 395, 1513–1524.
236- Rastogi, S.C. UV filters in sunscreen products—A survey. *Contact Dermat.* **2002**, 46, 348–351.
237- Battistin, M.; Dissette, V.; Bonetto, A.; Durini, E.; Manfredini, S.; Marcomini, A.; Casagrande, E.; Brunetta, A.; Ziosi, P.; Molesini, S.; et al. A new approach to UV protection by direct surface functionalization of TiO_2 with the antioxidant polyphenol dihydroxyphenyl benzimidazole carboxylic acid. *Nanomaterials* **2020**, 10, 231.
238- Sohn, M. UV booster and photoprotection. In Principles and Practice of Photoprotection. *Adis: Cham, Switzerland*, **2016**; pp. 227–245.
239- Juliano, C.; Magrini, G.A. Cosmetic ingredients as emerging pollutants of environmental and health concern. A mini-review. **Cosmetics** *2017*, 4, 11.
240- Senathirajah, K.; Attwood, S.; Bhagwat, G.; Carbery, M.; Wilson, S.; Palanisami, T. Estimation of the mass of microplastics ingested—A pivotal first step towards human health risk assessment. *J. Hazard. Mater.* **2021**, 404, 124004.
241- Sánchez-Quiles, D.; Tovar-Sánchez, A. Are sunscreens a new environmental risk associated with coastal tourism? *Environ. Int.* **2015**, 83, 158–170.
242- Gago-Ferrero, P.; Díaz-Cruz, M.S.; Barceló, D. An overview of UV-absorbing compounds (organic UV filters) in aquatic biota. *Anal. Bioanal. Chem.* **2012**, 404, 2597–2610.
243- Corinaldesi, C.; Marcellini, F.; Nepote, E.; Damiani, E.; Danovaro, R. Impact of inorganic UV filters contained in sunscreen products on tropical stony corals (*Acropora spp.). Sci. Total Environ.* **2018**, 637–638, 1279–1285.
244- Menard, A.; Drobne, D.; Jemec, A. Ecotoxicity of nanosized TiO_2. Review of in vivo data. *Environ. Pollut.* **2011**, 159, 677–684.
245- Huang, Y.; Law, J.C.F.; Lam, T.K.; Leung, K.S.Y. Risks of organic UV filters: A review of environmental and human health concern studies. *Sci. Total Environ.* **2021**, 755, 142486.
246- Nash, J.F.; Tanner, P.R. Relevance of UV filter/sunscreen product photostability to human safety. *Photodermatol. Photoimmunol. Photomed.* **2014**, 30, 88–95.
247- Santos, A.J.M.; Miranda, M.S.; Esteves da Silva, J.C.G. The degradation products of UV filters in aqueous and chlorinated aqueous solutions. *Water Res.* **2012**, 46, 3167–3176.
248- Damiani, E.; Astolfi, P.; Giesinger, J.; Ehlis, T.; Herzog, B.; Greci, L.; Baschong, W. Assessment of the photo-degradation of UV-filters and radical-induced peroxidation in cosmetic sunscreen formulations. *Free Radic. Res.* **2010**, 44, 304–312.
249- Lionetti, N.; Rigano, L. The New Sunscreens among Formulation Strategy, Stability Issues, Changing Norms, Safety and Efficacy Evaluations. *Cosmetics* **2017**, 4, 15.
250- Stein, H.V.; Berg, C.J.; Maung, J.N.; O'Connor, L.E.; Pagano, A.E.; Macmanus-Spencer, L.A.; Paulick, M.G. Photolysis and cellular toxicities of the organic ultraviolet filter chemical octyl methoxycinnamate and its photoproducts. *Environ. Sci. Process. Impacts* **2017**, 19, 851–860.
251- Lorigo, M.; Cairrao, E. Antioxidants as stabilizers of UV filters: An example for the UV-B filter octylmethoxycinnamate. *Biomed. Dermatology* **2019**, 3.
252- Hanson, K.M.; Gratton, E.; Bardeen, C.J. Sunscreen enhancement of UV-induced reactive oxygen species in the skin. *Free Radic. Biol. Med*. **2006**, 41, 1205–1212.
253- Napper, I.E.; Bakir, A.; Rowland, S.J.; Thompson, R.C. Characterisation, quantity and sorptive properties of microplastics extracted from cosmetics. *Mar. Pollut. Bull.* **2015**, 99, 178–185.
254- Ward, J.B.; Casagrande, S.S.; Cowie, C.C. Urinary phenols and parabens and diabetes among US adults, NHANES 2005–2014. *Nutr. Metab. Cardiovasc. Dis.* **2020**, 30, 768–776.
255- Kapelewska, J.; Kotowska, U.; Wiśniewska, K. Determination of personal care products and hormones in leachate and groundwater from Polish MSW landfills by ultrasound-assisted emulsification microextraction and GC-MS. *Environ. Sci. Pollut. Res*. **2016**, 23, 1642–1652.
256- Yang, C.; Lim, W.; Bazer, F.W.; Song, G. Avobenzone suppresses proliferative activity of human trophoblast cells and induces apoptosis mediated by mitochondrial disruption. *Reprod. Toxicol.* **2018**, 81, 50–57.
257- Ahn, S.; An, S.; Lee, M.; Lee, E.; Pyo, J.J.; Kim, J.H.; Ki, M.W.; Jin, S.H.; Ha, J.; Noh, M. A long-wave UVA filter avobenzone induces obesogenic phenotypes in normal human epidermal keratinocytes and mesenchymal stem cells. *Arch. Toxicol*. **2019**, 93, 1903–1915.

258- Klopčič, I.; Dolenc, M.S. Endocrine activity of AVB, 2MR, BHA, and their mixtures. *Toxicol. Sci*. **2017**.
259- Ruszkiewicz, J.A.; Pinkas, A.; Ferrer, B.; Peres, T.V.; Tsatsakis, A.; Aschner, M. Neurotoxic effect of active ingredients in sunscreen products, a contemporary review. *Toxicol. Rep.* **2017**, 4, 245–259
260- Janjua, N.R.; Mogensen, B.; Andersson, A.M.; Petersen, J.H.; Henriksen, M.; Skakkebæk, N.E.; Wulf, H.C. Systemic absorption of the sunscreens benzophenone-3, octyl- methoxycinnamate, and 3-(4-methyl-benzylidene) camphor after whole-body topical application and reproductive hormone levels in humans. *J. Investig. Dermatol*. **2004**, 123, 57–61.
261- Kunisue, T.; Chen, Z.; Buck Louis, G.M.; Sundaram, R.; Hediger, M.L.; Sun, L.; Kannan, K. Urinary concentrations of benzophenone-type UV filters in U.S. women and their association with endometriosis. *Environ. Sci. Technol.* **2012**, 46, 4624–4632.
262- Stiefel, C.; Schwack, W. Photoprotection in changing times—UV filter efficacy and safety, sensitization processes and regulatory aspects. *Cosmet. Sci.* **2014**, 37, 2–30.
263- Egambaram, O.P.; Kesavan Pillai, S.; Ray, S.S. Materials Science Challenges in Skin UV Protection: A Review. *Photochem. Photobiol*. **2020**, 96, 779–797.
264- Rojas, J.; Londoño, C.; Ciro, Y. The health benefits of natural skin uva photoprotective compounds found in botanical sources. *Int. J. Pharm. Pharm. Sci.* **2016**, 8, 13–23.
265- Morocho-Jácome, A.L.; Freire, T.B.; de Oliveira, A.C.; de Almeida, T.S.; Rosado, C.; Velasco, M.V.R.; Baby, A.R. In Vivo SPF from multifunctional sunscreen systems developed with natural compounds—A review. *J. Cosmet. Dermatol.* **2020**.
266- Korkina, L.; Kostyuk, V.; Potapovich, A.; Mayer, W.; Talib, N.; De Luca, C. Secondary plant metabolites for sun protective cosmetics: From pre-selection to product formulation. *Cosmetics* **2018**, 5, 32.
267- Korkina, L.G.; Mayer, W.; de Luca, C. Meristem plant cells as a sustainable source of redox actives for skin rejuvenation. *Biomolecules* **2017**, 7, 40.
268- Takshak, S.; Agrawal, S.B. Defense potential of secondary metabolites in medicinal plants under UV-B stress. *J. Photochem. Photobiol. B Biol.* **2019,** 193, 51–88.
269- Cavinato, M.; Waltenberger, B.; Baraldo, G.; Grade, C.V.C.; Stuppner, H.; Jansen-Dürr, P. Plant extracts and natural compounds used against UVB-induced photoaging. *Biogerontology* **2017**, 18, 499–516.
270- Nishida, Y.; Kumagai, Y.; Michiba, S.; Yasui, H.; Kishimura, H. Efficient extraction and antioxidant capacity of mycosporine-like amino acids from red alga dulse palmaria palmata in Japan. *Mar. Drugs* **2020**, 18, 502.
271- Whittock, A.L.; Turner, M.A.P.; Coxon, D.J.L.; Woolley, J.M.; Horbury, M.D.; Stavros, V.G. Reinvestigating the Photoprotection Properties of a Mycosporine Amino Acid Motif. *Front. Chem.* **2020**, 8.
272- Chrapusta, E.; Kaminski, A.; Duchnik, K.; Bober, B.; Adamski, M.; Bialczyk, J. Mycosporine-Like Amino Acids: Potential health and beauty ingredients. *Mar. Drugs* **2017**, 15, 326.
273- Pangestuti, R.; Siahaan, E.A.; Kim, S.K. Photoprotective substances derived from marine algae. *Mar. Drugs* **2018**, 16, 399.
274- Chiari, B.G.; Trovatti, E.; Pecoraro, É.; Corrêa, M.A.; Cicarelli, R.M.B.; Ribeiro, S.J.L.; Isaac, V.L.B. Synergistic effect of green coffee oil and synthetic sunscreen for health care application. *Ind. Crops Prod.* **2014**, 52, 389–393.
275- Tomaino, A.; Cristani, M.; Cimino, F.; Speciale, A.; Trombetta, D.; Bonina, F.; Saija, A. In vitro protective effect of a Jacquez grapes wine extract on UVB-induced skin damage. *Toxicol. In Vitro* **2006**, 20, 1395–1402.
276- Huynh, A.; Abou-Dahech, M.S.; Reddy, C.M.; O'Neil, G.W.; Chandler, M.; Baki, G. Alkenones, a renewably sourced, biobased wax as an SPF booster for organic sunscreens. *Cosmetics* **2019**, 6, 11.
277- Calcio Gaudino, E.; Tabasso, S.; Grillo, G.; Cravotto, G.; Dreyer, T.; Schories, G.; Altenberg, S.; Lauberte, L.; Telysheva, G. Wheat straw lignin extraction with bio-based solvents using enabling technologies. *Comptes Rendus Chem.* **2018**, 21, 563.
278- Xie, J.; Hse, C.-Y.; Shupe, T.F.; Hu, T. Physicochemical characterization of lignin recovered from microwave-assisted delignified lignocellulosic biomass for use in biobased materials. *J. Appl. Polym. Sci.* **2015**, 132, 42635–42642.
279- Brahim, M.; Checa Fernandez, B.L.; Regnier, O.; Boussetta, N.; Grimi, N.; Sarazin, C.; Husson, C.; Vorobiev, E.; Brosse, N. Impact of ultrasounds and high voltage electrical discharges on physico-chemical properties of rapeseed straw's lignin and pulps. *Bioresour. Technol.* **2017**, 237, 11–19
280- Gordobil, O.; Herrera, R.; Yahyaoui, M.; Ilk, S.; Kaya, M.; Labidi, J. Potential use of kraft and organosolv lignins as a natural additive for healthcare products. *RSC Adv.* **2018**, 8, 24525–24533.
281- Norgren, M.; Edlund, H. Lignin: Recent advances and emerging applications. *Curr. Opin. Coll. Interface Sci.* **2014**, 19, 409–416.
282- Stewart, D. Lignin as a base material for materials applications: Chemistry, application and economics. *Ind. Crops Prod.* **2008**, 27, 202–207.
283- Lendlein, A.; Balk, M.; Tarazona, N.A.; Oliver, E.C. Gould Bioperspectives for Shape-Memory Polymers as Shape Programmable. *Act. Mater.* **2019**, 20, 3627–3640.
284- Yuan, T.Q.; Xu, F.; Sun, R.C. Role of lignin in a biorefinery: Separation characterization and valorization. *J. Chem. Technol. Biotechnol.* **2013**, 88, 346–352.
285- Azadi, P.; Inderwildi, O.R.; Farnood, R.; King, D.A. Liquid fuels, hydrogen and chemicals from lignin: A critical review. *Renew. Sustain. Energy Rev.* **2013**, 21, 506–523.
286- Liao, J.J.; Latif, N.H.A.; Trache, D.; Brosse, N.; Hussin, M.H. Current advancement on the isolation, characterization and application of lignin. *Int. J. Biol. Macromol*. **2020**, 162, 985–1024.

287- Peart, C.; Ni, Y. UV-Vis spectra of lignin model compounds in the presence of metal ions and chelants. *J. Wood Chem. Technol.* **2001**, 21, 113–125.
288- Mahmood, Z.; Yameen, M.; Jahangeer, M.; Riaz, M.; Ghaffar, A.; Javid, I. Lignin as Natural Antioxidant Capacity. In Lignin.Trends and Applications; *IntechOpen: London*, UK, **2018**.
289- García, A.; González Alriols, M.; Spigno, G.; Labidi, J. Lignin as natural radical scavenger. Effect of the obtaining and purification processes on the antioxidant behaviour of lignin. *Biochem. Eng. J.* **2012**, 67, 173–185.
290- Yu, O.; Ho Kim, K. Lignin to Materials: A Focused Review on Recent Novel Lignin Applications. *Appl. Sci.* **2020**, 10, 4626.
291- In Vivo Toxicity Assessment of Chitosan-Coated Lignin Nanoparticles in Embryonic Zebrafish (Danio rerio). *Nanomaterials* **2021**, 11, 111.
292- Wang, B.; Sun, D.; Wang, H.M.; Yuan, T.Q.; Sun, R.C. Green and Facile Preparation of Regular Lignin Nanoparticles with High Yield and Their Natural Broad-Spectrum Sunscreens. *ACS Sustain. Chem. Eng.* **2019**, 7, 2658–2666.
293- Ratanasumarn, N.; Chitprasert, P. Cosmetic potential of lignin extracts from alkaline-treated sugarcane bagasse: Optimization of extraction conditions using response surface methodology. *Int. J. Biol. Macromol.* **2020**, 15, 138–145.
294- Gordobil, O.; Olaizola, P.; Banales, M.J.; Labidi, J. Lignins from Agroindustrial by-Products as Natural Ingredients for Cosmetics: Chemical Structure and In Vitro Sunscreen and Cytotoxic Activities. *Molecules* **2020**, 25, 1131.
295- Espinoza-Acosta, J.L.; Torres-Chávez, P.I.; Ramírez-Wong, B.; López-Saiz, C.M.; Montaño-Leyva, B. Antioxidant, antimicrobial, and antimutagenic properties of technical lignins and their applications. *BioResources* **2016**, 11, 5452–5481.
296- Jardim, J.M.; Hart, P.W.; Lucia, L.; Jameel, H. Insights into the Potential of Hardwood Kraft Lignin to Be a Green Platform Material for Emergence of the Biorefinery. *Polymers* **2020**, 12, 1795.
297- Kirsi, S. Mikkonen. Strategies for structuring diverse emulsion systems by using wood lignocellulose-derived stabilizers. *Green Chem.* **2020**, 22, 1019–1037.
298- Kleinert, M.; Barth, T. Phenols from lignin. *Chem. Eng. Technol.* **2008**, 31
299- Martínez, Á.T.; Rencoret, J.; Marques, G.; Gutiérrez, A.; Ibarra, D.; Jiménez-Barbero, J.; del Río, J.C. Monolignol acylation and lignin structure in some nonwoody plants: A 2D NMR study. *Phytochemistry* **2008**, 69, 2831–2843.
300- Guerriero, G.; Hausman, J.F.; Strauss, J.; Ertan, H.; Siddiqui, K.S. Lignocellulosic biomass: Biosynthesis, degradation, and industrial utilization. *Eng. Life Sci.* **2016**, 16, 1–16.
301- Wang, Y.; Chantreau, M.; Sibout, R.; Hawkins, S. Plant cell wall lignification and monolignol metabolism. *Front. Plant Sci.* **2013**, 4.
302- Davin, L.B.; Lewis, N.G. Lignin primary structures and dirigent sites. *Curr. Opin. Biotechnol.* **2005**, 16, 407–41.
303- Crestini, C.; Melone, F.; Sette, M.; Saladino, R. Milled wood lignin: A linear oligomer. *Biomacromolecules* **2011**, 12, 3928–3935.
304- Liu, Q.; Luo, L.; Zheng, L. Lignins: Biosynthesis and biological functions in plants. *Int. J. Mol. Sci.* **2018**, 19, 335.
305- Gellerstedt, G.; Henriksson, G. Monomers, Polymers and Composites from Renewable Resources; *Elsevier Science: Amsterdam, The Netherlands,* **2008**; ISBN 9780080453163.
306- Schutyser, W.; Renders, T.; Van den Bossche, G.; Van den Bosch, S.; Koelewijn, S.-F.; Ennaert, T.; Sels, B.F. Catalysis in Lignocellulosic Biorefineries: The Case of Lignin Conversion. *In Nanotechnology in Catalysis; Van de Voorde, M., Sels, B., Eds.; Wiley: Hoboken,* NJ, USA, **2017.**
307- Wang, H.; Male, J.; Wang, Y. Recent advances in hydrotreating of pyrolysis bio-oil and its oxygen-containing model compounds. *ACS Catal.* **2013**, 3, 1047–1070.
308- Giummarella, N.; Pu, Y.; Ragauskas, A.J.; Lawoko, M. A critical review on the analysis of lignin carbohydrate bonds. *Green Chem.* **2019**, 21, 1573–1595.
309- Duval, A.; Lawoko, M.; Hatakka, P.A.; Maciejewska, A.; Veringa, H.; Sanders, J.; Peteves, S.D.; Fernandes, E.M.; Pires, R.A.; Mano, J.F.; et al. A review on lignin-based polymeric, micro- and nano-structured materials. *React. Funct. Polym.* **2014**, 85, 78–96.
310- Espinoza-Acosta, J.L.; Torres-Chávez, P.I.; Carvajal-Millán, E.; Ramírez-Wong, B.; Bello-Pérez, L.A.; Montaño-Leyva, B. Ionic liquids and organic solvents for recovering lignin from lignocellulosic biomass. *BioResources* **2014**, 9, 3660–3687.
311- Baurhoo, B.; Phillip, L.; Ruiz-Feria, C.A. Effects of purified lignin and mannan oligosaccharides on intestinal integrity and microbial populations in the ceca and litter of broiler chickens. *Poult. Sci.* **2007**, 86, 1070–1078.
312- Baurhoo, B.; Ruiz-Feria, C.A.; Zhao, X. Purified lignin: Nutritional and health impacts on farm animals-A review. *Anim. Feed Sci. Technol.* **2008**, 144, 175–184.
313- Calvo-Flores, F.G.; Dobado, J.A. Lignin as renewable raw material. *ChemSusChem* **2010**, 3, 1227–1235.
314- Eastwood, M.; Kritchevsky, D. Dietary fiber: How did we get where we are? *Annu. Rev. Nutr.* **2005**, 25, 1–8.
315- Nasrullah, A.; Bhat, A.H.; Isa, M.H. Lignin: A sustainable biosorbent for heavy metal adsorption from wastewater, a review. *AIP Conf. Proc.* **2016**, 1787, 040001.
316- Vinardell, M.P.; Ugartondo, V.; Mitjans, M. Potential applications of antioxidant lignins from different sources. *Ind. Crops Prod.* **2008**, 27, 220–223.
317- Yamamoto, Y.; Shirono, H.; Kono, K.; Ohashi, Y. Immunopotentiating activity of the water-soluble lignin rich fraction prepared from lem—The extract of the solid culture medium of 90yridine edodes mycelia. *Biosci. Biotechnol. Biochem.* **1997**, 61, 1909–1912.

318- Vinardell, M.P.; Mitjans, M. Lignins and their derivatives with beneficial effects on human health. *Int. J. Mol. Sci.* **2017**, 18, 1219.
319- Evstigneyev, E.I.; Shevchenko, S.M. Structure, chemical reactivity and solubility of lignin: A fresh look. *Wood Sci. Technol.* **2019**, 53, 7–47.
320- Chollet, B.; Lopez-Cuesta, J.M.; Laoutid, F.; Ferry, L. Lignin nanoparticles as a promising way for enhancing lignin flame retardant effect in polylactide. *Materials* **2019**, 12, 2132.
321- Yang, W.; Rallini, M.; Wang, D.Y.; Gao, D.; Dominici, F.; Torre, L.; Kenny, J.M.; Puglia, D. Role of lignin nanoparticles in UV resistance, thermal and mechanical performance of PMMA nanocomposites prepared by a combined free-radical graft polymerization/masterbatch procedure. *Compos. Part A Appl. Sci. Manuf.* **2018**, 107, 61–69.
322- Rivière, G.N.; Korpi, A.; Sipponen, M.H.; Zou, T.; Kostiainen, M.A.; Österberg, M. Agglomeration of Viruses by Cationic Lignin Particles for Facilitated Water Purification. *ACS Sustain. Chem. Eng.* **2020**, 8, 416–4177.
323- Zhang, X.; Yang, M.; Yuan, Q.; Cheng, G. Controlled Preparation of Corncob Lignin Nanoparticles and their Size-Dependent Antioxidant Properties: Toward High Value Utilization of Lignin. *ACS Sustain. Chem. Eng*. **2019**, 7, 17166–17174.
324- Garver, T.M.; Callaghan, P.T. Hydrodynamics of Kraft Lignins. *Macromolecules* **1991**, 24, 420–430.
325- Lu, Y.; Fan, H.; Stump, A.; Ward, T.L.; Rieker, T.; Brinker, C.J. Aerosol-assisted self-assembly of mesostructured spherical nanoparticles. *Nature* **1999**, 398, 223–226.
326- Borisova, O.V.; Billon, L.; Cernochova, Z.; Lapp, A.; Stepanek, P.; Borisov, O.V. Effect of temperature on self-assembly of amphiphilic block-gradient copolymers of styrene and acrylic acid. *Macromol. Symp.* **2015**, 348, 25–32.
327- Guerra, A.; Gaspar, A.R.; Contreras, S.; Lucia, L.A.; Crestini, C.; Argyropoulos, D.S. On the propensity of lignin to associate: A size exclusion chromatography study with lignin derivatives isolated from different plant species. *Phytochemistry* **2007**, 68, 2570–2583.
328- Deng, Y.; Feng, X.; Yang, D.; Yi, C.; Qiu, X. π-π Stacking of the aromatic groups in lignosulfonates. *BioResources* **2012**, 7, 1145–1156.
329- Zhao, W.; Xiao, L.P.; Song, G.; Sun, R.C.; He, L.; Singh, S.; Simmons, B.A.; Cheng, G. From lignin subunits to aggregates: Insights into lignin solubilization. *Green Chem.* **2017**, 19, 3272–3281.
330- Whitesides, G.M.; Boncheva, M. Beyond molecules: Self-assembly of mesoscopic and macroscopic components. *Proc. Natl. Acad. Sci.* USA **2002**, 99, 4769–4774.
331- Lindström, T. The colloidal behaviour of kraft lignin. *Colloid Polym. Sci.* **1980**, 258, 390–397.
332- Lindström, T.; Westman, L. The colloidal behaviour of kraft lignin. *Colloid Polym. Sci.* **1982**, 260, 594–598.
333- Gupta, A.K.; Mohanty, S.; Nayak, S.K. Synthesis, Characterization and Application of Lignin Nanoparticles (LNPs). *Mater. Focus* **2015**, 3, 444–454.
334- Low, L.E.; I, K.C.; Siva, S.P.; Chew, I.M.L.; Mwangi, W.W.; Chew, C.L.; Goh, B.H.; Chan, E.S.; Tey, B.T. Lignin nanoparticles: The next green nanoreinforcer with wide opportunity. *Environ. Nanotechnol. Monit. Manag.* **2021**, 15, 100398.
335- Chowdhury, M.A. The controlled release of bioactive compounds from lignin and lignin-based biopolymer matrices. *Int. J. Biol. Macromol.* **2014**, 65, 136–147.
336- Ago, M.; Huan, S.; Borghei, M.; Raula, J.; Kauppinen, E.I.; Rojas, O.J. High-throughput synthesis of lignin particles (~30 nm to ~2 μm) via aerosol flow reactor: Size fractionation and utilization in pickering emulsions. *ACS Appl. Mater. Interfaces* **2016**, 8, 23302–23310.
337- C. Frangville, M. Rutkevičius, A. P. Richter, O. D. Velev, S. D. Stoyanov, V. N. Paunov. Fabrication of Environmentally Biodegradable Lignin Nanoparticles. *ChemPhysChem* **2012**, 13, 4235
338- Chen, L.; Zhou, X.; Shi, Y.; Gao, B.; Wu, J.; Kirk, T.B.; Xu, J.; Xue, W. Green synthesis of lignin nanoparticle in aqueous hydrotropic solution toward broadening the window for its processing and application. *Chem. Eng. J*. **2018**, 346, 217–225.
339- Ju, T.; Zhang, Z.; Li, Y.; Miao, X.; Ji, J. Continuous production of lignin nanoparticles using a microchannel reactor and its application in UV-shielding films. *RSC Adv.* **2019**, 9, 24915–24921.
340- Beisl, S.; Friedl, A.; Miltner, A. Lignin from micro- to nanosize: Applications. *Int. J. Mol. Sci.* **2017**, 18, 2367.
341- Myint, A.A.; Lee, H.W.; Seo, B.; Son, W.S.; Yoon, J.; Yoon, T.J.; Park, H.J.; Yu, J.; Yoon, J.; Lee, Y.W. One pot synthesis of environmentally friendly lignin nanoparticles with compressed liquid carbon dioxide as an antisolvent. *Green Chem.* **2016**, 18, 2129–2146.
342- Yiamsawas, D.; Beckers, S.J.; Lu, H.; Landfester, K.; Wurm, F.R. Morphology-Controlled Synthesis of Lignin Nanocarriers for Drug Delivery and Carbon Materials. *ACS Biomater. Sci. Eng.* **2017**, 3, 2375–2383.
343- Sauce, R.; Aparecida Sales de Oliveira Pinto, C.; Robles Velasco, M.V.; Rosado, C.; Rolim Baby, A. Ex Vivo penetration analysis and anti-inflammatory efficacy of the association of ferulic acid and UV filters. *Eur. J. Pharm. Sci.* **2021**, 156, 105578.
344- De Lima Cherubim, D.J.; Buzanello Martins, C.V.; Oliveira Fariña, L.; da Silva de Lucca, R.A. Polyphenols as natural antioxidants in cosmetics applications. *J. Cosmet. Dermatol.* **2020**, 19, 33–37.
345- Dizhbite, T.; Telysheva, G.; Jurkjane, V.; Viesturs, U. Characterization of the radical scavenging activity of lignins—Natural antioxidants. Bioresour. Technol. 2004, 95, 309–317.
346- Ibrahim, M.N.M.; Iqbal, A.; Shen, C.C.; Bhawani, S.A.; Adam, F. Synthesis of lignin based composites of TiO2 for potential application as radical scavengers in sunscreen formulation. *BMC Chem*. **2019**, 13, 17.

347- Freitas, F.M.C.; Cerqueira, M.A.; Gonçalves, C.; Azinheiro, S.; Garrido-Maestu, A.; Vicente, A.A.; Pastrana, L.M.; Teixeira, J.A.; Michelin, M. Green synthesis of lignin nano- and micro-particles: Physicochemical characterization, bioactive properties and cytotoxicity assessment. *Int. J. Biol. Macromol.* **2020**, 163, 1798–1809.
348- Pylypchuk, I.V.; Lindén, P.A.; Lindström, M.E.; Sevastyanova, O. New Insight into the Surface Structure of Lignin Nanoparticles Revealed by 1H Liquid-State NMR Spectroscopy. *ACS Sustain. Chem. Eng.* **2020**, 8, 13805–13812.
349- Trevisan, H.; Rezende, C.A. Pure, stable and highly antioxidant lignin nanoparticles from elephant grass. *Ind. Crops Prod.* **2020**, 145, 112105.
350- Morsella, M.; D'Alessandro, N.; Lanterna, A.E.; Scaiano, J.C. Improving the Sunscreen Properties of TiO_2 through an Understanding of Its Catalytic Properties. *ACS Omega* **2016**, 1, 464–469.
351- Widsten, P.; Tamminen, T.; Liitiä, T. Natural Sunscreens Based on Nanoparticles of Modified Kraft Lignin (CatLignin). *ACS Omega* **2020**, 5, 13438–13446.
352- Liu, R.; Dai, L.; Xu, C.; Wang, K.; Zheng, C.; Si, C. Lignin-Based Micro- and Nanomaterials and their Composites in Biomedical Applications. *ChemSusChem* **2020**, 13, 4266–4283.
353- Sadeghifar, H.; Ragauskas, A. Lignin as a UV Light blocker-a review. *Polymers* **2020**, 12, 1134.
354- Tribulová, T.; Kacík, F.; Evtuguin, D.; Cabalová, I. Assessment of chromophores in chemically treated and aged wood by uv-vis diffuse reflectance spectroscopy. *Cellul. Chem. Technol.* **2016**, 50, 659–667.
355- Wang, M.; Zhao, Y.; Li, J. From hollow lignin microsphere preparation to simultaneous preparation of urea encapsulation for controlled release using industrial kraft lignin via slow and exhaustive acetone-water evaporation. *Holzforschung* **2019**, 74, 77–87.
356- Ma, Z.; Liu, C.; Niu, N.; Chen, Z.; Li, S.; Liu, S.; Li, J. Seeking Brightness from Nature: J-Aggregation-Induced Emission in Cellulolytic Enzyme Lignin Nanoparticles. *ACS Sustain. Chem. Eng.* **2018**, 6, 3169–3175.
357- Furman, G.S.; Lonsky, W.F.W. Charge-transfer complexes in kraft lignin part 1: Occurrence. *J. Wood Chem. Technol.* **1988**, 8, 165–189.
358- Chang, H.T.; Su, Y.C.; Chang, S.T. Studies on photostability of butyrylated, milled wood lignin using spectroscopic analyses. *Polym. Degrad. Stab.* **2006**, 91, 816–822.
359- Li, Y.; Yang, D.; Lu, S.; Qiu, X.; Qian, Y.; Li, P. Encapsulating TiO2 in Lignin-Based Colloidal Spheres for High Sunscreen Performance and Weak Photocatalytic Activity. *ACS Sustain. Chem. Eng.* **2019**, 7, 6234–6242.
360- Yaqoob Khan, A.; Talegaonkar, S.; Iqbal, Z.; Jalees Ahmed, F.; Krishan Khar, R. Multiple Emulsions: An Overview. *Curr. Drug Deliv.* **2006**, 3, 429–443.
361- Benvegnu, T.; Plusquellec, D.; Lemiègre, L. Surfactants from renewable sources: Synthesis and applications. In Monomers, Polymers and Composites from Renewable Resources; Belgacem, M.N., Gandini, A., Eds.; *Elsevier Science: Amsterdam, The Netherlands*, **2008**; pp. 15–178.
362- Ruwoldt, J. A Critical Review of the Physicochemical Properties of Lignosulfonates: Chemical Structure and Behavior in Aqueous Solution, at Surfaces and Interfaces. *Surfaces* **2020**, 3, 42.
363- Low, L.E.; Siva, S.P.; Ho, Y.K.; Chan, E.S.; Tey, B.T. Recent advances of characterization techniques for the formation, physical properties and stability of Pickering emulsion. *Adv. Colloid Interface Sci.* **2020**, 277, 102117.
364- Oh-Hara, T.; Sakagami, H.; Kawazoe, Y.; Kaiya, T.; Komatsu, N.; Ohsawa, N.; Fujimaki, M.; Tanuma, S.I.; Konno, K. Antimicrobial spectrum of lignin-related pine cone extracts of pinus parviflora Sieb. Et Zucc. *In Vivo* **1990**, 4, 7–12.
365- Sláviková, E.; Košíková, B. Inhibitory effect of lignin by-products of pulping on yeast growth. *Folia Microbiol. Off. J. Inst. Microbiol. Acad. Sci. Czech Repub.* **1994,** 39, 241–243.
366- Richter, A.P.; Brown, J.S.; Bharti, B.; Wang, A.; Gangwal, S.; Houck, K.; Cohen Hubal, E.A.; Paunov, V.N.; Stoyanov, S.D.; Velev, O.D. An environmentally benign antimicrobial nanoparticle based on a silver-infused lignin core. *Nat. Nanotechnol.* **2015**, 10, 817–823.
367- Mohan, D.; Pittman, C.U.; Steele, P.H. Single, binary and multi-component adsorption of copper and cadmium from aqueous solutions on Kraft lignin—A biosorbent. *J. Coll. Interface Sci*. **2006**, 297, 489–504.
368- Wu, Y.; Zhang, S.; Guo, X.; Huang, H. Adsorption of chromium (III) on lignin. *Bioresour. Technol.* **2008**, 99, 7709–7715.
369- Harmita, H.; Karthikeyan, K.G.; Pan, X.J. Copper and cadmium sorption onto kraft and organosolv lignins. *Bioresour. Technol.* **2009**, 100, 6183–6191.
370- Guo, X.; Zhang, S.; Shan, X.-Q. Adsorption of metal ions on lignin. *J. Hazard. Mater.* **2008**, 28, 134–142.
371- Oviedo, C.; Rodríguez, J. EDTA: The chelating agent under environmental scrutiny. *Quim. Nova* **2003**, 26, 901–905.
372- Wang, J.; Deng, Y.; Qian, Y.; Qiu, X.; Ren, Y.; Yang, D. Reduction of lignin color via one-step UV irradiation. *Green Chem.* **2016**, 18, 695–699.
373- Li, C.; Ping, Q.; Shi, H.; Li, N.; Zhang, J.; Wang, C. A rapid and quantitative method for assessing the whiteness of whitened lignin based on an in-depth analysis of reported methods. *Int. J. Biol. Macromol.* **2020**, 156, 1483–1490.
374- Vainio, U.; Maximova, N.; Hortling, B.; Laine, J.; Stenius, P.; Simola, L.K.; Gravitis, J.; Serimaa, R. Morphology of dry lignins and size and shape of dissolved kraft lignin particles by X-ray scattering. *Langmuir* **2004**, 20, 9736–9744.
375- Zhang, H.; Chen, F.; Liu, X.; Fu, S. Micromorphology Influence on the Color Performance of Lignin and Its Application in Guiding the Preparation of Light-colored Lignin Sunscreen. *ACS Sustain. Chem. Eng.* **2018**, 6, 12532–12540.
376- Lee, S.C.; Yoo, E.; Lee, S.H.; Won, K. Preparation and application of light-colored lignin nanoparticles for broad-spectrum sunscreens. *Polymers* **2020**, 12, 699.
377- Hang, H.; Bai, Y.; Yu, B.; Liu, X.; Chen, F. A practicable process for lignin color reduction: Fractionation of lignin using methanol/water as a solvent. *Green Chem.* **2017**, 19, 5152–5162.

378- Tjeerdsma, B.F.; Boonstra, M.; Pizzi, A.; Tekely, P.; Militz, H. Characterisation of thermally modified wood: Molecular reasons for wood performance improvement. *Holz Roh Werkst.* **1998**, 56, 149–153.
379- Sundqvist, B.; Karlsson, O.; Westermark, U. Determination of formic-acid and acetic acid concentrations formed during hydrothermal treatment of birch wood and its relation to colour, strength and hardness. *Wood Sci. Technol.* **2006**, 40, 549–561.
380- Zhang, P.; Wei, Y.; Liu, Y.; Gao, J.; Chen, Y.; Fan, Y. Heat-induced discoloration of chromophore structures in Eucalyptus lignin. *Materials* **2018**, 11, 1686.
381- Zhang, H.; Bai, Y.; Zhou, W.; Chen, F. Color reduction of sulfonated eucalyptus kraft lignin. *Int. J. Biol. Macromol.* **2017**, 97, 201–208.
382- Podschuna, J.; Saakea, B.; Lehnenb, R. Reactivity enhancement of organosolv lignin by phenolation for improved bio-based thermosets. *Eur. Polym. J.* **2011**, 67, 1–11.
383- Matsushita, Y.; Yasuda, S. Preparation and evaluation of lignosulfonates as a dispersant for gypsum paste from acid hydrolysis lignin. *Bioresour. Technol.* **2005**, 96, 465–470.
384- Zhang, H.; Liu, X.; Fu, S.; Chen, Y. High-value utilization of kraft lignin: Color reduction and evaluation as sunscreen ingredient. *Int. J. Biol. Macromol*. **2019**, 133, 86–92.
385- Ahmed, M. B.; Johir, M. A. H.; Zhou, J. L.; Ngo, H. H.; Guo, W. S.; Sornalingam, K. Photolytic and photocatalytic degradation of organic UV filters in contaminated water. *Curr. Opin. Green Sustainable Chem.* **2017**, 6, 85−92.
386- Maier, H.; Schauberger, G.; Martincigh, B. S.; Brunnhofer, K.; Honigsmann, H. Ultraviolet protective performance of photoprotective lipsticks: change of spectral transmittance because of ultraviolet exposure. *Photodermatol., Photoimmunol. Photomed.* **2005,** 21, 84−92.
387- Benevenuto, C. G.; Di Matteo, M. A. S.; Campos, P. M. B. G. M.; Gaspar, L. R. Influence of the Photostabilizer in the Photoprotective Effects of a Formulation Containing UV-Filters and Vitamin A. *Photochem. Photobiol.* **2010**, 86, 1390−1396.
388- Fu, P. P.; Xia, Q. S.; Yin, J. J.; Cherng, S. H.; Yan, J.; Mei, N.; Chen, T.; Boudreau, M. D.; Howard, P. C.; Wamer, W. G. Photodecomposition of vitamin a and photobiological implications for the skin. *Photochem. Photobiol.* **2007**, 83, 409−424.
389- Butt, S. T.; Christensen, T. Toxicity and phototoxicity of chemical sun filters. *Radiat. Prot. Dosim.* **2000**, 91, 283−286.
390- Franca, C. C. V.; Ueno, H. M. Green cosmetics: perspectives and challenges in the context of green chemistry. *Desenvolv. Meio Ambiente* **2020**, 53, 133−150.
391- Haile, A.; Gelebo, G. G.; Tesfaye, T.; Mengie, W.; Mebrate, M. A.; Abuhay, A.; Limeneh, D. Y. Pulp and paper mill wastes: utilizations and prospects for high value-added biomaterials. *Bioresour. Bioprocess.* **2021**, 8, 35.
392- Garcia, A.; Amendola, D.; Gonzalez, M.; Spigno, G.; Labidi, J. 93yridine93 Natural Radical Scavenger. Study of the Antioxidant Capacity of Apple Tree Pruning Lignin Obtained by Different Methods. *Chem. Eng. Trans.* **2011**, 24, 925.
393- Alzagameem, A.; Klein, S. E.; Bergs, M.; Do, X. T.; Korte, I.; Dohlen, S.; Huwe, C.; Kreyenschmidt, J.; Kamm, B.; Larkins, M.; Schulze, M. Antimicrobial Activity of Lignin and Lignin-Derived Cellulose and Chitosan Composites against Selected Pathogenic and Spoilage Microorganisms. *Polymers* **2019**, 11, 670.
394- Ruthran, V. B.; Barman, P.; Kadam, R.; Kumar, A. Lignin-based adsorbent for effective removal of toxic heavy metals from wastewater. *Emergent Mater.* **2022**, 5, 923−943.
395- Stine, J. S.; Harper, B. J.; Conner, C. G.; Velev, O. D.; Harper, S. L. In Vivo Toxicity Assessment of Chitosan-Coated Lignin Nanoparticles in Embryonic Zebrafish (Danio rerio). *Nanomaterials* **2021**, 11, 111.
396- Bao, D. D.; Xie, Y. T.; Ma, S. L.; Wu, Z. B.; Piao, J. G. Self-assembly of a renewable lignin biopolymer in nanoparticles with multiple morphologies. *J. Appl. Polym. Sci.***2019**, 136 ().
397- Tran, M. H.; Phan, D. P.; Lee, E. Y. Review on lignin modifications toward natural UV protection ingredient for lignin-based sunscreens. *Green Chem.* **2021**, 23, 4633−4646.
398- Alqahtani, M. S.; Alqahtani, A.; Kazi, M.; Ahmad, M. Z.; Alahmari, A.; Alsenaidy, M. A.; Syed, R. Wound-healing potential of curcumin loaded lignin nanoparticles. *J. Drug Delivery Sci. Technol*. **2020**, 60, No. 102020.
399- Pang, Y. X.; Sun, Y. N.; Luo, Y. L.; Zhou, M. S.; Qiu, X. Q.; Yi, C. H.; Lou, H. M. Preparation of novel all-lignin microcapsules via interfacial cross-linking of pickering emulsion. *Ind. Crops Prod.* **2021**, 167, No. 113468.
400- Chaiyabutr, C.; Sukakul, T.; Kumpangsin, T.; Bunyavaree, M.; Charoenpipatsin, N.; Wongdama, S.; Boonchai, W. Ultraviolet filters in sunscreens and cosmetic products-A market survey. *Contact Dermatitis* **2021**, 85, 58−68.
401- Mturi, G. J.; Martincigh, B. S. Photostability of the sunscreening agent 4-tert-butyl-4'-methoxydibenzoylmethane (avobenzone) in solvents of different polarity and proticity. *J. Photochem. Photobiol., A* **2008**, 200, 410−420.
402- Jentzsch, F.; Olsson, O.; Westphal, J.; Reich, M.; Leder, C.; Kummerer, K. Photodegradation of the UV filter ethylhexyl methoxycinnamate under ultraviolet light: Identification and in silico assessment of photo-transformation products in the context of grey water reuse. *Sci. Total Environ.* **2016**, 572, 1092−1100.
403- Berenbeim, J. A.; Wong, N. G. K.; Cockett, M. C. R.; Berden, G.; Oomens, J.; Rijs, A. M.; Dessent, C. E. H. Unravelling the Keto-Enol Tautomer Dependent Photochemistry and Degradation Pathways of the Protonated UVA Filter Avobenzone. *J. Phys. Chem. A* **2020**, 124, 2919−2930.
404- Karlsson, I.; Hillerstrom, L.; Stenfeldt, A. L.; Martensson, J.; Borje, A. Photodegradation of Dibenzoylmethanes: Potential Cause of Photocontact Allergy to Sunscreens. *Chem. Res. Toxicol.* **2009**, 22, 1881−1892.
405- Hanson, K. M.; Narayanan, S.; Nichols, V. M.; Bardeen, C. J. Photochemical degradation of the UV filter octyl methoxycinnamate in solution and in aggregates. *Photochem. Photobiol. Sci*. **2015**, 14, 1607−1616.

406- Pattanaargson, S.; Limphong, P. Stability of octyl methoxycinnamate and identification of its photo-degradation product. *Int. J. Cosmet. Sci.* **2001**, 23, 153−160.
407- Broadbent, J. K.; Martincigh, B. S.; Raynor, M. W.; Salter, L. F.; Moulder, R.; Sjoberg, P.; Markides, K. E. Capillary supercritical fluid chromatography combined with atmospheric pressure chemical ionisation mass spectrometry for the investigation of photoproduct formation in the sunscreen absorber 2-ethylhexyl-p-methoxycinnamate. *J. Chromatogr. A* **1996**, 732, 101−110.
408- Lhiaubet-Vallet, V.; Marin, M.; Jimenez, O.; Gorchs, O.; Trullas, C.; Miranda, M. A. Filter-filter interactions. Photostabilization, triplet quenching and reactivity with singlet oxygen. *Photochem. Photobiol. Sci.* **2010**, 9, 552−558.
409- Afonso, S.; Horita, K.; Sousa e Silva, J. P.; Almeida, I. F.; Amaral, M. H.; Lobao, P. A.; Costa, P. C.; Miranda, M. S.; Esteves da Silva, J. C.; Sousa Lobo, J. M. Photodegradation of avobenzone: stabilization effect of antioxidants. *J. Photochem. Photobiol., B* **2014**, 140, 36−40.
410- Gaspar, L. R.; Campos, P. M. A HPLC method to evaluate the influence of photostabilizers on cosmetic formulations containing UV-filters and vitamins A and E. *Talanta* **2010**, 82, 1490−1494.
411- De Vaugelade, S.; Nicol, E.; Vujovic, S.; Bourcier, S.; Pirnay, S.; Bouchonnet, S. UV-vis degradation of alpha-tocopherol in a model system and in a cosmetic emulsion-Structural elucidation of photoproducts and toxicological consequences. *J. Chromatogr. A* **2017**, 1517, 126−133.
412- Qiu, X. Q.; Li, Y.; Qian, Y.; Wang, J. Y.; Zhu, S. P. Long-Acting and Safe Sunscreens with Ultrahigh Sun Protection Factor via Natural Lignin Encapsulation and Synergy. *ACS Appl. Bio Mater.* **2018**, 1, 1276−1285.
413- Chen, K.; Lei, L.; Qian, Y.; Xie, A. L.; Qiu, X. Q. Biomass Lignin Stabilized Anti-UV High Internal Phase Emulsions: Preparation, Rheology, and Application As Carrier Materials. *ACS Sustainable Chem. Eng.* **2019**, 7, 810−818.
414- Bertelli, M.; Kiani, A. K.; Paolacci, S.; Manara, E.; Kurti, D.; Dhuli, K.; Bushati, V.; Miertus, J.; Pangallo, D.; Baglivo, M.; Beccari, T.; Michelini, S. Hydroxytyrosol: A natural compound with promising pharmacological activities. *J. Biotechnol.* **2020**, 309, 29−33.
415- Pazos, M.; Alonso, A.; Sanchez, I.; Medina, I. Hydroxytyrosol prevents oxidative deterioration in foodstuffs rich in fish lipids. *J. Agric. Food Chem.* **2008**, 56, 3334−3340.
416- Aissa, I.; Kharrat, N.; Aloui, F.; Sellami, M.; Bouaziz, M.; Gargouri, Y. Valorization of antioxidants extracted from olive mill wastewater. *Biotechnol. Appl. Biochem.* **2017**, 64, 579−589.
417- Britton, J.; Davis, R.; O'Connor, K. E. Chemical, physical and biotechnological approaches to the production of the potent antioxidant hydroxytyrosol. *Appl. Microbiol. Biotechnol.* **2019**, 103, 5957−5974.
418- Guo, W.; An, Y.; Jiang, L.; Geng, C.; Zhong, L. The protective effects of hydroxytyrosol against UVB-induced DNA damage in HaCaT cells. *Phytother. Res.* **2010**, 24, 352−359.
419- Maitz, S.; Schlemmer, W.; Hobisch, M. A.; Hobisch, J.; Kienberger, M. Preparation and Characterization of a Water-Soluble Kraft Lignin. *Adv. Sustainable Syst.* **2020**, 4, No. 2000052.
420- Sztucki, M.; Narayanan, T. Development of an ultra-small-angle X-ray scattering instrument for probing the microstructure and the dynamics of soft matter. *J. Appl. Crystallogr.* **2007**, 40, S459−S462.
421- Wijaya, C. J.; Ismadji, S.; Gunawan, S. A Review of Lignocellulosic-Derived Nanoparticles for Drug Delivery Applications: Lignin Nanoparticles, Xylan Nanoparticles, and Cellulose Nanocrystals. *Molecules* **2021**, 26, 676.
422- Toro-Uribe, S.; Ibanez, E.; Decker, E. A.; McClements, D. J.; Zhang, R. J.; Lopez-Giraldo, L. J.; Herrero, M. Design, Fabrication, Characterization, and In Vitro Digestion of Alkaloid-, Catechin-, and Cocoa Extract-Loaded Liposomes. *J. Agric. Food Chem.* **2018**, 66, 12051−12065.
423- d'Agostino, S.; Azzali, A.; Casali, L.; Taddei, P.; Grepioni, F. Environmentally Friendly Sunscreens: Mechanochemical Synthesis and Characterization of beta-CD Inclusion Complexes of Avobenzone and Octinoxate with Improved Photostability. *ACS Sustainable Chem. Eng.* **2020**, 8, 13215−13225.
424- Sayre, R. M.; Dowdy, J. C.; Gerwig, A. J.; Shields, W. J.; Lloyd, R. V. Unexpected photolysis of the sunscreen octinoxate in the presence of the sunscreen avobenzone. *Photochem. Photobiol.* **2005**, 81, 452−456.
425- Kikuchi, A.; Yagi, M. Direct observation of the intermolecular triplet−triplet energy transfer from UV-A absorber 4-tert-butyl-4′-methoxydibenzoylmethane to UV-B absorber octyl methoxycinnamate. *Chem. Phys. Lett.* **2011**, 513, 63−66.
426- Isherwood, F.A.; Chen, Y.T.; Mapson, L.W. Synthesis of l-ascorbic acid in plants and animals. *Nature* **1953**, 171, 348–349.
427- Njus, D.; Kelley, P.M.; Tu, Y.J.; Schlegel, H.B. Ascorbic acid: The chemistry underlying its antioxidant properties. *Free Radic. Biol. Med.* **2020**, 159, 37–43.
428- Carita, A.C.; Fonseca-Santos, B.; Shultz, J.D.; Michniak-Kohn, B.; Chorilli, M.; Leonardi, G.R. Vitamin C: One compound, several uses. Advances for delivery, efficiency and stability. *Nanomed. Nanotechnol. Biol. Med.* **2020**, 24, 102117.
429- Levine, M. New concepts in the biology and biochemistry of ascorbic acid. *N. Engl. J. Med.* **1986**, 314, 892–902.
430- Drouin, G.; Godin, J.R.; Page, B. The Genetics of Vitamin C Loss in Vertebrates. *Curr. Genom.* **2011**, 12, 371–3787
431- Rowe, S.; Carr, A.C. Global Vitamin C Status and Prevalence of Deficiency: A Cause for Concern? *Nutrients* **2020**, 12, 2008.
432- Ravetti, S.; Clemente, C.; Brignone, S.; Hergert, L.; Allemandi, D.; Palma, S. Ascorbic Acid in Skin Health. *Cosmetics* **2019**, 6, 58.
433- Santos, P.H.S.; Silva, M.A. Retention of Vitamin C in Drying Processes of Fruits and Vegetables. A Review. *Dry Technol.* **2008**, 26, 1421–1437.

434- Ma, S. Formulation and Stability of Ascorbic Acid in Liquid and Semisolid Preparations; Baqai Medical University: Clachi, Pakistan, **2009**.
435- Smuda, M.; Glomb, M.A. Maillard Degradation Pathways of Vitamin C. *Angew. Chem. Int. Ed.* **2013**, 52, 4887–4891.
436- Spagnol, C.M.; Ferreira, G.A.; Chiari-Andreo, B.G.; Isaac, V.L.B.; Correa, M.A.; Salgado, H.R.N. Ascorbic acid in cosmetic formulations: Stability, in vitro release, and permeation using a rapid, inexpensive, and simple method. *J. Dispers. Sci. Technol.* **2017**, 38, 901–908.
437- Peyrat-Maillard, M.N.; Bonnely, S.; Rondini, L.; Berset, C. Effect of vitamin E and vitamin C on the antioxidant activity of malt rootlets extracts. *LWT Food Sci. Technol.* **2001**, 34, 176–182.
438- Karmee, S.K. Biocatalytic synthesis of ascorbyl esters and their biotechnological applications. *Appl. Microbiol. Biotechnol.* **2009**, 81, 1013–1022.
439- Sharma, S.; Kanwar, K.; Kanwar, S.S. Ascorbyl palmitate synthesis in an organic solvent system using a Celite-immobilized commercial lipase (Lipolase 100L). *3 Biotech* **2016**, 6, 183.
440- Amiri, S.; Rezazadeh-Bari, M.; Alizadeh-Khaledabad, M.; Amiri, S. New formulation of vitamin C encapsulation by nanoliposomes: Production and evaluation of particle size, stability and control release. *Food Sci. Biotechnol.* **2019**, 28, 423–432.
441- Esposito, E.; Cervellati, F.; Menegatti, E.; Nastruzzi, C.; Cortesi, R. Spray dried Eudragit microparticles as encapsulation devices for vitamin C. *Int. J. Pharm.* **2002**, 242, 329–334.
442- Abbas, S.; Da Wei, C.; Hayat, K.; Zhang, X.M. Ascorbic Acid: Microencapsulation Techniques and Trends-A Review. *Food Rev. Int.* **2012**, 28, 343–374.
443- Bajwa, D.S.; Pourhashem, G.; Ullah, A.H.; Bajwa, S.G. A concise review of current lignin production, applications, products and their environmental impact. *Ind. Crop. Prod.* **2019**, 139, 111526.
444- Garlapati, V.K.; Chandel, A.K.; Kumar, S.P.J.; Sharma, S.; Sevda, S.; Ingle, A.P.; Pant, D. Circular economy aspects of lignin: Towards a lignocellulose biorefinery. Renew. *Sustain. Energy Rev.* **2020**, 130, 109977.
445- Lu, X.Y.; Gu, X.L.; Shi, Y.J. A review on lignin antioxidants: Their sources, isolations, antioxidant activities and various applications. *Int. J. Biol. Macromol.* **2022**, 210, 716–741.
446- Dai, L.; Liu, R.; Hu, L.Q.; Zou, Z.F.; Si, C.L. Lignin Nanoparticle as a Novel Green Carrier for the Efficient Delivery of Resveratrol. *ACS Sustain. Chem. Eng.* **2017**, 5, 8241–8249
447- Piccinino, D.; Capecchi, E.; Trifero, V.; Tomaino, E.; Marconi, C.; Del Giudice, A.; Galantini, L.; Poponi, S.; Ruggieri, A.; Saladino, R. Lignin Nanoparticles as Sustainable Photoprotective Carriers for Sunscreen Filters. *ACS Omega* **2022**, 7, 37070–37077.
448- Gabellone, S.; Piccinino, D.; Filippi, S.; Castrignano, T.; Zippilli, C.; Del Buono, D.; Saladino, R. Lignin Nanoparticles Deliver Novel Thymine Biomimetic Photo-Adducts with Antimelanoma Activity. *Int. J. Mol. Sci.* **2022**, 23, 915.
449- Liao, W.C.; Huang, Y.T.; Lu, L.P.; Huang, W.Y. Antioxidant Ability and Stability Studies of 3-O-Ethyl Ascorbic Acid, a Cosmetic Tyrosinase Inhibitor. *J. Cosmet. Sci.* **2018**, 69, 233–243.
450- Benedini, L.; Schulz, E.P.; Messina, P.V.; Palma, S.D.; Allemandi, D.A.; Schulz, P.C. The ascorbyl palmitate-water system: Phase diagram and state of water. *Colloids Surface A* **2011**, 375, 178–185.
451- Hui, A.L.; Wang, Y.; Zhu, K.L.; Chen, J.C.; Fan, Q.P.; Zhou, A.; Zhang, W.C.; Wu, Z.Y. Synthesis and evaluation of novel ascorbyl cinnamates as potential anti-oxidant and antimicrobial agents. *Res. Chem. Intermed.* **2017**, 43, 5901–5916.
452- Spiclin, P.; Gasperlin, M.; Kmetec, V. Stability of ascorbyl palmitate in topical microemulsions. *Int. J. Pharm.* **2001**, 222, 271–279.
453- Tomaino, E.; Capecchi, E.; Piccinino, D.; Saladino, R. Lignin Nanoparticles Support Lipase-Tyrosinase Enzymatic Cascade in the Synthesis of Lipophilic Hydroxytyrosol Ester Derivatives. *Chemcatchem* **2022**, 14, e202200380.
454- Syedd-Leon, R.; Sandoval-Barrantes, M.; Trimino-Vasquez, H.; Villegas-Penaranda, L.R.; Rodriguez-Rodriguez, G. Revisiting the fundamentals of p-nitrophenol analysis for its application in the quantification of lipases activity. A graphical update. *Uniciencia* **2020**, 34, 31–43.
455- Dash, S.; Murthy, P.N.; Nath, L.; Chowdhury, P. Kinetic Modeling on Drug Release from Controlled Drug Delivery Systems. *Acta Pol. Pharm.* **2010**, 67, 217–223.
456- Huang, X.B.; Zhang, B.C.; Xu, H. Synthesis of some monosaccharide-related ester derivatives as insecticidal and acaricidal agents. *Bioorg. Med. Chem. Lett.* **2017**, 27, 4336–4340.
457- Kumar, S.; Singh, B.K.; Arya, P.; Malhotra, S.; Thimmulappa, R.; Prasad, A.K.; Van der Eycken, E.; Olsen, C.E.; De Pass, A.L.; Biswal, S.; et al. Novel natural product-based cinnamates and their thio and thiono analogs as potent inhibitors of cell adhesion molecules on human endothelial cells. *Eur. J. Med. Chem*. **2011**, 46, 5498–5511.
458- Shi, H.M.; Xie, D.S.; Yang, R.L.; Cheng, Y.Q. Synthesis of Caffeic Acid Phenethyl Ester Derivatives, and Their Cytoprotective and Neuritogenic Activities in PC12 Cells. *J. Agric. Food Chem.* **2014**, 62, 5046–5053.
459- Andrew Williams, I.T.I. Carbodiimide chemistry: Recent advances. Chem. Rev. 1981, 81, 589–636.
460- Yang, Y.H.; Raku, T.; Song, E.; Park, S.H.; Yoo, D.; Park, H.Y.; Kim, B.G.; Kim, H.J.; Lee, S.H.; Kim, H.S.; et al. Lipase catalyzed reaction of L-ascorbic acid with cinnamic acid esters and substituted cinnamic acids. *Biotechnol. Bioprocess Eng.* **2012**, 17, 50–54.
461- Chen, B.; Miller, M.E.; Gross, R.A. Effects of porous polystyrene resin parameters on Candida antarctica Lipase B adsorption, distribution, and polyester synthesis activity. *Langmuir* **2007**, 23, 6467–6474.
462- Hernandez-Garcia, S.; Garcia-Garcia, M.I.; Garcia-Carmona, F. An improved method to measure lipase activity in aqueous media. *Anal. Biochem.* **2017**, 530, 104–106.

463- Simeo, Y.; Sinisterraa, J.V.; Alcantara, A.R. Regioselective enzymatic acylation of pharmacologically interesting nucleosides in 2-methyltetrahydrofuran, a greener substitute for THF. *Green Chem.* **2009**, 11, 855–862.
464- Zippilli, C.; Bizzarri, B.M.; Gabellone, S.; Botta, L.; Saladino, R. Oxidative Coupling of Coumarins by Blue-LED-Driven in situ Activation of Horseradish Peroxidase in a Two-Liquid-Phase System. *Chemcatchem* **2021**, 13, 4151–4158.
465- Gerard, V.; Ay, E.; Graff, B.; Morlet-Savary, F.; Galopin, C.; Mutilangi, W.; Lalevee, J. Ascorbic Acid Derivatives as Potential Substitutes for Ascorbic Acid To Reduce Color Degradation of Drinks Containing Ascorbic Acid and Anthocyanins from Natural Extracts. *J. Agric. Food Chem.* **2019**, 67, 12061–12071.
466- Benazzouz, A.; Moity, L.; Pierlot, C.; Molinier, V.; Aubry, J.M. Hansen approach versus COSMO-RS for predicting the solubility of an organic UV filter in cosmetic solvents. *Colloids Surface A* **2014**, 458, 101–109.
467- Pereira, A.D.S.; de Oliveira, J.L.; Savassa, S.M.; Rogerio, C.B.; de Medeiros, G.A.; Fraceto, L.F. Lignin nanoparticles: New insights for a sustainable agriculture. *J. Clean. Prod.* **2022**, 345, 131145.
468- Ali, S.M.; Yosipovitch, G. Skin pH: From Basic Science to Basic Skin Care. *Acta Derm. Venereol.* **2013**, 93, 261–267.
469- Pinnell, S.R.; Yang, H.S.; Omar, M.; Riviere, N.M.; DeBuys, H.V.; Walker, L.C.; Wang, Y.H.; Levine, M. Topical L-ascorbic acid: Percutaneous absorption studies. *Dermatol. Surg.* **2001**, 27, 137–142.
470- Cailotto, S.; Gigli, M.; Bonini, M.; Rigoni, F.; Crestini, C. Sustainable Strategies in the Synthesis of Lignin Nanoparticles for the Release of Active Compounds: A Comparison. *ChemSusChem* **2020**, 13, 4759–4767.
471- Wu, I.Y.; Bala, S.; Skalko-Basnet, N.; di Cagno, M.P. Interpreting non-linear drug diffusion data: Utilizing Korsmeyer-Peppas model to study drug release from liposomes. *Eur. J. Pharm. Sci.* **2019**, 138, 105026.
472- Shikinaka, K.; Nakamura, M.; Navarro, R.R.; Otsukar, Y. Plant-Based Antioxidant Nanoparticles without Biological Toxicity. *Chemistryopen* **2018**, 7, 709–712.
473- Bae, S.; Choi, J.-H.; Ahn, M.; Kim, R.; Kim, H. Ethanol organosolv lignin as a substitute for commercial antioxidants, focusing on the structural properties and synergistic effect with myricetin. *Food Chem.* **2023**, 418, 136009.
474- Liu, D.; Li, Y.; Qian, Y.; Xiao, Y.; Du, S.J.; Qiu, X.Q. Synergistic Antioxidant Performance of Lignin and Quercetin Mixtures. *ACS Sustain. Chem. Eng.* **2017**, 5, 8424–8428.
475- Amorati, R.; Ferroni, F.; Lucarini, M.; Pedulli, G.F.; Valgimigli, L. A quantitative approach to the recycling of alpha-tocopherol by coantioxidants. *J. Org. Chem.* **2002**, 67, 9295–9303.
476- Olszowy-Tomczyk, M. Synergistic, antagonistic and additive antioxidant effects in the binary mixtures. *Phytochem. Rev.* **2020**, 19, 63–103.
477- Lauberte, L.; Fabre, G.; Ponomarenko, J.; Dizhbite, T.; Evtuguin, D.V.; Telysheva, G.; Trouillas, P. Lignin Modification Supported by DFT-Based Theoretical Study as a Way to Produce Competitive Natural Antioxidants. *Molecules* **2019**, 24, 1794.
478- Baschieri, A.; Amorati, R.; Benelli, T.; Mazzocchetti, L.; D'Angelo, E.; Valgimigli, L. Enhanced Antioxidant Activity under Biomimetic Settings of Ascorbic Acid Included in Halloysite Nanotubes. *Antioxidants* **2019**, 8, 30.

CHAPTER 5

MULTIENZYME CASCADE APPLICATIONS OF LIGNIN NANOPARTICLES

5.1. Lignin Nanoparticles Support Lipase-Tyrosinase Enzymatic Cascade in the Synthesis of Lipophilic Hydroxytyrosol Ester Derivatives

5.1.1 Aim of work

In the last years, lignin nanoparticles received a great attention due to the optimal chemo-physical properties they showed in the immobilization of different enzymes.[130-132,479,480,126] In this context, organosolv lignin nanoparticles (OLNPs) have been applied as functional nanoplatforms for the immobilization of laccase,[132,131] horseradish peroxidase,[480] and hydrolase,[126] showing the beneficial effect to improve the enzymatic activity by pseudo direct electron transfer (pseudo-DET) and mediated electron transfer (MET) processes.[132,481] Tyrosol, [2-(4-hydroxyphenyl) ethanol] and hydroxytyrosol [2-(3,4-dihydroxyphenyl)ethanol] are secondary metabolites produced in the cell by the shikimic acid pathway.[482] These compounds are well-recognized components in olive oil wastes, where they are recovered in high amount (about 1.0 g/L),[483] representing a valuable resource for sustainable green processes.[484] Tyrosol is resistant toward microbial degradation,[485] and it is characterized by a lower biological activity than hydroxytyrosol.[486] Pharmaceutical, nutraceutical and cosmeceutical properties of hydroxytyrosol are reported, including antioxidant activity,[487] and protective effect against cardiovascular diseases,[488] inflammation and neurodegenerative disorders.[488-490] Unfortunately, the high polarity of hydroxytyrosol limited its absorption, distribution, and excretion properties.[491] Chemical procedures for the oxidation of tyrosol to hydroxytyrosol are reported, encompassing the use of toxic halogenated reagents and solvents,[492] and tedious multi steps-procedures.[493,494] Enzymes are potent and selective catalysts in the transformation of phenol derivatives[492,495] under mild experimental conditions.[496] Examples of the enzymatic mediated oxidation of tyrosol to hydroxytyrosol are reported[492,497,498] under both homogeneous and heterogeneous conditions.[499] In addition, the activity and biological availability of hydroxytyrosol was improved through the synthesis of lipophilic esters[500] with high affinity for the cellular membrane,[501,502] by using multi-steps chemical[503] and enzymatic procedures.[504,505] These compounds showed antioxidant and antiviral activity dependent from the number of carbon atoms in the side-chain.[506] Enzymatic cascade is an advanced tool for multiple synthetic transformations in one-pot condition,[507,508] promoting the fast exchange of substrate between adjacent enzymes.[509,136] Supported multienzyme cascades are reported, and their efficiency, selectivity, stability and reusability deeply discussed.[479,142] Here we describe the one-pot synthesis of lipophilic hydroxytyrosol esters from tyrosol and long side-chain carboxylic acids by lignin nanoparticles supported enzymatic cascade involving lipase M from *Mucor javanicus* (MJL) and tyrosinase (Ty) from *Agaricus bisporus*. Previous examples of immobilization of Ty and MJL alone on lignin nanoparticles were reported by us in connection to the synthesis of bioactive catechols[130] and the esterification of butyric acid,[126] respectively. The novel lignin nanoparticles supported enzymatic cascade worked in mild experimental conditions using bio-renewable 2-methyltetrahydrofuran[510] and sodium phosphate buffer as reaction medium. MJL performed as a lyase between tyrosol and carboxylic acids,[511] while Ty catalyzed the selective ortho-hydroxylation of newly produced tyrosol esters to corresponding hydroxytyrosol counterpart. MJL and Ty were co-immobilized on lignin nanoparticles by a layer-by-layer (LBL) procedure using chitosan (CH) as positive charged polyelectrolyte to balance negative charged lignin and enzymes. Concanavalin A (Con A) was also used as a molecular spacer to confer an

ordered co-orientation at the two enzymes, thus favouring the optimal distance between their active sites.[512] The molecular recognition properties of Con A in the immobilization of enzymatic cascade was previously reported in the preparation of glucose oxidase and horseradish peroxidase biosensors.[479,512]

5.1.2 Experimental part

Materials
Organosolv lignin (OL) was purchased from Chemical Point (Oberhaching, Germany). Chitosan (medium molecular weight: 100.000-300.000), 2-(4-Hydroxyphenyl)ethanol (Tyrosol), octanoic acid, lauric acid, oleic acid, Amano lipase M from *Mucor javanicus* (300 U/mg), Concanavalin A (Con A) type IV from *Canavalia ensiformis* (Jack bean), mushroom tyrosinase from *Agaricus bisporus* (1000 U/mg), 4-nitrophenyl laurate, L-tyrosine, trizma base (primary standard and buffer) and sodium sulfate anhydrous (Na_2SO_4), were purchased from Sigma Chemical Co. (St Louis, MO, USA). Reagents including n-hexane, 2-methyltetrahydrofuran, and ethanol were purchased from Sigma Chemical Co. (St Louis, MO, USA) and were used without further purification. Sodium phosphate buffer (PBS 0.1 M, pH 7) and Tris-HCl (0.1 M, pH 7.4) were prepared using Milli-Q water (ρ=18.2 MΩ cm a 25 °C; TOC <10 μg L^{-1}, Millipore, Molsheim, France). Spectrophotometric analysis was performed with Cary 60 UV-Vis spectrophotometer equipped with a single cell peltier thermostated cell holder, Agilent, Santa Clara, USA. Data were elaborated with Cary Win UV software. Chemical reactions were monitored using thin layer chromatography on precoated aluminium silica gel Merck 60 F254 plates and a UV lamp (λ_{max} =254 nm) was used for visualization

*Preparation of **Catalyst I***
Organosolv lignin nanoparticles (OLNPs) were prepared by previously reported nanoprecipitation procedure.[132] Briefly, CH solution (5 mg, 1.0 mg mL^{-1} in diluted acetic acid 1.0 % v/v) that was added dropwise to OLNPs (5 mg, 1.0 mg mL^{-1}) in Milli-Q water under slow magnetic stirring (200 rpm) for 2 h at room temperature. The final suspension was centrifuged (2616 g, 20 min) and rinsed with deionized water, followed by centrifugation (2616 g, 20 min) and freeze-dry to yield OLNPs/CH intermediate. The yield of OLNPs/CH intermediate is defined as total amount in weight of nanoparticles recovered with respect to the total amount of the two components (lignin and CH) (yield 96 %). In order to prepare **Catalyst I**, the OLNPs/CH intermediate (1.5 mg mL^{-1}) were dispersed in sodium phosphate buffer (PBS 1.0 mL; 0,1 M, pH 7) and added of the appropriate amount of MJL (25 U; 3.0 mg mL^{-1}) and Ty (25 U; 1.0 mg mL^{-1}) dissolved in PBS (0.1 M; pH 7) under gentle stirring (200 rpm). The mixture was stirred at 4 °C in orbital shaking for 24 h and the suspension was centrifuged and washed two times with PBS (pH 7, 0.1 M) to afford **Catalyst I** (yield 85 %). Note that the enzymes were not released from **Catalyst I** in the reaction conditions (that is 2-MeTHF and PBS), as evaluated by Bradford analysis of the supernatant after recovery of the catalyst by centrifugation.

*Preparation of **Catalyst II***
For the preparation of **Catalyst II**, 0.5 mL of Con A solution (1.0 mg mL^{-1}) in PBS (0.1 M, pH 7.3) was added to OLNPs/CH intermediate (1.5 mg mL^{-1}) in PBS (1.0 mL; 0,1 M, pH 7) under gentle sonication conditions at 25 °C, followed by the addition of MJL (25 U; 3.0 mg mL^{-1}) and Ty (25 U; 1.0 mg mL^{-1}) dissolved in PBS (0.1 M; pH 7). The

mixture was stirred at 4 °C in orbital shaking for 24 h. The solution was centrifuged and washed two times with PBS (pH 7; 0.1 M) to afford **Catalyst II** (yield 88 %).

Field emission scanning electron microscopy (FE-SEM) characterization.
The field emission scanning electron microscopy (FE-SEM) of **Catalyst I** and **Catalyst II** was acquired on FESEM ZEISS GeminiSEM500, operated at 5 kV after drop 20μL (with deionized water) of sample dispersion on specimen stubs, air dried and coated with gold by sputtering with AGAR (Auto Sputter Coater). Before the observations, the sample received a deposition of chromium thin film (5 nm) by sputter coating using a QUORUM Q 150T ES plus coater.

Hydrodynamic diameter and ζ-potential analyses
The hydrodynamic diameter and ζ-potential values were evaluated in H_2O by dynamic light scattering (DLS) using a Zetasizer Nano ZS (Malvern Instruments, Malvern, UK) apparatus, equipped with an He−Ne laser (633 nm, fixed scattering angle of 173°, 25 °C). Measurements were performed in triplicate at 25 °C.

Fourier-transform infrared spectroscopy (FT-IR)
Catalyst I and **II** were analyzed by attenuated total reflection Fourier transform infrared (ATR-IR) spectroscopic using an Agilent Cary 630 FT-IR spectrometer (UATR unit cell) averaging 32 scans (resolution of 4 cm^{-1}).

Kinetic and activity parameters
The enzymatic activity and kinetic parameters of MJL and Ty were determined by using the *p*-NPL[513,514] and dopachrome assay,[515] respectively. In particular, the activity of MJL was evaluated by measuring the increase in absorbance (λ_{max} 405 nm) produced during the release of para-nitrophenol in the hydrolysis of para-nitrophenyl laurate (*p*-NPL) in Tris-HCl (0.1 M, pH 7.4) at 25 °C for 15 min. In a typical experiment, free MJL (25 U), or in alternative, **Catalyst I** and **Catalyst II** (1.5 mg mL^{-1} in PBS, 0.1 M, pH 7) were added to *p*-NPL solution (0.1 mL; 20 mM; $CNCH_3$: water 1 : 1) in Tris-HCl. The international unit of lipase activity was defined as the amount of enzyme necessary to hydrolyse 1.0 μmol of *p*-NPL in 1.0 min at 25 °C and optimal pH. The activity of Ty was measured by the dopachrome assay (λ_{max} 475 nm) in PBS (pH 7; 0.1 M) at 25 °C for 10 min. In a typical experiment, free Ty (25 U), or in alternative Catalyst I and Catalyst II (1.5 mg mL^{-1} in PBS, 0.1 M, pH 7), were added to L-tyrosine solution (1.0 mL; 2.5 mM) in PBS (pH 7; 0.1 M). The international unit of tyrosinase activity was defined as the amount of enzyme necessary to oxidize 1.0 μmol of L-tyrosine in 1.0 min at 25 °C and optimal pH. Kinetic parameters (Km and Vmax) of MJL, Ty and **Catalyst I** and **Catalyst II** were determined by measuring the activity of the appropriate enzyme (25 U) kept constant using different concentration of *p*-NPL (from 0 to 10 mM) in Tris-HCl (pH 7.4) and L-tyrosine (from 0.1 to 0.33 mM) in PBS (pH 7), respectively.

Förster resonance energy transfer (FRET)
The detailed procedure for the labelling of MJL and Ty and for the calculation of the FRET effect are reported in supporting (SI#3). The confocal images of **Catalyst I** and **Catalyst II** were obtained by ZEISS LSM-710 NLO confocal system equipped with a Plan Apochromat 100×/1.40 oil DIC M 27 objectives.

*Synthesis of tyrosol oleate **5** by esterification of tyrosol **1** with **Catalyst I** and **II***
The reactions were performed starting from different amount of tyrosol **1** (0.25, 0.14 and 0.36 mmol) and oleic acid **2** (0.25, 0.25 and 0.12 mmol) in the appropriate organic solvent

(5.0 mL) and PBS (0.1 mL) containing **Catalyst I–II** (165 μg) at 50 °C for 48 h under argon atmosphere. The reactions were monitored at regular intervals of time by thin layer chromatography (CH_2Cl_2: MeOH 9.8:0.2). At the end of the reaction the catalyst was recovered by centrifugation (6000 rpm) for 20 min, and the organic phase was evaporated under reduce pressure. The crude was dissolved in EtOAc (5.0 mL) and washed with NaCl saturated solution, dried over anhydrous Na_2SO_4 and evaporated. Reaction products were recovered after chromatographic purification using CH_2Cl_2: MeOH as eluent. The reaction with free MJL was also performed as a reference. Briefly, different amount of tyrosol **1** (0.25, 0.14 and 0.36 mmol) and oleic acid **2** (0.25, 0.25 and 0.12 mmol) were reacted in the appropriate organic solvent (5.0 mL) and PBS (0.1 mL) with MJL (25 U) at 50 °C for 48 h. The reactions were monitored at regular intervals by thin layer chromatography (CH_2Cl_2: MeOH 9.8:0.2). At the end of the reaction the organic phase was recovered and evaporated under reduce pressure. The crude was dissolved in EtOAc (5.0 mL) and washed with NaCl saturated solution, dried over anhydrous Na_2SO_4 and evaporated.

4-Hydroxyphenethyl oleate (tyrosol oleate) ***5***. Yield 50 % (47 mg); yellow oil. ^{1}H NMR (400 MHz, [D]$CDCl_3$): δ=0.90 (3H, m, CH_3), 1.29-1.30 (20H, m, CH_2), 1.59 (2H, m, CH_2), 2.02 (4H, m, CH_2), 2.30 (2H, m, O=C-CH_2), 2.88 (2H, m, CH_2), 4.26 (2H, m, OCH_2), 5.37 (2H, m, CH=CH), 6.79 (2H, d, J 9.0 Hz, Ph−H), 7.09 (2H, d, J 8.4 Hz, Ph−H) ppm. ^{13}C NMR (100 MHz, $CDCl_3$) δ: 14.8 (CH_3), 23.2 (CH_2), 25.4 (CH_2), 28.2 (CH_2x2), 28.7–30.8 (CH_2, x8), 32.4 (CH_2), 34.2 (CH_2), 36.3 (CH_2), 66.4 (CH_2), 117.2 (CH x2), 128 (CH x2), 129.9 I, 130.8 (CH, x2), 156.3 I, 173.2 I ppm. MS (EI) m/z 402.62

Synthesis of hydroxytyrosol esters ***8–11*** *by cascade enzymatic transformation of tyrosol* ***1*** *and carboxylic acids* ***2–4***

The reactions were performed starting from tyrosol **1** (0.25 mmol) and the appropriate carboxylic acid **2–4** (0.25 mmol) in 2-MeTHF (5.0 mL) and PBS (0.1 mL) containing **Catalyst I–II** (165 μg) and ascorbic acid (0.5 mmol) under dioxygen atmosphere (O_2) at 50 °C for 48 h. The reaction was monitored at regular times by thin layer chromatography (CH_2Cl_2: MeOH 9.8:0.2). At the end of the reaction the catalyst was recovered by centrifugation (2616 g) for 20 min, followed by evaporation of the solvent under reduced pressure. The crude was dissolved in EtOAc (5.0 mL) and washed with NaCl saturated solution, dried over anhydrous Na_2SO_4 and evaporated. Reaction products were recovered after chromatographic purification using CH_2Cl_2: MeOH as eluent. In one selected case, tyrosol **1** (0.25 mmol) was reacted with **2** (0.25 mmol) and **Catalyst II** (165 μg) in absence of ascorbic acid under previously reported experimental conditions. The work-up of the reaction was performed in the same conditions previously described to yield hydroxytyrosol ester **8** and hydroxytyrosol quinone ester **11**. As an alternative, tyrosol **1** (0.25 mmol) and oleic acid **2** (0.25 mmol) in 2-MeTHF (5.0 mL) and PBS (0.1 mL) were reacted in the presence of Catalyst III (165 μg) and Catalyst IV (165 μg) and ascorbic acid (0.5 mmol) under dioxygen atmosphere (O_2) at 50 °C for 48 h. The reaction was monitored at regular times by thin layer chromatography (CH_2Cl_2: MeOH 9.8:0.2). The work-up of the reaction was performed as reported in the previous procedures. The reusability of **Catalyst II** was evaluated after its recovering at the end of the reaction by centrifugation at 15000 g for 10 mins, followed by washing with PBS (pH 7.0, 0.1 M) and re-using it in next runs.

4-Hydroxyphenethyl dodecanoate (tyrosol laurate) ***6***. Yield 7 % (6 mg); yellow oil. ^{1}H NMR (400 MHz, [D] $CDCl_3$): δ=0.90 (3H, m, CH_3), 1.29 (16H, m, CH_2), 1.62 (2H, m, CH_2), 2.31 (2H, m, O=C CH_2), 2.88 (2H, m, CH_2), 4.27 (2H, m, OCH_2), 6.80 (2H, d, J

9.0 Hz, Ph−H), 7.07 (2H, d, J 8.4 Hz, Ph−H) ppm. ^{13}C NMR (100 MHz, [D]CDCl$_3$) δ=12.8 (CH$_3$), 22.5 (CH$_2$), 25.4 (CH$_2$), 28.2-30.5 (CH$_2$, x6), 32.4 (CH$_2$), 34.3 (CH$_2$, x2), 66.4 (CH$_2$), 116.2 (CH, x2), 130.9 I, 132.8 (CH, x2), 156.3 I, 173.9 I ppm. MS (EI) m/z 320.47.

4-Hydroxyphenethyl octanoate (tyrosol octanoate) ***7***. Yield 6 % (4.26 mg); yellow oil. ^{1}H NMR (400 MHz, [D]CDCl$_3$): δ=0.94 (3H, m, CH$_3$), 1.26-1.30 (8H, m, CH$_2$), 1.64 (2H, m, CH$_2$), 2.31 (2H, m, O=C CH$_2$), 2.89 (2H, m, CH$_2$), 4.26 (2H, m, OCH$_2$), 6.79 (2H, d, J 9.0 Hz, Ph−H), 7.09 (2H, d, J 8.4 Hz, Ph−H) ppm. ^{13}C NMR (100 MHz, [D]CDCl$_3$): δC=14.8 (CH$_3$), 22.7 (CH$_2$), 25.4 (CH$_2$), 28.2–30.5 (CH$_2$, 3x), 34.3 (CH$_2$), 35.2 (CH$_2$), 66.4 (CH$_2$), 115.9 (CH, x2), 130.9 I, 132.8 (CH, x2), 156.3 I, 174.2 I ppm. MS (EI) m/z 264.37.

3,4-Dihydroxyphenethyl oleate (Hydroxytyrosol oleate) ***8***. Yield 49 % (48 mg); colourless oil. ^{1}H NMR (400 MHz, [D]CDCl$_3$): δ=0.88 (3H, m, CH$_3$), 1.27-1.33 (20H, m, CH$_2$), 1.66 (2H, m, CH$_2$), 2.03 (4H, m, CH$_2$), 2.37 (2H, m, O=C-CH$_2$), 2.83 (2H, m, CH$_2$), 4.24 (2H, m, OCH$_2$), 5.35 (2H, m, CH=CH), 6.67 (1H, dd, J 7.9 Hz, Ph−H), 6.76 (1H, d, J 2.1 Hz, Ph−H), 6.81 (1H, d, J 8.0 Hz, Ph−H) ppm. ^{13}C NMR (100 MHz, [D]CDCl$_3$) δ=14.5 (CH$_3$), 23.2 (CH$_2$), 25.4 (CH$_2$), 27.2 (CH$_2$ x2), 28.5–30.1 (CH$_2$, x8), 30.2 (CH$_2$ x2), 31.5 (CH$_2$), 34.3 (CH$_2$), 35.2 (CH$_2$), 66.7 (CH$_2$), 116.2 (CH), 117.9 (CH), 122.5 (CH) 130.9 (CH x2), 131.7 (CH), 145.8 I, 146.3 I, 173.2 I ppm. MS (EI) m/z 418.62.

3,4-Dihydroxyphenethyl dodecanoate (Hydroxytyrosol laurate) ***9***. Yield 63 % (46 mg); yellow oil. ^{1}H NMR (400 MHz, [D]CDCl$_3$): δ=0.90 (3H, m, CH$_3$), 1.28–1.32 (16H, m, CH$_2$), 1.63 (2H, m, CH$_2$), 2.37 (2H, m, O=C-CH$_2$), 2.83 (2H, m, CH$_2$), 4.25 (2H, m, OCH$_2$), 6.65 (1H, dd, J 7.9 Hz, Ph−H), 6.76 (1H, d, J 2.1 Hz, Ph−H), 6.79 (1H, d, J 8.0 Hz, Ph−H) ppm. ^{13}C NMR (100 MHz, [D]CDCl$_3$): δ=13.9 (CH$_3$), 22.5 (CH$_2$), 24.8 (CH$_2$), 28.2–29.8 (CH$_2$ x6), 32.8 (CH$_2$), 34.3 (CH$_2$), 35.8 (CH$_2$), 65.4 (CH$_2$), 116.2 (CH), 117.2 (CH), 120.2 (CH), 131.9 I, 142.3 I, 145.1 I 173.2 I ppm. MS (EI) m/z 336.47.

3,4-Dihydroxyphenethyl octanoate (Hydroxytyrosol octanoate) ***10***. Yield 80 % (56.8 mg); colourless oil. ^{1}H NMR (400 MHz, [D]CDCl$_3$): δ=0.90 (3H, m, CH$_3$), 1.27–1.29 (8H, m, CH$_2$), 1.66 (2H, m, CH$_2$), 2.35 (2H, m, O=C-CH$_2$), 2.83 (2H, m, CH$_2$), 4.23 (2H, m, OCH$_2$), 6.76 (1H, dd, J 7.9 Hz, Ph−H), 6.77 (1H, d, J 2.1 Hz, Ph−H), 6.81 (1H, d, J 8.0 Hz, Ph−H) ppm. ^{13}C NMR (100 MHz, [D]CDCl$_3$): δ=13.8 (CH$_3$), 23.2 (CH$_2$), 24.8 (CH$_2$), 29.3–29.5 (CH$_2$ x2), 31.8 (CH$_2$), 33.9 (CH$_2$), 34.5 (CH$_2$), 64.8 (CH$_2$), 115.7 (CH), 116.3 (CH), 121.2 (CH), 130.9 I, 145.3 I, 146.3 I, 173.4 I ppm. MS (EI) m/z 280.36.

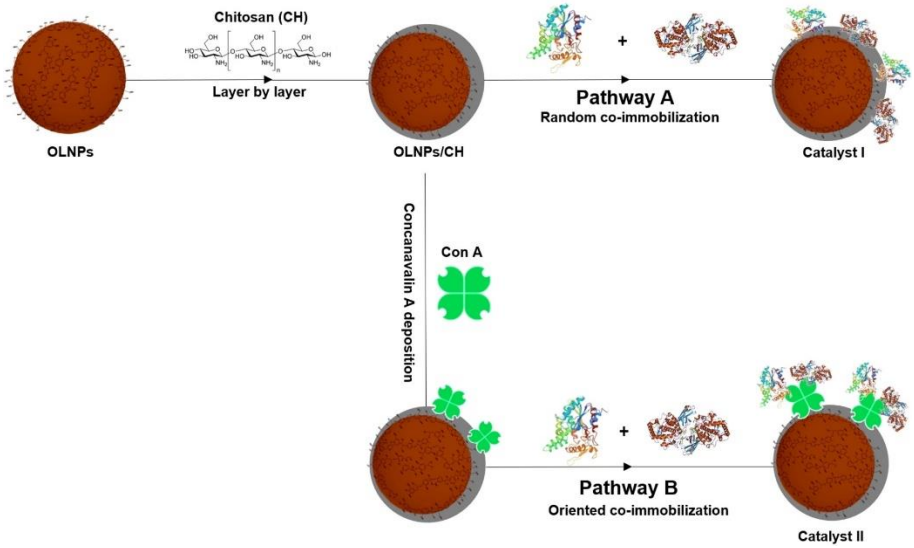
2-(3,4-Dioxocyclohexa-1,5dien-1-yl) ethyl oleate (hydroxyl tyrosol quinone oleate) ***11***. Yield 25 % (26.5 mg); yellow oil. ^{1}H NMR (400 MHz, [D]CDCl$_3$: δ=0.88 (3H, m, CH$_3$), 1.28 (21H, m, CH$_2$), 1.62 (2H, m, CH$_2$), 2.10 (4H, m, CH$_2$), 2.29 (2H, m, CH$_2$), 2.80 (2H, m, CH$_2$), 4.13 (2H, m, CH$_2$), 5.30 (2H, m, CH=CH), 5.89 (1H, s, Ph−H), 6.80 (1H, s, Ph−H), 7.25 (1H, s, Ph−H) ppm. ^{13}C NMR (100 MHz, [D]CDCl$_3$): δ=14.3 (CH$_3$), 23.2 (CH$_2$), 25.2 (CH$_2$), 27.2 (CH$_2$ x2), 28.5–29.9 (CH$_2$ x8), 32.3 (CH$_2$), 34.2 (CH$_2$), 39.1 (CH$_2$), 64.7 (CH$_2$), 113.5 (CH), 127.5 (CH), 130.7 (CH x2), 153.8 (CH), 156.3 I, 173.8 I, 180.4 I, 183.1 I ppm. MS (EI) m/z 416.60.

3,4-dihydroxyphenethyl alcohol (hydroxytyrosol) ***12***. Yield 10 % (10.6 mg); white solid. ^{1}H NMR (400 MHz, [D]CDCl$_3$): δ=2.77 (2H, m, CH$_2$), 3.85 (2H, m, CH$_2$), 4.58 (OH, m), 6.67 (1H, s, Ph−H), 6.77 (1 h, m, PH−H), 6.84 (1H, s, Ph−H) ppm. ^{13}C NMR (100 MHz,

[D]$CDCl_3$): δ=39.2 (CH_2), 61.1 (OCH_2), 115.9 (CH), 116.4 (CH), 122.2 (CH), 131.5 I, 144.5 I, 145.6 I ppm. MS (EI) m/z 154.06.

5.7.3 Results and discussions

OLNPs were prepared by nanoprecipitation of organosolv lignin (OL) in the presence of tetrahydrofuran (THF) as primary solvent and deionized water as anti-solvent.[195] In order to immobilize MJL and Ty, the positive charged layer of chitosan (CH) was initially coated on the negative charged surface of OLNPs to yield the OLNPs/CH intermediate (**Scheme 5.1**).[516] Briefly, a solution of CH in diluted acetic acid was added dropwise to a suspension of OLNPs in Milli-Q water under gentle magnetic stirring for 2 h at room temperature. The final suspension was centrifuged and lyophilized to afford OLNPs/CH intermediate in 96 % yield. Catalyst I was prepared by random immobilization of similar enzymatic units of MJL and Ty on OLNPs/CH intermediate. MJL (25 U) and Ty (25 U) in sodium phosphate buffer were added to OLNPs/CH intermediate (1.5 mg mL^{-1}) in PBS. The mixture was stirred at 4 °C in orbital shaking for 24 h. The suspension was centrifuged and washed two times with PBS to afford **Catalyst I** in 85 % yield (**Scheme 5.1,** pathway A). **Catalyst II** was prepared by co-oriented immobilization of MJL and Ty on OLNPs/CH intermediate by using Con A as a molecular spacer. Negative charged (ζ-potential −14 mV) Con A (0.5 mg)[517] in PBS was deposited on OLNPs/CH intermediate (1.5 mg mL^{-1}) in PBS under gentle sonication conditions for 5 min at room temperature to afford OLNPs/CH/Con A intermediate (Scheme 1, pathway B). Next, MJL (25 U) and Ty (25 U) in PBS were added to OLNPs/CH/Con A intermediate (1.5 mg mL^{-1}) in PBS, and the mixture was stirred at 4 °C for 24 h. The suspension was centrifuged and washed two times with PBS to afford **Catalyst II** in 88 % yield (**Scheme 5.1**, pathway B).



Scheme 5.1. Schematic representation of Catalyst I and Catalyst II. Random immobilization (pathway A); Oriented co-immobilization (pathway B)

Field emission scanning electron microscopy (FE-SEM) analysis of **Catalyst I** and **Catalyst II** (**Figure 5.1**) showed nanoparticles with regular spherical shape characterized, in the case of **Catalyst II**, by the typical corona-like structural motif associated to the presence of Con A (**Figure 5.1**, panel B) (FE-SEM analysis of OLNPs are reported in Supporting Information #1).[149] This different morphology was appreciable

from that observed for **Catalyst I**, in which case roughly aggregates of small clumps, typical of CH,[518] were present on the surface of the nanoparticles (**Figure 5.1**, panel A).

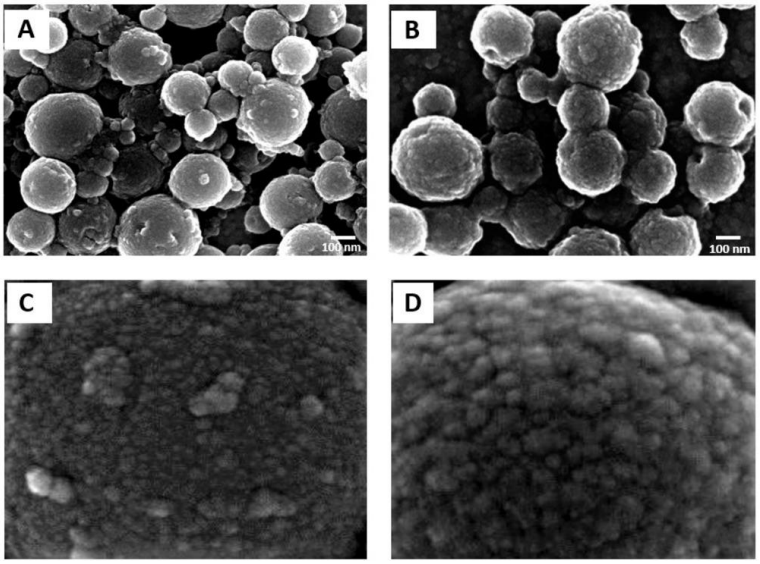


Figure 5.1. Field emission scanning electron microscopy (FE-SEM) images of **Catalyst I** (panel A) and **Catalyst II** (panel B). Panel C–D: magnification (x800k) of **Catalyst I** and **Catalyst II**, respectively.

Dynamic light scattering (DLS) and ζ-potential values of **Catalyst I** and **Catalyst II** are reported in **Table 15** and compared with OLNPs, and OLNPs/CH and OLNPs/CH/Con A intermediates, respectively (entries 1–5). **Catalyst I** and **Catalyst II** showed an average diameter of 378.8 nm and 526.5 nm, respectively, higher than OLNPs (**Table 15**, entries 4–5 versus entry 1). Note that, the diameter of **Catalyst I** increased of c.a. 50 nm with respect to OLNPs/CH intermediate after the deposition of the enzymes (**Table 15**, entry 4 versus entry 2, respectively). In a similar way, the diameter of **Catalyst II** increased of c.a. 74 nm with respect to OLNPs/CH/Con A intermediate (**Table 15**, entry 5 versus entry 3). In addition, an increase of about 100 nm was measured after deposition of Con A on OLNPs/CH intermediate. This latter trend was in accordance with previous reported data on the immobilization of enzymes on organic supports when mediated by Con A.[151] The value of the ζ-potential confirmed the occurrence of the expected coating sequence in the preparation of **Catalyst I** and **Catalyst II. Catalyst I** inverted the ζ-potential value with respect to OLNPs/CH intermediate which was characterized by a positive ζ-potential value (+26 mV), as a consequence of the balance with the negative charged enzymes (**Table 15**, entry 4 versus entry 2). Conversely, the ζ-potential of **Catalyst II** was similar to that of OLNPs/CH/Con A intermediate, having this latter compound a negative ζ-potential (**Table 15**, entry 5 versus entry 3). Probably, the efficacy of the supramolecular recognition between OLNPs/CH/Con A intermediate and MJL and Ty was controlled by the formation of H-bonding network than electrostatic interactions, in accordance with data previously reported.[519]

Table 15. DLS and ζ-potential of OLNPs/CH and OLNPs/CH/Con A intermediates and **Catalyst I–II**.

Entry	Sample	Size (nm)	ζ-potential (mV)
1	OLNPs	290.8	-43
2	OLNPs/CH	328.6	+26
3	OLNPs/CH/Con A	452.2	-30
4	Catalyst I	378.8	-36
5	Catalyst II	526.5	-48

The immobilization of MJL and Ty on OLNPs/CH intermediate was further confirmed by attenuated total reflectance FT-IR analysis (FT-IR analysis of OLNPs, OLNPs/CH and OLNPs/CH/Con A intermediates are reported in SI#2; Figure S2). The FT-IR spectrum of Catalyst I showed the typical bands of OLNPs/CH intermediate (**Figure 5.2**). In addition, the signal about 1500 cm^{-1} and 1600–1700 cm^{-1} were attributed to the stretching vibration of the amide II and amide I bands, respectively, which are characteristic of the polypeptide structure. FT-IR analysis was not diagnostic in the case of **Catalyst II**, due to the presence of bands associated to Con A.

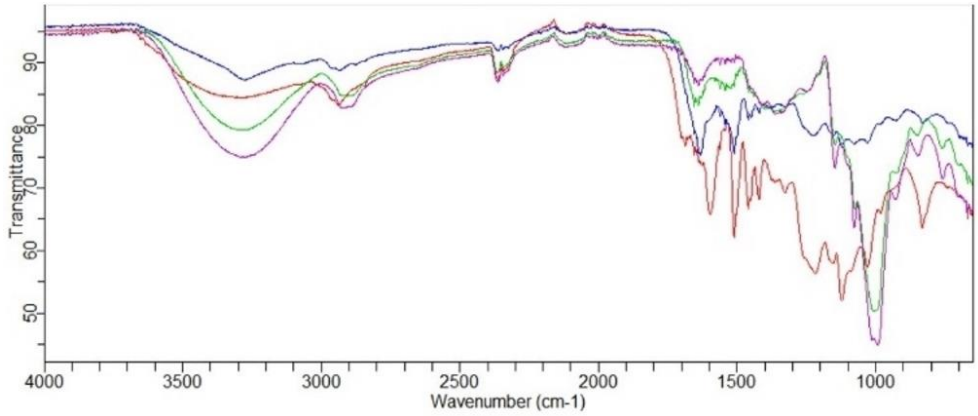


Figure 5.2. FT-IR spectra of **Catalyst I** (red line) and **Catalyst II** (blue line). The FT-IR spectra of free MJL (green line) and Ty (purple line) are reported as reference.

The activity parameters of **Catalyst I** and **Catalyst II** were evaluated as reported in Equations (1)-(3), respectively:

$$\text{Activity yield (\%)} = [U_x/(U_a — U_r)] \times 100 \quad (1)$$

$$\text{Immobilization yield (\%)} = [(U_a — U_r)/U_a] \times 100 \quad (2)$$

$$\text{Activity (units/mg)} = U_x/W_{support} \quad (3)$$

where U_x are the immobilized enzyme units, U_a are the total units of the enzyme added to the solution, and Ur are the residual units of the enzyme in the washing solution. The activity parameters of MJL were evaluated following the increase in absorbance (λ_{max} 405 nm) produced during the release of para-nitrophenol in the hydrolysis of para-nitrophenyl laurate (*p*-NPL) in Tris-HCl (0.1 M, pH 7.4) at 25 °C for 15 min.[513,514] In a typical

experiment, **Catalyst I** and **Catalyst II** (1.5 mg mL^{-1} in PBS) were added to *p*-NPL solution (20 mM) in Tris-HCl at 25 °C. The international unit of lipase activity was defined as the amount of enzyme necessary to hydrolyze 1.0 μmol of *p*-NPL in 1 min at 25 °C and optimal pH. The activity of Ty was measured by the dopachrome assay (λ_{max} 475 nm) in PBS at 25 °C for 10 min.[515] In a typical experiment, **Catalyst I** and **Catalyst II** (1.5 mg mL^{-1} in PBS) were added to L-tyrosine solution (2.5 mM) in PBS at 25 °C. The activity of Ty was determined following the increase in absorbance (λ_{max} 475 nm) during the oxidation of L-tyrosine in PBS at 25 °C for 10 min. The international unit of tyrosinase activity was defined as the amount of enzyme necessary to oxidize 1.0 μmol of L-tyrosine in 1 min at 25 °C and optimal pH. As reported in **Table 16**, the immobilization yield of MJL and Ty in **Catalyst II** was higher than that of **Catalyst I**, confirming the beneficial role of Con A in the immobilization procedure (entry 4 versus entry 3). In a similar way, the activity yield and the activity of MJL and Ty in **Catalyst II** were higher than that of **Catalyst I**. This effect was most probably due to the optimal co-orientation of the two enzymes, as successively confirmed by FRET analysis (see next paragraph).

Table 16. Immobilization and activity parameters of **Catalyst I** and **Catalyst II**.[a]

Entry	Catalyst	IY[b] of MJL (%)	IY of Ty (%)	AY[c] (%) and A[d] of MJL	AY (%) and A of Ty
1	MJL	-	-	10.6	-
2	Ty	-	-	-	11.8
3	I	80	50	20(8.4)[d]	14(12.2)[d]
4	II	87	69	60(15.9)[d]	45(15.7)[d]

[a] All experiments were conducted in triplicates. [b] Immobilization yield (%). [c] Activity yield (%). [d] Activity ($U/W_{support}$).

Kinetic parameters (K_m and V_{max}) of MJL and Ty in **Catalyst I** and **Catalyst II** (**Table 17**, entries 3 and 4) were determined by measuring the activity of the appropriate enzyme at different concentration of *p*-NPL (0–10 mM) and L-tyrosine (0.1–0.33 mM) by using the *p*-NPL[513] and dopachrome assays,[515] respectively. All measurements were performed by using the same amount of catalyst (1.5 mg). The data were analyzed by Lineweaver-Burk plots and the Michaelis-Menten constant and Vmax calculated in triplicate with the GraphPad software. Kinetic parameters of MJL and Ty were also calculated as a reference (**Table 17**, entries 1 and 2). **Catalyst II** showed a value of V_{max} for both MJL and Ty of the same order of magnitude than the native counterpart (**Table 17**, entries 3–4 versus 1–2), and higher than **Catalyst I** (**Table 17**, entry 4 versus entry 3), confirming the beneficial effect played by Con A in the immobilization process. K_m of MJL and Ty followed a similar trend (**Table 17**). This result is in accordance with data previously reported on the role played by the correct spatial distribution of the enzymes during the immobilization process in the overall catalytic activity of the enzymatic cascade.[479,520]

Table 17. Kinetic parameters of **Catalyst I** and **Catalyst II**.[a]

Entry	Catalyst	K_m (mM)[b] of MJL	K_m (mM) of Ty	V_{max} (μmol L^{-1} s^{-1})[c] of MJL	V_{max} (μmol L^{-1} s^{-1}) of Ty
1	MJL	5.3	-	0.24	-
2	Ty	-	0.18	-	0.62
3	**I**	8.30	0.45	0.22	0.54
4	**II**	3.17	0.16	0.45	0.75

[a] All experiments were conducted in triplicates. [b] Average error is 2–4 %. [c] Average error is 1–3 %.

In order to unambiguously confirm the proximity of MJL and Ty on the surface of **Catalyst II**, we measured the Förster resonance energy transfer (FRET) spectra by Zeiss LSM-710 laser confocal microscopy (CLSM) analysis,[521] comparing the result with **Catalyst I** as a reference (**Figure 5.3**, panel a-h). The FRET effect occurs between two fluorophores by non-radiative dipole-dipole coupling as a consequence of the energy transfer between a donor and acceptor dyes in close proximity (typically 1–10 nm).[522] **Catalyst I** and **Catalyst II** were labelled with fluorescein isothiocyanate (FITC) as donor dye, and with rhodamine B (Rho B) as the acceptor counterpart, respectively (labelling of MJL and Ty and confocal FRET microscopy procedure are reported in SI#3).[523] The effective presence of FITC-MJL on **Catalyst I–II** was detected in the donor channel mode at 490 nm (**Figure 5.3**, panel a and e; green fluorescence signal), while Rho B−Ty was detected in the acceptor channel mode at 560 nm (**Figure 5.3**, panel b and f; red fluorescence signal). The proximal localization of fluorophores, highlighted by the presence of a merged fluorescent signal, was observed only in the case **Catalyst II**, (**Figure 5.3**, panel g versus panel c). The elaboration of the FRET signal of **Catalyst II** (**Figure 5.3**, panel h)[524] indicated the presence of a distance of 6.7 nm between the two enzymes, a value that is comprised in the range of values for which the substrate channelling effect was operative.[525] The absence of the FRET signal in the case of **Catalyst I** (**Figure 5.3** panel d) suggested the random co-immobilization of the enzymes.

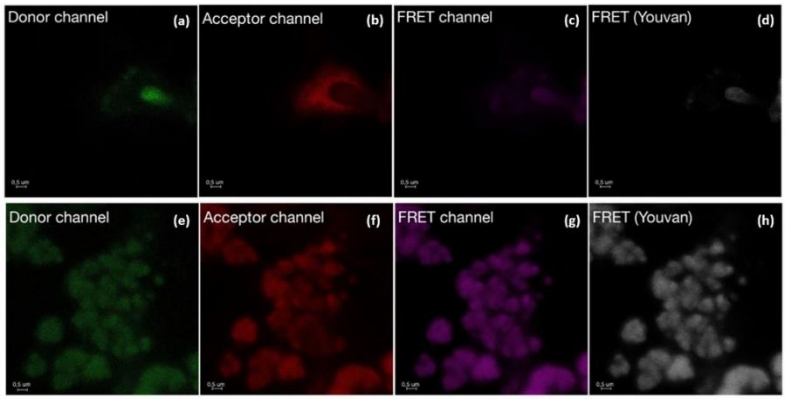
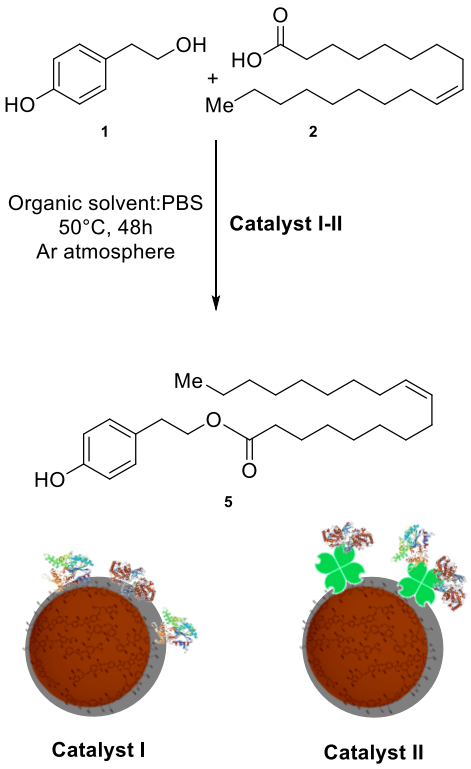


Figure 5.3. Laser confocal scanning microscopy of **Catalyst I–II**. Panel a: MJL labelled with FITC in the donor channel at 490 nm (green pixels) of **Catalyst I**. Panel b: Ty labelled with Rho B in the acceptor channel at 560 nm (red pixels) of **Catalyst I**. Panel c: FRET channel of merged fluorescence effect of **Catalyst I**. Panel d: original FRET signal of **Catalyst I**. PANEL e-h: donor, acceptor, FRET and original FRET channels respectively of **Catalyst II**.

Lipophilic esters of hydroxytyrosol were synthesized by reaction of tyrosol **1** with long-chain carboxylic acids including oleic acid (C18:1) **2**, lauric acid (C12) **3** and octanoic acid (C8) **4**. We first evaluated the effect played by the ratio between the two reagents and the polarity of the reaction solvent in the esterification step, analyzing the reaction of **1** and **2** as a selected case under argon atmosphere in order to selectively inhibit the activity of Ty (**Scheme 5.2**).



Scheme 5.2. Synthesis of tyrosol oleate **5** by reaction of tyrosol **1** and oleic acid **2** in the presence of **Catalyst I** and **Catalyst II**. The tyrosinase activity of **Catalyst I** and **Catalyst II** was inhibited by performing the reaction under argon atmosphere.

The reaction was performed using three different molar ratio of the reagents (1 : 1, 1 : 1.78 and 3 : 1 ratio, respectively). Compounds **1** and **2** were solubilized in organic solvents (5.0 mL) with different polarity (n-hexane, 2-methyltetrahydrofuran, and n-hexane/ethanol 9 : 1 v/v) in the presence of a low amount of PBS (0.1 mL) containing the appropriate amount of catalyst (165 μg) under argon atmosphere at 50 °C and gentle magnetic stirring (200 rpm). The organic solvents were selected among that previously reported in the lipase transformations,[510,526,527] while the low amount of PBS was required to hydrate the enzyme.[528] Higher amount of aqueous buffer is known to inhibit the esterase activity of lipase.[527] The range of temperature between 40 °C and 50 °C is a well-recognized temperature for the enzymatic synthesis of ester derivatives.[529] Similar reactions were performed with free MJL as a reference. **Table 18** summarizes the conversion of **1** and the yield of tyrosol oleate **5** depending on the ratio value of the reagents, the nature of the reaction solvent and the catalyst applied in the transformation. As expected, hydroxytyrosol was not detected in the reaction mixture due to the presence of the argon atmosphere inhibiting Ty activity. As a general trend, 2-methyltetrahydrofuran (2-MeTHF) performed as the best organic solvent in the synthesis of **5** under both homogeneous and heterogeneous conditions (**Table 18**, entries 10–18).

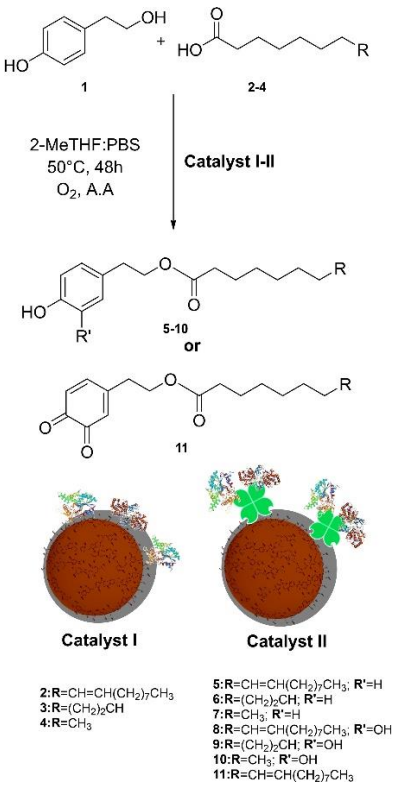
A lower yield of **5** was obtained in the presence of n-hexane (n-Hex) and n-Hex/Ethanol (EtOH; 9 : 1 v/v). Irrespective from the experimental conditions, the highest yield of **5** was generally obtained using the 1 : 1 ratio of the two reagents. 2-MeTHF is a bio-renewable reaction solvent[530] widely applied in bio-catalysis and esterification processes.[128,455] Among the different experimental conditions tested with 2-MeTHF, **Catalyst II** afforded **5** in yield higher than **Catalyst I** (**Table 18**, entry 16 versus entry 13). This result is in accordance with the higher activity and kinetic parameters of **Catalyst II** than **Catalyst I**. In addition, the reaction performed with **Catalyst II** in 2-MeTHF afforded **5** in a yield comparable to (**Table 18**, entry 16 versus entry 10), or higher than (**Table 18**, entries 17 and 18 versus entries 11 and 12), free MJL. On the basis of these data, we selected 2-MeTHF and the molar ratio value of 1 : 1 between **1** and long-chain carboxylic acids **2–4** to generalize the procedure for the synthesis of hydroxytyrosol ester derivatives **8–10**. In this latter case, the reaction was performed under dioxygen atmosphere (O_2) to activate the catecholase activity of Ty in the enzymatic cascade (**Scheme 5.3**).

Table 18. Synthesis of tyrosol oleate **5** from tyrosol **1** and oleic acid **2** in the presence of **Catalyst I** and **Catalyst II**.[a]

Entry	Organic solvent	MJL/Catalyst	1 (mmol)	2 (mmol)	Ratio ½	Conversion[b] [%]	Yield[c] [%]
1	n-Hex	MJL	0.25	0.25	1:1	38	35
2	n-Hex	MJL	0.14	0.25	1:2	5	3.2
3	n-Hex	MJL	0.36	0.12	3:1	16	15
4	n-Hex	**Catalyst I**	0.25	0.25	1:1	3.8	2.7
5	n-Hex	**Catalyst I**	0.14	0.25	1:2	1.6	1.4
6	n-Hex	**Catalyst I**	0.36	0.12	3:1	3.0	3.0
7	n-Hex	**Catalyst II**	0.25	0.25	1:1	12.5	11
8	n-Hex	**Catalyst II**	0.14	0.25	1:2	2.3	2.1
9	n-Hex	**Catalyst II**	0.36	0.12	3:1	5.6	5.6
10	2-Me-THF	MJL	0.25	0.25	1:1	57	57
11	2-Me-THF	MJL	0.14	0.25	1:2	23	22
12	2-Me-THF	MJL	0.36	0.12	3:1	29.5	29
13	2-MeTHF	**Catalyst I**	0.25	0.25	1:1	27	27
14	2-MeTHF	**Catalyst I**	0.14	0.25	1:2	20	19
15	2-MeTHF	**Catalyst I**	0.36	0.12	3:1	13	12
16	2-MeTHF	**Catalyst II**	0.25	0.25	1:1	51	50
17	2-MeTHF	**Catalyst II**	0.14	0.25	1:2	30	30

18	2-MeTHF	**Catalyst II**	0.36	0.12	3:1	40	40
19	n-Hex/ EtOH	MJL	0.25	0.25	1:1	19	18
20	n-Hex/ EtOH	MJL	0.14	0.25	1:2	7	5.6
21	n-Hex/ EtOH	MJL	0.36	0.12	3:1	8.5	6.0
22	n-Hex/ EtOH	**Catalyst I**	0.25	0.25	1:1	2.3	1.1
23	n-Hex/ EtOH	**Catalyst I**	0.14	0.25	1:2	0.4	0.4
24	n-Hex/ EtOH	**Catalyst I**	0.36	0.12	3:1	1.6	1.6
25	n-Hex/ EtOH	**Catalyst II**	0.25	0.25	1:1	6	5.9
26	n-Hex/ EtOH	**Catalyst II**	0.14	0.25	1:2	4.2	4.0
27	n-Hex/ EtOH	**Catalyst II**	0.36	0.12	3:1	4.7	4.7

[a] All experiments were conducted in triplicates at 50 °C for 48 h. MJL: Lipase M. [b] Conversion of tyrosol 1 was evaluated on the basis of the recovered mmol of substrate. [c] The yield of tyrosol oleate 5 was evaluated on the basis of the recovered mmol of the reaction product.



Scheme 5.3. Synthesis of hydroxytyrosol esters **8–10** from tyrosol 1 and carboxylic acids **2–4** in the presence of **Catalyst I** and **Catalyst II**. The reaction was performed under dioxygen atmosphere to activate also tyrosinase.

Briefly, tyrosol **1** (35 mg, 0.25 mmol) and carboxylic acids **2–4** (0.25 mmol) were added with **Catalyst I–II** (165 μg in PBS, 0.1 mL) and ascorbic acid (0.5 mmol) in 2-MeTHF (5.0 mL) under dioxygen atmosphere at 50 °C for 48 h. Ascorbic acid (A.A) was used to avoid the formation of quinone side chain derivatives.[531] Under these experimental

conditions, hydroxytyrosol esters **8–10** were synthesized as the main reaction products from acceptable to high yield (from 49 % to 80 %), besides low amount of tyrosol esters **5** and **6–7**, and unreacted substrate (**Table 19**). As a general trend, the highest conversion of **1** and yield of compounds **8–10** were obtained in the presence of **Catalyst II**, further confirming the beneficial effect of Con A as molecular spacer (**Table 19**, entries 4–7 versus entries 1–3). Irrespective from the experimental conditions, a low amount of tyrosol esters **5–7** was also obtained. In order to evaluate the possible occurrence of substrate-tunnelling effect between the active sites of the two enzymes, the performance of **Catalyst II** was compared with that of **Catalyst III** and **Catalyst IV**, prepared by the individual immobilization of MJL and Ty on OLNPs/CH/Con A intermediate (the preparation and structural characterization of **Catalyst III** and **Catalyst IV** are reported in SI#4). The treatment of **1** and **2** under previously reported experimental conditions in the presence of a mixture of **Catalyst III** and Catalyst IV, bearing the same total amount of the two enzymes as in **Catalyst II**, afforded hydroxytyrosol ester **8** in low yield, besides to appreciable amount of tyrosol ester **5** and hydroxytyrosol **12** (**Table 19**, entry 8 versus entry 4). The presence of relevant amount of **5** and **12** in the reaction mixture suggested that the occurrence of the substrate-tunnelling effect cannot be completely ruled out. As a general trend, the yield of esters **8–10** increased by decreasing the number of carbon atoms in the side-chain of the molecule (**Table 19**, entry 4 versus entries 6–7). The role of carboxylic acids in the efficacy of esterification of tyrosol and hydroxytyrosol under biocatalytic conditions is reported, focusing on the deleterious effect exerted by the increase of the number of carbon atoms in the efficacy of the transformation.[532] Note that, the treatment of **1** with **Catalyst II** in the absence of ascorbic acid afforded a mixture of hydroxytyrosol ester **8** and quinone **11** in a similar yield (**Table 19**, entry 5), opening the possibility to apply this procedure for the synthesis of hydroxytyrosol quinone esters.

Table 19. Synthesis of lipophilic hydroxytyrosol esters **8–10** from 1 by **Catalyst I** and **Catalyst II**[a]

Entry	Catalyst	Carboxylic acid	Product(s)	Conversion[b] (%)	Yield (%) [c]
1	**I**	2	**5 (8)**	24	6.1 (18)
2	**I**	3	**6 (9)**	32	8.0 (24)
3	**I**	4	**7 (10)**	38	5.1 (33)
4	**II**	2	**5 (8)**	53	4.2 (49)
5	**II**	2[d]	**5 (8) [11]**	53	5.3 (25) [25]
6	**II**	3	**6 (9)**	70	7 (63)
7	**II**	4	**7 (10)**	86	6 (80)
8	**III-IV**	2	**5 (8) [12]**	70	32.4 (9) [27]
9	**II**	2	**8**	51 (Run n.1) [e]	49
10	**II**	2	**8**	49 (Run n.2)	47
11	**II**	2	**8**	43 (Run n.3)	39
12	**II**	2	**8**	38 (Run n.4)	35
13	**II**	2	**8**	35 (Run n.5)	29

[a] All experiments were conducted in triplicate. [b] Conversion of tyrosol **1**. [c] The yield was evaluated on the basis of the recovered mmol of reaction product. [d] Reaction performed in the absence of ascorbic acid. [e] **Catalyst II** was recovered by centrifugation and re-used in next runs.

The reusability of **Catalyst II** was evaluated after its recovering at the end of the reaction (centrifugation, followed by washing with PBS) and its re-using in the next runs. As a general trend, **Catalyst II** retained a relevant reactivity after 5 runs in the synthesis of hydroxytyrosol ester **8** as a selected example (**Table 19**, entries 9–13). The decrease in conversion of the substrate observed during the recycling experiments (c.a. 20 % with respect to the first run) may be probably due to the partial thermic denaturation of Con A,[533,534] responsible for the occurrence of unfavourable conformational changes of immobilized enzymes.

5.2. Synthesis of Bioactive Hydroxytyrosol Esters via Multienzyme Cascade on Electroactive Melanin Lignin Nanoparticles: A One-Pot Approach without Extra Reducing Agents

5.2.1 Aim of work

Hydroxytyrosol [2-(3,4-dihydroxyphenyl) ethanol] is a natural polyphenol with powerful health benefits, including antioxidant, anti-inflammatory, anti-cancer, and neuroprotective properties.[489,535-538] It is a very polar molecule with limited absorption, distribution, metabolism and excretion (ADME) properties.[539,506] Esters of hydroxytyrosol with lipophilic carboxylic acids have been synthesized to enhance bioavailability and cell membrane affinity, thus improving the therapeutic efficacy.[499,540]
Up to now, hydroxytyrosol esters have been obtained by multistep protocols encompassing tedious protecting methods and time-consuming procedures.[540,541] Enzymatic cascades can solve this problem. They emerged as a sustainable and efficient strategy to perform multisteps reaction in one-pot conditions.[542] In this latter case, the product of the first enzymatic transformation became the substrate for the next enzyme, simplifying the overall transformation.[543] The possibility to support multienzyme cascades on smart and functional nanoplatforms further improved their synthetic application.[544]
In this context, we recently reported that lipase and tyrosinase could work in a cascade transformation for the one-pot synthesis of esters of hydroxytyrosol.[453] The oriented immobilization of these enzymes on lignin nanoparticles was obtained by the aid of Concanavalin A (Con A) as spatial orienting agent able to selectively bind the carbohydrate region of glycoenzymes.[479,480,519,149] As confirmed by previous study, tyrosinase and lipase MJL are both glycoenzymes bearing nonreducing terminal α-D-mannosyl and α-D-glucosyl groups located far from their active sites.[545,546] In addition, the role played by Con A in the orientation of lipase and tyrosinase by Förster resonance energy transfer (FRET) confocal microscopy analysis has been reported and the possibility of the occurrence of substrate channelling effect discussed in detail.[453,525]
Lignin nanoparticles are effective platforms for the immobilization of redox enzymes, thanks to the capability to improve both stability and reactivity.[130-132,547] Note that the use of tyrosinase in the enzymatic cascade irremediably required the presence of extra reducing agents in order to counteract the prevalence of the diphenolase activity of tyrosinase to yield desired catechols instead of quinone derivatives.[548-550] On the other hand, extra reducing agents inhibit tyrosinase leading to low conversion of substrate and product yield.[550] The presence of extra reducing agents also require further purification steps and complex work-up procedures.[551]
To address these challenges, we report here the one-pot synthesis of lipophilic esters of hydroxytyrosol by using the lipase-tyrosinase multienzyme cascade in the absence of extra reducing agents. This result was obtained by supporting the multienzyme cascade on hybrid lignin nanoparticles containing electroactive eumelanin and pheomelanin.[552-554] Eumelanin and pheomelanin were selected in order to lowering the HOMO-LUMO energy gap between the aromatic subunits of lignin, thus improving the redox properties of the overall platform.[555] The electrochemical properties of eumelanin and pheomelanin are reviewed, and the capability of these polyphenols to perform as semiconductor in dark conditions discussed in detail.[556,557]

The redox potential of hybrid melanin lignin nanoparticles was favourable for the regeneration of the active site of tyrosinase from unproductive met-form to reversible *deoxy/oxy*-form as indicated by optoelectronic and electrochemical analyses.[558] This effect improved the overall activity of tyrosinase in the multienzyme cascade with respect to lignin alone and favoured the reduction of undesired quinones to corresponding catechols.[551,559]

5.2.2 Experimental part

Materials and methods.
Enzymatic hydrolysis lignin (EHL) was purchased from Chemical Point (Oberhaching, Germany). L-3,4-dihydroxyphenylalanine (L-DOPA), L-cysteine, 2-(4-hydroxyphenyl)ethanol (Tyrosol), octanoic acid, lauric acid, butyric acid, propionic acid, Amano lipase M from *Mucor javanicus* (MJL, 300 U/mg), concanavalin A (Con A) type IV from *Canavalia ensiformis* (Jack bean), mushroom tyrosinase from *Agaricus bisporus* (Ty, 1000 U/mg), 4-nitrophenyl palmitate and para-coumaric acid, were purchased from Sigma-Aldrich. 2-methyltetrahydrofuran, tetrahydrofuran and ethanol were purchased from Sigma-Aldrich and were used without further purification. Sodium phosphate buffer (PBS 0.1 M, pH 7) was prepared by using Milli Q water. Spectrophotometric analysis was performed with Cary 60 UV-Vis spectrophotometer equipped with a single cell peltier thermostated holder. Chemical reactions were monitored by using thin layer chromatography on pre-coated aluminium silica gel Merck 60 F_{254} plates and UV lamp (λ_{max}=254 nm) for visualization. ^{1}H NMR and ^{13}C NMR spectra were recorded on a Bruker (400 MHz) spectrometer using $CDCl_3$. Chemical shifts (δ) are expressed in parts per million (ppm). Coupling constants J are expressed in hertz (Hz). Spin multiplicities are given as s (singlet), d (doublet), dd (doublet of doublets), and m (multiplet). MS data were obtained by using LC/MS Agilent 1100 LC-MSD VL system (G1946C) interfaced with an ESI source (spray voltage of 4.5 kV and nitrogen as sheath gas).

Preparation of melanin samples
Water-soluble eumelanin (EM) was prepared by dissolution of L-DOPA (0.76 mmol; 150 mg) in deionized water (30 mL), followed by addition of NH_4OH (0.2 mL) to reach pH 9. The mixture was stirred for 15 hours at room temperature under bubbling oxygen.[560] At the end, the solution was kept in a dialysis membrane of 3.5K MWCO against deionized water for 24 hours and then the sample was freeze-dried. Water soluble pheomelanin (PM) was synthesized from L-DOPA (0.76 mmol; 150 mg) and L-Cysteine (1.14 mmol, 138 mg) in the optimal ratio of 1 : 1.5, dissolved in deionized water (30 mL) followed by addition of NH_4OH (0.2 mL) to reach pH 9. The purification of pheomelanin followed the same protocol described for EM.

Preparation of hybrid melanin-lignin nanoparticles
For the synthesis of hybrid melanin-lignin nanoparticles, EHL (170 mg) was dissolved in the ternary mixture (primary solvent) water (22 % v/v, 0.54 mL), ethanol (39 % v/v, 0.98 mL) and THF (39 % v/v, 0.98 mL) and added to EM (8.5 mg) in deionized water (12.5 mL) as anti-solvent under gentle mechanical stirring to yield EHLNPs/EM.[561] Next, EHLNPs/EM were isolated by rotary evaporation under reduced pressure at 60 °C for 25 min, followed by centrifugation (14339 RCF, 4 °C for 10 minutes) and freeze dry. A similar procedure was applied in the case of PM to afford EHLNPs/PM. The UV-vis scan analysis of the supernatant recovered after isolation of the hybrid nanoparticles by centrifugation was recorded in the range between 290 nm to 800 nm.

Electrochemical characterization of EHLNPs/EM and EHLNPs/PM
Cyclic voltammetry (CV) measurements were performed in a conventional three-electrode thermostated glass-cell (Metrohm) using a Multi Walled Carbon Nanotubes Screen-Printed Electrode (MWCNTs/SPE) modified by drop casting technique with EHLNPs/EM and EHLNPs/PM as a working electrode, Ag/AgCl/Kclsat as reference electrode (198 mV versus NHE) and Glassy Carbon rod as a counter electrode. Autolab Potentiostat/Galvanostat (Eco Chemie) was utilized for the electrochemical measurements. Cyclic voltammetry (CV) experiments were performed in 5 mM $[Fe(CN)_6]3^-/4^-$ containing 0.1 M KCl solution and scan rate 25 mV s^{-1}.

*Procedure for the preparation of **Catalyst I–III***
For the preparation of **Catalysts I–III**, 0.5 mL of Con A solution (2.0 mg/mL) in PBS (0.1 M, pH 7.0) were added to EHLNPs, EHLNPs/EM and EHLNPs/PM (2.0 mg/mL) in PBS (1.0 mL; 0.1 M, pH 7.0) under gentle sonication conditions at 25 °C, followed by the addition of MJL (110 U; 5.0 mg/mL) and Ty (32 U; 1.0 mg/mL) dissolved in PBS (0.1 M, pH 7.0). The mixture was stirred at 4 °C in orbital shaking for 24 h. The solution was centrifuged (14339 RCF, 4 °C for 10 minutes) and washed two times with PBS (0.1 M, pH 7.0) to afford **Catalysts I–III**.[453] The immobilization and activity parameters for MJL were evaluated by measuring the increase in absorbance (λ_{max} 405 nm) during the release of para-nitrophenol in the hydrolysis of *para*-nitrophenyl palmitate (*para*-NPP) in PBS (0.1 M, pH 7.0) at 25 °C for 10 min.[514,562] In a typical experiment, **Catalysts I–III** (1.0 mg/mL; in PBS 0.1 M, pH 7.0) were added to *para*-NPP solution (15 mM; $CNCH_3$: water 17 : 50; 1 mL) in PBS (0.1 M, pH 7.0). The immobilization and activity parameters for Ty were determined following the increase in absorbance (λ_{max} 311 nm) produced during the oxidation of *para*-coumaric acid to caffeic acid in PBS (0.1 M, pH 7.0) for 30 min at 20 °C.[525] In a typical experiment, **Catalysts I–III** (1.0 mg/mL; in PBS 0.1 M, pH 7.0) were added to *para*-coumaric acid solution (4.9 mM; PBS : $CH_3(CH_2)_2OH$ 4 : 1; 0.077 mL) in PBS (0.1 M, pH 7.0).

Synthesis of lipophilic hydroxytyrosol esters
The reactions were performed starting from tyrosol **1** (0.25 mmol) and octanoic acid **2 a**, lauric acid **2 b**, butyric acid **2 c** and propionic acid **2 d** (0.25 mmol) in 2-MeTHF (5.0 mL) and PBS (0.15 mL) in the presence of **Catalysts I–III** (150 μg) at 50 °C for 48 h under bubbling oxygen.[453] The reaction was monitored by thin layer chromatography (TLC, n-hexane/EtOAc=8.0 : 2.0 and n-hexane/EtOAc=6.0 : 4.0). At the end, the reaction was filtered to remove the catalysts and the solvent was evaporated under reduced pressure. The crude was purified by flash chromatography. The reusability of **Catalyst III** in the synthesis of hydroxytyrosol esters **3 b** and **4 b** was evaluated after its recovering at the end of the reaction by filtration followed by washing with PBS (0.1 M, pH 7.0) and freeze dry. The original ^{1}H NMR and ^{13}C NMR spectra of the reaction products are in Supporting information S8.

3,4-Dihydroxyphenethyl octanoate (Hydroxytyrosyl octanoate) **3 a**. Colourless oil. ^{1}H NMR (400 MHz, $CDCl_3$): δ=0.90 (m, 3H), 1.28 (m, 8H), 1.59–1.63 (m, 2H), 2.28–2.32 (m, 2H), 2.82–2.88 (m, 2H), 4.24–4.27 (m, 2H), 6.65–6.67 (dd, J 7.9 Hz, 1H), 6.76–6.82 (m, 2H) ppm. ^{13}C NMR (100 MHz, $CDCl_3$): δ=14.0 (CH_3), 22.7 (CH_2), 24.9 (CH_2), 28.9–29.0 (CH_2×2), 31.6 (CH_2), 34.2 (CH_2), 34.4 (CH_2), 65.2 (CH_2), 115.9 (CH_2×2), 122.3 (CH), 131.3 I, 144.6 I, 145.5 I, 173.2 I ppm. MS (ESI) m/z 280.36.

2-(3,4-Dioxocyclohexa-1,5-dien-1-yl)ethyl octanoate (Hydroxytyrosyl octanoate quinone) **4 a**. Yellow oil. ^{1}H NMR (400 MHz, $CDCl_3$: δ=0.90 (m, 3H), 1.28 (m, 8H), 1.60–1.63 (m, 2H), 2.23–2.24 (m, 2H), 2.33–2.35 (m, 2H), 4.07–4.10 (m, 2H), 5.86–5.87 (d, J 5 Hz, 1H), 6.09 (s, 1H), 7.22–7.23 (d, j 4.9 Hz, 1H) ppm. ^{13}C NMR (100 MHz, $CDCl_3$): δ=14.1 (CH_3), 22.7 (CH_2), 24.9 (CH_2), 28.9–29.0 (CH_2×2), 31.6 (CH_2), 34.0 (CH_2), 37.3 (CH_2), 62.7 (CH_2), 112.9 (CH), 126.9 (CH), 152.7 (CH), 157.6 I, 173.2 I, 180.6 I, 181.9 I ppm. MS (ESI) m/z 278.15.

4-Hydroxyphenethyl octanoate (Tyrosyl octanoate) **5 a**. Yellow oil. ^{1}H NMR (400 MHz, $CDCl_3$): δ=0.88–0.92 (m, 3H), 1.29–1.31 (m, 8H), 1.57–1.64 (m, 2H), 2.28–2.32 (m, 2H), 2.86–2.90 (m, 2H), 4.24–4.28 (m, 2H), 6.78–6.80 (d, J 8.0 Hz, 2H), 7.09–7.11 (d, J 8.1 Hz, 2H) ppm. ^{13}C NMR (100 MHz, $CDCl_3$): δ=14.0 (CH_3), 22.6 (CH_2), 24.9 (CH_2), 28.9–29.0 (CH_2, x2), 31.6 (CH_2), 34.2–34.4 (CH_2 x2), 65.1 (CH_2), 115.3 (CH, ×2), 129.6 I, 130.0 (CH, ×2), 154.5 I, 174.2 I ppm. MS (ESI) m/z 264.37.

3,4-Dihydroxyphenethyl dodecanoate (Hydroxytyrosyl laurate) **3 b**. Yellow oil. ^{1}H NMR (400 MHz, $CDCl_3$): δ=0.90 (m, 3H), 1.28 (m, 16H), 1.62-1.67 (m, 2H), 2.28–2.31 (m, 2H), 2.82–2.87 (m, 2H), 4.23–4.28 (m, 2H), 6.65–6.68 (dd, J 7.9 Hz, 1H), 6.76–6.82 (m, J 8 Hz, 2H) ppm. ^{13}C NMR (100 MHz, $CDCl_3$): δ=13.9 (CH_3), 22.5 (CH_2), 24.8 (CH_2), 28.2–29.8 (CH_2 ×6), 32.8 (CH_2), 34.3 (CH_2), 35.8 (CH_2), 65.4 (CH_2), 116.2 (CH), 117.2 (CH), 120.2 (CH), 131.9 I, 142.3 I, 145.1 I 173.2 I ppm. MS (ESI) m/z 336.47.

2-(3,4-Dioxocyclohexa-1,5-dien-1-yl)ethyl dodecanoate (Hydroxytyrosyl laurate quinone) **4 b**. Yellow oil. ^{1}H NMR (400 MHz, $CDCl_3$): δ=0.89 (m, 3H), 1.28 (m, 16H), 1.60–1.62 (m, 2H), 2.23–2.24 (m, 2H), 2.33–2.35 (m, 2H), 4.07–4.11 (m, 2H), 5.86–5.87 (d, J 5 Hz, 1H), 6.08 (s, 1H), 7.22–7.24 (d, j 4.9 Hz, 1H) ppm. ^{13}C NMR (100 MHz, $CDCl_3$): δ=14.1 (CH_3), 22.7 (CH_2), 24.9 (CH_2), 28.9–29.3 (CH_2 ×6), 31.6 (CH_2), 34.0 (CH_2), 37.3 (CH_2), 62.6 (CH_2), 112.5 (CH), 126.7 (CH), 152.8 (CH), 157.6 I, 173.1 I, 180.6 I, 182.0 I ppm. MS (ESI) m/z 334.21.

4-Hydroxyphenethyl dodecanoate (Tyrosyl laurate) **5 b**. Yellow oil. ^{1}H NMR (400 MHz, $CDCl_3$): δ=0.88–0.91 (m, 3H), 1.29 (m, 16H), 1.59–1.66 (m, 2H), 2.28–2.32 (m, 2H), 2.86–2.89 (m, 2H), 4.24–4.28 (m, 2H), 6.77–6.79 (d, J 8.0 Hz, 2H), 7.08–7.10 (d, J 8.1 Hz, 2H) ppm. ^{13}C NMR (100 MHz, $CDCl_3$): δ=14.0 (CH_3), 22.6 (CH_2), 24.9 (CH_2), 28.9–29.0 (CH_2, 6×), 31.5 (CH_2), 34.0 (CH_2), 34.4 (CH_2), 65.2 (CH_2), 115.6 (CH, x2), 130.1 I, 130.8 (CH, ×2), 155.5 I, 173.2 I ppm. MS (ESI) m/z 320.24.

3,4-Dihydroxyphenethyl butyrate (Hydroxytyrosyl butyrate) **3 c**. Colourless oil. ^{1}H NMR (400 MHz, $CDCl_3$): δ=0.92–0,95 (m, 3H), 1.62–1.68 (m, 2H), 2.27–2.31 (m, 2H), 2.86–2.89 (m, 2H), 4.26–4.28 (m, 2H), 6.77–6.79 (dd, J 7.9 Hz, 1H), 6.86–6.99 (m, 2H) ppm. ^{13}C NMR (100 MHz, $CDCl_3$): δ=13.5 (CH_3), 18.2 (CH_2), 34.9–36.0 (CH_2 x2), 65.2 (CH_2), 116.0 (CH_2 ×2), 122.8 (CH), 131.4 I, 144.6 I, 145.5 I, 173.2 I ppm. MS (ESI) m/z 224.25.

4-Hydroxyphenethyl butyrate (Tyrosyl butyrate) **5 c**. Yellow oil. ^{1}H NMR (400 MHz, $CDCl_3$): δ=0.92–0.96 (m, 3H), 1.62-1.68 (m, 2H), 2.27–2.31 (m, 2H), 2.86–2.89 (m, 2H), 4.25–4.28 (m, 2H), 6.78–6.80 (d, J 8.0 Hz, 2H), 7.08–7.10 (d, J 8.1 Hz, 2H) ppm. ^{13}C NMR (100 MHz, $CDCl_3$): δ=13.5 (CH_3), 18.4 (CH_2), 34.9–36.0 (CH_2, ×2), 65.2 (CH_2), 115.9 (CH, ×2), 130.2 (CH ×2), 130.8 I, 155.6 I, 173.2 I ppm. MS (ESI) m/z 208.25.

3,4-Dihydroxyphenethyl propionate (Hydroxytyrosyl proprionate) **3 d**. Yellow oil. ^{1}H NMR (400 MHz, $CDCl_3$): δ=1.28–1.29 (m, 3H), 2.28–2.32 (m, 2H), 2.87–2.89 (m, 2H),

4.25–4.27 (m, 2H), 6.75–6.77 (dd, J 7.9 Hz, 1H), 6.84–6.87 (m, 2H) ppm. ^{13}C NMR (100 MHz, $CDCl_3$): δ=9.2 (CH_3), 27.3 (CH_2), 34.9 (CH_2), 65.2 (CH_2), 116.0 (CH_2 ×2), 122.7 (CH), 131.4 I, 144.6 I, 145.6 I, 173.2 I ppm. MS (ESI) m/z 210.09.

4-Hydroxyphenethyl propionate (Tyrosyl proprionate) **5 d**. Colourless oil. ^{1}H NMR (400 MHz, $CDCl_3$): δ=1.28–1.29 (m, 3H), 2.28–2.32 (m, 2H), 2.86–2.89 (m, 2H), 4.25–4.28 (m, 2H), 6.76–6.80 (d, J 8.0 Hz, 2H), 7.08–7.12 (d, J 8.1 Hz, 2H) ppm. ^{13}C NMR (100 MHz, $CDCl_3$): δ=9.4 (CH_3), 27.5 (CH_2), 34.6 (CH_2), 65.2 (CH_2), 115.8 (CH, ×2), 130.2 (CH ×2), 130.8 I, 155.6 I, 173.4 I ppm. MS (ESI) m/z 194.23.

4-(2-hydroxyethyl) benzene-1,2-diol (Hydroxytyrosol) **6**. Solid (b. p. 355.4 °C). ^{1}H and ^{13}C NMR spectra were in accordance with those of an authentic sample.[561]

5.7.3 Results and discussions

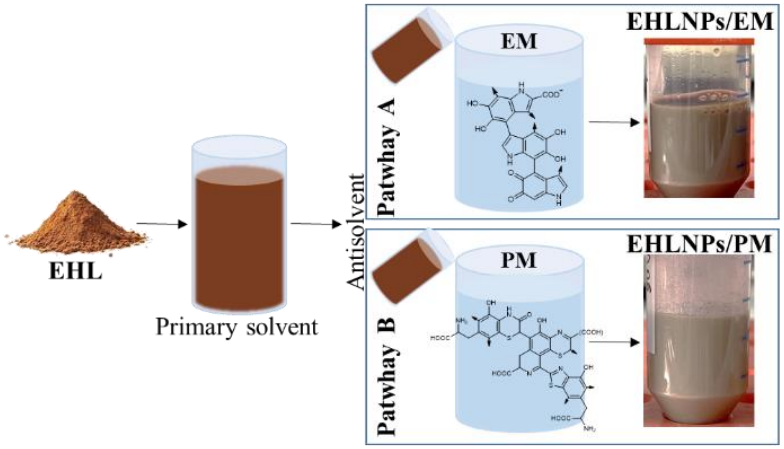
Preparation of melanin samples

Water-soluble eumelanin (EM) and pheomelanin (PM) were synthesized by a modification of previously reported procedure based on the use of molecular oxygen as primary oxidant.[560] UV-vis analysis (Supporting Information S1; Figure S1) showed the absorption bands expected for eumelanin and pheomelanin.[562] Field emission scanning electron microscopy (FE-SEM) confirmed the formation of amorphous aggregates typical for both type of water-soluble melanin (Supporting Information S2, Figure S2, panel A and panel B, respectively).[560,563] Energy-dispersive X-ray elemental analysis (EDX) of PM showed the incorporation of 10-wt % of cysteine (Figure S2, panel C and panel D, respectively). Electron paramagnetic resonance (EPR) spectra of EM was characterized by giso value of 2.0037 in accordance with data reported in the literature.[564] In a similar way, the giso value of PM (2.0041) was in accordance with the expected structure (Supporting Information S3, Figure S3).[565,566] In addition, the presence of C−N and C=O stretching bands at 1400–1700 cm^{-1} confirmed the standard fingerprint of EM,[567,568] and the C−S bending at 685 cm^{-1} and the stretching of S−O at 1213 cm^{-1} that of PM (Supporting Information S4, Figure S4).[569]

Preparation of hybrid melanin lignin nanoparticles

Hybrid melanin lignin nanoparticles were prepared from enzymatic hydrolysis lignin (EHL) by nanoprecipitation in the presence of water-soluble EM and PM samples.[570,571,447,194,171]

The general procedure is reported in **Scheme 5.4**.[561] Briefly, EHL (170 mg) dissolved in the ternary mixture (primary solvent) water (22 % v/v, 0.54 mL), ethanol (39 % v/v, 0.98 mL) and THF (39 % v/v, 0.98 mL) was added to EM (8.5 mg) in deionized water (12.5 mL) as anti-solvent under gentle mechanical stirring (Pathway A) to yield EHLNPs/EM isolated by centrifugation and freeze dry. A similar procedure was applied for PM to afford EHLNPs/PM. EM and PM were quantitatively loaded in the nanoparticles as confirmed by the UV-vis analysis of the supernatant recovered after isolation of the hybrid nanoparticles by centrifugation. In this latter cases, the typical UV-vis fingerprint of melanin was no detected. The yield of EHLNPs/EM and EHLNPs/PM (**Table 20**) was calculated as the total amount by weight of particles compared to the starting amount of lignin and melanin. Irrespective from the experimental conditions both yields were higher than 65 %.



Scheme 5.4. Synthesis of hybrid melanin-lignin nanoparticles. Pathway A: preparation of EHLNPs/EM. Pathway B: preparation of EHLNPs/PM.

Table 20. Yields, HOMO-LUMO energy gap values and electrochemical parameters of EHLNPs/EM and EHLNPs/PM by using EHLNPs as reference.

Entry	Sample	Yield %[b)]	HLG (eV)[c)]	I_{pa} (mA)	I_{pc} (mA)	ΔE (mV)[d)]	E^0 (V)[e)]
1	EHLNPs/EM	69	2.75	-33.3	+37.6	147	0.16
2	EHLNPs/PM	68	2.45	-31.6	+35.6	147	0.15
3	EHLNPs[a)]	67	2.85	-36.3	+40.5	154	0.18

[a] Parent lignin nanoparticles used as reference, [b] Each experiment was conducted in triplicate and the average errors in yields were ±1–2 %. [c] Average errors in HLG values calculated from Tauc's plot were ±2–3 %. [d]ΔE range of reversibility is 59–180 mV and the average errors in ΔE were ±1–2 %. [e] Average errors in E0 were ±1–2 %.

The presence of melanin in hybrid nanoparticles was confirmed by spectroscopic and morphological analyses by using parent lignin nanoparticles (EHLNPs) as a reference. FT-IR spectra of EHLNPs/EM and EHLNPs/PM are reported in **Figure 5.4** (Panel A and Panel B**,** green line, respectively) and compared with EHLNPs (orange line). EHLNPs/EM (Panel A) showed peaks in the range of 1400–1700 cm^{-1} associated to the stretching of C−N and C=O groups. These signals were typical of eumelanin, and were absent in EHLNPs (**Figure 5.4,** Panel A**;** orange line).[567,568] In the case of EHLNPs/PM, the presence of the S−O symmetric stretching vibration at 100—1300 cm^{-1} (Panel B, green line) was in accordance with the benzothiazine units (this peak was absent in EHLNPs; Panel B, orange line).[569-572]

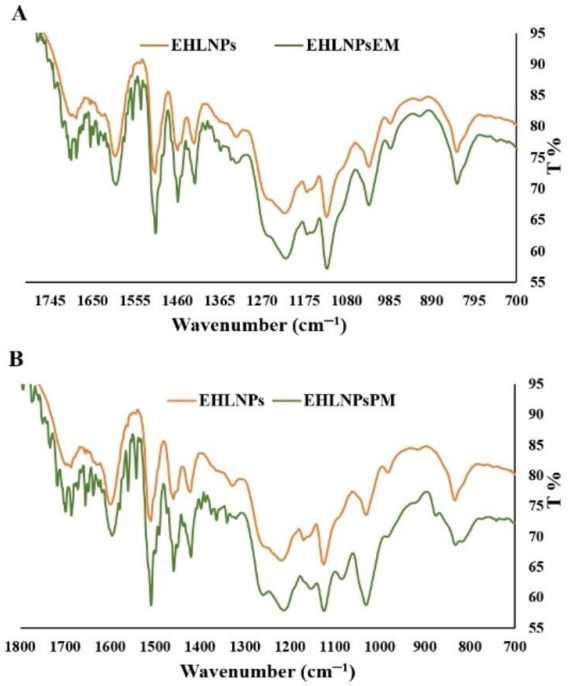


Figure 5.4. FTIR spectra of hybrid melanin lignin nanoparticles. Panel (A): EHLNPs/EM, green line. Panel (B) EHLNPs/PM, green line. EHLNPs orange line.

FE-SEM images are reported in **Figure 5.5** EHLNPs/EM and EHLNPs/PM were characterized by agglomerates of melanin on the surface of LNPs (**Figure 5.5,** Panel A and Panel B, respectively). The irregular shape of these agglomerates suggested the presence of variable layers of amorphous melanin in accordance with data previously reported.[560,563] These layers were absent in EHLNPs (Supporting Information S5, Figure S5). The average diameter of nanoparticles was c. a. 200 nm.

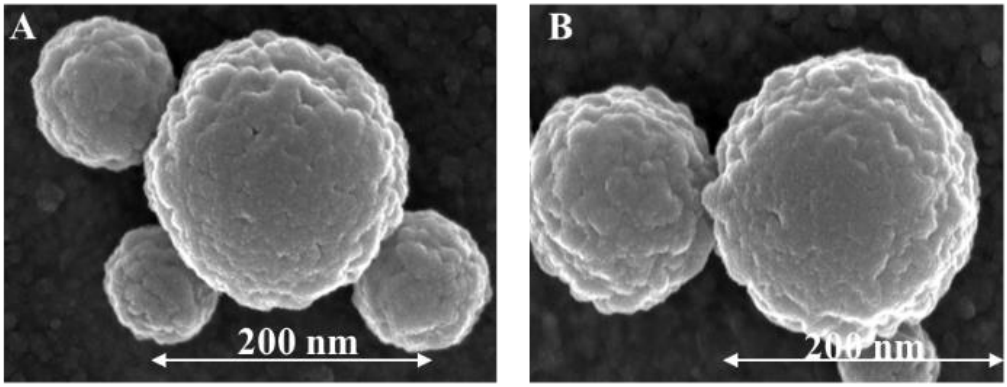


Figure 5.5. FE-SEM images of hybrid melanin lignin nanoparticles. Panel (A): EHLNPs/EM. Panel (B) EHLNPs/PM.

Optoelectronic and electrochemical properties of EHLNPs/EM and EHLNPs/PM

The HOMO-LUMO energy gap (HLG) values of EHLNPs/EM and EHLNPs/PM were calculated by UV-Vis analysis (Experimental details are in Supporting Information S6).[573,574] Plots deriving from the Tauc's equation are reported in Figure S6, while HLG values are in **Table 20**. EHLNPs/EM and EHLNPs/PM showed values of HLG lower than parent lignin (**Table 20,** entries 1 and 2 versus entry 3). This result confirmed the emergence of novel redox properties associated to the presence of melanin. The very fact that EHLNPs/PM showed HLG values lower than EHLNPs/EM was in accordance with

the improved redox properties of benzothiazine units with respect to the indolic counterpart.[556]
Cyclic voltammetry (CV) of EHLNPs/EM and EHLNPs/PM was performed by using a Multi Walled Carbon Nanotubes Screen-Printed Electrode (MWCNTs/SPE) modified by drop casting technique. The CVs were recorded in 5 mM $[Fe(CN)_6]3^-/4^-$ and 0.1 M KCl at the scan rate of 25 mV s^{-1} (**Figure 5.6**). The main electrochemical parameters are summarized in **Table 20**. The samples were characterized by good electrochemical reversibility (**Figure 5.6**) measured as the difference between the anodic and cathodic peak potentials (Δ_E).[575-577]

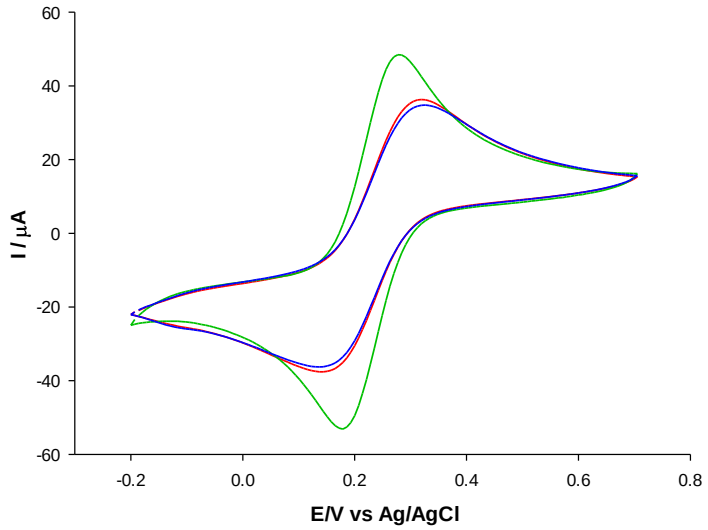


Figure 5.6. CVs of EHLNPs/EM (red line), EHLNPs/PM (blue line) and EHLNPs (green line). Redox probe: 5 mM $[Fe(CN)_6]3^-/4^-$ containing 0.1 M KCl. Scan rate: 25 mV/s.

In addition, EHLNPs/EM and EHLNPs/PM showed Δ_E values lower than EHLNPs in accordance with the trend of the HLG data (**Table 20** entries 1 and 2). The redox potential (E_0) values (**Table 20**) showed a similar pattern and suggest the higher reducing character for the hybrid platform with respect to EHLNPs.[578]

Immobilization of the multienzyme cascade lipase-tyrosinase on EHLNPs/EM and EHLNPs/PM
The immobilization of the enzymatic cascade lipase-tyrosinase on the surface of EHLNPs/EM and EHLNPs/PM required the initial optimization of the immobilization parameters for the redox active tyrosinase, followed by the co-immobilization with lipase.

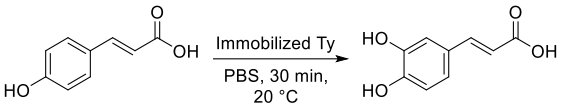
Procedure for the immobilization of tyrosinase
We studied the immobilization of tyrosinase (Ty) on EHLNPs in order to find the optimal immobilization parameters for the enzyme.[517] Briefly, Concanavalin A used as co-orienting agent (Con A; from 0.2 mg/mL to 0.5 mg/mL) was added to EHLNPs (1.0 mg/mL) in PBS at room temperature and the mixture was sonicated for 5 minutes. At the end, Ty (16 U and 32 U) in PBS (0.1 M, pH 7.0) was added to the mixture, and the system was left for 24 hours under orbital shaking at 4 °C. EHLNPs/Con A/Ty were recovered by centrifugation, washed with PBS (0.1 M, pH 7.0) and freeze-dry. The loading of Con A on EHLNPs (% in weight) was evaluated by Bradford assay (Supporting Information S7). The loading factor was always higher than 75 % confirming the presence of interactions between lectins and polyphenols (Figure S7).[579] The immobilization and

activity parameters of EHLNPs/Con A/Ty are reported in **Table 21**. The activity of Ty was determined following the oxidation of *para*-coumaric acid to caffeic acid (λ_{max} 311 nm) in PBS (0.1 M, pH 7.0) for 30 min at 20 °C.[525] The immobilization parameters were evaluated as reported in equation (1) and (2).

$$\text{Immobilization yields (\%)} = [(U_a - U_r)/U_a] \times 100 \quad (\mathbf{1})$$

$$\text{Activity (units/mg)} = U_x/mg_{support} \quad (\mathbf{2})$$

Table 21. Immobilization and activity parameters of EHLNPs/EM/Con A/Ty, EHLNPs/PM/Con A/Ty and EHLNPs/Con A/Ty.



p-coumaric acid caffeic acid

Entry	Sample	Ratio Con A (w/w)	Ty (U)	Immobilization yield (%) [a]	Activity [b]
1	EHLNPs	/	16	90	3.8
2	EHLNPs	1:0.2	16	92	5.4
3	EHLNPs	1:0.2	32	89	5.2
4	EHLNPs	1:0.3	32	89	5.3
5	EHLNPs	1:0.5	32	89	7.5
6	EHLNPs/EM	1:0.5	32	83	12.4
7	EHLNPs/PM	1:0.5	32	84	13.2

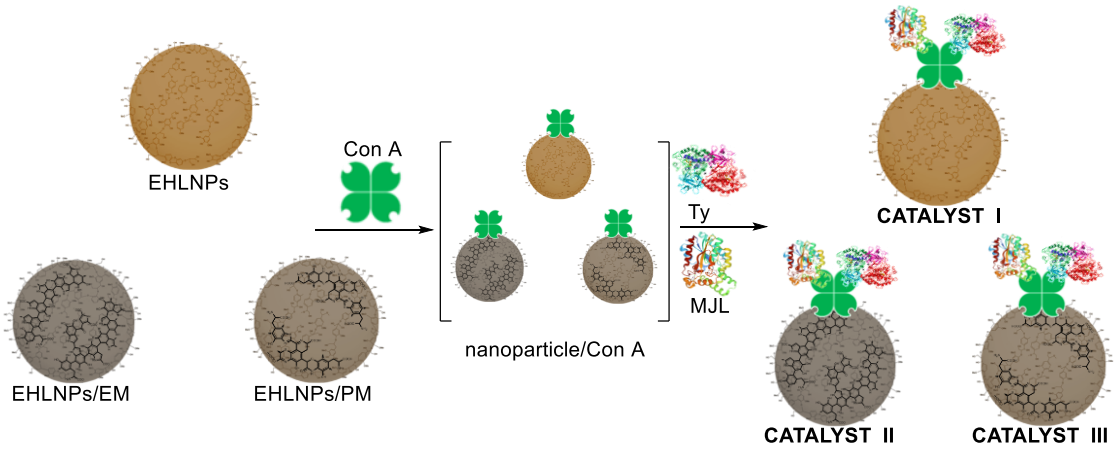
[a] The experiments were conducted in triplicate; the average error in the immobilization yield was ±1–4 %. [b] Average error in the enzyme activity was ±2–3 %.

Where U_x are the immobilized enzyme units, U_a are the total units of the enzyme added to the solution, and U_r are the residual units of the enzyme in the washing solution. Irrespective from the experimental conditions, the highest value of activity was obtained in the presence of Con A (**Table 21** entries 2–6 versus entry 1), highlighting the beneficial effect played by the spacer in the oriented immobilization of the enzyme.[525] The optimal immobilization protocol consisted in the use of 0.5 mg/mL of Con A and 32 U/mg of Ty (**Table 21**, entry 5). The immobilization procedure was next applied to EHLNPs/EM and EHLNPs/PM. EHLNPs/EM/Con A/Ty and EHLNPs/PM/Con A/Ty showed activity parameters higher than the parent EHLNPs/Con A/Ty (**Table 21**, entries **6** and 7 versus entry 5). This result suggests a possible role played by both electrochemical active melanin in favouring the prevalence of the reversible *deoxy/oxy*form of the enzyme.[556,558]

Procedure for the immobilization of the lipase-tyrosinase multienzyme cascade

The multienzyme cascade was immobilized on EHLNPs/EM and EHLNPs/PM by a modification of the protocol previously reported for the co-immobilization of the two enzymes on lignin nanoparticles from organosolv lignin and chitosan.[453] Lipase-tyrosinase multienzyme cascade was immobilized also on EHLNPs as a reference. As a general procedure, Con A (1.0 mg/mL) in PBS was suspended with the appropriate support (2.0 mg/mL) in PBS under gentle sonication conditions for 5 min at room temperature to yield the corresponding nanoparticle/Con A intermediate. Next, lipase from *Mucor Javanicus* MJL (110 U) (selected on the basis of the high activity at the optimal pH for Ty)[513] and Ty (32 U) in PBS were added to freshly prepared nanoparticle/Con A and the mixture was stirred at 4 °C for 24 h under orbital shaking. EHLNPs/ConA/MJL-Ty (**Catalysts I**), EHLNPs/EM/Con A/MJL-Ty, (**Catalyst II**), and

EHLNPs/PM/Con A/MJL-Ty, (**Catalyst III**), were recovered by centrifugation, washed two times with PBS and freeze-dry (**Scheme 5.5**).



Scheme 5.5. Preparation of **Catalyst I–III**.

The activity parameters of **Catalysts I–III** were calculated for both immobilized enzymes by using the equations described above. In particular, the activity parameters of MJL were evaluated following the increase in absorbance produced during the release of *para*-nitrophenol (λ_{max} 405 nm) in the hydrolysis of *para*-nitrophenil palmitate (*p*-NPP, 15 mM) in PBS (0.1 M, pH 7.0) at 25 °C for 10 min.[514,562] The activity parameters of Ty were determined following the increase in absorbance (λ_{max} 311 nm) produced during the oxidation of *para*-coumaric acid (4.9 mM) to caffeic acid in PBS for 30 min at 20 °C.[525] In the case of MJL, **Catalysts I–III** showed comparable values of immobilization yield and activity (**Table 22**). A different behaviour was observed for Ty. In this latter case, the activity of Ty was significantly improved in the case of **Catalysts II–III**, in accordance with the major redox properties associated to the presence of melanin. (**Table 22**, entries 2–3 versus entry 1).

Table 22. Activity parameters of **Catalyst I–III**.

Entry	Catalyst	Yield (%)[a)] MJL	Activity[b)] MJL	Yield (%) Ty[a]	Activity[b)] Ty
1	I	58	55	97	8
2	II	53	53	96	16
3	III	50	54	99	20

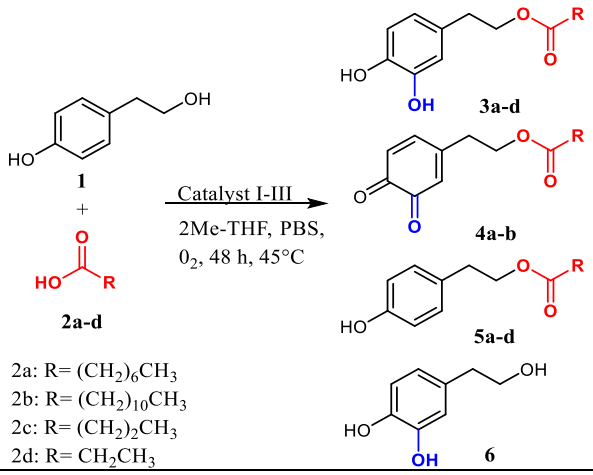
[a] Each experiment was conducted in triplicate, average errors in immobilization yield were ±1–4 %. [b] Average errors in enzyme activity were ±2–3 %.

Synthesis of lipophilic hydroxytyrosol esters via heterogeneous multienzymatic cascade

The one-pot synthesis of lipophilic hydroxytyrosol esters was studied starting from tyrosol **1** and two selected carboxylic acids differing in the number of carbon atoms in the side chain, octanoic acid (C_8) **2 a**, and lauric acid (C_{12}) **2 b** (0.25 mmol; molar ratio 1 : 1). The reaction was performed by addition of the appropriate catalyst (150 μg in PBS, 0.15 mL) to substrate in 2-methyltetrahydrofuran (2-MeTHF; 5.0 mL) at 50 °C for 48 h in the presence of bubbled dioxygen.[453] 2-MeTHF was previously used by us as a sustainable organic solvent[581,464] in different bio-catalytic and photo-biocatalytic applications.[453,557] The reaction was repeated using a mixture of native MJL (8 U) and Ty (2 U) in the same ratio by which the enzymes were contained in **Catalyst I–III** as a reference. At the end, the reaction was filtered to recover the catalyst and the filtrate was concentrated under reduced pressure. The residue was purified by flash chromatography

and the reaction products identified by spectroscopic and spectrometric analyses. Irrespective from the experimental conditions, lipophilic hydroxytyrosol esters **3 a–b** were recovered as the major reaction products in appreciable amount in the presence of **Catalyst II–III**, besides to quinone esters **4 a–b** and tyrosol esters **5 a–b** as side products (**Table 23**, entries 2–3 and 6–7). Quinone esters **4 a–b** were produced by over oxidation of compounds **3 a–b** due to the diphenolase activity of Ty, while tyrosol esters **5 a–b** derived from the prevalence of MJL activity. **Catalyst II–III** showed a selectivity different than **Catalyst I**, in which case quinone esters 4 a–b were isolated in the highest yield (**Table 23**, entries 2–3 versus entry 1, and entries 6–7 versus entry 5), suggesting the role of electroactive melanin in counteracting the diphenolase activity of Ty. In this latter case, hydroxytyrosol esters **3 a–b** were obtained in low yield. The selectivity observed with **Catalyst II–III** was probably due to the role played by melanin in the control of the redox equilibrium between the quinone and catechol moieties, even if the occurrence of electron transfer processes able to tune the oxy-form of Ty cannot be completely ruled out.[556,558] This effect was not operative in the case of **Catalyst I**. As a general trend, **Catalysts II–III** were more effective than native enzymes in the conversion of tyrosol (**Table 23**, entries 1–3 versus entry 4, and entries 5–7 versus entry 8), confirming the efficacy of the enzymatic cascade process. Overall, **Catalyst III** was the most effective tool in the synthesis of hydroxytyrosol esters **3 a–b.**

Table 23. Synthesis of lipophilic hydroxytyrosol esters.



Entry	Catalyst	Conversion [%][a)]	Product(s)	Products Yield (%)[b)]
1	I	36	3a (4a) [5a]	10 (58) [28]
2	II	35	3a (4a) [5a]	51 (25) [23]
3	III	36	3a (4a) [5a]	54 (23) [22]
4	MJL+Ty	19	4a [5a]	46 [47]
5	I	45	3b (4b) [5b]	12 (61) [25]
6	II	46	3b (4b) [5b]	52 (25) [21]
7	III	46	3b (4b) [5b]	56 (22) [20]
8	MJL+Ty	25	4b [5b]	48 [47]
9	I	22	[5c]{6}	[15] {80}
10	II	21	3c [5c] {6}	8 [10] {80}
11	III	23	3c [5c] {6}	8 [10] {80}
12	I	22	[5d] {6}	[13] {80}
13	II	22	3d [5d] {6}	8 [10] {80}
14	III	23	3d [5d] {6}	8 [10] {83}
15	III	46 (Run n . 1)[c]	3 b (4 b) [5 b]	55 (21) [20]
16	III	42 (Run n . 2)	3 b (4 b) [5 b]	55 (21) [20]
17	III	40 (Run n . 3)	3 b (4 b) [5 b]	53 (20) [19]
18	III	38 (Run n . 4)	3 b (4 b) [5 b]	52 (20) [18]
19	III	36 (Run n . 5)	3 b (4 b) [5 b]	51 (21) [18]

All experiments were conducted in triplicate. A) Conversion of tyrosol 1. B) The yields were evaluated on the basis of the recovered mmol of the reaction products. C) Catalyst III was recovered by filtration and re-used in next runs. The parentheses were used to indicate the yield of different reaction products: () for series 4, [] for series 5, {} for compound 6

Next, the synthetic procedure was extended to butyric acid (C_4) **2 c** and propionic acid (C_3) **2 d**. These compounds are reported to generate pH value in the microenvironment of the active site of lipase lower than long chain derivatives **2 a–b**.[582] The relevance of pH in the effectiveness of the esterification process is reviewed and discussed in detail.[583] Irrespective from the experimental conditions, hydroxytyrosol esters **3 c–d** were recovered in low yield, besides to hydroxytyrosol **6** as the major reaction product, and tyrosol esters **5 c–d** as side products. The corresponding quinone esters were not isolated probably due to the formation of oligomers not recovered under our experimental conditions (**Table 23**, entries 9–14).[584,585]

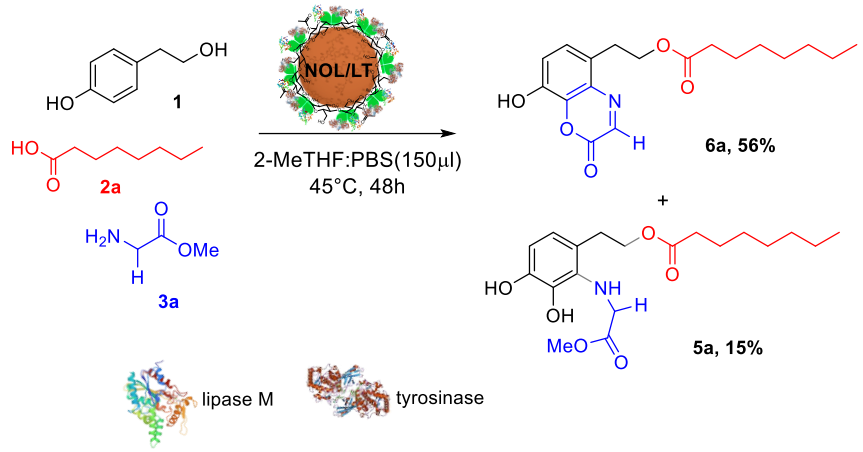
Note that, the high amount of hydroxytyrosol **6** may be due to the low efficacy of lipase in the enzymatic cascade in the esterification of tyrosol with acids **2 c–d**, compound **6** being accumulated as a product of the Ty mediated oxidation of tyrosol. This result was in accordance with the reported inhibitory effect exerted by local low pH value in the activity of lipase, probably associated to the low stability of hydroxytyrosol esters bearing short chain carboxylic acids.[582,586] Thus, the enzymatic cascade performed selectively and with high efficacy in the synthesis of lipophilic (long chain) hydroxytyrosol esters.

The reusability of **Catalyst III** in the synthesis of hydroxytyrosol esters **3 b** and **4 b** was evaluated for more runs. As a general trend, it retained an appreciable reactivity after 5 runs (**Table 23**, entries 15–19) suggesting the overall stability of the system.

5.3. Synthesis of benzoxazines by heterogeneous multicomponent bio-chemo multienzymes cascade reaction

5.3.1 Aim of work

Benzoxazines are heterocyclic derivatives[587,588] characterized by different biological activities, including neuroprotective[589], anticancer[590] and antioxidant properties.[591] They are usually synthesized by harsh and tedious multi-step reactions,[592,593] the only exception being a limited number of procedures based on heavy metals[594] or, in alternative, electrochemistry.[595] Multi-enzymes cascade reactions[596] and multi-component chemistry[597] are considered as a sustainable and green alternative for the synthesis of heterocyclic derivatives. These procedures show similar features. Multi-component chemistry yields the desired compound by condensing three or more reagents in one-pot conditions.[598,599] Multi-enzymes cascade reactions couples together several synthetic steps during which the end product of the first transformation becomes the substrate for the next-one and so on.[136] They undoubtedly have numerous advantages over the classic step-by-step procedures and their combination in a unique reactive framework may represents a valuable and innovative tool for sustainable organic synthesis. We recently reported the one-pot synthesis of hydroxytyrosol esters by multi-enzymes cascade reaction composed by lipase M and tyrosinase after their co-immobilization on electroactive lignin nanoparticles.[551] In this latter case, *ortho*-quinones were irremediably recovered as side-products due to the prevalence of the diphenolase activity of tyrosinase[130,551] in the overall catalytic cycle. Examples of application of the electrophilic reactivity[550] of *ortho*-quinones are reported, they include the preparation of neuroprotective DOPA peptidomimetics[600] by the use of α-amino acid methyl esters as nucleophiles.[601] Inspired by these results, herein we describe the combination of multi-component chemistry and multi-enzymes cascade reaction in a unique reactive framework to yield highly functionalized 1,4-benzoxazines under favorable heterogeneous conditions. The multi-enzymes cascade catalyst (indicated as NOL/LT) was composed by lipase M from *Mucor javanicus* and tyrosinase from *Agaricus bisporus* immobilized on lignin nanoparticles bearing chitosan and concanavalin A (Con A) as specific glycoprotein orienting agents.[512,479] Experimental details for the preparation of NOL/LT, morphology and corresponding activity parameters are reported in **S1** (Figure S1 and Table S1). Lignin nanoparticles are renewable and functional platforms effective for the immobilization of enzymes due to their excellent chemical-physical properties.[194,447,132,480] The starting reagents included the ternary mixture of tyrosol **1**, carboxylic acids **2a-d** (octanoic acid **2a,** lauric acid **2b**, oleic acid **2c,** phloretic acid **2d**) and selected α-amino acid methyl esters **3a-e** (glycine **3a**, alanine **3b,** valine **3c**, leucine **3d,** phenylalanine **3e**). When tyrosol **1** (38.7mg, 0.28 mmol), octanoic acid **2a** (40.4mg, 0.28 mmol) and glycine methyl ester **3a** (37.6mg, 0.30 mmol), dissolved in 2-methyltetrahydrofuran (2-MeTHF; 5.0 mL) and limiting amount of PBS buffer (150 μL, pH 7, 0.1M), were treated at 45°C in air atmosphere and in the presence of catalytic amount of NOL/LT (280 μg; 40U/mg of both lipase and tyrosinase), the 8-hydroxy-5-phenethyloctanoate-2(H)-benzo-1,4-oxazin-2-one **6a** was obtained in one-pot conditions as the main reaction product (56%), besides low amount of catechol derivative **5a** (15%) and traces amount of tyrosol-octanoate **4a** (2%) (**Scheme 5.6**). The low mass balance we observed in the multicomponent reaction involving compounds **1**, **2a** and **3a**, was probably due to the formation of polar oligomers we were not able to isolate from the reaction mixture due to spontaneous oxidative polymerization of quinone intermediate.[512]



Scheme 5.6. Heterogeneous multi-component bio-chemo multienzymes cascade synthesis of 2(H)-benzo-1,4-oxazin-2-one 1,4-benzoxazine **6a** and catechol **5a**.

5.3.2 Experimental part

General information.

Organosolv lignin (OL) was purchased from Chemical Point (Oberhaching, Germany). Chitosan (medium molecular weight: 100.000-300.000), 2-(4-hydroxyphenyl)ethanol, octanoic acid, lauric acid, oleic acid, phloretic acid, 2,2-Dimethylbutyric acid, Amano lipase M from *Mucor javanicus* (300 U/mg), Concanavalin A (Con A) type IV from *Canavalia ensiformis* (Jack bean), tyrosinase from *Agaricus bisporus* (1000 U/mg), glycine methyl ester, valine methyl ester, alanine methyl ester, leucine methyl ester, and phenylalanine methyl ester, benzylamine, ethanolamine, and 2-pycolylamine were purchased from Sigma Chemical Co. (St Louis, MO, USA). 2-Methyltetrahydrofuran was purchased from Sigma Chemical Co. (St Louis, MO, USA) and used without further purification. 4-Nitrophenyl 2-aminoacetate was purchased from Biosynth Ltd and used without further purification. Sodium phosphate buffer (PBS 0.1 M, pH 7) was prepared from Milli Q water. Reactions were monitored by using thin-layer chromatography (TLC) on precoated aluminum silica gel Merck 60 F_{254} plates and the visualization was achieved by UV lamp (λ_{max} =254 nm). ^{1}H NMR and ^{13}C NMR spectra were recorded on Bruker (400 MHz) spectrometer using $CDCl_3$. Chemical shifts (δ) are expressed in parts per million (ppm). Coupling constants J are expressed in Hertz (Hz). Spin multiplicities are given as s (singlet), d (doublet), dd (doublet of doublets), and m (multiplet). High-resolution mass spectra (HRMS) were recorded on a Bruker Daltonics, Inc. APEXIII 7.0 TESLA FTMS instrument. The field emission scanning electron microscopy (FE-SEM) was acquired on FESEM ZEISS GeminiSEM500 at 5 kV after drop 20µL of the sample dispersion (deionized water) on specimen stubs, dried and coated with gold by sputtering with AGAR (Auto Sputter Coater). The sample was coated with chromium thin film (5 nm) by sputter coating using QUORUM Q 150T ES plus coater. Spectrophotometric analysis was performed with Cary 60 UV-Vis spectrophotometer equipped with a single cell peltier thermostated cell holder, Agilent, Santa Clara, USA. Data were elaborated with Cary Win UV software. Attenuated total reflection Fourier transform infrared (ATR-IR) spectroscopy was performed by using Agilent Cary 630 FT-IR spectrometer (UATR unit cell), averaging 32 scans (resolution of 4 cm^{-1}).

Synthesis of 1,4-benzoxazine derivatives with NOL/LT.

As a general procedure, tyrosol **1** (38.6 mg, 0.28 mmol), carboxylic acid **2a-d** (0.28 mmol) and selected α-amino acids methyl esters **3a-e** (0.30 mmol) (glycine **3a,** 37.6mg; alanine **3b,** 41.9mg; valine **3c,** 50.3mg; leucine **3d** 54.5mg; phenylalanine **3e,** 64.7mg, and 4-Nitrophenyl 2-aminoacetate **3f,** 58.8mg) in 2-methyltetrahydrofuran (2-MeTHF; 5.0 mL) were added with NOL/LT (280 μg in 150 μL PBS, pH 7, 0.1M) under dioxygen atmosphere (O_2) and gentle stirred (200 rpm) at 45 °C for 48 h in oil bath. The reaction was monitored by thin layer chromatography (TLC, n-hexane/EtOAc = 8.0:2.0). At the end, the reaction was filtered to recover NOL/LT and the solvent was collected and evaporated under reduced pressure. The crude was purified by flash chromatography (n-hexane/EtOAc = 8.0:2.0) and the reaction products identified by spectrometric and spectroscopic analyses. Original NMR spectra are reported in **S8**.

4-Hydroxyphenethyl octanoate (tyrosol octanoate) (**4a**). Yield 2 % (1.16 mg). Yellow oil. MS (EI) m/z 264.37. Purified by flash chromatography (CH_2Cl_2=MeOH 9.8:0.2). ^{1}H NMR (400 MHz, $CDCl_3$) δ 7.10-7.08 (d, 2H, J 8.4 Hz), 6.79-6.77 (d, 2H, J 9.0 Hz), 4.28-4.24 (m, 2H), 2.89-2.86 (m, 2H), 2.32 -2.28 (m, 2H), 1.66-1.59 (m, 2H), 1.29 (m, 8H), 0.91-0.88 (m, 3H) ppm. ^{13}C{^{1}H} NMR (100 MHz, $CDCl_3$) δ 174.2, 154.5, 130.0 (2C), 129.6, 115.3 (2C), 65.1, 34.4, 34.2, 31.6, 29.0, 28.9, 24.9, 22.6, 14.0 ppm.

2-(8-hydroxy-2-oxo-2H-benzo[b][1,4]oxazin-5-yl)ethyl octanoate **(6a).** Yield 56% (53 mg). Clear oil. MS (EI) m/z 333.16. Purified by flash chromatography (n-hexane/EtOAc = 8.0:2.0). ^{1}H NMR (400 MHz, $CDCl_3$) δ 8.45 (s, 1H, J 9.0 Hz), 7.10-7.08 (d, 1H, J 9.0 Hz), 6.79-6.77 (d, 1H, J 9.0 Hz), 4.28-4.24 (m, 2H), 2.89-2.86 (m, 2H), 2.32-2.28 (m 2H), 1.66-1.59 (m, 2H), 1.29 (m, 8H), 0.91-0.88 (m, 3H) ppm. ^{13}C{^{1}H} NMR (100 MHz, $CDCl_3$) δ 174.2, 157.8, 154.5, 144.2, 143.1, 133.5, 128.9, 127.2, 115.3, 65.1, 34.4, 31.6, 29.0, 28.9 (2C), 24.9, 22.6, 14.0 ppm. HRMS (ESI-TOF) m/z: Calcd for $C_{18}H_{23}NO_5$ 333.1581, found $[M+H]^+$ 333.1600.

2-(8-hydroxy-3-methyl-2-oxo-2H-benzo[b][1,4]oxazin-5-yl)ethyl octanoate **(6b).** Yield 53% (49 mg). Clear oil. MS (EI) m/z 347.17. Purified by flash chromatography (n-hexane/EtOAc = 8.0:2.0). ^{1}H NMR (400 MHz, $CDCl_3$) δ 7.10-7.08 (d, 1H, J 9.0 Hz), 6.79-6.77 (d, 1H, J 9.0 Hz), 4.28-4.24 (m, 2H), 2.89-2.86 (m, 2H), 2.32-2.28 (m, 2H), 2.01-2.00 (s, 3H), 1.66-1.59 (m, 2H), 1.29 (m, 8H), 0.91-0.88 (m, 3H) ppm. ^{13}C{^{1}H} NMR (100 MHz, $CDCl_3$) δ 174.2, 159.0, 154.5, 152.2, 143.2, 134.4, 130.0, 129.6, 115.3, 65.1, 34.4, 31.6, 29.0, 28.9 (2C), 24.9, 22.6, 17.5, 14.0 ppm. HRMS (ESI-TOF) m/z: Calcd for $C_{19}H_{25}NO_5$ 347.1738, found $[M+H]^+$ 347.1758.

2-(8-hydroxy-3-isopropyl-2-oxo-2H-benzo[b][1,4]oxazin-5-yl)ethyl octanoate **(6c).** Yield 49% (43 mg). Clear oil. MS (EI) m/z 375.20. Purified by flash chromatography (n-hexane/EtOAc = 8.0:2.0). ^{1}H NMR (400 MHz, $CDCl_3$) δ 7.10-7.08 (d, 1H, J 9.0 Hz), 6.79-6.77 (d, 1H, J 9.0 Hz), 4.28-4.24 (m, 2H), 2.89-2.86 (m, 2H), 2.32-2.28 (m, 2H), 1.66-1.59 (m, 3H, CH+CH_2), 1.29 (m, 8H), 0.91-0.88 (m, 9H), ppm. ^{13}C{^{1}H} NMR (100 MHz, $CDCl_3$) δ 174.2, 160.0, 154.5, 151.9, 142.6, 134.0, 127.3, 126.5, 114.2, 65.1, 34.4, 31.7, 30.0, 29.9 (3C), 24.9, 22.6, 18.7 (2C), 14.0 ppm. HRMS (ESI-TOF) m/z: Calcd for $C_{21}H_{29}NO_5$ 375.2051, found $[M+H]^+$ 375.2073.

2-(8-hydroxy-3-isobutyl-2-oxo-2H-benzo[b][1,4]oxazin-5-yl)ethyl octanoate **(6d).** Yield 45% (40 mg). Clear oil. MS (EI) m/z 389.22. Purified by flash chromatography (n-hexane/EtOAc = 8.0:2.0). ^{1}H NMR (400 MHz, $CDCl_3$) δ 7.10-7.09 (d, 1H, J 9.0 Hz), 6.79-6.78 (d, 1H, J 9.0 Hz), 4.27-4.23 (m, 2H), 2.89-2.86 (m, 2H), 2.32-2.28 (m, 2H), 2.04 (m, 2H), 1.78 (m, 1H), 1.66-1.59 (m, 2H), 1.29 (m, 8H), 0.93-0.88 (m, 9H) ppm. ^{13}C{^{1}H} NMR (100 MHz, $CDCl_3$) δ 174.2, 157.6, 153.5, 152.9, 143.0, 134.2, 130.0,

129.6, 115.3, 65.1, 38.0, 34.4, 31.6, 29.0, 28.9 (2C), 25.6, 24.5, 23.0 (2C), 22.6, 14.0 ppm. HRMS (ESI-TOF) m/z: Calcd for $C_{22}H_{31}NO_5$ 389.2207, found $[M+H]^+$ 389.2230.

2-(8-hydroxy-2-oxo-2H-benzo[b][1,4]oxazin-5-yl)ethyl dodecanoate (**6e**). Yield 50% (47 mg). Clear oil. MS (EI) m/z 389.22. Purified by flash chromatography (n-hexane/EtOAc = 8.0:2.0). ^{1}H NMR (400 MHz, $CDCl_3$) δ 8.45 (s, 1H, J 7.9 Hz), 7.10-7.08 (d, 1H, J 9.0 Hz), 6.79-6.77 (d, 1H, J 9.0 Hz), 4.28-4.24 (m, 2H), 2.89-2.86 (m, 2H), 2.32-2.28 (m, 2H), 1.66-1.59 (m, 2H), 1.29 (m, 16H), 0.91-0.88 (m, 3H) ppm. ^{13}C{^{1}H} NMR (100 MHz, $CDCl_3$) δ 174.2, 156.9, 152.0, 145.5, 142.3, 133.6, 129.6, 127.5, 113.4, 65.2, 34.4, 31.6, 29.0 (4C), 28.9 (3C), 25.0, 22.6, 14.0, ppm. HRMS (ESI-TOF) m/z: Calcd for $C_{22}H_{31}NO_5$ 389.2207, found $[M+H]^+$ 389.2222.

2-(8-hydroxy-2-oxo-2H-benzo[b][1,4]oxazin-5-yl)ethyl oleate (**6f**). Yield 47% (43 mg). Clear oil. MS (EI) m/z 471.30. Purified by flash chromatography (n-hexane/EtOAc = 8.0:2.0). ^{1}H NMR (400 MHz, $CDCl_3$) δ 8.39 (s, 1H, J 7.9 Hz), 7.10-7.08 (d, 1H, J 9.0 Hz), 6.79-6.75 (d, 1H, J 9.0 Hz), 5.45-5.35 (m, 2H), 4.28-4.24 (m, 2H), 2.95-2.93 (m, 2H), 2.32-2.30 (m, 2H), 2.03-2.00 (m, 4H), 1.66-1.59 (m, 2H), 1.33-1.29 (m, 20H), 0.91-0.88 (m, 3H) ppm. ^{13}C{^{1}H} NMR (100 MHz, $CDCl_3$) δ 174.2, 157.4, 153.5, 145.0, 142.2, 133.6, 130.0 (C=C), 127.5 (2C), 114.0, 65.1, 34.4, 31.6, 29.0 (8C), 27.3 (2C), 25.0, 22.6, 14.0 ppm. HRMS (ESI-TOF) m/z: Calcd for $C_{28}H_{41}NO_5$ 471.2990, found $[M+H]^+$ 471.3018.

*2-(3-benzyl-8-hydroxy-2-oxo-3,4-dihydro-2H-benzo[b][1,4]oxazin-5-yl)ethyl octanoate (**6g**).* Yield 58% (53 mg). Clear oil. MS (EI) m/z 425.53. Purified by flash chromatography (n-hexane/EtOAc = 8.0:2.0). ^{1}H NMR (400MHz), $CDCl_3$) δ 7.23-7.22 (m, 5H, J 7.9 Hz), 6.79-6.77 (d, 1H, J 9.0 Hz), 6.68-6.66 (d, 1H, J 9.0 Hz), 4.28-4.24 (m, 2H), 4.13-4.10 (m, 1H), 2.89-2.87 (m, 2H), 2.32-2.28 (m, 2H), 1.66-1.59 (m, 2H), 1.29 (m, 8H), 0.91-0.88 (m, 3H) ppm. ^{13}C{^{1}H} NMR (100 MHz, $CDCl_3$) δ 173.8, 158.5, 155.5, 151.5, 144.0, 136.0, 133.3, 128.8 (2C), 127.8 (2C), 126.8, 125.7, 124.5, 114.3, 65.1, 33.8, 31.9, 29.9, 29.0, 27.5, 25.5, 22.6, 14.0 ppm. HRMS (ESI-TOF) m/z: Calcd for $C_{25}H_{29}NO_5$ 423.2051, found $[M+H]^+$ 423.2076.

2-(8-hydroxy-2-oxo-2H-benzo[b][1,4]oxazin-5-yl)ethyl 3-(4-hydroxyphenyl)propanoate **(6h).** Yield 55% (50 mg). Yellow oil. MS (EI) m/z 355.35. Purified by flash chromatography (n-hexane/EtOAc = 8.0:2.0). ^{1}H NMR (400 MHz, $CDCl_3$) δ 8.49 (s, 1H, J 9.0 Hz), 7.10-7.07 (d, 2H, J 9.0 Hz), 6.98-6.75 (dd, 2H, J 9.0 Hz), 6.70 (d, 2H, J 9.0 Hz), 4.28-4.24 (m, 2H), 2.89-2.86 (m, 2H), 2.85-2.84 (m, 2H), 2.53-2.52 (m, 2H) ppm. ^{13}C{^{1}H} NMR (100 MHz, $CDCl_3$) δ 173.2, 157.2, 155.6, 151.5, 145.2, 142.5, 134.2, 133.9, 130.0 (2C), 127.1, 126.9, 115.3 (2C), 113.5, 65.1, 34.4, 29.0, 28.9, ppm. HRMS (ESI-TOF) m/z: Calcd for $C_{19}H_{17}NO_6$ 355.1061, found $[M+H]^+$ 355.1082.

3,4-dihydroxy-2-((2-methoxy-2-oxoethyl)amino)phenethyl octanoate **(5a).** Yield 15% (11 mg). Yellow oil. MS (EI) m/z 367.20. Purified by flash chromatography (n-hexane/EtOAc = 8.0:2.0). ^{1}H NMR (400 MHz, $CDCl_3$) δ 6.79-6.77 (d, 1H, J 8.9 Hz), 6.04-6.03 (d, 1H, J 9.0 Hz), 4.28-4.24 (m, 2H), 4.02 (s, 2H), 3.68 (s, 3H), 2.89-2.86 (m, 2H), 2.32-2.28 (m, 2H), 1.66-1.59 (m, 2H), 1.29 (m, 8H), 0.91-0.88 (m, 3H) ppm. ^{13}C{^{1}H} NMR (100 MHz, $CDCl_3$) δ 174.2, 171.0, 145.5, 138.4, 130.0, 122.9, 115.3, 104.5, 65.1, 53.1, 44.8, 34.2, 31.6, 29.0, 28.9 (2C), 24.9, 22.6, 14.0 ppm. HRMS (ESI-TOF) m/z: Calcd for $C_{19}H_{29}NO_6$ 367.2000, found $[M+H]^+$ 367.2022.

3,4-dihydroxy-2-((1-methoxy-1-oxopropan-2-yl)amino)phenethyl octanoate **(5b).** Yield 10% (8 mg). Yellow oil. MS (EI) m/z 381.22. Purified by flash chromatography (n-hexane/EtOAc = 8.0:2.0). ^{1}H NMR (400 MHz, $CDCl_3$) δ 6.45-6.44 (d, 1H, J 8.8 Hz), 6.03 (d, 1H, J 9.0 Hz), 4.28-4.24 (m, 2H), 3.95-3.94 (m, 1H), 3.65 (s, 3H), 2.92-2.89 (m, 2H), 2.32-2.29 (m, 2H), 1.66-1.58 (m, 2H), 1.28-1.26 (m, 8H), 0.91-0.88 (m, 6H) ppm. ^{13}C{^{1}H} NMR (100 MHz, $CDCl_3$) δ 174.2, 173.4, 146.1, 138.6, 130.0, 122.3, 116.3,

103.9, 65.1, 56.9, 52.0, 34.5, 31.6, 29.0, 28.9 (2C), 24.9, 22.6, 18.7, 14.1 ppm. HRMS (ESI-TOF) m/z: Calcd for $C_{20}H_{31}NO_6$ 381.2156, found $[M+H]^+$ 381.2178.

3,4-dihydroxy-2-((1-methoxy-3-methyl-1-oxobutan-2-yl)amino)phenethyl octanoate **(5c).** Yield 10% (8.5 mg). Yellow oil. MS (EI) m/z 409.25. Purified by flash chromatography (n-hexane/EtOAc = 8.0:2.0). ^{1}H NMR (400 MHz, $CDCl_3$) δ 6.79-6.77 (d, 1H, J 8.9 Hz), 6.12 (d, 1H, J 9.0 Hz), 4.28-4.24 (m, 2H), 3.52 (s, 3H), 3.49 (m, 1H), 2.89-2.86 (m, 2H), 2.52-2.51 (m, 1H), 2.32-2.28 (m, 2H), 1.66-1.59 (m, 2H), 1.29 (m, 8H), 0.99-0.80 (m, 9H) ppm. ^{13}C{^{1}H} NMR (100 MHz, $CDCl_3$) δ 174.2, 171.6, 145.6, 138.4, 129.4, 122.3, 115.3, 103.9, 74.2, 65.1, 52.0, 34.2, 31.6, 29.0 (2C), 28.9 (2C), 24.9, 22.6, 18.9 (2C), 14.0 ppm. HRMS (ESI-TOF) m/z: Calcd for $C_{22}H_{35}NO_6$ 409.2469, found $[M+H]^+$ 409.2493.

3,4-dihydroxy-2-((1-methoxy-4-methyl-1-oxopentan-2-yl)amino)phenethyl octanoate (**5d**). Yield 12% (10 mg). Yellow oil. MS (EI) m/z 423.26. Purified by flash chromatography (n-hexane/EtOAc = 8.0:2.0). ^{1}H NMR (400 MHz, $CDCl_3$) δ 6.46-6.45 (d, 1H, J 9.0 Hz), 6.12-6.11 (d, 1H, J 9.0 Hz), 4.28-4.26 (m, 2H), 4.03-4.02 (m, 1H), 3.65 (s, 3H), 2.95-2.88 (m, 2H), 2.32-2.28 (m, 2H), 1.92-1.84 (m, 2H), 1.66-1.59 (m, 2H), 1.49 (m, 1H), 1.30-1.29 (m, 8H), 0.90-0.88 (m, 9H) ppm. ^{13}C{^{1}H} NMR (100 MHz, $CDCl_3$) δ 174.2, 172.2, 140.9, 138.9, 130.0, 123.1, 116.3, 105.0, 65.1 (2C), 51.0, 40.1, 34.2, 31.6, 29.0, 28.9 (2C), 24.9 (2C), 22.8 (3C), 14.1 ppm. HRMS (ESI-TOF) m/z: Calcd for $C_{23}H_{37}NO_6$ 423.2626, found $[M+H]^+$ 423.2651.

3,4-dihydroxy-2-((2-methoxy-2-oxoethyl)amino)phenethyl dodecanoate ***(5e).*** Yield 13% (11 mg). Yellow oil. MS (EI) m/z 423.55. Purified by flash chromatography (n-hexane/EtOAc = 8.0:2.0). ^{1}H NMR (400 MHz, $CDCl_3$) δ 6.79-6.77 (d, 1H, J 9.0 Hz), 6.04-6.03 (d, 1H, J 9.0 Hz), 4.28-4.24 (m, 2H), 4.02 (s, 2H), 3.68 (s, 3H), 2.89-2.86 (m, 2H), 2.32-2.28 (m, 2H), 1.66-1.59 (m, 2H), 1.29 (m, 16H), 0.91-0.88 (m, 3H) ppm. ^{13}C{^{1}H} NMR (100 MHz, $CDCl_3$) δ 174.2, 171.0, 145.5, 138.4, 130.0, 122.9, 115.3, 104.5, 65.1, 53.1, 44.8, 34.2, 31.6, 29.0 (3C), 28.9 (3C), 24.9, 22.6, 14.0 ppm. HRMS (ESI-TOF) m/z: Calcd for $C_{23}H_{37}NO_6$ 423.2626, found $[M+H]^+$ 423.2653.

3,4-dihydroxy-2-((2-methoxy-2-oxoethyl)amino)phenethyl oleate **(5f).** Yield 17% (15 mg). Yellow oil. MS (EI) m/z 367.20. Purified by flash chromatography (n-hexane/EtOAc = 8.0:2.0). ^{1}H NMR (400 MHz, $CDCl_3$) δ 6.48-6.46 (d, 1H, J 8.9 Hz), 6.05-6.03 (d, 1H, J 9.0 Hz), 5.35 (m, 2H), 4.28-4.24 (m, 2H), 4.02 (s, 2H), 3.68 (s, 3H), 2.96-2.93 (m, 2H), 2.32-2.30 (m, 2H), 2.03-2.00 (m, 4H), 1.66-1.59 (m, 2H), 1.33-1.29 (m, 20H), 0.91-0.80 (m, 3H) ppm. ^{13}C{^{1}H} NMR (100 MHz, $CDCl_3$) δ 174.2, 171.0, 145.5, 138.4, 130.0, 129.6 (C=C), 122.9, 115.3, 104.5, 65.1, 52.0, 44.2, 34.2, 31.6, 29.0 (8C), 27.3 (2C), 25.0, 22.6, 14.0 ppm. HRMS (ESI-TOF) m/z: Calcd for $C_{29}H_{47}NO_6$ 505.3408, found $[M+H]^+$ 505.3438.

*3,4-dihydroxy-2-((1-methoxy-1-oxo-3-phenylpropan-2-yl)amino)phenethyl octanoate (**5g**)*. Yield 15% (10 mg). Yellow oil. MS (EI) m/z 457.57. Purified by flash chromatography (n-hexane/EtOAc = 8.0:2.0). ^{1}H NMR (400 MHz, $CDCl_3$) δ 7.19-7.16 (m, 5H, J 8.9 Hz), 6.47-6.46 (d, 1H, J 9.0 Hz), 6.04-6.03 (d, 1H, J 9.0 Hz), 4.28-4.24 (m, 2H), 4.12-4.11 (m, 1H), 3.66 (s, 3H), 3.55-3.26 (m, 2H), 2.89-2.86 (m, 2H), 2.32-2.28 (m, 2H), 1.66-1.59 (m, 2H), 1.29 (m, 8H), 0.91-0.88 (m, 3H) ppm. ^{13}C{^{1}H} NMR (100 MHz, $CDCl_3$) δ 173.7, 171.7, 145.5, 138.2, 136.7, 130.8, 128.8 (2C), 127.7, 125.8, 122.5, 115.3, 104.8, 68.1, 65.1, 51.2, 36.1, 33.9, 31.9, 30.3, 29.6-29.3 (2C), 24.4, 22.6, 14.0 ppm. HRMS (ESI-TOF) m/z: Calcd for $C_{26}H_{35}NO_6$ 457.2469, found $[M+H]^+$ 457.2496.

*3,4-dihydroxy-2-((2-methoxy-2-oxoethyl)amino)phenethyl 3-(4-hydroxyphenyl)propanoate (**5h**)*. Yield 12% (9 mg). Yellow oil. MS (EI) m/z 389.40. Purified by flash chromatography (n-hexane/EtOAc = 8.0:2.0). ^{1}H NMR (400 MHz, $CDCl_3$) δ 7.10-7.08 (d, 2H, J 9.0 Hz), 6.79-6.77 (d, 2H, J 9.0 Hz), 6.49-6.47 (d, 1H, J 9.0

Hz), 6.06-6.03 (d, 1H, J 9.0 Hz), 4.28-4.24 (m, 2H), 4.05 (s, 2H), 3.66 (s, 3H), 2.98-2.95 (m, 2H), 2.89-2.86 (m, 2H), 2.53-2.52 (m, 2H) ppm. $^{13}C\{^{1}H\}$ NMR (100 MHz, $CDCl_3$) δ 173.2, 170.1, 156.4, 144.5, 138.5, 134.0, 130.0, 129.6 (2C), 122.2, 116.8, 115.3 (2C), 104.3, 65.1, 51.2, 44.5, 34.2, 29.9, 29.9 ppm. HRMS (ESI-TOF) m/z: Calcd for $C_{20}H_{23}NO_7$ 389.1480, found $[M+H]^+$ 389.1503.

3,4-dihydroxy-2-((2-(4-nitrophenoxy)-2-o-oethyl)amino)phenethyl octanoate (**5i**). Yield 10% (7.6 mg). Clear yellow oil. MS (EI) m/z 474.50. Purified by flash chromatography (n-hexane/EtOAc = 8.0:2.0). ^{1}H NMR (400 MHz, $CDCl_3$) δ 8.43-8.34 (d, 2H, J 8.4 Hz), 7.50-7.49 (d, 2H, J 8.4 Hz), 6.43-6.32 (d, 1H, J 8.4 Hz), 6.13-6.09 (d, 1H, J 9.0 Hz), 4.28-4.24 (m, 2H), 4.19 (s, 2H), 2.89-2.86 (m, 2H), 2.32-2.28 (m, 2H), 1.66-1.59 (m, 2H), 1.29 (m, 8H), 0.91-0.88 (m, 3H) ppm. $^{13}C\{^{1}H\}$ NMR (100 MHz, $CDCl_3$) δ 174.2, 167.5, 157.5, 145.0, 144.6, 137.3, 130.0, 125.3 (2C), 122.3 (3C), 115.3, 105.3, 65.1, 44.0, 34.4, 31.6, 29.0, 28.9, 24.9, 22.6, 14.0 ppm. HRMS (ESI-TOF) m/z: Calcd for $C_{24}H_{30}N_2O_8$ 474.2007, found $[M+H]^+$ 474.2036.

*Synthesis of catechol derivatives **8a-c**.*

As a general procedure, tyrosol **1** (0.28 mmol), octanoic acid **2a** and selected primary amines (benzylamine **7a**, ethanolamine **7b** and 2-pycolylamine **7c**) (0.30 mmol) were treated with a catalytic amount of NOL/LT (280 μg, 40U/mg) at 45°C in 2-MeTHF (5.0 mL) and limiting amount of PBS buffer (150 μL, pH 7) in air atmosphere to afford catechol derivatives **8a-c** as the main products in high yield besides to traces amount of tyrosol-octanoate **4a**. Original NMR spectra are reported in **SI4**.

*2-(benzylamino)-3,4-dihydroxyphenethyl octanoate **(8a).*** Yield 45% (40 mg). Clear oil. MS (EI) m/z 385.23. Purified by flash chromatography (n-hexane/EtOAc = 8.0:2.0). ^{1}H NMR (400 MHz, $CDCl_3$) δ 7.32-7.29 (m, 5H), 6.42-6.41 (d, 1H, J 9.0 Hz), 6.04-6.03 (d, 1H, J 9.0 Hz), 4.29-4.28 (m, 2H), 4.19 (s, 2H), 2.96-2.95 (m, 2H), 2.32-2.29 (m, 2H), 1.66-1.61 (m, 2H), 1.29 (m, 8H), 0.92-0.88 (m, 3H) ppm. $^{13}C\{^{1}H\}$ NMR (100 MHz, $CDCl_3$) δ 174.2, 145.3, 140.0, 138.6, 131.2, 128.0 (2C), 126.6 (3C), 122.6, 115.9, 104.2, 65.1, 48.7, 34.4, 31.6, 30.0, 29.2 (2C), 25.1, 22.6, 14.0 ppm. HRMS (ESI-TOF) m/z: Calcd for $C_{23}H_{31}NO_4$ 385.2258, found $[M+H]^+$385.2281.

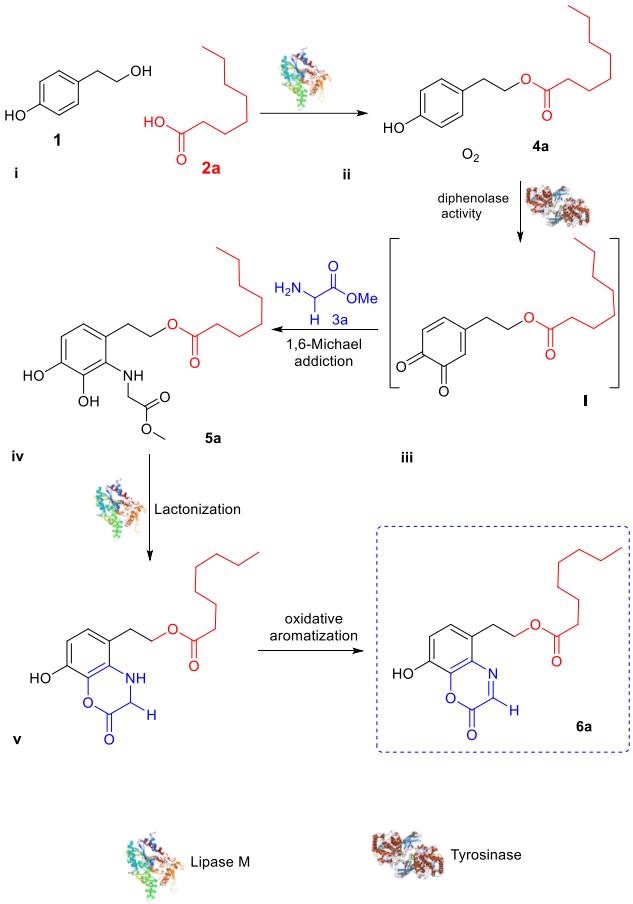
3,4-dihydroxy-2-((2-hydroxyethyl)amino)phenethyl octanoate (**8b**). Yield 34% (22.8 mg). Yellow oil. MS (EI) m/z 339.20. Purified by flash chromatography (n-hexane/EtOAc = 8.0:2.0). ^{1}H NMR (400 MHz, $CDCl_3$) δ 6.47-6.45 (d, 1H, J 9.0 Hz), 6.02-6.01 (d, 1H, J 9.0 Hz), 4.28-4.24 (m, 2H), 3.68-3.67 (m, 2H), 3.55-3.54 (2H, m), 2.96-2.95 (m, 2H), 2.32-2.29 (m, 2H), 1.66-1.59 (m, 2H), 1.32 (m, 8H), 0.91-0.89 (m, 3H) ppm. $^{13}C\{^{1}H\}$ NMR (100 MHz, $CDCl_3$) δ 173.5, 145.7, 138.3, 129.6, 123.2, 115.9, 104.2, 65.1, 61.9, 46.5, 33.9, 31.6, 30.0, 29.2 (2C), 25.1, 23.6, 14.1 ppm. HRMS (ESI-TOF) m/z: Calcd for $C_{18}H_{29}NO_5$ 339.2051, found $[M+H]^+$ 339.2071.

3,4-dihydroxy-2-((130yridine-2-ylmethyl)amino)phenethyl octanoate (**8c).** Yield 42% (39 mg). Clear oil. MS (EI) m/z 386.22. Purified by flash chromatography (n-hexane/EtOAc = 8.0:2.0). ^{1}H NMR (400 MHz, $CDCl_3$) δ 8.49-8.46 (m, 1H), 7.75-7.30 (m, 1H, J 7.9 Hz), 7.26-7.23 (m, 2H, J 7.9 Hz), 6.42-6.40 (d, 1H, J 9.0 Hz), 6.03-6.02 (d, 1H, J 9.0 Hz), 4.70-4.69 (s, 2H), 4.30-4.27 (m, 2H), 2.91-2.89 (m, 2H), 2.32-2.29 (m, 2H), 1.66-1.59 (m, 2H), 1.33-1.30 (m, 8H), 0.91-0.88 (m, 3H) ppm. $^{13}C\{^{1}H\}$ NMR (100 MHz, $CDCl_3$) δ 174.2, 159.0, 148.9, 144.9, 139.8, 138.5, 130.9, 122.5, 121.2 (2C), 115.8, 103.9, 65.1, 48.4, 34.2, 31.6, 29.0, 28.9 (2C), 24.9, 22.6, 14.1 ppm. HRMS (ESI-TOF) m/z: Calcd for $C_{22}H_{30}N_2O_4$ 386.2211, found $[M+H]^+$ 386.2234.

5.7.3 Results and discussions

The reaction pathway involved the following steps: i) lipase M catalyzed synthesis of tyrosol-octanoate **4a** (isolated in traces amount) from tyrosol **1** and octanoic acid **2a**; ii) selective hydroxylation of tyrosol-octanoate **4a** by tyrosinase to yield *ortho*-quinone **I** (not isolated in our case); iii) 1,6-Michael addition of glycine methyl ester **3a** on *ortho*-quinone **I** and successive keto-enolic aromatization to catechol **5a** (side-product); and iv) intramolecular lactonization involving the ester moiety of glycine and the proximal hydroxyl group of the catechol moiety, followed by v) spontaneous oxidative aromatization to yield benzoxazine **6a** (**Scheme 5.7**). The sequence of lipase and tyrosinase activity in the cascade of **Scheme 5.7** was hypothesized on the basis of the consideration that the activity of lipase increased more significantly in the cascade system than tyrosinase (Supporting information), the latter being in part limited by the prevalence of the organic solvent with respect to the buffer (just the amount required for the hydration shell of tyrosinase). The presence of tyrosol ester **4a** as side-product instead of hydroxytyrosol ester counterpart further confirmed the highest efficacy of lipase in the first step of the transformation. The selective addition of compound **3a** at C3 position of ortho-quinone **I** (1,6-type regiochemistry) was not expected, since nucleophiles usually add at C5 position (1,4-type regiochemistry). Probably, this selectivity was a consequence of the favorable ring closure of the oxazine ring, even if, the occurrence of radical addition than ionic mechanism, affording 1,6-type regiochemistry, cannot be completely ruled out.[615] Note that the reaction between tyrosol **1**, glycine methyl ester **3a** and tyrosol-octanoate **4a**, performed in the presence of NOL/T deprived of Lipase M (for the preparation and characterization of NOL/T see S2, Table S2), yielded catechol **5a** as the only recovered product (26%) besides to unreacted substrates. The yield of benzoxazine **6a** with NOL/LT was higher than that obtained with NOL/T, showing that the activity of tyrosinase was improved by the cascade system, in accordance with data previously reported.[130,508,603,604] Conversely, when the reaction was performed with NOL/L deprived of Tyrosinase, tyrosol octanoate **4a** was detected as single product. Thus, both the enzymes were essential ingredients for the multicomponent synthesis of benzoxazine **6a**. In order to better investigate the multi-enzyme cascade effect in the overall yield of benzoxazine **6a**, the reaction was repeated with a mixture of NOL/T and NOL/L, taking into due account the use of appropriate amount of biocatalysts. The mixture of NOL/T and NOL/L afforded benzoxazine **6a** in low yield (10%), besides to tyrosol-octanoate **4a** (50%) and catechol derivative **5a** (27%), confirming the lack of tunnelling effect[138] (see S4).

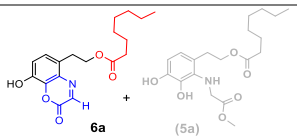
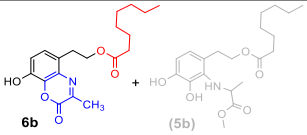
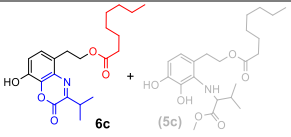
The total yield of benzoxazine **6a** was higher, or of the same order of magnitude, than that previously reported for traditional multi-steps procedures.[605-608] Since we operated in one-pot conditions, the multicomponent cascade enzyme approach appears to be of significant green interest with respect to the state of art. Experimental details for the reaction are reported in S4. This result confirmed the role played by Lipase M in the intramolecular lactonization (step iv). In addition, the synthesis of imines from aromatic N-alkylamines (step v) by tyrosinase is reported and the hydrogen transfer from the alkylamino group of the substrate to the oxy form of the enzyme discussed in detail.[609] The effective isolation of tyrosol-octanoate **4a** and catechol derivative **5a** from the reaction mixture was in accordance with the proposed reaction pathway. It cannot escape to our attention that the overall transformation was (highly) resemblant to the last metabolic steps in the biosynthesis of benzothiazines from DOPA-quinone and cysteine during melanogenesis.[610]

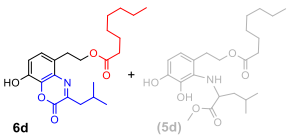
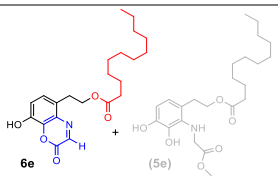
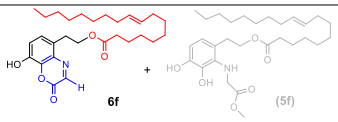
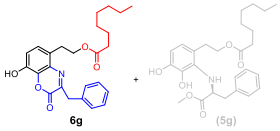
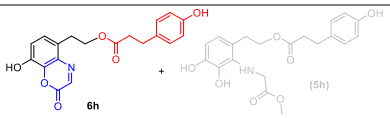
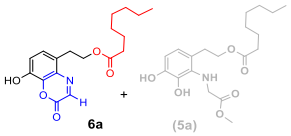
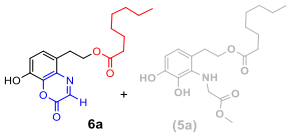
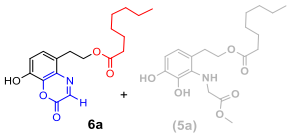
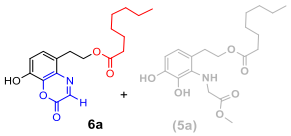
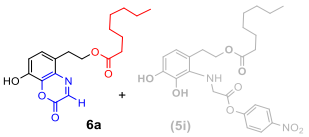


Scheme 5.7. Proposed reaction pathway for the synthesis of 2(H)-benzo-1,4-oxazin-2-one **6a** and catechol derivative **5a** from the ternary mixture of compounds **1**, 2a and **3a**.

Next, we extended the reaction to ternary mixtures containing α-amino acids **3b-d.** Irrespective to experimental conditions, *8-hydroxy-3-methyl-5-phenethyloctanoate-2(H)-benzo-1,4-oxazin-2-one* **6b**, *8-hydroxy-3-isopropyl-5-phenethyloctanoate-2(H)-benzo-1,4-oxazin-2-one* **6c**, and *8-hydroxy-3-isobutyl-5-phenethyloctanoate-2(H)-benzo-1,4-oxazin-2-one* **6d** were recovered as the main reaction products from moderate to excellent yield, besides low amount of catechol derivatives **5b-d** and traces-amount of tyrosol-octanoate **4a** (**Table 24**).

Table 24. Synthesis of 1,4-benzoxazine derivatives by NOL/LT.

Entry	Substrate 1	Substrate 2	Substrate 3	Products	Conversion (%)	Yield (%)
1	1	2a	3a	 **6a** (5a)	80	56[a](15)[b]
2	1	2a	3b	 **6b** (5b)	78	53(10)
3	1	2a	3c	 **6c** (5c)	75	49(10)

4	1	2a	3d		68	45(12)
5	1	2b	3a		70	50(13)
6	1	2c	3a		70	47(17)
7	1	2a	3e		77	58(15)
8	1	2d	3a		73	55(12)
9	1	2a	3a		80 (Run n.1)[c]	55(11)
10	1	2a	3a		78(Run n.2)	51(9)
11	1	2a	3a		75(Run n.3)	52(9)
12	1	2a	3a		70(Run n.4)	48(8)
13	1	2a	3f		85%	66(5)

The products yield was evaluated based on recovered mmol of the reaction product. [a] Data refers to yield of compound **6a-h**. [b] Data refers to yield of compound **5a-i**. Traces amount of tyrosol octanoate **4a** (c.a. 1-2%) were detected in the reaction mixture. [c] NOL/LT was re-covered by centrifugation and re-used in next runs.

The steric hindrance of the carboxylic acid was not detrimental to the overall transformation in the case of linear carboxylic acids, while the reaction was not operative with highly hindered 2,2-dimethylbutyric acid. The latter result is in accordance with the reported inhibitory effect of fatty acids with branching carbon chain at the position neighboring the carboxylic group against esterase activity.[611] As a selected example,

when tyrosol **1** (38.7mg, 0.28 mmol), long side-chain and heterocyclic carboxylic acids lauric acid **2b** (56.08mg, 0.28 mmol), oleic acid **2c** (79.08mg, 0.28 mmol), and glycine methyl ester **3a** (37.6mg, 0.30 mmol) were treated at 45°C in 2-MeTHF (5.0 mL) and limiting amount of PBS buffer (150 μL, pH 7, 0.1M) in air atmosphere and in the presence of NOL/LT (280 μg; 40U/mg of both lipase and tyrosinase), the 8-hydroxy-5-phenethyllaurate-2(H)-benzo-1,4-oxazin-2-one **6e**, and 8-hydroxy-5-phenethyloleate-2(H)-benzo-1,4-oxazin-2-one **6f** were obtained, respectively, as the main reaction products besides low amount of catechol derivatives **5e-f** (**Scheme 5.7, Table 24**, entries 5-6). The reusability of NOL/LT was evaluated after its recovering at the end of the reaction by centrifugation (15000 g) for 10 mins, followed by washing with PBS (pH 7.0, 0.1 M). NOL/LT effectively retained the reactivity for at least 4 runs in the synthesis of benzoxazine derivative **6a** as a selected example (**Table 24**, entries 9-12). In order to further evaluate the method's adaptability, the reaction was repeated under similar experimental conditions including the aryl-like derivative phenylalanine methyl ester **3e**, and the aromatic phloretic acid **2d**, respectively. As reported in **Table 24** (entries 7-8), benzoxazines **6g** and **6h** were obtained in significant yield besides low amounts of corresponding catechol derivatives **5g** and **5h**, confirming the generality of the procedure. Finally, the reaction between **1** and **2a** was repeated, as a selected case, with (4-nitrophenyl)-2-amino acetate **3f** instead than glycine methyl-ester **3a** under similar experimental conditions, in order to reduce the formation of catechol derivative **5a**. As reported in **Table 24** (entry 13), benzoxazine **6a** was obtained in higher yield and similar conversion than the reference counterpart (**Table 24**, entry 1). Note that the use of mild bases to further enhance the yield of the lactonization step was not possible due to the reported inhibition of lipase from Mucor javanicus activity at pH > 7.[514,612,613]

The synthetic relevance of the multicomponent biochemo multi-enzymes cascade reaction was further demonstrated in the synthesis of highly functionalized catechol derivatives by using simple primary amines as nucleophiles. For example, when tyrosol **1** (38.7mg, 0.28 mmol), octanoic acid **2a** (40.4mg, 0.28 mmol) and selected amines **7a-c** (0.30 mmol) (benzylamine **7a**, 32.14mg; ethanolamine **7b**, 18.32mg; and 2-pycolylamine **7c**, 32.44mg) were treated at 45°C in 2-MeTHF (5.0 mL) and limiting PBS buffer (150 μL, pH 7, 0.1M) in air atmosphere and in the presence of NOL/LT (280 μg; 40U/mg of both lipase and tyrosinase), catechol derivatives **8a-c** were isolated in high yield as the only recovered products besides traces-amount of tyrosol-octanoate **4a** (**Scheme 5.7, Figure 5.7**). The reaction proceeded with high chemo-selectivity in the case of bifunctional ethanolamine, the product deriving from N-addition being the only recovered compound.

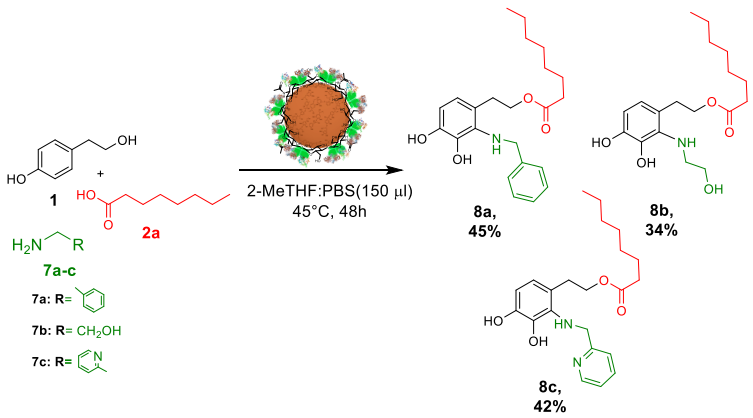


Figure 5.7. Heterogeneous multicomponent bio-chemo multienzymes cascade synthesis of catechols **8a-c** from the ternary mixture of compounds **1**, **2a** and **7a-c**. The yield was evaluated on the basis of mmol of the recovered product. Traces amount of tyrosol octanoate **4a** (1-2%) were detected in the reaction mixture.

References

479- Capecchi, E., Piccinino, D., Tomaino, E., Bizzarri, B.M., Polli, F., Antiochia, R., Mazzei, F. and Saladino, R., Lignin nanoparticles are renewable and functional platforms for the concanavalin a oriented immobilization of glucose oxidase–peroxidase in cascade bio-sensing. *RSC advances*, **2020**,10(48), pp.29031-29042.

480- Capecchi, E., Piccinino, D., Bizzarri, B.M., Botta, L., Crucianelli, M. and Saladino, R., Oxidative bio-desulfurization by nanostructured peroxidase mediator system. *Catalysts*, **2020**, 10(3), p.313.

481- Kim, Eunkyoung, W. Taylor Leverage, Yi Liu, Ian M. White, William E. Bentley, and Gregory F. Payne. "Redox-capacitor to connect electrochemistry to redox-biology." *Analyst 139*, no. 1 **(2014):** 32-43.

482- Rodríguez-Morató, J., Boronat, A., Kotronoulas, A., Pujadas, M., Pastor, A., Olesti, E., Perez-Mana, C., Khymenets, O., Fito, M., Farre, M. and de la Torre, R. Metabolic disposition and biological significance of simple phenols of dietary origin: Hydroxytyrosol and tyrosol. *Drug Metabolism Reviews*, **2016**, 48(2), pp.218-236

483- R. Delisi, F. Saiano, M. Pagliaro, R. Ciriminna, *Chem. Cent.* J. **2016**, 10, 63.

484- Safarzadeh Markhali, F. Effect of processing on phenolic composition of olive oil products and olive mill by-products and possibilities for enhancement of sustainable processes. *Processes*, **2021**, 9(6), p.953.

485- Allouche, N., Damak, M., Ellouz, R. and Sayadi, S. Use of whole cells of Pseudomonas aeruginosa for synthesis of the antioxidant hydroxytyrosol via conversion of tyrosol. *Applied and environmental microbiology*, **2004**, 70(4), pp.2105-2109.

486- Karković Marković, A., Torić, J., Barbarić, M. and Jakobušić Brala, C. Hydroxytyrosol, tyrosol and derivatives and their potential effects on human health. *Molecules*, **2019**, 24(10), p.2001.

487- Manna, C., Galletti, P., Cucciolla, V., Montedoro, G. and Zappia, V. Olive oil hydroxytyrosol protects human erythrocytes against oxidative damages. *The Journal of nutritional biochemistry,* **1999**, 10(3), pp.159-165.

488- Lopez-Huertas Leon E., Geerlings A., Morales Sanchez J. C., J. Boza Puerta, WO-200308798 A1, **2003**.

489- Fuccelli, R., Fabiani, R. and Rosignoli, P. Hydroxytyrosol exerts anti-inflammatory and anti-oxidant activities in a mouse model of systemic inflammation. *Molecules*, **2018**, 23(12), p.3212.

490- De Pablos, R.M., Espinosa-Oliva, A.M., Hornedo-Ortega, R., Cano, M. and Arguelles, S. Hydroxytyrosol protects from aging process via AMPK and autophagy; a review of its effects on cancer, metabolic syndrome, osteoporosis, immune-mediated and neurodegenerative diseases. *Pharmacological research*, **2019**, 143, pp.58-72.

491- Robles-Almazan, M., Pulido-Moran, M., Moreno-Fernandez, J., Ramirez-Tortosa, C., Rodriguez-Garcia, C., Quiles, J.L. and Ramirez-Tortosa, M., Hydroxytyrosol: Bioavailability, toxicity, and clinical applications. *Food Research International*, **2018**, 105, pp.654-667.

492- Ziosi, P., Paolucci, C., Santarelli, F., Tabanelli, T., Passeri, S., Cavani, F. and Righi, P. A Two-Step Process for the Synthesis of Hydroxytyrosol. *ChemSusChem,* **2018**, 11(13), pp.2202-2210.

493- Bernini, R., Mincione, E., Barontini, M. and Crisante, F. Convenient synthesis of hydroxytyrosol and its lipophilic derivatives from tyrosol or homovanillyl alcohol. *Journal of agricultural and food chemistry*, **2008**, 56(19), pp.8897-8904.

494- Kalampaliki, A.D., Giannouli, V., Skaltsounis, A.L. and Kostakis, I.K. A three-step, gram-scale synthesis of hydroxytyrosol, hydroxytyrosol acetate, and 3, 4-dihydroxyphenylglycol. *Molecules*, **2019**, 24(18), p.3239.

495- Li, Z., Chen, H., Fang, Y., Ma, Y., Chen, H., Yang, B. and Wang, Y., A highly efficient three-liquid-phase-based enzymatic one-pot multistep reaction system with recoverable enzymes for the synthesis of biodiesel. *Journal of Agricultural and Food Chemistry,* **2021**, 69(19), pp.5481-5490.

496- B. Zieniuk, K. Groborz, M. Wołoszynowska, K. Ratusz, E. Białecka-florjańczyk, A. Fabiszewska, *Biomol. Eng.* **2021**, 11, 1–12.

497- Liebgott, P.P., Labat, M., Casalot, L., Amouric, A. and Lorquin, J., Bioconversion of tyrosol into hydroxytyrosol and 3, 4-dihydroxyphenylacetic acid under hypersaline conditions by the new Halomonas sp. strain HTB24. *FEMS Microbiology Letters*, **2007**, 276(1), pp.26-33.

498- Annunziata, F., Contente, M.L., Pinna, C., Tamborini, L. and Pinto, A. Biocatalyzed flow oxidation of tyrosol to hydroxytyrosol and efficient production of their acetate esters. *Antioxidants*, **2021**, 10(7), p.1142.

499- Bozzini, T., Botta, G., Delfino, M., Onofri, S., Saladino, R., Amatore, D., Sgarbanti, R., Nencioni, L. and Palamara, A.T., Tyrosinase and Layer-by-Layer supported tyrosinases in the synthesis of lipophilic catechols with antiinfluenza activity. *Bioorganic & Medicinal Chemistry*, **2013**, 21(24), pp.7699-7708.

500- Zhou, D.Y., Sun, Y.X. and Shahidi, F., Preparation and antioxidant activity of tyrosol and hydroxytyrosol esters. *Journal of Functional Foods,* **2017**, 37, pp.66-73.

501- Ginex, T., Vazquez, J., Gilbert, E., Herrero, E. and Luque, F.J., Lipophilicity in drug design: An overview of lipophilicity descriptors in 3D-QSAR studies. *Future medicinal chemistry,* **2019**, 11(10), pp.1177-1193.

502- Rutkowska, E., Pajak, K. and Jóźwiak, K., Lipophilicity--methods of determination and its role in medicinal chemistry. *Acta poloniae pharmaceutica*, **2013**, 70(1), pp.3-18.

503- Bernini, R., Carastro, I., Santoni, F. and Clemente, M., Synthesis of lipophilic esters of tyrosol, homovanillyl alcohol and hydroxytyrosol. *Antioxidants,* **2019**, 8(6), p.174.

504- Fotiadou, R., Chatzikonstantinou, A.V., Hammami, M.A., Chalmpes, N., Moschovas, D., Spyrou, K., Polydera, A.C., Avgeropoulos, A., Gournis, D. and Stamatis, H. Green synthesized magnetic nanoparticles as effective nanosupport for the immobilization of lipase: Application for the synthesis of lipophenols. *Nanomaterials,* **2021**, 11(2), p.458.
505- Botta, G., Bizzarri, B.M., Garozzo, A., Timpanaro, R., Bisignano, B., Amatore, D., Palamara, A.T., Nencioni, L. and Saladino, R. Carbon nanotubes supported tyrosinase in the synthesis of lipophilic hydroxytyrosol and dihydrocaffeoyl catechols with antiviral activity against DNA and RNA viruses. *Bioorganic & Medicinal Chemistry,* **2015**, 23(17), pp.5345-5351.
506- Tofani, D., Balducci, V., Gasperi, T., Incerpi, S. and Gambacorta, A., Fatty acid hydroxytyrosyl esters: structure/antioxidant activity relationship by ABTS and in cell-culture DCF assays. *Journal of agricultural and food chemistry,* **2010**, 58(9), pp.5292-5299.
507- Schrittwieser, J.H., Velikogne, S., Hall, M. and Kroutil, W., Artificial biocatalytic linear cascades for preparation of organic molecules. *Chemical reviews,* **2018**, 118(1), pp.270-348.
508- Chauhan, K., Zárate-Romero, A., Sengar, P., Medrano, C. and Vazquez-Duhalt, R., Catalytic Kinetics Considerations and Molecular Tools for the Design of Multienzymatic Cascade Nanoreactors. *ChemCatChem*, **2021**, 13(17), pp.3732-3748.
509- Giannakopoulou, A., Chatzikonstantinou, A.V., Chalmpes, N., Tsapara, G., Gournis, D., Polydera, A.C. and Stamatis, H., Development of a novel bi-enzymatic nanobiocatalyst for the efficient bioconversion of oleuropein to hydroxytyrosol. *Catalysts*, **2021**, 11(6), p.749.
510- Simeó, Y., Sinisterra, J.V. and Alcántara, A.R. Regioselective enzymatic acylation of pharmacologically interesting nucleosides in 2-methyltetrahydrofuran, a greener substitute for THF. *Green Chemistry,* **2009**, 11(6), pp.855-862.
511- Adlercreutz, P., Immobilisation and application of lipases in organic media. *Chemical Society Reviews*, **2013**, 42(15), pp.6406-6436.
512- Ortiz, E., Gallay, P., Galicia, L., Eguílaz, M. and Rivas, G. Nanoarchitectures based on multi-walled carbon nanotubes non-covalently functionalized with Concanavalin A: A new building-block with supramolecular recognition properties for the development of electrochemical biosensors. *Sensors and Actuators B: Chemical*, **2019**, 292, pp.254-262.
513- Hernández-García, S., García-García, M.I. and García-Carmona, F., An improved method to measure lipase activity in aqueous media. *Analytical Biochemistry,* **2017**, 530, pp.104-106.
514- Verma, S.K., Ghosh, K.K., Verma, R. and Verma, S. Influence of cationic surfactants and inorganic salts on the enzyme kinetic activity of Mucor javanicus lipase. *International Journal of Chemical Kinetics*, **2021**, 53(2), pp.308-316.
515- Y. Masamoto, S. Lida, M. Kubo, *J. Med. Plants Res.* **1980**, 40, 361–365.
516- Decher, G., Fuzzy nanoassemblies: toward layered polymeric multicomposites. *Science*, **1997**, 277(5330), pp.1232-1237.
517- Makky, A., Michel, J.P., Maillard, P. and Rosilio, V., Biomimetic liposomes and planar supported bilayers for the assessment of glycodendrimeric porphyrins interaction with an immobilized lectin. *Biochimica et Biophysica Acta (BBA)-Biomembranes,* **2011**, 1808(3), pp.656-666.
518- Perchyonok, V.T., Souza, J., Küll, M.F., Suzuki, T.Y.U., Maluly-Proni, A.T. and Santos, P.H.D., Color stability and surface roughness of chitosan-and nanodiamond-modified bisacrylic resin. *Brazilian oral research*, **2019**, 33.
519- Zhang, Y., Yong, Y., Ge, J. and Liu, Z., Lectin agglutinated multienzyme catalyst with enhanced substrate affinity and activity. *ACS Catalysis,* **2016**, 6(6), pp.3789-3795.
520- Idan, O. and Hess, H., Engineering enzymatic cascades on nanoscale scaffolds. *Current opinion in biotechnology*, **2013**, 24(4), pp.606-611.
521- Wu, F. and Minteer, S.D., Fluorescence Characterization of Co-immobilization-Induced Multi-Enzyme Aggregation in a Polymer Matrix Using Forster Resonance Energy Transfer (FRET): Toward the Metabolon Biomimic. *Biomacromolecules*, **2013**, 14(8), pp.2739-2749.
522- Shrestha, D., Jenei, A., Nagy, P., Vereb, G. and Szöllősi, J., Understanding FRET as a research tool for cellular studies. *International journal of molecular sciences*, **2015**, 16(4), pp.6718-6756.
523- Zhang, Y., Lyu, F., Ge, J. and Liu, Z., Ink-jet printing an optimal multi-enzyme system. *Chemical Communications,* **2014**, 50(85), pp.12919-12922.
524- Xia, Z. and Liu, Y. Reliable and global measurement of fluorescence resonance energy transfer using fluorescence microscopes. *Biophysical journal,* **2001**, 81(4), pp.2395-2402.
525- J. Fu, Y. R. Yang, A. Johnson-Buck, M. Liu, Y. Liu, N. G. Walter, N. W. Woodbury, H. Yan, Nat. *Nanotechnol.* **2014**, 9, 531–536.
526- Zaidi, A., Gainer, J.L., Carta, G., Mrani, A., Kadiri, T., Belarbi, Y. and Mir, A. Esterification of fatty acids using nylon-immobilized lipase in n-hexane: kinetic parameters and chain-length effects. *Journal of Biotechnology,* **2002**, 93(3), pp.209-216.
527- Sun, J. and Liu, S.Q. Ester synthesis in aqueous media by lipase: alcoholysis, esterification and substrate hydrophobicity. *Journal of Food Biochemistry,* **2015**, 39(1), pp.11-18.
528- Chowdary, G.V. and Prapulla, S.G. The influence of water activity on the lipase catalyzed synthesis of butyl butyrate by transesterification. *Process Biochemistry,* **2002**, 38(3), pp.393-397.
529- Wang, S., Meng, X., Zhou, H., Liu, Y., Secundo, F. and Liu, Y., Enzyme stability and activity in non-aqueous reaction systems: a mini review. *Catalysts*, **2016**, 6(2), p.32.
530- Englezou, G., Kortsen, K., Pacheco, A.A., Cavanagh, R., Lentz, J.C., Krumins, E., Sanders-Velez, C., Howdle, S.M., Nedoma, A.J. and Taresco, V. 2-Methyltetrahydrofuran (2-MeTHF) as a versatile green solvent for the synthesis of

amphiphilic copolymers via ROP, FRP, and RAFT tandem polymerizations. *Journal of Polymer Science*, **2020**, 58(11), pp.1571-1581.
531- Bradshaw, M.P., Barril, C., Clark, A.C., Prenzler, P.D. and Scollary, G.R. Ascorbic acid: A review of its chemistry and reactivity in relation to a wine environment. *Critical reviews in food science and nutrition*, **2011**, 51(6), pp.479-498.
532- Liu, Y., Lotero, E. and Goodwin Jr, J.G. Effect of carbon chain length on esterification of carboxylic acids with methanol using acid catalysis. *Journal of Catalysis,* **2006**, 243(2), pp.221-228.
533- Vetri, V., Canale, C., Relini, A., Librizzi, F., Militello, V., Gliozzi, A. and Leone, M., Amyloid fibrils formation and amorphous aggregation in concanavalin A. *Biophysical chemistry*, **2007**, 125(1), pp.184-190.
534- Locke, A.K., Cummins, B.M., Abraham, A.A. and Cote, G.L. PEGylation of concanavalin A to improve its stability for an in vivo glucose sensing assay. *Analytical chemistry*, **2014**, 86(18), pp.9091-9097.
535- Leri, M., Scuto, M., Ontario, M.L., Calabrese, V., Calabrese, E.J., Bucciantini, M. and Stefani, M. Healthy effects of plant polyphenols: molecular mechanisms. *International journal of molecular sciences*, **2020**, 21(4), p.1250.
536- Manna, C., D'Angelo, S., Migliardi, V., Loffredi, E., Mazzoni, O., Morrica, P., Galletti, P. and Zappia, V., Protective effect of the phenolic fraction from virgin olive oils against oxidative stress in human cells. *Journal of agricultural and food chemistry,* **2002**, 50(22), pp.6521-6526.
537- Fabiani, R.D.B.A., De Bartolomeo, A., Rosignoli, P., Servili, M., Montedoro, G.F. and Morozzi, G., Cancer chemoprevention by hydroxytyrosol isolated from virgin olive oil through G_1 cell cycle arrest and apoptosis. *European Journal of Cancer Prevention*, **2002**, pp.351-358.
538- J. Rodrígue-Morató, L. Xicota, M. Fitó, M. Farré, M. Dierssen, R. de la Torre, *Molecules*. **2015**, 20, 4655–80.
539- Fiorentino, A., Gentili, A., Isidori, M., Monaco, P., Nardelli, A., Parrella, A. and Temussi, F., Environmental effects caused by olive mill wastewaters: toxicity comparison of low-molecular-weight phenol components. *Journal of Agricultural and Food Chemistry,* **2003**, 51(4), pp.1005-1009.
540- Bernini, R., Gilardini Montani, M.S., Merendino, N., Romani, A. and Velotti, F., Hydroxytyrosol-derived compounds: A basis for the creation of new pharmacological agents for cancer prevention and therapy. *Journal of medicinal chemistry,* **2015**, 58(23), pp.9089-9107.
541- Irving, C.D., Floreancig, J.T., Gasonoo, M., Kelley, A.S. and Laulhé, S. Synthesis of Imide and Amine Derivatives via Deoxyamination of Alcohols Using N-Haloimides and Triphenylphosphine. *ChemistrySelect,* **2021**, 6(33), pp.8874-8878.
542- Benítez-Mateos, A.I., Roura Padrosa, D. and Paradisi, F. Multistep enzyme cascades as a route towards green and sustainable pharmaceutical syntheses. *Nature chemistry,* **2022**, 14(5), pp.489-499.
543- Zhang, Y. and Hess, H. Toward rational design of high-efficiency enzyme cascades. *ACS Catalysis*, **2017**, 7(9), pp.6018-6027.
544- de Jesús Rostro-Alanis, M., Mancera-Andrade, E.I., Patiño, M.B.G., Arrieta-Baez, D., Cardenas, B., Martinez-Chapa, S.O. and Saldívar, R.P. Nanobiocatalysis: Nanostructured materials–a minireview. *Biocatalysis*, **2016***,* 2(1), pp.1-24.
545- G. Imokawa, Y. Mishima, JID **1985**, 85, 165–168.
546- van Schaick, G., Pot, S., Schouten, O., den Hartog, J., Akeroyd, M., van der Hoeven, R., Bijleveld, W., Abello, N., Wuhrer, M., Olsthoorn, M. and Dominguez-Vega, E. Evaluating the effect of glycation on lipase activity using boronate affinity chromatography and mass spectrometry. *Food Chemistry*, **2023**, 421, p.136147.
547- Tortolini, C., Capecchi, E., Tasca, F., Pofi, R., Venneri, M.A., Saladino, R. and Antiochia, R. Novel nanoarchitectures based on lignin nanoparticles for electrochemical eco-Friendly biosensing development. *Nanomaterials*, **2021**, 11(3), p.718.
548- Espín, J.C., Soler-Rivas, C., Cantos, E., Tomás-Barberán, F.A. and Wichers, H.J. Synthesis of the antioxidant hydroxytyrosol using tyrosinase as biocatalyst. *Journal of Agricultural and Food Chemistry*, **2001**, 49(3), pp.1187-1193.
549- Hernández-Romero, D., Sanchez-Amat, A. and Solano, F. A tyrosinase with an abnormally high tyrosine hydroxylase/dopa oxidase ratio: role of the seventh histidine and accessibility to the active site. *The FEBS journal*, **2006**, 273(2), pp.257-270.
550- Ito, S., Sugumaran, M. and Wakamatsu, K. Chemical reactivities of ortho-quinones produced in living organisms: Fate of quinonoid products formed by tyrosinase and phenoloxidase action on phenols and catechols. *International Journal of Molecular Sciences,* **2020**, 21(17), p.6080.
551- Guazzaroni, M., Crestini, C. and Saladino, R. Layer-by-Layer coated tyrosinase: An efficient and selective synthesis of catechols. *Bioorganic & medicinal chemistry*, **2012**, 20(1), pp.157-166.
552- Kim, E., Gordonov, T., Liu, Y., Bentley, W.E. and Payne, G.F. Reverse engineering to suggest biologically relevant redox activities of phenolic materials. *ACS chemical biology*, **2013**, 8(4), pp.716-724.
553- Napolitano, A., Panzella, L., Leone, L. and d'Ischia, M. Red hair benzothiazines and benzothiazoles: Mutation-inspired chemistry in the quest for functionality. *Accounts of Chemical Research*, **2013**, 46(2), pp.519-528.
554- Ye, T., Hong, L., Garguilo, J., Pawlak, A., Edwards, G.S., Nemanich, R.J., Sarna, T. and Simon, J.D. Photoionization thresholds of melanins obtained from free electron laser-photoelectron emission microscopy, femtosecond transient absorption spectroscopy and electron paramagnetic resonance measurements of oxygen photoconsumption. *Photochemistry and photobiology*, **2006**, 82(3), pp.733-737.
555- M. C. Scharber, N. S. Sariciftci, *Adv. Mater. Technol.* **2021**, 2000857.
556- Kim, E., Panzella, L., Micillo, R., Bentley, W.E., Napolitano, A. and Payne, G.F. Reverse engineering applied to red human hair pheomelanin reveals redox-buffering as a pro-oxidant mechanism. *Scientific reports,* **2015**, 5(1), p.18447.

557- Gabellone, S., Capecchi, E., Ortelli, L.A. and Saladino, R., First Evidence of Pheomelanin-UVA-Driven Synthesis of Pummerer's Ketones by Peroxidase-Mediated Oxidative Coupling of Substituted Phenols. *ACS omega,* **2022**, 7(49), pp.45688-45696.
558- C. A. Ramsden, P. A. Riley, *Bioorg. Med. Chem.* **2014**, 22, 2388–95.
559- Lerch, K., Protein and active-site structure of tyrosinase. *Progress in clinical and biological research*, **1988**, 256, pp.85-98.
560- Bronze-Uhle, E.S., Paulin, J.V., Piacenti-Silva, M., Battocchio, C., Rocco, M.L.M. and Graeff, C.F.D.O., Melanin synthesis under oxygen pressure. *Polymer International*, **2016**, 65(11), pp.1339-1346.
561- Lintinen, K., Xiao, Y., Ashok, R.B., Leskinen, T., Sakarinen, E., Sipponen, M., Muhammad, F., Oinas, P., Österberg, M. and Kostiainen, M., Closed cycle production of concentrated and dry redispersible colloidal lignin particles with a three solvent polarity exchange method. *Green Chemistry,* **2018**, 20(4), pp.843-850.
562- Ito, S., Wakamatsu, K. and Sarna, T. Photodegradation of eumelanin and pheomelanin and its pathophysiological implications. *Photochemistry and photobiology,* **2018**, 94(3), pp.409-420.
563- Al Khatib, M., Costa, J., Spinelli, D., Capecchi, E., Saladino, R., Baratto, M.C. and Pogni, R., Homogentisic acid and gentisic acid biosynthesized pyomelanin mimics: Structural characterization and antioxidant activity. *International journal of molecular sciences*, **2021**, 22(4), p.1739.
564- Mostert, A.B., Hanson, G.R., Sarna, T., Gentle, I.R., Powell, B.J. and Meredith, P. Hydration-controlled X-band EPR spectroscopy: A tool for unravelling the complexities of the solid-state free radical in eumelanin. *The Journal of Physical Chemistry B,* **2013**, 117(17), pp.4965-4972.
565- Chikvaidze, E.N., Partskhaladze, T.M. and Gogoladze, T.V. Electron spin resonance (ESR/EPR) of free radicals observed in human red hair: a new, simple empirical method of determination of pheomelanin/eumelanin ratio in hair. *Magnetic Resonance in Chemistry*, **2014**, 52(7), pp.377-382.
566- Al Khatib, M., Harir, M., Costa, J., Baratto, M.C., Schiavo, I., Trabalzini, L., Pollini, S., Rossolini, G.M., Basosi, R. and Pogni, R., Spectroscopic characterization of natural melanin from a Streptomyces cyaneofuscatus strain and comparison with melanin enzymatically synthesized by tyrosinase and laccase. *Molecules*, **2018**, 23(8), p.1916.
567- Kim, D.J., Ju, K.Y. and Lee, J.K. The synthetic melanin nanoparticles having an excellent binding capacity of heavy metal ions. *Bulletin of the Korean Chemical Society*, **2012**, 33(11), pp.3788-3792.
568- Stanic, V., Maia, F.C.B., de Oliveira Freitas, R., Montoro, F.E. and Evans-Lutterodt, K. The chemical fingerprint of hair melanosomes by infrared nano-spectroscopy. *Nanoscale*, **2018**, 10(29), pp.14245-14253.
569- De Souza, R.A., Kamat, N.M. and Nadkarni, V.S. Purification and characterisation of a sulphur rich melanin from edible mushroom Termitomyces albuminosus Heim. *Mycology*, **2018**, 9(4), pp.296-306.
570- Cho, J., Chu, S., Dauenhauer, P.J. and Huber, G.W. Kinetics and reaction chemistry for slow pyrolysis of enzymatic hydrolysis lignin and organosolv extracted lignin derived from maplewood. *Green Chemistry,* **2012**, 14(2), pp.428-439.
571- Liu, Q., Bai, Y., Chen, H., Chen, M., Sang, Y., Wu, K., Ma, Z., Ma, Y. and Li, Y., Catalytic conversion of enzymatic hydrolysis lignin into cycloalkanes over a gamma-alumina supported nickel molybdenum alloy catalyst. *Bioresource Technology*, **2021**, 323, p.124634.
572- Fuentes-López, D., Ortega-Zambrano, D., Fernández-Herrera, M.A. and Mercado-Uribe, H., The growth of Escherichia coli cultures under the influence of pheomelanin nanoparticles and a chelant agent in the presence of light. *Plos one*, **2022**, 17(3), p.e0265277.
573- Johannes, A.Z., Pingak, R.K. and Bukit, M. Tauc Plot Software: Calculating energy gap values of organic materials based on Ultraviolet-Visible absorbance spectrum. *In IOP conference series: materials science and engineering* **2020**, (Vol. 823, No. 1, p. 012030). IOP Publishing.
574- J. Tauc, Mat. Res. Bull. 1968, 3, 37–46.
575- Elgrishi, N., Rountree, K.J., McCarthy, B.D., Rountree, E.S., Eisenhart, T.T. and Dempsey, J.L., A practical beginner's guide to cyclic voltammetry. *Journal of chemical education,* **2018**, 95(2), pp.197-206.
576- Mazzaracchio, V., Tomei, M.R., Cacciotti, I., Chiodoni, A., Novara, C., Castellino, M., Scordo, G., Amine, A., Moscone, D. and Arduini, F., Inside the different types of carbon black as nanomodifiers for screen-printed electrodes. *Electrochimica Acta,* **2019**, 317, pp.673-683.
577- A. S. Elewi, S. A. W. Al-Shammaree, A. K. Sammarraie, *Sens. Bio-Sens. Res.* **2020**, 28, 100340.
578- Matsui, T., Kitagawa, Y., Okumura, M. and Shigeta, Y. Accurate standard hydrogen electrode potential and applications to the redox potentials of vitamin C and NAD/NADH. *The Journal of Physical Chemistry A*, **2015**, 119(2), pp.369-376.
579- Fish, B.C. and Thompson, L.U. Lectin-tannin interactions and their influence on pancreatic amylase activity and starch digestibility. *Journal of agricultural and food chemistry,* **1991**, 39(4), pp.727-731.
580- Scheibel, D.M. and Gitsov, I. Unprecedented enzymatic synthesis of perfectly structured alternating copolymers via "green" reaction cocatalyzed by laccase and lipase compartmentalized within supramolecular complexes. *Biomacromolecules*, **2018**, 20(2), pp.927-936.
581- De Marchi, E., Botta, L., Bizzarri, B.M. and Saladino, R. A Green Blue LED-Driven Two-Liquid-Phase One-Pot Procedure for the Synthesis of Estrogen-Related Quinol Prodrugs. *Molecules*, **2022**, 27(24), p.8961.
582- Adlercreutz, P. Immobilisation and application of lipases in organic media. *Chemical Society Reviews*, **2013**, 42(15), pp.6406-6436.
583- Zhang, Z., Chen, F., Zhang, R., Deng, Z. and McClements, D.J. Encapsulation of pancreatic lipase in hydrogel beads with self-regulating internal pH microenvironments: retention of lipase activity after exposure to gastric conditions. *Journal of agricultural and food chemistry*, **2016**, 64(51), pp.9616-9623.

584- Ito, S., Fujiki, Y., Matsui, N., Ojika, M. and Wakamatsu, K., Tyrosinase-catalyzed oxidation of resveratrol produces a highly reactive ortho-quinone: Implications for melanocyte toxicity. *Pigment Cell & Melanoma Research,* **2019**, 32(6), pp.766-776.
585- Dunsmore, L., Navo, C.D., Becher, J., de Montes, E.G., Guerreiro, A., Hoyt, E., Brown, L., Zelenay, V., Mikutis, S., Cooper, J. and Barbieri, I., Controlled masking and targeted release of redox-cycling ortho-quinones via a C–C bond-cleaving 1, 6-elimination. *Nature Chemistry,* **2022**, 14(7), pp.754-765.
586- Bartella, L., Mazzotti, F., Napoli, A., Sindona, G. and Di Donna, L., A comprehensive evaluation of tyrosol and hydroxytyrosol derivatives in extra virgin olive oil by microwave-assisted hydrolysis and HPLC-MS/MS. *Analytical and bioanalytical chemistry,* **2018**, 410, pp.2193-2201.
587- Cui S.; Arza C.R.; Froimowicz P.; Ishida H. Developing Further Ver-satility in Benzoxazine Synthesis via Hydrolytic Ring-Opening. *Polym.* **2020**, 12, 694.
588- Shariat M.; Abdollahi S. Synthesis of Benzoxazinone Derivatives: A New Route to 2-(N-Phthaloylmethyl)-4H-3,1-benzoxazin-4-one. *Mol*. **2004**, 9, 705-712.
589- Nguyen K. M. H.; Schwendimann L.; Gressensb P.; Largeron M. Regiospecific synthesis of neuroprotective 1,4-benzoxazine deriva-tives through a tandem oxidation–Diels–Alder reaction. *Org. Bio-mol. Chem.,* **2015**,13, 3749-3756.
590- Pegklidou K.; Papastavrou N.; Gkizis P.; Komiotis D.; Balzarini J.; Nicolaou I. N-substituted pyrrole-based scaffolds as potential anti-cancer and antiviral lead structures. *Med Chem.* **2015**,11(6): 602-8.
591- Bavandi H.; Shahedi M.; Habibi Z.; Yousefi M.; Brask J.; Moham-madi M. Biocatalytic decarboxylative Michael addition for synthesis of 1,4-benzoxazinone derivatives. *Sci. Rep.,* **2022**, 12, 12713.
592- Zheng B-F.; Zuo Y.; Huang G-Y.; Wang Z-Z.; Ma J-Y.; Wu Q-Y.; Yang G-F. Synthesis and Biological Activity Evaluation of Benzoxa-zinone-Pyrimidinedione Hybrids as Potent Protoporphyrinogen IX Oxidase-Inhibitor. *J. Agric. Food Chem*. **2023**, 71, 39, 14221–14231.
593- Gambacorta N.; Gasperi V.; Guzzo T.; Di Leva F.S.; Ciriaco F.; Sanchez C.; Tullio V.; Rozzi D.; Marinelli L.; Topai A.; Nicolotti O.; Maccarone M. Exploring the 1,3-benzoxazine chemotype for canna-binoid receptor 2 as a promising anti-cancer therapeutic. *Eur. J. Med. Chem.* **2023**, 259, 115647.
594- Xu F.; Qian X.Y.; Li Y.J.; Xu H.C. Synthesis of 4H-1,3-Benzoxazines via Metal- and Oxidizing Reagent-Free Aromatic C–H Oxygenation. *Org. Lett.* **2017**, 19, 23, 6332–6335.
595- Wei W.J.; Zhan L.; Jiang C.N.; Tang H.T.; Pan Y.M.; Ma X.L.; Mo Z.Y. Electrochemical oxidative cascade cyclization of olefinic am-ides and alcohols leading to the synthesis of alkoxylated 4H-3,1-benzoxazines and indolines. *Green Chem.,* **2023**, 25, 928-933.
596- Zumbrägel N.; Gröger H. Merging Heterocyclic Chemistry and Bio-catalysis in One-Pot Processes through Compartmentalization of the Reaction Steps. *Bioeng.* **2018**, 5, 60.
597- Bizzarri B. M.; Fanelli A.; Botta L.; De Angelis M.; Palamara A. T.; Nencioni L.; Saladino R. Aminomalononitrile inspired prebiotic chemistry as a novel multicomponent tool for the synthesis of imidazole and purine derivatives with anti-influenza A virus activity. *RSC Adv.,* **2021**, 11, 30020.
598- Răzvan C.C.; Eelco R.; Romano V.A. Orru. Multicomponent Reactions: Advanced Tools for Sustainable Organic Synthesis. *Green Chem.,* **2014**, 16, 00-00.
599- Botta L.; Cesarini S.; Zippilli C.; Bizzarri B. M.; Fanelli A.; Saladino R. Multicomponent Reactions in the Synthesis of Antiviral Com-pounds. *Curr. Med. Chem.,* **2022**, 12, 2013–2050.
600- Bizzarri B. M.; Pieri C.; Botta G.; Arabuli L.; Mosesso P.; Cinelli S.; Schinoppia A.; Saladino R. Synthesis and antioxidant activity of DOPA peptidomimetics by a novel IBX mediated aromatic oxidative functionalization. *RSC Adv.*, **2015**, 5, 60354.
601- Bizzarri B. M.; Martini A.; Serafini F.; Aversa D.; Piccinino D.; Botta L.; Berretta N.; Guatteo E.; Saladino R. Tyrosinase mediated oxidative functionalization in the synthesis of DOPA-derived peptidomimetics with anti-Parkinson activity. *RSC Adv.,* **2017**, 7, 20502.
602- Witayakran S. and Ragauskas A.J. Co-catalytic Enzyme System for the Michael Addition Reaction of in-situ-Generated ortho-Quinones. *Eur. J. Org. Chem.,* **2009**, 3, 358-363.
603- Alfieri M.L.; Cariola A.; Panzella L.; Napolitano A.; d'Ischia M.; Valgimigli L.; Crescenzi O. Disentangling the Puzzling Regiochemi-stry of Thiol Addition to o-Quinones. *J. Org. Chem.,* **2022**, 87, 4580-4589.
604- Han P.; Zhou X.; You C. Efficient Multi-Enzymes Immobilized on Porous Microspheres for Producing Inositol From Starch. *Front Bioeng Biotechnol*., **2020**, 8, 380.
605- Heinks T., Koopmeiners S., Montua N., Sewald N., Höhne M., Bornscheuer U. T., Fischer von Mollard G., *ChemBioChem*, **2023**, 24, e202300425.
606- Su S.; Hu J.; Cui Y.; Tang C.; Chen Y.; Li J. A formal (5+1) annula-tion reaction from heterodimerization of two different isocyanides: stereoselective synthesis of 2H-benzo[b] [1,4]oxazin-2-one. *Chem Comm.,* **2019**, 55, 12243.
607- Su S.; J Li.; Sun M.; Zhao H.; Chen Y.; Li J. A domino reaction of 2-isocyanophenyloxyacrylate and aryne to synthesize arenes with vicinal olefin and benzoxazole, *Chem. Commun.,* **2018**, 9611-9614.
608- Choudhary G.; Naganaboina R.T.; Peddinti R.K. Expedient synthesis of novel 1,4-benzoxazine and butenolide derivatives. *RSC Adv.,* **2014**, 4, 17969.
609- Muñoz-Muñoz J. L.; Garcia-Molina F.; Garcia-Ruiz P. A.; Varon R.; Tudela J.; Rodriguez- Lopez J. N.; Garcia-Canovas F. Catalytic oxidation of o-aminophenols and aromatic amines by mushroom tyrosinase. *Biochim. Biophys. Acta*, **2011**, 1814, 1974–1983.

610- D'Mello S. A. N.; Finlay G. J.; Baguley B. C.; Askarian-Amiri M. E. Signaling Pathways in Melanogenesis. *Int. J. Mol. Sci.*, **2016,** 17, 1144.
611- Takahashi K., Yoshimoto T., Ajima A., Tamaura Y., Inada Y. Modified Lipoprotein Lipase Catalyzes Ester Synthesis in Benzene. *Enzyme*, **1984**, 32(4), 235–240.
612- Abbas H., Comeau L. Aroma synthesis by immobilized lipase from Mucor sp. *Enzyme Microb. Technol*., **2003**, 32, 5, 589-595.
613- Salis A., Meloni D., Ligas S., Casula M.F., Monduzzi M., Solinas V., Dumitriu E. Physical and chemical adsorption of Mucor javanicus lipase on SBA-15 mesoporous silica. Synthesis, structural characterization, and activity performance. *Langmuir*, **2005**, 21, 5511-5516.

Conclusions

Nano-biotechnologies based on the application of lignin nanoparticles are of large industrial interest for the design of novel biobased materials with antioxidant, antimicrobial and UV-protecting properties, as well as for the preparation of biocatalysts. The renewable and biodegradable properties showed by lignin nanoparticles, associated to the possibility to prepare them by sustainable and efficient nanoprecipitation procedures using eco-certified organic solvents and deionized water, favoured their effective application in the encapsulation of chemical sunscreen filters useful for the preparation of novel sunscreen products and photoprotective carriers. In this context, lignin nanoparticles showed high biocompatibility, complete biodegradability and antimicrobial activity, improving the antioxidant and UV shielding properties of the end products with respect to the homopolymer counterpart. The emergence of these latter beneficial chemo-physical properties was a direct consequence of their nano-aggregation state ("exciton" theory"), favouring the emergence of synergistic effects.

Next, composite lignin nanoparticles have been studied in the context of the design of innovative cosmeceutical products. Lignin nanoparticles coated with chitosan by layer-by-layer technology showed remarkable properties as functional and renewable support for the immobilization of enzymes, including lipase B from *Candida antarctica*. In this case, a dual-target strategy was applied for the lipase mediated biosynthesis of novel 3-O-ethyl-L-ascorbyl-6-ferulate and 3-O-ethyl-L-ascorbyl-6-palmitate and in their successive solvent-shift encapsulation in order to improve stability and antioxidant activity against temperature and pH-dependent degradation. After the encapsulation process, loaded LNPs showed improved thermal and pH stability, 3-Oethyl-L-ascorbyl-6-ferulate and 3-O-ethyl-L-ascorbyl-6-palmitate being preserved toward degradation with respect to free ascorbic acid (AA) and other AA derivatives as references.

In the context of advanced materials, lignin nanoparticles containing saccharides from fishery wastes were produced by a sustainable nanoprecipitation process and used as sustainable bio-fillers in the preparation of bioplastic blends. The chemo-physical and biological activities of composite lignin/saccharide nanoparticles, such as UV-shielding, antioxidant, and antimicrobial activities, were found to be dependent on both molecular weight and deacetylation degree of saccharides, the best results being obtained with low molecular-weight and highly deacetylated chito-oligosaccharides. In addition, chito-oligosaccharides increased the melting point, antioxidant activity, UV protection, and antimicrobial effects of lignin nanoparticles with respect to the chitosan counterpart.

Lignin nanoparticles showed also significant applications in biocatalysis under green conditions. Thus, organosolv lignin nanoparticles coated with chitosan were used as support for the co-immobilization of lipase M and tyrosinase in the synthesis of lipophilic hydroxytyrosol esters by one-pot esterification and *ortho*-hydroxylation of tyrosol with long-medium side chain carboxylic acids. The highest yield was obtained in the presence of Concanavalin A, which was able to control the optimal orientation and distance between the two enzymes, favouring the occurrence of substrate-tunnelling effect. In order to avoid the use of external and toxic reducing agents, which can also inhibit the enzyme, the multienzyme cascade of lipase M and tyrosinase was also supported on hybrid lignin nanoparticles containing electroactive eumelanin and pheomelanin. It was demonstrated that eumelanin and pheomelanin embedded into the lignin nanoplatform were able to control the selectivity of lipase-tyrosinase multienzyme cascade in the one-pot synthesis of lipophilic hydroxytyrosol esters. In particular, the redox activity of tyrosinase in the multienzyme cascade was significantly improved with respect to native

enzyme. This effect was probably due to the shift of the active site of tyrosinase from unproductive met-form to reversible *deoxy/oxy*-form mediated by the presence of electroactive melanin.[569] The reactivity observed for the novel biocatalysts was confirmed by cyclic voltammetry and optoelectronic analysis (E_0 and HOMO-LUMO energy gap values). Biocatalysts retained their activity for at least five runs, preserving the morphological integrity of the lignin nanoparticle.

Next, the possibility to combine multi-component chemistry and multi-enzymes cascade transformations in a unique reactive framework was demonstrated focusing on the synthesis of highly functionalized 1,4-benzoxazines from a ternary mixture under mild reaction conditions. The desired products were obtained from moderate to high yield under mild reaction conditions and excellent atom economy and chemo-selectivity.

The immobilization of the multienzymes cascade on electroactive lignin nanoparticles improved the sustainability and recyclability of the overall system.

This approach extends the wide application of multienzymes cascade reaction and multicomponent chemistry in a unique chemical framework providing a new entry for sustainable organic synthesis.